The development of multiwire drift chambers for high energy physics

K. A. Short

THE DEVELOPMENT OF MULTIWIRE DRIFT CHAMBERS

FOR

HIGH ENERGY PHYSICS

by

K.A. SHORT B.Sc.

A thesis submitted to the University of Durham
for the Degree of Doctor of Philosophy.

Being an account of the work carried out at the University of Durham during the period October 1972 to September 1975.

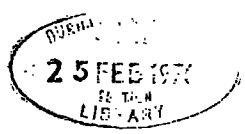

ABSTRACT

An array comprising eight multiwire drift chambers has been developed and installed in the g-2 muon storage ring at CERN with the main objectives being to measure the circulating beam profile and the momenta of decay electrons.

Constructional design features include narrow framework and an extremely thin curved end member, the latter having been converted into a sensitive drift space.

Prototype models of the chambers have been used to select the operating parameters and to investigate the general properties and capabilities of such detectors. Argon(90%) and Methane(10%) has been chosen from several gas mixtures tested and has been used extensively throughout this work.

Prototype and production chambers have been operated in the e^+ accelerator beam at the Daresbury Laboratory using a computerised data acquisition system and spatial resolutions of the order 100 to 150 μm have been recorded in magnetic fields up to 7.5 KGauss. This system has also enabled a qualitative study of certain simulated g-2 conditions.

A simple model based on classical equations has been used to select an electric field configuration, which enables good operation

in a strong non-uniform magnetic field up to 14.75 KGauss, and to predict the behaviour of drifting electrons in such an environment.

The operation of the chambers under experimental conditions has been studied, and initial results from the storage ring are discussed together with proposed future work.

CONTENTS

CHAPTER 1

THE DRIFT CHAMBER TECHNIQUE

1.1 Particle Detectors in High Energy Physics

Over the past forty years, with the advent of accelerator machines and the many breakthroughs made in cosmic ray physics, a vast amount of effort has been required in the field of high energy radiation detection. The earliest detectors included the ionization chamber and the Wilson cloud chamber (1) in 1912 and, since this pioneering work, there has been a great and diverse expansion in this particular branch of nuclear physics. Many hybrid devices have appeared and it is the purpose of this thesis to consider the development and application of one such device, the multiwire drift chamber.

Particle detectors can be subdivided into various categories. There are non-triggerable devices such as the bubble chamber and expansion cloud chamber; electrically pulsed, triggerable devices such as the spark chamber, streamer chamber, projection chamber and flash tube; and continuously sensitive devices such as the diffusion cloud chamber, the scintillation counter, the Cerenkov counter and the proportional counter.

The multiwire drift chamber is a gaseous detector belonging

to the last group.

1.2 The Drift Chamber Principle

The easiest way to introduce the multiwire drift chamber (MWDC) is to consider first the operation of its closest neighbour, the multiwire proportional chamber (MWPC). This device itself is a recent development by Charpak (2) of the traditional proportional counter, and has already found a significant role in high energy nuclear physics. It consists of two parallel planes of wires separated by say 10 to 20 mm and maintained at a negative high voltage. In between and equidistant from these cathode planes is a series of finer (sense) wires which are spaced every 2 mm say and are usually orthogonal to the cathode wires. Such a configuration is shown in figure 1.1(a), the whole structure being contained in an enclosed gaseous volume.

A particle traversing a MWPC as shown in the diagram, leaves a trail of ion pairs along its trajectory. If the cathode voltage is high enough, there exists around each sense wire a field strong enough to enable the primarily deposited electrons to undergo a series of ionizing collisions with gas molecules, building up to a sizeable avalanche (a multiplication factor of approximately 10^7) towards the sense wire. Thus a current is induced in the wire which is usually manifested as a negative going pulse across a resistor between the sense wire and earth. It so happens that the avalanche is localized to the nearest wire and in effect, each wire acts as an individual counter.

The basic principle of the drift chamber is to drift, in an electric field, the electrons deposited by a particle towards the

FIG 1.1.a Normal Wire Proportional Chamber

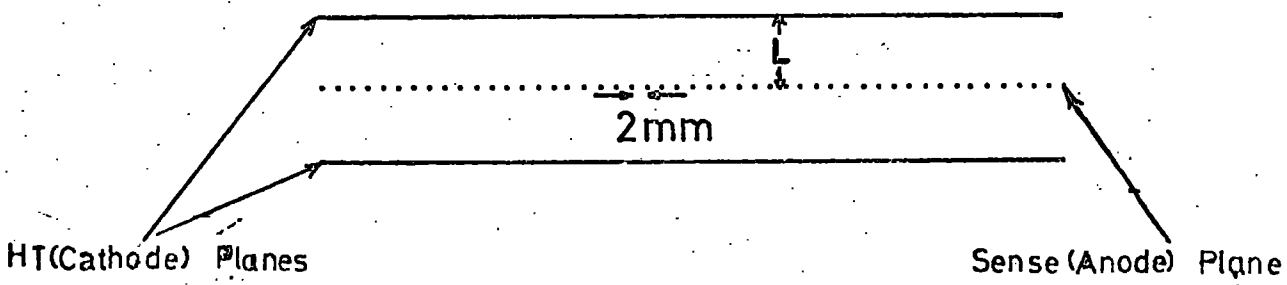

FIG 1.1.b Basic Drift Chamber

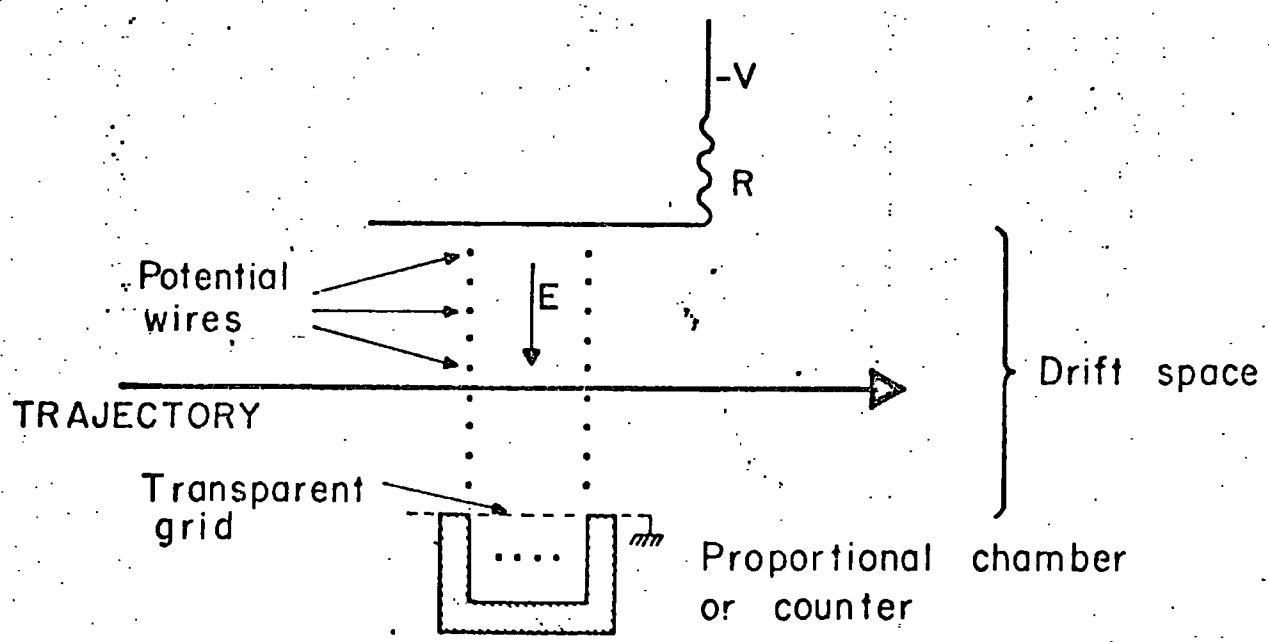

sense wire of a proportional chamber and obtain a signal in the manner described above. If the conditions of field and gas composition are correctly chosen so as to produce a uniform drift velocity, then the elapsed time between the traversal of the particle (usually determined electronically using a scintillator as a trigger) and the appearance of a pulse from the sense wire gives a direct and accurate indication of the spatial position at one point of the particle trajectory. With this idea in mind, the basic drift chamber configuration is shown in figure 1.1 (b) (3).

1.2.1 The Evolution of Drift Chambers.

A first modification was to incorporate the drift principle into the MWPC structure itself, simply by increasing the separation of sense wires and drifting electrons over distances of the order 10 to 20 mm in the sense wire plane. This method was first realized by Walenta et al. (4), the configuration of such a system being illustrated in figure 1.1(c). Note the appearance of the so called "potential" or "field" wires interspaced between the sense wires. These are wires of similar type and maintained at a similar potential to the cathode wires, their purpose being to maintain high electric fields in regions where this parameter normally falls to zero, the field obviously being important to the drift velocity of electrons.

Further improvement to the uniformity of the electric field was introduced by Charpak et al. (5), the idea being to have a fixed and controllable electric field gradient in the sense wire plane. This was achieved by having the high voltage and sense wires in the same direction as shown in figure 1.1(d), and grading the voltage from a maximum value above and below the field wire to a

FIG 1.1 c Walenta-type Drift Chamber

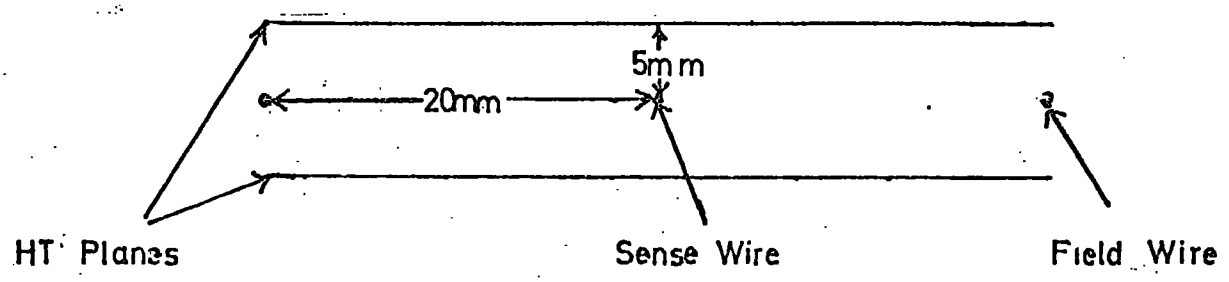

FIG 1.1 d Charpak-type (adjustable-field) Drift Chamber

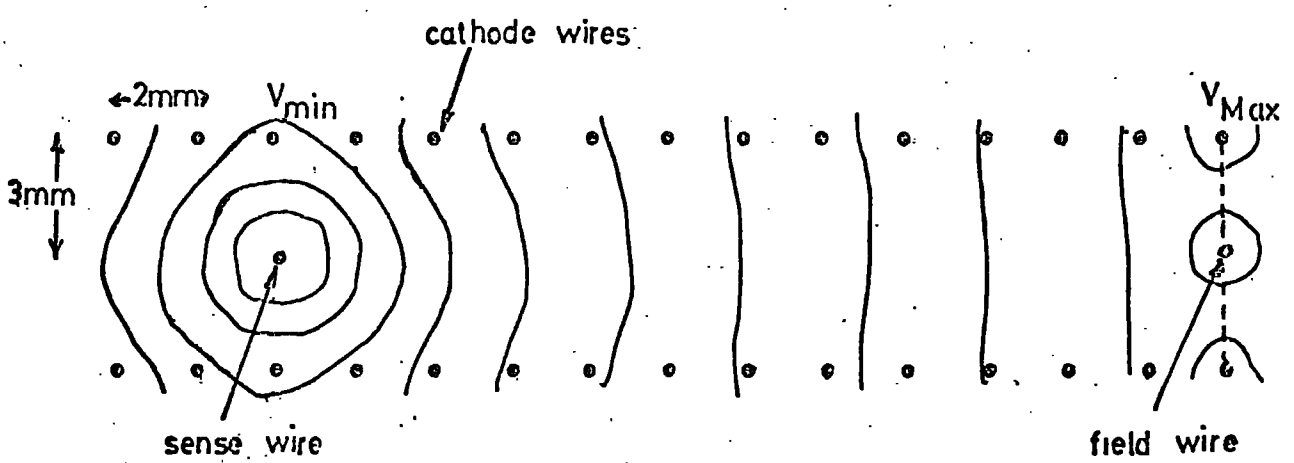

minimum above and below the sense wire. The electric field thus produced is illustrated in figure 1.2 where it can also be compared with the field of a Walenta type chamber of similar dimensions.

1.3 The Life History of Electrons in a Drift Chamber.

Having described the basic method of drift chamber operation, in order to understand better the development work described in this thesis, it is worth considering more fully what happens between the time of particle traversal and the receiving of a signal pulse from the sense wire.

1.3.1 Ion Formation.

The first process is the initial production of ionization in the gaseous volume by a traversing particle. This is the result of the particle losing energy by inelastic Coulomb collisions with electrons, that is, excitation and ionization of gas molecules.

The amount of energy deposited in this manner can be determined from the "dE/dx curve" and is not discussed here. More important in drift chambers, perhaps, is the number of ion pairs produced per unit length (cm. say) (6). This depends on the gas composition, but to consider a commonly used gas, Argon, at atmospheric pressure, the number is about 30.

The energies of the electrons liberated will depend on the collision distance; "knock on" electrons (δ rays) of high energy being produced when the distance involved is small and the energy transfer is large. Many primary electrons (of energies around 70 eV) cause secondary ionization within 1 μm of their initial position and, in the case of Argon, the total number of ion pairs deposited along

FIG 1.2 Drift Chamber Electric Fields

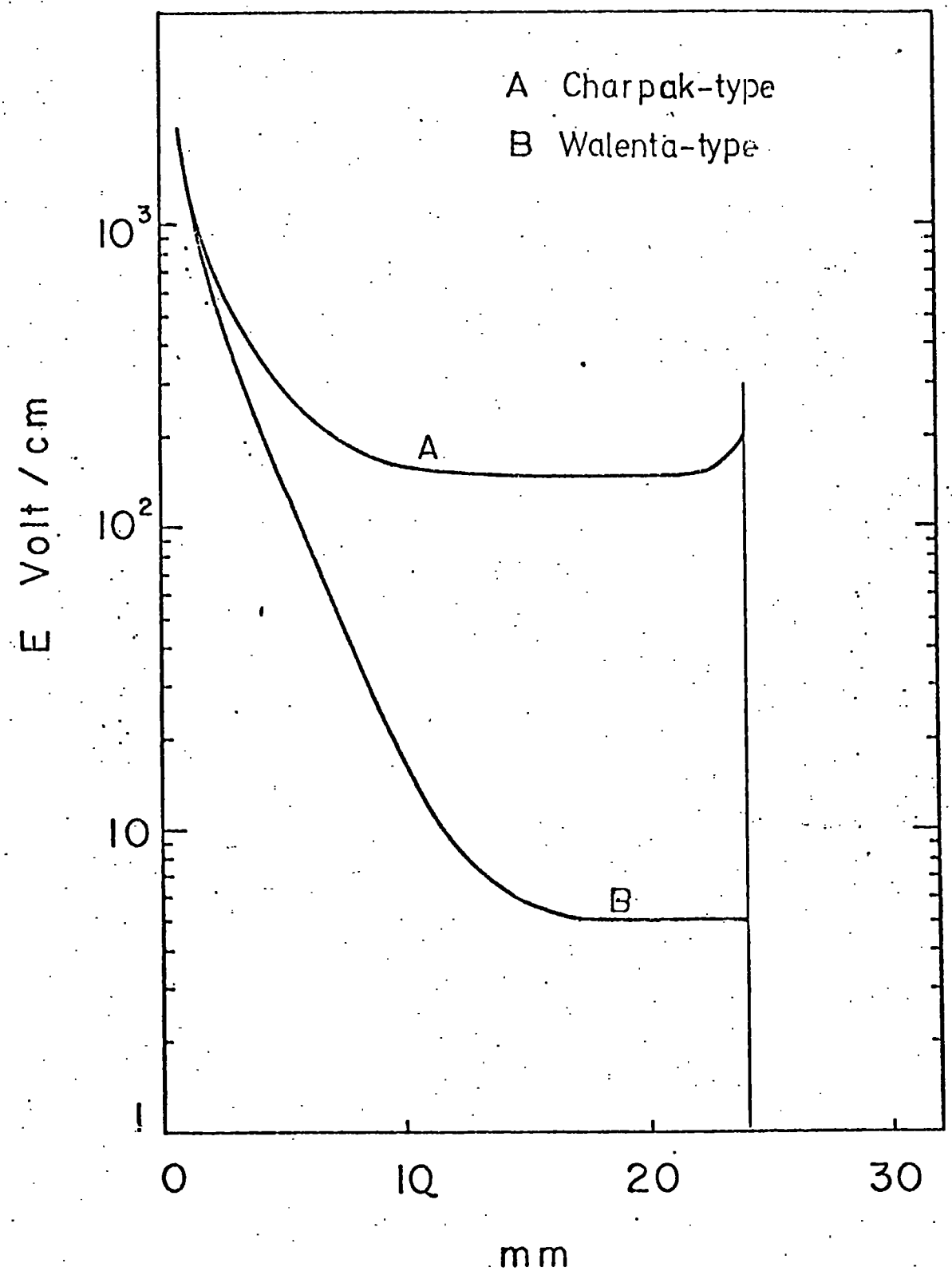

a track will be taken to ~90/cm in this manner. It may also be noted here that other effects, such as Bremstrahlung in the case of electrons, can be responsible for further ion production. By keeping the chamber width small, the chance of δ ray production is reduced and the initial track thickness is negligible.

1.3.2 The Drift Process.

The resulting electrons thermalise rapidly by a series of collisions to energies given by the Maxwell formula $3kT/2$ (1/30 eV at room temperature). If an external electric field is applied, each electron will retain its random-direction thermal velocity but will also start to accelerate in the electric field direction. As the electron swarm is in a viscous medium, a series of elastic collisions will occur with gas molecules, momentum exchange being small due to the comparatively low electron mass.

In a drift chamber, a resultant mean drift velocity will be exhibited in the direction of the sense wire given by:-

$$w = \langle v_x \rangle = \int v_x \, F(\vec{r},\vec{v},t) \, d\vec{v} \qquad (1.1)$$

where $F(\vec{r},\vec{v},t)$ is the velocity distribution (not necessarily Maxwellian) at the point $\vec{r}$ and time t. As already indicated, control over the value of w and hence precise knowledge of drift times can be achieved. A fuller account of drift velocities of electrons in specific gases is to be presented in chapter 4

An important process occuring in the drift region is the diffusion of the swarm, the spread in the direction of the electric field being critical to drift chamber work. If the electron mobility

in a field E is defined by $\mu = w/E$, then the diffusion is given by:-

$$\sigma_x = \sqrt{\frac{2D}{\mu} \cdot \frac{x}{Ee}} = \sqrt{2\,\varepsilon_K \cdot \frac{x}{Ee}} \qquad (1.2)$$

where D is the diffusion coefficient and is dependent on the mean free path for collision. ε_K is a quantity referred to as the characteristic energy, equalling eD/μ and closely related to the electron temperature.

Once again, a certain degree of control can be exercised on the diffusion parameter.

1.3.3 The Avalanche Process.

The final process is the one producing the signal pulse. For a periodic wire structure it has been shown (7) that the potential at any point (x,y) from a sense wire in a chamber of sense wire spacing S, and distance between the sense and H.T. planes, L, is given by:-

$$V = \frac{q}{4\pi E_o}\left[2\pi \frac{L}{S} - \ln\left(4 \sin^2 \frac{\pi x}{S} + 4 \sinh^2 \frac{\pi y}{S}\right) \right] \qquad (1.3)$$

where the charge density, q, for wires of radius r and applied voltage V_o (usually the operating potential above a sense wire) is given by:-

$$q = \frac{4\pi\, \varepsilon_o\, V_o}{2\left[\frac{\pi L}{S} - \ln \frac{2\pi r}{S}\right]} \qquad (1.4)$$

Thus it is evident from equation (1.3) that there is a rapid increase in electric field around the sense wire. In this region, a drifting electron can gain enough energy between collisions to ionize (and excite) gas molecules thus liberating electrons and leaving positive ions, the number of ion pairs being dramatically increased as the process continues.

The current pulse obtained on the wire is not due to the collection of charge from incident electrons, but rather to the movement of both negative and positive ions (in opposite directions), and thus exhibits a finite rise time. As the final ions created are very near to the wire, the positive ions moving down the entire potential are mainly responsible for the induced pulse, whereas the electrons move only a small distance before being neutralised at the wire surface.

1.4 Applications of Drift Chambers to High Energy Physics.

Drift chambers are of use in similar circumstances to those involving proportional or spark chambers, their major usefulness lying in the possibility of very high spatial resolution of the order 100μm. Thus they may be found in spectrometer arrays and track locating systems of all types. Large detecting areas can easily be covered and as such, the drift chamber may well find a useful place in cosmic ray arrays such as the Durham "Muon Automated Research Spectrograph" (M.A.R.S.)

To operate in accelerator environments, several developments have been necessary, some important ones being listed in the next section.

1.4.1 Developments in Drift Chamber Technique.

In order to obtain the very high spatial and timing resolutions (100μm and 5 ns respectively) which make drift chambers an attractive proposition, much work is required on the control of mechanical, electrical and gas parameters as well as the accurate electronic signal processing and timing. The various contributions to expected inaccuracies have been documented by Walenta (8) and are discussed at various points in this thesis.

The first problem to arise in using drift chambers in a track locating system is that of the "left-right ambiguity", that is to say, a single chamber can give no indication of which side of the sense wire the particle traversed. This has been solved in several ways to date (4, 9), namely:-

a) The use of a sense wire doublet (separation 0.2 - 1 mm). Each sense wire is found to act independently, but electrostatic instabilities can occur and difficulties arise from tracks passing between the two wires.

b) The staggering by half-cell distances of alternate chambers, (a "cell" being the detection zone common to one sense wire).

c) For curved trajectories, the geometry provided by four or more chambers will yield unambiguous tracks (to be illustrated in chapter 7).

d) Use in conjunction with MWPC devices.

An important aspect of drift chamber operation is their use

in strong magnetic fields as is often the requirement of a high energy experiment. If the magnetic field has a component parallel to the sense wires, electrons drifting towards the avalanche region may easily be deflected out of the chamber. This can be overcome in chambers of the Charpak design by tilting the electric field potentials to set up a specific electric field vector which in conjunction with the magnetic force vector, will produce a resultant motion of electrons directly towards the sense wire. This subject is discussed more fully in chapter 6.

Problems have been encountered with the multitrack resolution attainable with drift chambers. The first limitation is the usual one for wire chambers, that is electronic occupation time of the amplifier-discriminator, and can be minimised (to about 25 ns) by careful electronic design. The second limitation is the collection time of all the electrons and the time required for the resulting positive space charge to dissipate (200 ns or more); obviously gas composition is important in this case. Finally, confusion between events occuring within a time less than the maximum drift time can now be eliminated (up to a point) using more sophisticated timing circuits.

Two dimensional readout methods have been investigated (10, 11) examples being given below:-

a) Induced positive pulses on the cathode wires can be duly processed using either delay line or pulse centre of gravity techniques.

b) The measurement of the position of the avalanche along

the length of a sense wire can be achieved using a current division method.

Second spatial coordinates can be obtained to within ±2mm.

Drift chambers have been proved capable of high efficiency operation in environments of high rates and angled particle trajectories (12, 13).

Having discussed some of the major developments in this field over recent years, it is now worth-while looking at some typical applications.

1.4.2 A Range of Applications of Drift Chambers in High Energy Physics.

One of the first applications of multiwire drift chambers in a high energy physics experiment involved a series of large chambers (dimensions varying in the range 1 to 2 metres) developed by the CERN-Heidelberg group under Walenta (8). These were used at the CERN PS from 1971-2 in an experiment to determine the branching ratio $K^+ \rightarrow e^+\nu/K^+ \rightarrow \mu^+\nu$, successfully operating at particle rates of 6×10^6 per second.

Charpak's group at CERN (14) have developed drift chambers of dimensions $(2.2 \times 1.5)m^2$ for use together with spark chambers in the OMEGA spectrometer during a neutron experiment. These chambers each comprise several planes of sense wires and employ 25 mm drift spaces, they have been successfully operated in particle rates of 10^5 per second and magnetic fields of 18 KGauss.

A magnificent set of $(3.6 \times 3.6)m^2$ chambers have been built at Harvard University by Rubbia et al. (15) for momentum measurements of high energy muons in a neutrino experiment at NAL. 5 cm drift

spaces yielded time and spatial resolutions of 11 nsec. and 0.35 mm. respectively.

A chamber of the type described in figure 1.2(b) with two 50 cm. drift spaces has been developed by Saudinos et al. at Saclay (16), in order to investigate the feasibility of cheaply covering large areas in experiments. Spatial resolutions of between 0.4 and 1.3 mm. (for drift lengths of 7 and 50 cm. respectively) have proved to be very encouraging.

A novel device has been proposed by an Oxford University group (17), the idea being to sample, using 300 MWPC wires, the energy deposited by a particle. Drift lengths of up to 2m will be employed and 300 positional measurements will be yielded (each to within $\pm$ 2mm.) for each track. Such a device will be used to distinguish kaons, pions and protons from 5 GeV/c to 100 GeV/c.

A proposal has been made by the European Muon collaboration (18) to build many multiwire drift chambers of various sizes for use in an extensive programme of muon physics at the CERN SPS. Spatial resolutions of the order 0.3 to 0.6 mm. will be required as will the efficient operation in high magnetic fields and with high particle rates.

In general, there is currently an extensive programme of work in the development of drift chambers for high energy physics. The fundamental work on discharge properties is usually done using small, single sense wire chambers, whereas the experimental demand is often for large area devices such as those described above.

1.4.3 The Comparison of Drift Chambers with other Particle Detectors.

The most reasonable comparisons to be made are with the wire

spark and proportional chambers, these being by now well established as tools in accelerator physics experiments. The multiwire drift chamber stands on an equal footing with these said devices in the following respects:-

The basic construction is of a simple nature and to vary the shape and size is fairly easy (extensive work is already in progress on spherical drift chambers (19)). Reasonably cheap gas mixtures and building materials exist.

Operation is possible in high rates and strong magnetic fields (although the proportional chamber is slightly superior in these respects).

Little absorptive material is presented to incident radiation, thus Coulomb scattering effects are minimal for high energy particles.

By using a series of chambers, energy deposited can be sampled thus allowing an estimation of incident particle energy.

The advantages of multiwire drift chambers are:-

Mainly the extremely good spatial resolution (of the order 100 μm). With the arrival of accelerators of the 300 GeV plus generation (eg. the CERN SPS) there is a demand for the accurate detection of high rigidity particles as, in this case, momentum determination is made difficult due to the small bending experienced

in magnetic fields presently in use. For charged particles of all typical machine product energies, a series of drift chambers presents a rapid momentum selection system, capable of distinguishing different particle types.

The corresponding good time resolution (of the order 5 ns.) is also of value. For instance, at the CERN Intersecting Storage Rings, proportional chambers alone give too poor timing information to distinguish beam-beam and beam-gas interactions using time of flight measurements.

Another great advantage is the ability to cover large areas using drift chambers. Construction is easier than in other chambers and overall readout is cheaper due simply to the fact that there are fewer wires. Large detecting areas become important in experiments when low event rates are encountered such as neutrino experiments where the cross section of interaction is extremely small. Also, the construction of two dimensional chambers is relatively easy.

With the use of converters, drift chambers can provide reasonable efficiency detectors of photons and neutral particle beams, however in this respect they are not as pliable as scintillator sandwich devices or flash tube hodoscopes (20).

Some further useful properties are: the ability to gate out random events using a half-cell staggered system, and the absence of electrostatic instabilities (as occur in a closely spaced wire system).

It might also be mentioned at this point that there is certainly a future for drift chambers in low energy radiation detection, however this field is outside the scope of the present work.

There are however, several limitations to the usefulness of drift chambers, these being listed below:-

Severe multitrack limitations occur due to the long drift time values encountered and higher rate operation can be realized using MWPCs

Drift chamber operation is more complicated than for other wire chambers, especially in magnetic fields.

In certain arrays, drift chambers may be an unfeasible financial proposition as readout systems tend to be complicated resulting in a high cost of electronics per wire.

To summarise this section, the drift chamber offers many attractive properties to the high energy physicist, and track measuring systems (spectrometers) will probably tend towards a combination of multiwire drift and proportional chambers, there remaining still much scope for development in drift chambers.

1.5 Present Work.

This thesis describes the research work carried out on a system of multiwire drift chambers with the application to a

particular high energy physics experiment in mind, the chamber design itself being of a specialist nature.

It is proposed that the work described here concerning the testing and selection of operating parameters is typical of the requirements of any such system, this being performed using laboratory and accelerator facilities.

Finally, the problems of operating the drift chambers in their experimental environment are investigated (in particular concerning a strong, non-uniform magnetic field) and initial results from the system are presented.

References

1 C.T.R. Wilson. Proc. Roy. Soc. 87 (1912) 277

2 G. Charpak, R. Bouclier, T. Bressani, J. Favier, C. Zupancic. Nucl. Inst. Meth. 62 (1968) 262

3 G. Charpak. Rutherford Laboratory Meeting on Proportional Wire Chambers, (Ed. W.M. Evans), 3-4 (June 1972)

4 A.H. Walenta, J.Heintze, B. Schürlein. Nucl. Inst. Meth. 92 (1971) 373

5 G. Charpak, F. Sauli, W.Duinker. Nucl. Inst. Meth. 108 (1973) 613

6 S.A. Korff. Electron and Nuclear Counters: Theory and Use. (Van Nostrand, 1955)

7 G.A. Erskine. Nucl. Inst. Meth. 105 (1972) 565

8 A.H. Walenta. Nucl. Inst. Meth. 3 (1973) 467

9 G. Charpak, F. Sauli. Nucl. Inst. Meth. 107 (1973) 371

10 G. Charpak, F. Sauli, J-C. Santiard. CERN N.P. Internal Report 73-16

11 A.H. Walenta. Proc. Int. Conf. on High Energy Physics, Batavia, 1972

12 A. Breskin, G. Charpak, B. Gabioud, F. Sauli, N. Trautner, W. Duinker, G. Shultz. Nucl. Inst. Meth. 119 (1974) 9

13 A. Breskin, G. Charpak, F. Sauli, M. Atkinson, G. Shultz. Nucl. Inst. Meth. 124 (1975) 189

14 F. Sauli. Private Document. October 1974, CERN

15 D.C. Cheng, W.A. Kozanecci, R.L. Piccioni, C. Rubbia, L.R. Sulak, H.J. Weedon, J. Whittaker. Nucl. Inst. Meth. 117 (1975) 157

16 R. Chaminade, J.C. Duchazeaubeneix, C. La Spalles, J. Saudinos. Nucl. Inst. Meth. 111 (1973) 77

17 G. Charpak. Proceedings of the Workshop on Research Goals for Cosmic Ray Astrophysics in the 1980's. Frascati, 1974

18 The European Muon Collaboration. Proposed Experiments and Equipment for a Programme of Muon Physics at the SPS. CERN Report SPSC/74-78 July 1974

19 G. Charpak, Z. Hajduk, A. Jeavons, R. Kahn, R.J. Stubbs. Nucl. Inst. Meth. 122 (1974) 307

20 J.E. Chaney. Ph.D. Thesis, University of Durham, 1974

CHAPTER 2

DRIFT CHAMBER REQUIREMENTS OF A HIGH ENERGY PHYSICS EXPERIMENT

2.1 Introduction

This chapter describes the multiwire drift chamber requirements of a typical high energy physics experiment, that is, one which requires particle detectors capable of a high spatial resolution, high efficiency, cheap readout and operation in a strong magnetic field. The experiment in question is the latest of a long line of "g-2" measurements involving the new muon storage ring at CERN, Geneva.

The discussion starts with a brief resumé of the motivations and experimental arrangements of g-2 and is followed by a description of the reasons for and requirements of drift chambers in this experiment. Subsequent chapters are to deal in detail with the development and operation of these "g-2 chambers".

2.2 A Brief Discussion of the Theory of g-2 of the Muon (1)

For a relativistic particle of spin $\frac{1}{2}$ (such as the electron or muon) in an external magnetic field $\vec{B}$, Dirac theory predicts a magnetic moment of μ_0 (one Bohr magneton):-

$$\vec{\mu} = -g\,\mu_0\vec{s} \qquad (2.1)$$

where $\mu_0 = eh/2m_0c$ in usual notation and $\vec{s}$ is the spin as obtained from the Pauli spin matrices. The g factor is 2 for a Dirac particle, yielding $\bar{\mu} = \mu_0$, but is slightly modified by various radiative corrections and hence an "anomaly" (a) is introduced; so (for the muon):-

$$\bar{\mu} = -2(1+ a_\mu)\mu_0\vec{s} \qquad (2.2)$$

where it can be seen that:-

$$a_\mu \equiv (g_\mu - 2)/2 \qquad (2.3)$$

From quantum electrodynamic theory (Q.E.D.), a_μ can be expressed as a power series in α (the fine structure constant $\equiv e^2/\hbar c$) which is a well known quantity. To date, terms have been calculated, using many Feynmann diagrams, to the sixth order in α, yielding a prediction:-

$$a^{Q.E.D.} = \frac{\alpha}{2\pi} + 0.76578\,\frac{\alpha^2}{\pi^2} + 21.8\,\frac{\alpha^3}{\pi^3} \qquad (2.4)$$

To this value must be added corrections estimated from the contributions due to the strong and weak interactions, giving finally:-

$$a_\mu = a^{Q.E.D.} + a^{STRONG} + a^{WEAK} \qquad (2.5)$$

In this way, a latest theoretical estimate for the anomaly

has been found as $a_\mu(\text{theory}) = (1{,}165{,}897 \pm 8) \times 10^{-9}$.

2.2.1 Motivation for a g-2 Experiment

The anomaly, a, is a useful quantity to measure as it provides a good test of Q.E.D., the muon in particular allowing, by virtue of its higher mass, a probing of action over smaller distances than for the electron.

Although Q.E.D. is a well understood and proven theory, there still remains the mystery of the existence of both the muon and the electron. A particle basically interacts by virtue of its mass and, as all other properties of these two particles are the same, there is no explanation for their mass difference, ($m_\mu/m_e \sim 207$). A Q.E.D. experiment of the g-2 type may discover a coupling to a stronger field in the case of the muon and hence explain its existence.

There are, in fact, various differences between the (g-2) of the muon and electron; for instance, additional contributions from strongly interacting particles and virtual electron pairs are evident in the muon system.

The (g-2) of the electron has been measured by various methods and several collaborations are continuing this work (2). Regarding the muon, the previous determination using a 5m diameter ring magnet at CERN (3) returned a value of $a_\mu(\text{exp}) = (1{,}166{,}160 \pm 310) \times 10^{-9}$, yeilding a difference between experiment and theory, $(a_\mu(\text{exp})-a_\mu(\text{theory}))$, of $+(240 \pm 270)$ppm. This shows good agreement between experiment and theory but, because of the possible fluctuation contained in the error, a more accurate experimental determination of a is required if any discrepancy is to be uncovered. It has been established (4) that a measurement to a level of 10 to 20 ppm would either validate once more Q.E.D. or indicate a violation which would

lead to several interesting theoretical implications (apart from the one already mentioned).

It may also be noted that there are three interesting by-products of the main experiment: a verification of Einstein's "clock paradox" by muon lifetime measurement, a measurement of the electric dipole moment of the muon and a comparison of μ^+ and μ^-.

2.3 The Present g-2 Experiment at CERN

The experiment involves trapping longitudinally polarized muons in the magnetic field of a 14 m diameter storage ring and observing the decay products (electrons) using a series of 20 shower counters placed at regular intervals on the inside of the ring (see figure 2.1). As the stored muons (positive in this case) undergo the following decay:-

$$\mu^+ \rightarrow e^+ + \nu_e + \bar{\nu}_e$$

the observed counting rate of "electrons" (in fact positrons in the above decay) will be exponential in form. However, the anomalous moment will cause the spin vector of the muons to precess with frequency ω_a relative to the momentum vector, thus altering the direction of electron emission (since this is preferentially in the direction of spin) and causing the count rate to be modulated. The asymmetry introduced into the electron counts in this way is shown in an example from a previous g-2 experiment (3) in figure 2.2. The modulation frequency is given by:-

$$\omega_a = a(e/m_o)B \qquad (2.6)$$

FIG 2.1 g-2 Muon Storage Ring

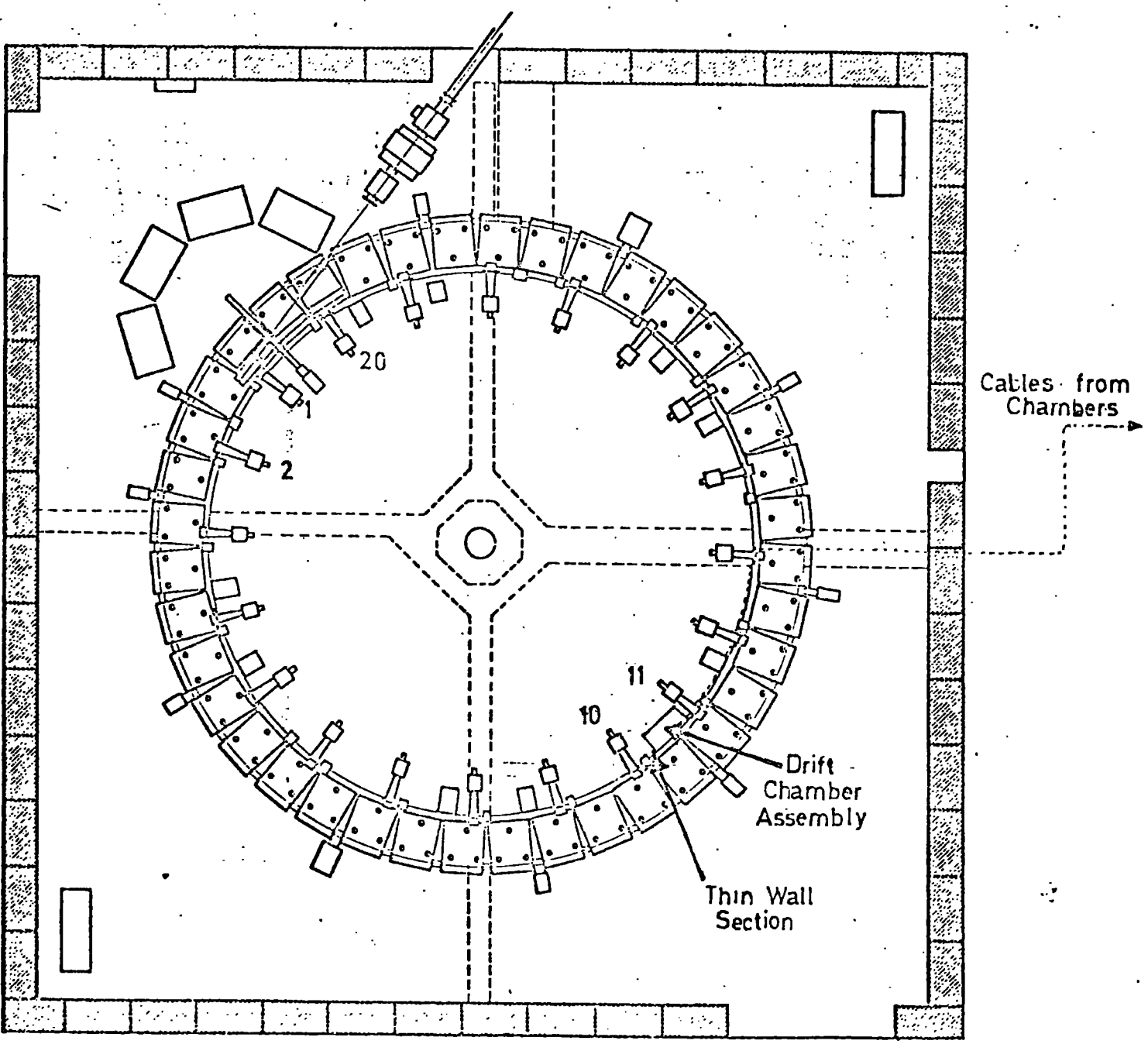

FIG 2.2 g-2 Count Modulation Curve from Previous Experiment

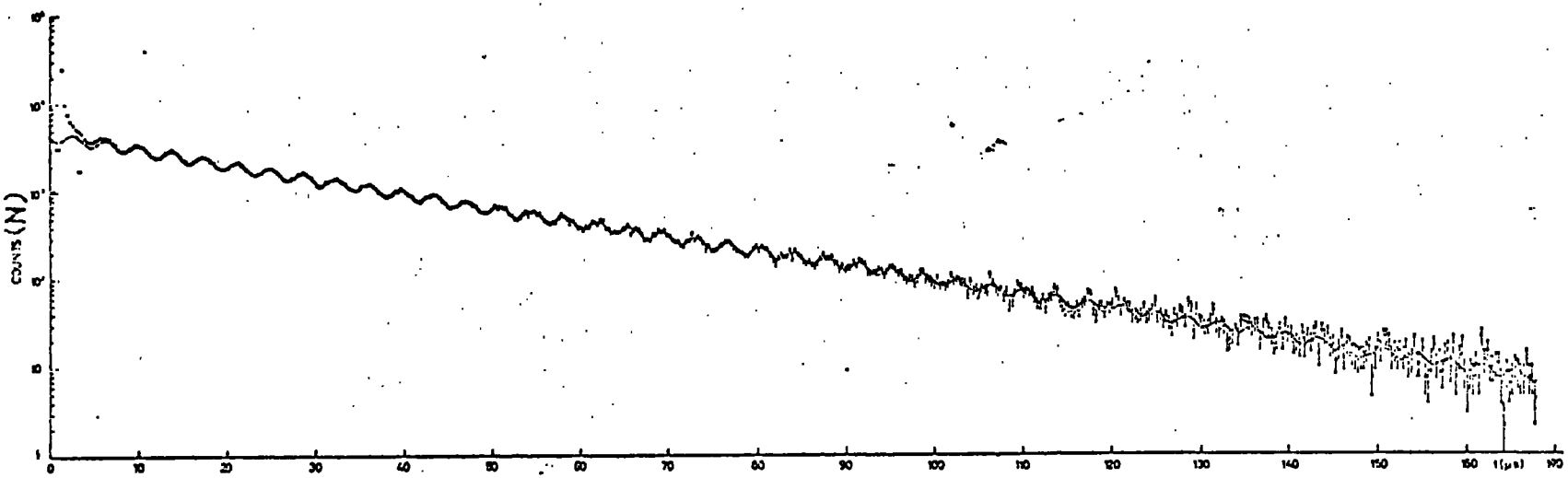

$$N(E_e > E_o) = N \exp(-t/T) \{1 + A \cos \omega t\}$$

where the charge to mass ratio of the muon (e/m_o) is derived from other experiments (5) determining the ratio of muon to proton precession frequencies ($\lambda \equiv \omega_\mu / \omega_p$) in the same field. This work has yielded:-

$$(1 + a)(e/m_o)(1-\epsilon)\vec{B} = \lambda \omega_p \qquad (2.7)$$

and combining equations (2.6) and (2.7) produces the ratio to be measured:-

$$\frac{\omega_a}{\omega_p} = a(1 + a)^{-1} \lambda (1 - \epsilon)^{-1} \qquad (2.8)$$

where $(1-\epsilon)$ is a diamagnetic shielding correction. Hence a value for the anomaly a can be calculated provided λ and ϵ are known.

It is useful now to dwell on some particular experimental facts concerning the new g-2 storage ring as it is evident that these points provide the environment in which the drift chambers will operate, several factors being of direct importance:-

a) The most important improvement on the last g-2 experiment at CERN is the extra effort in obtaining a uniform magnetic field, as ω_a is directly proportional to this value. Previously, a radial magnetic field gradient was necessary to provide vertical focussing this has now been superseded by a quadrapole electrostatic field, thus allowing $\vec{B}$ to be radially independent. Assuming E to be radial

(that is E_r), the expression for precession frequency in the combined fields is (6):-

$$\omega_a = \frac{ea}{m_o}\left[\frac{-E_r}{V}\left(1 - \frac{a^{-1}+1}{\gamma^2}\right) + B\right] \qquad (2.9)$$

where V is the muon velocity and an approximate value of 858 can be inserted for a^{-1} for muons.

Comparing this with equation 2.6 it can be seen that there now exists a "spin effective field" given by:-

$$B^s_{eff} = B + \frac{E_r}{V}\left(\frac{859}{\gamma^2} - 1\right) \qquad (2.10)$$

Hence it is apparent that a correct choice of $\gamma = 29.3$ effectively removes the dependence of ω_a on E_r, leaving $B^s_{eff} = B$. This corresponds to a muon momentum of 3.098 GeV/c, a figure on which the storage ring parameters are designed. This value is in fact larger than for the previous storage ring, allowing the measurement of ω_a for 2 to 3 times longer than before and thus increasing statistical accuracies.

A magnetic field uniform to a few ppm and of value 14.745 KGauss is produced in 40 C-magnets to define muons of the above momentum in a 7m radial orbit. A section through the vacuum storage tank and one magnet block is shown in figure 2.3. The magnetic field is monitored regularly throughout the experiment with a series of plunging NMR probes.

FIG 2.3 Section Through Magnet Block and Storage Tank Showing Drift Chamber Position

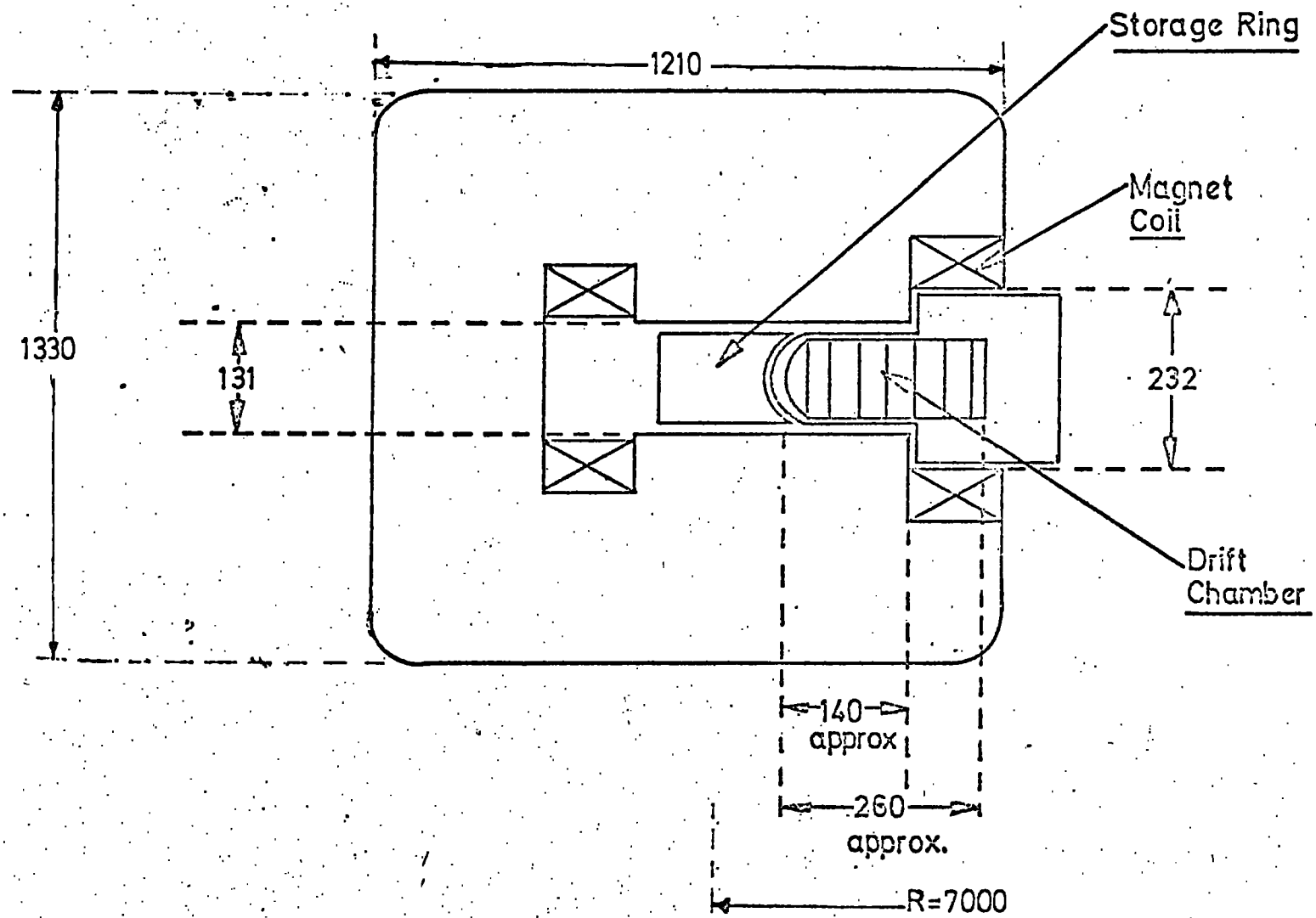

b) The initial polarization of muons is ~90% due to the use of momentum-selected pion injection as opposed to the previously employed proton injection in which a pion momentum spread, and hence low polarization, existed. Injection is achieved by means of a pulsed inflector which temporarily compensates for the magnetic field. After one revolution, the inflected pions will either be lost by hitting the inflector or decay into muons by the process:-

$$\pi^+ \rightarrow \mu^+ + \nu_\mu$$

The muons having momenta very close to that of the pions will be stored with a high polarization. This method of muon production reduces considerably the non-rotating background evident when using an internal target for injected protons.

c) For a one bunch injection from the CERN proton synchrotron (P.S.), approximately 330 muons are stored. For a number of electron counts N_e and an asymmetry A (basically the count modulation amplitude), it is desireable to optimize the quantity $N_e A^2$. The decay electrons have a wide spread in momenta and, as the value of the threshold energy E_{thresh} of detection is raised, N_e decreases and A increases. An optimum value of 1.75 GeV for E_{thresh} is predicted. This being the case for 16% of the muons, approximately 53 electrons will bend out of the storage tank with energies high enough to be detected in one of the 20 counters. Because of the geometry of the detecting system, approximately one or two electrons will be detected in each counter every P.S. burst (2 seconds). In this manner the "stop rate" will be an order of magnitude higher than previously

and the asymmetry will be a factor of 2 better, statistically improving the accuracy of measurement of ω_a. The high discrimination level of the counters ensures the collection of forward decaying electrons; (this level is in fact varied during a g-2 run to observe the effect on the asymmetry, but is always above 1 GeV).

d) Muon losses are minimized by the correct shaping of electric and magnetic fields as described in the Daresbury proposal (4). The stored muons will in fact undergo a series of betatron oscillations resulting in the possibility of radially selective losses which could alter the mean polarization of the sample, thus affecting the measured value of ω_a; the muon lifetime measurement would also be affected. Losses due to scattering from gas molecules are reduced by using a storage tank pressure of 10^{-6} Torr.

2.4 The Reasons for Multiwire Drift Chambers in the g-2 Experiment

In the previous g-2 experiment, a knowledge of the muon spatial distribution was necessary because of the radial dependence of $\vec{B}$. As $\vec{B}$ is uniform in the present experiment, the importance of this measurement is reduced, but is still valuable for the following reasons:-

The stored muons are constrained by the vacuum tank to radii between 6920 and 7080 mm. and those on a trajectory other than the equilibrium orbit of 7000 mm. will have a value of γ different from 29.3 and hence the cancellation of the electric field effect will be incomplete. The correction factor from the direct change in γ is a linear function of radius and is increased to a quadratic function by the fact that the electric field strength is also linearly dependent

on radius. By correctly shaping the magnetic field (7), the spin effective field (equation 2.10) can be restored approximately to uniformity with radius, but in so doing, the radial uniformity of the magnetic field is obviously disturbed. Magnetic field corrections are also applied to compensate for the effects of surrounding material such as the vacuum tank. As the g-2 measurement is dependent on the average field experienced by the muons, a full mapping of the field is necessary as is a knowledge of the circulating beam profile.

As mentioned in the previous section, slight losses of muons may occur and be dependent on radius, again indicating the need for a beam profile measurement

Because of the betatron motion, the time average field for the sample is altered, hence a valuable measurement would be that of the beam profile in some fixed plane and its variation over a g-2 cycle.

A radial muon distribution can be successfully predicted (4) by a programme based on the comparison of the phase space distributions of pions and muons. However it is highly desirable to make a direct measurement of the distribution and this can be achieved in two distinct ways (without directly affecting the beam):-

A measurement of the longitudinal spread (with time) of the injected muon bunch can be transformed into a radial distribution as the spread is due to the different path lengths encountered by muons at different radii. Such a method is refered to as "fast rotation" and is achieved by measuring the electron count rate at one point in the ring the rate being modulated by the rotational period in this

case. This method however is only useful for the first 20 μsec. of the cycle, by which time the bunch has overlapped itself.

The second method is to use a series of multiwire chambers introduced into one section of the ring to record the tracks of decay electrons. By tracing such a trajectory back into the storage ring until a point tangential with the latter is reached, the radial position of electron origin and hence the parent muon position can be determined. To obtain a reasonable beam profile, this position should be estimated to an accuracy of the order $\pm$ 1 mm. On considering the simplified case of three points on the external electron path lying on a circular trajectory; to obtain a leverage of 1 mm. by projecting the fitted curve a reasonable distance back into the vacuum tank requires that each of the three points is determined to the order $\pm$ 0.1 mm (Appendix 1). Thus, MWPC's are ruled out and the track locating system must consist of drift chambers which can produce this order of spatial resolution.

Such a system is capable of determining the beam profile as accurately as the fast rotation technique and has the added advantage of being continuously sensitive and thus capable of operation even when muons are uniformly distributed throughout the ring. A series of drift chambers can also provide a count rate meter similar to a g-2 shower counter and should display a g-2 modulation curve of similar form to figure 2.2 on integration over all g-2 cycles. Another useful function is the provision of a momentum calibration mechanism for the shower counter used to trigger events.

One further profile measuring technique which has been

employed in g-2 is the scanning of shutters across the storage tank. However, such a method is undesireable as the muon sample is severely disturbed.

2.4.1 Positioning of the Drift Chambers in the Storage Ring

One region of the storage ring is left free of electrostatic focusing electrodes to allow pion injection. To balance this and thus reduce closed orbit distortion, another non-electrode region exists diametrically opposite the inflector. This is a convenient position in which to arrange the drift chamber system for the following reasons:-

The electrostatic field would distort the back-projection of the electron trajectory as it would seriously affect the electron motion within the vacuum tank.

The non-electrode region is a convenient section of the ring in which to install an extremely thin vacuum tank wall to reduce the otherwise severe scattering of emergent electrons. In fact, for the normal vacuum tank wall, a showering of the decay electron may eventually yield an electron-positron pair, and it may be possible that neither of these particles is detected because of the direction of curvature of one of them, and the possibility of energies lower than the detection threshold. This effect will be observed by comparing the results from the counter (number 11 of figure 1) in the non-electrode region with other counters. In this context, it will also be the responsibility of the drift chambers to provide, by track reconstruction, an estimate of the frequency of multiple particle events in the thin wall region.

A description of the final experimental arrangement of the

track locating system is left until chapter 7, save to say that eight drift chambers will be employed with counter 11 providing the trigger.

2.5 Special Requirements for the g-2 Chambers (8)

The design criteria for the chambers were initially presented by collaborators to the g-2 experiment from the Daresbury Nuclear Physics Laboratory (D.N.P.L.) (9) and various extra necessities have since arisen.

The immediate requirements concerned the construction of the chambers. Figure 2.3 shows one chamber in its location between the poles of a magnet block, and from this illustration several points regarding the mechanical design are evident, mainly concerning the presentation of maximum sensitive area for detection of electrons. In this respect each chamber requires an extremely thin end wall for the track measuring system to be sensitive to high energy electrons having trajectories of little curvature (note that this member will be curved to fit exactly the profile of the thin vacuum tank wall), thin side members to make use of as much of the gap between the pole pieces as possible and a detecting area extending to at least the outer edge of the sensitive region of the shower counter.

A minimum of scattering material is ensured by the thin end wall and also to this effect, thin "mylar" sheeting provides the material for the chamber windows.

A minimum requirement of "hits" on three or four chambers will be set as the condition of a sufficiently informative event, and in order to ensure the collection of enough data to accurately reconstruct the sharply bending tracks of the softer decay electrons, the chambers near the electron counter will be packed as closely as

possible. To achieve this, the chamber widths must be made as small as possible within the limits of practicability. The final spacing arrangements between the eight chambers, together with the above mechanical design criteria ensures the optimum detection system for the range of electron energies encountered.

From the discussion in section 2.3, it is evident that the following environmental conditions will influence the drift chamber performance requirements:-

Although the storage ring magnetic field is uniform within the pole pieces, there is a gradual fall-off of magnetic flux outside this region. The form of this field is to be discussed in chapter 6 where the compensation technique is developed, the main point being that as the detecting area of each chamber protrudes out of the pole pieces (figure 2.4) they must be capable of operation in a strong, non-uniform magnetic field.

The chambers will be in an environment of high noise and low event rate. Much of the noise comes from the "initial flash" which consists of pions traversing the ring diameter directly, and electromagnetic pickup from the inflector and electrostatic field (which is in fact pulsed). A detailed study of such noise sources in an enclosure and the delayed noise of γ fluxes from target-produced neutrons decaying has been made (10). The initial flash can be electronically gated out but, because of the low event rate already mentioned, the longer term background radiation does provide a source of error i.e. possible random stops associated with genuine electron counter triggers.

The angle of incidence between the particle direction and the normal to the sense wire plane is important in drift chambers (11), but the effects are minimal at small angles ($< 30^{o}$ for a threshold of 1 GeV) which are applicable in this case (see appendix 1). To decrease these angles of incidence further, a tilting of the chambers near to the electron counter can be arranged if necessary.

One further noise source which causes a problem in drift chamber operation at CERN is the electromagnetic pickup by a sense wire of the local Suisse-Romande television transmission. This can be reduced by the use of earthed aluminized mylar windows.

A final consideration is of the efficiency requirements. If the efficiency of a chamber is E, then the efficiency for detection in each of n such chambers is E^{n}, indicating that near 100% efficiency of detection is desireable for the g-2 chambers.

References

1 B.E. Lautrup, A. Peterman, E. de Rafael. Phys. Reports 3c (1972) 193

2 F.H. Combley, E. Picasso. Phys. Reports 14c (1974) 1

3 J.M. Bailey, E. Picasso. Prog. Nuclear Phys. 12 (1970) 43

4 J.M. Bailey, F.H. Combley, P.M. Hattersley. Daresbury Proposal DNPL/SCP 77 May 1972

5 D.P. Hutchinson, J. Menes, G. Shapiro, A.M. Patlach. Phys. Rev. 131 (1963) 1351

6 V. Bargmann, L. Michel, V. Telegdi. Phys. Rev. Letters 2 (1959) 435

7 J.M. Bailey, F.J.M. Farley, H. Jootlein, G. Petrucci, E. Picasso, F. Wickens. CERN Proposal PH I/COM-69/20 (1969)

8 J.M. Breare, R. Browell, K.A. Short, J. Webster. Durham University Internal Report, NI-74-7

9 J.M. Bailey. Private Communication, Daresbury Laboratory, 1973

10 F.J.M. Farley, B.S. Carter. Nucl. Inst. Meth 28 (1964) 279

11 A. Breskin, G. Charpak, F. Sauli, M. Atkinson, G. Shultz. Nucl. Inst. Meth. 124 (1975) 189

CHAPTER 3

THE DESIGN AND DEVELOPMENT OF THE g-2 CHAMBERS AND ASSOCIATED HARDWARE

3.1 The Design and Construction of Prototype Models

Having determined the basic requirements for g-2 drift chambers as set out in chapter 2, this chapter will now deal with their actual design, mechanical and electrical, and development to a final production model stage.

The main criterion was to produce a mechanically sound structure capable of presenting maximum sensitive area within the constraints of the 140 mm. pole gaps of the g-2 magnets. Detection was required over a distance of ~220 mm. from the inner vacuum tank wall and for convenience (that is, compatibility with commercial electronics), this sensitive region was divided into 8 detection zones or "cells" each of 28 mm. width. Thus 14 mm. drift spaces were employed, this short length proving to be convenient as will be shown in following chapters.

A small, test drift chamber, consisting basically of one such cell, was designed, and this was followed by a series of 3 prototype models related closely to the final production chambers. These chambers were built at Durham University, and provided most of the data on general drift chamber properties to be described in

chapter 4 and part of the accelerator data of chapter 5. Any important developments between prototype and production models will be indicated in the relevant parts of the following text.

3.2 Mechanical Properties and Dimensions

The mechanical features and overall dimensions of the production models are summarised in the schematic sketch of figure 3.1, and the more detailed drawings of figures 3.2 and 3.3. The chamber design has been documented in detail (1) and the main points will now be discussed.

3.2.1 The Main Frame

The supporting part of the main frame was designed to be as massive as possible within the space restrictions of the storage ring, to provide maximum overall strength for the chamber and a rigid mounting facility. Thus this component was constructed from 37 mm. thick laminated glass-fibre epoxy-resin (G10) material.

The side members were designed under two conflicting criteria. They had to be as thin as possible in order to utilize the restricted space between the g-2 magnet pole pieces, but also had to support the tension ($\sim$12 kgm in total) presented by two vertical H.T. wire planes without any additional support from the end member as it turns out. Original side members were constructed from 11 mm. thick G10 which has a Young's modulus of 2×10^{10} Wm^{-2}, however these necessitated several special constructional techniques such as prestressing the frame before wiring and spring loading the main support frame after wiring.

It was suggested by the International Research and

FIG 3.1 Schematic Sketch of g-2 Chamber

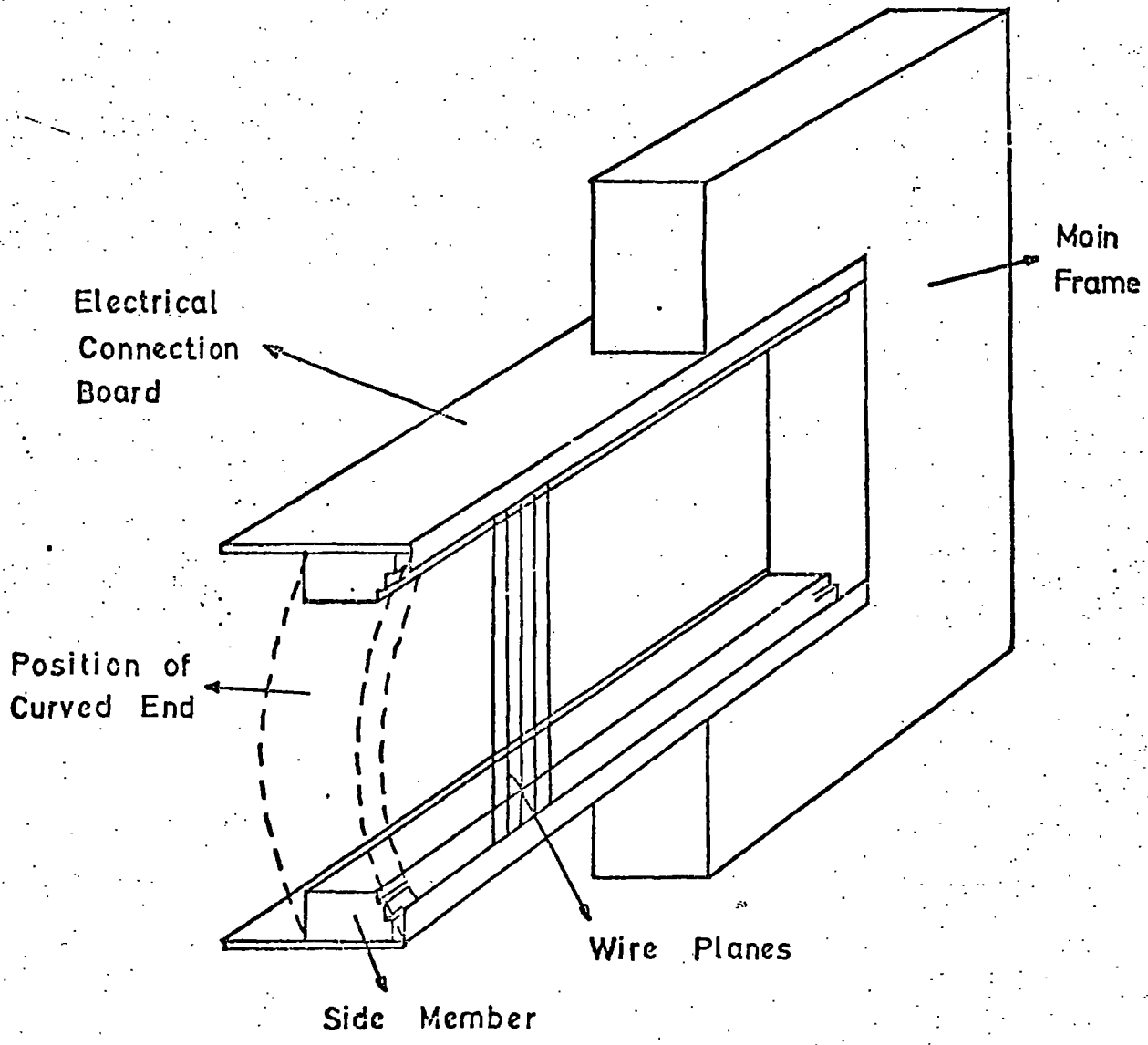

FIG 3.2 Chamber Dimensions (mm)

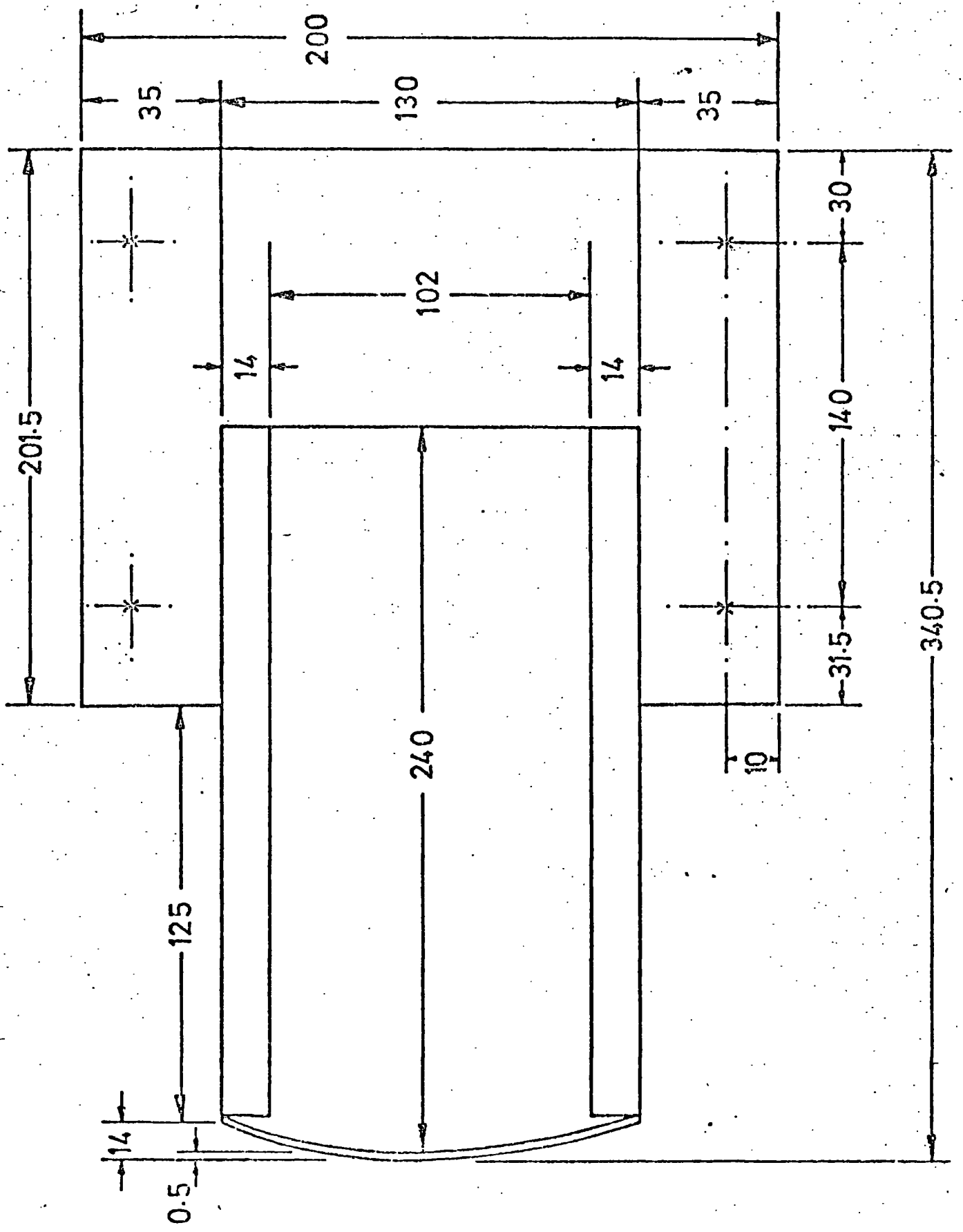

FIG 3.3 Section through Wire Mounting Assembly

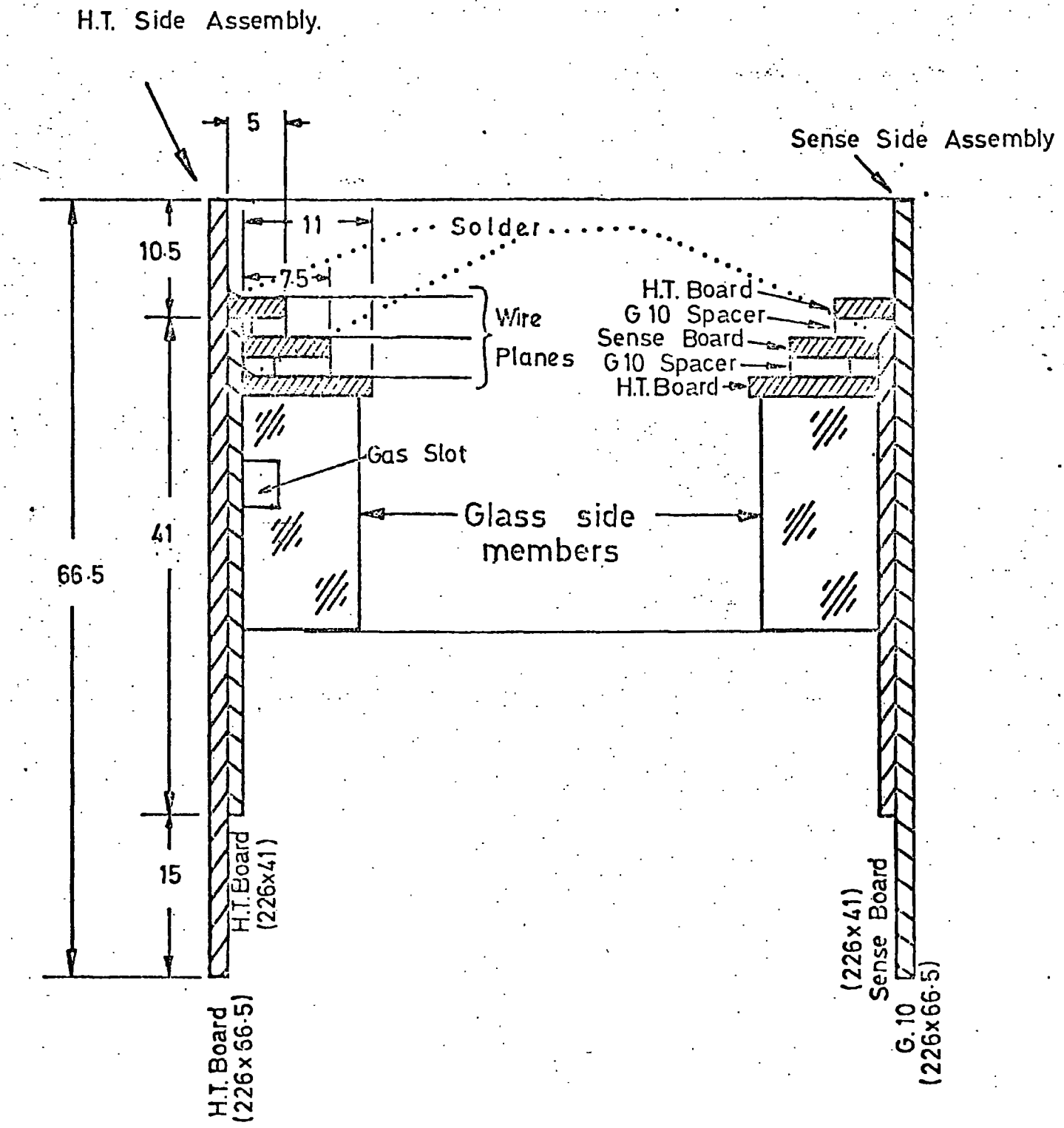

All Measurements in mm.

Development Co. Ltd. (I.R.D.) that glass side members be used instead of G10, these having a Young's modulus some 30 times greater than the latter. Problems concerning machining and adhesives were overcome and later models incorporated these rigid side members. One side member accomodated along its length a central channel to allow the input of gas, the gas outlet channel was in the main frame block near the opposite side member. The separation of the outer edges of the side members was 130 mm.

A thin end wall (0.5 mm G10) allowed the sensitive volume of the chamber to approach closely the vacuum tank, thus permitting detection of electrons shortly after their exit from the storage region, and at the same time presenting a minimum of scattering material in the electron path. The scattering factor was also reduced by a thin section (0.8 mm. Titanium) of vacuum tank in the drift chamber region. This section assumes a concave shape because of the pressure differential across it and thus the end wall of the drift chamber was designed to have a compatible curvature as indicated in figure 3.2, this being achieved by bending the G10 material after unsuccessful attempts at machining.

In order to achieve a minimum separation between chambers (required at the shower counter end of the array as mentioned in section 2.5), the chamber width was made as small as possible, the wire accomodation requirements of the electrical connection board setting a minimum requirement of 67 mm. on this value.

3.2.2 Internal Construction

Figure 3.3 is a section across the width of the detecting region of the chamber showing how the wire planes were attached

between the side members. Wires were soldered onto copper strips deposited onto thin G10 boards, these being prepared using a photo-lithographic technique. The H.T. and sense wire boards were separated by spacers to produce a step construction, as shown in the figure, thus facilitating replacement of broken wires.

The outer H.T. wire planes were separated by 6.4 mm. and comprised 120 μm. diameter Copper-Beryllium wires spaced at 2 mm. intervals. The sense wire plane contained eight gold-plated Tungsten wires of diameter 20 μm and separation of 28 mm. In the same plane and equally spaced between the sense wires, were field wires of the same type as those of the H.T. plane. The wire configuration in the curved end region was modified from the above and will be described in the electrical design section. Thus, the wire configuration resulted in drift cells of similar design to those used by Charpak (2).

The wire tensions were 50 gm and 30 gm for the H.T. and sense wires respectively, these values being checked occasionally by measuring the deflection of a weight hung at the wire centre (3).

3.2.3 External Construction

Electrical connection between the wire planes and the outside of the chamber was achieved by the use of copper coated G10 boards, with solder connections as indicated in figure 3.3. H.T. input and signal output were from different sides of the chamber. As a field gradient was to be applied along the H.T. planes (section 3.3), several different values of high voltage were distributed onto the H.T. boards by means of copper rails connecting relevant wires and again deposited onto thin G10 board. Application of the voltages onto these strips was achieved using multiway ribbon cable from a voltage

controlling resistor network mounted on top of the main frame block in a metal box.

Final signal output from the sense wires was achieved by short lengths (few ns) of miniature Lemo coaxial cable.

3.2.4 Gas Sealing

This was achieved using windows of 120 μm Mylar sheeting, which was thick enough to retain its seal when bowing out as the chamber was filled with gas, yet thin enough to introduce negligible scattering material into the g-2 storage ring. It is necessary to remove one window if a wire is to be replaced, therefore a temporary adhesive material (3M "Twinstick") was used between each G10 sealing surface and the Mylar. This method produced a 100% gas tight seal.

3.2.5 Further Points

The length and spacing of wires in a chamber of this size conveniently negate any electrostatic instabilities and hence no wire supports are necessary (4). Also, the chamber design has deliberately excluded the use of separable wire planes, as the gas sealing of such a structure usually involves rubber gaskets which can lead to electrical-shorting problems where voltage gradients along a wire plane are involved (5).

Although chamber sensitivity over the full pole-piece gap is desireable, most particle trajectories will be in the median plane (this has since been verified by vertical readout data using MWPC's), and thus any scattering produced by side members, or electric field distortion in the wire attachment regions will be relatively unimportant.

The main-structure components of the chambers were machined to a tolerance of 0.125 mm and the sense wires were installed by a process of repeated attempts to within 0.1 mm of their required positions. At various stages in the construction, rigorous mechanical testing was applied in the form of loading heavy weights at susceptible points. For the final design, no wire breakage or loosening occurred.

It was carefully ensured that no ferro-magnetic material was involved in the construction of the chambers as this would distort the g-2 magnetic field as well as introduce additional stress points in the chambers.

The photograph of figure 3.4 illustrates most of the mechanical features discussed in the foregoing sections.

3.3 Electrical Design and Properties

The method of Charpak et al. (2) of obtaining uniform and controllable drift fields was adopted for the g-2 chambers. By tilting such an applied electric field, a mechanism capable of operation in an external magnetic field could be realised. (This subject is to be discussed more fully)

3.3.1 Application of Drift Fields

Electric field gradients were applied to chamber cells using a single H.T. power supply, individual wire voltages being tapped from various points of a potential divider chain such as the one shown in figure 3.5. By varying the value of the final resistance to earth (R_E) and adjusting the supply voltage (V_S) so that the basic accelerating voltage (V_{MIN}, with some additional influence from the

FIG 3.4 THE MULTIWIRE DRIFT CHAMBER
DESIGNED FOR THE g-2 EXPERIMENT

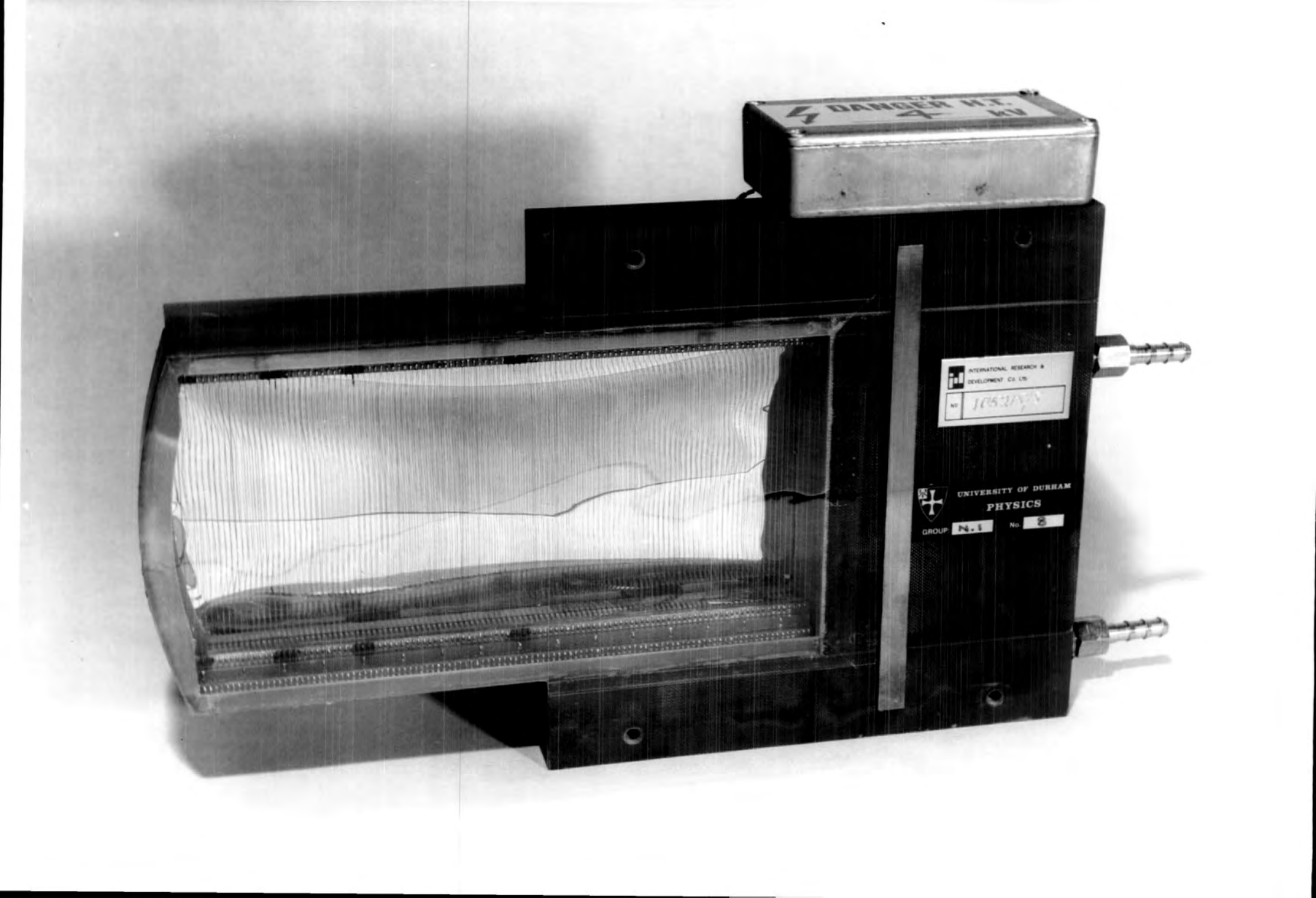
DANGER H.T.
kV
INTERNATIONAL RESEARCH & DEVELOPMENT Co. LTD
UNIVERSITY OF DURHAM
PHYSICS
GROUP N.1
No. 8

FIG 3.5 Example of HT Distribution to Wires

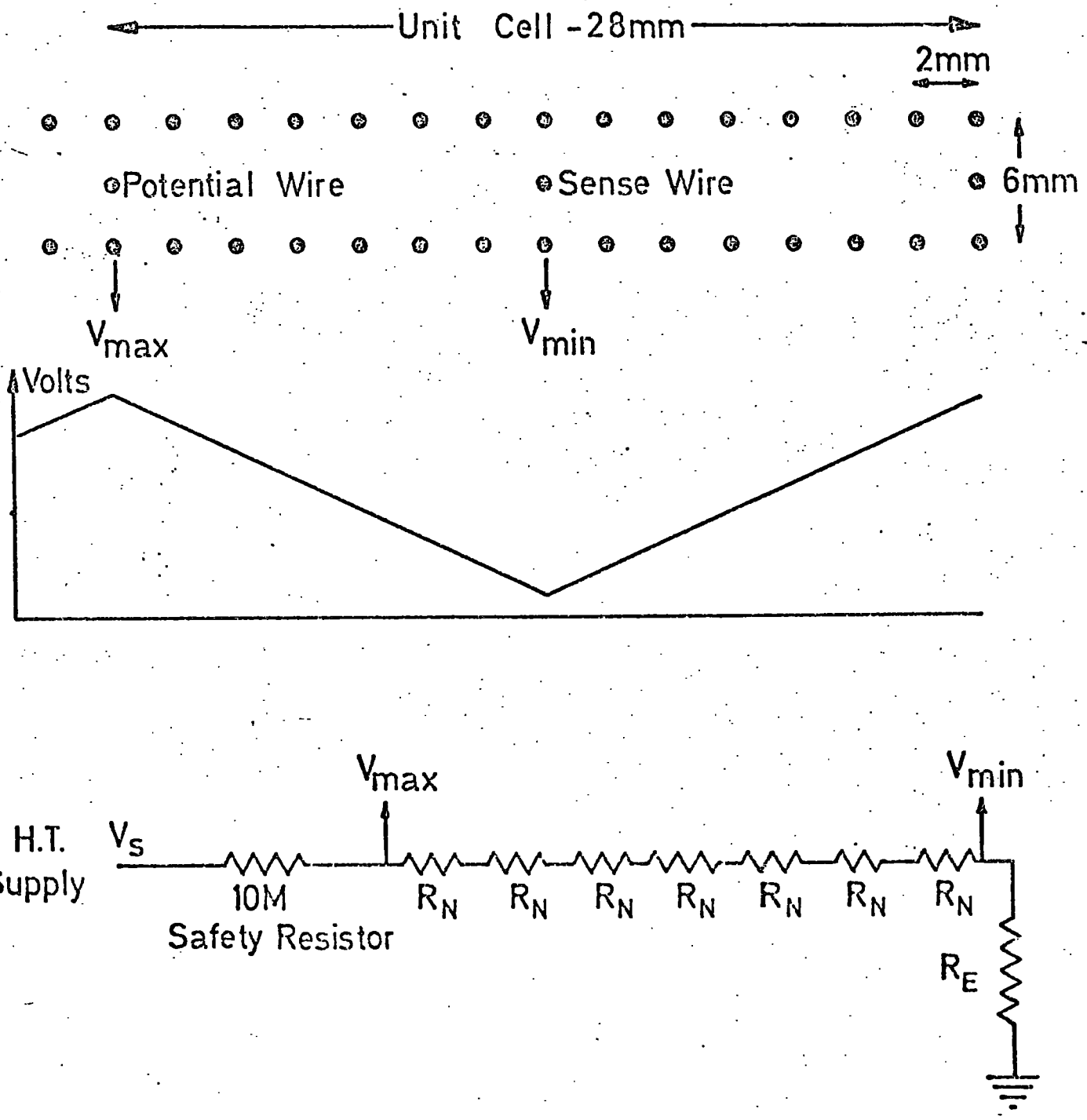

graded field) reaches an operational level, a large range of drift fields ($(V_{MAX} - V_{MIN})/1.4$ Vcm^{-1}) can be realised. An example is shown in figure 3.6 where the field is plotted against V_S for various values of R_E (R_N = 3.3 MΩ); only the working voltage ranges of the chamber being shown.

Two different wire configurations have been used for the curved end regions as indicated in figure 3.7, the prototype field requiring voltages > V_{MAX} and thus a modification of the resistor network of figure 3.5. The final curved end design (figure (b)) reduced the length of the distorted field region and also lowered the values of V_S and maximum drift time to be measured. The final H.T. rails were in the form of thin copper strips adhered to the inside face of the curved end. Normal H.T. wires were continued into this region as far as was practically possible in order to reduce the inevitable field distortion. The effectiveness of such a drift space is investigated in following chapters.

As a result of the work to be discussed in chapters 4, 5 and 6, a final design for the applied drift field, including the magnetic field compensating mechanism, was derived. The resistor network required for this, and the resulting wire potentials (at V_S=3.0kV) are shown in figure 3.8. A reversal of the direction of field slant could be achieved by unsoldering wires on the resistor board, as plug and socket mechanisms were found to be impractical at high voltages. Note that a more gradual field variation was applied in the sense wire region than for a staight forward tilting of uniform voltage drops between adjacent rails. This reduced breakdown problems which otherwise occurred due to the presence of too high a voltage directly above or below the sense wires.

FIG 3.6 Chamber Electric Field vs Supply Voltage

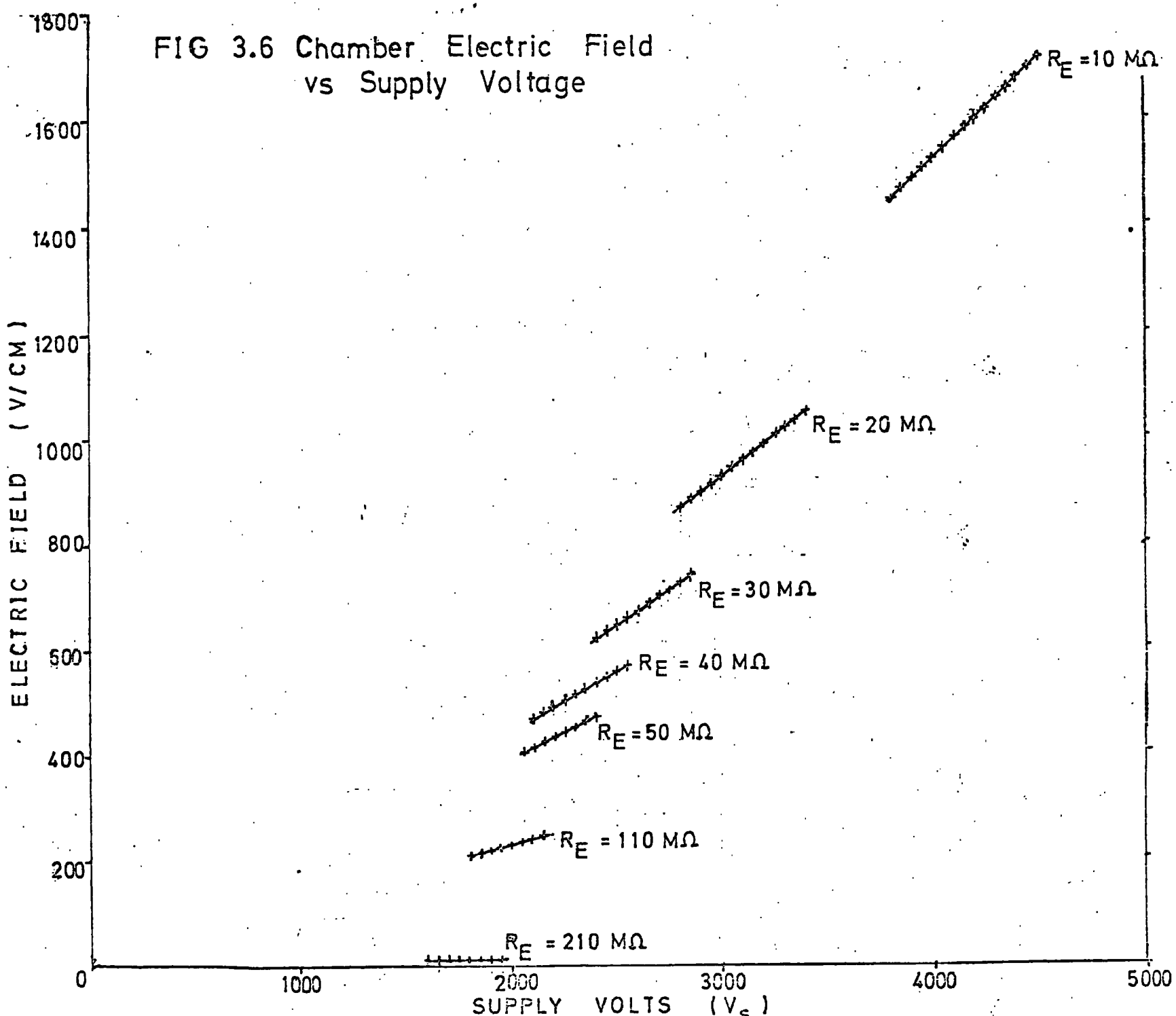

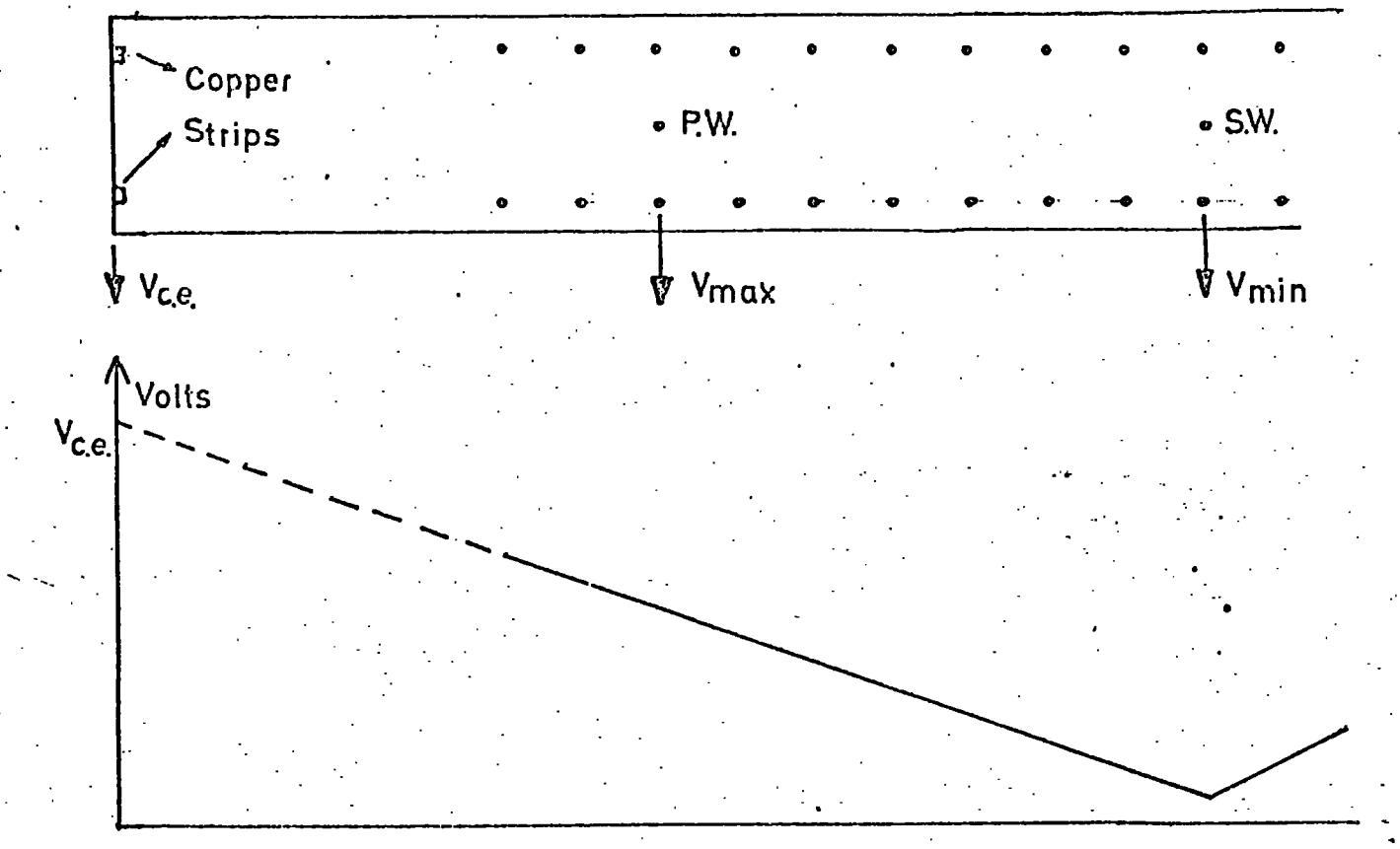

FIG 3.7(a) Original Curved End Wire Configuration

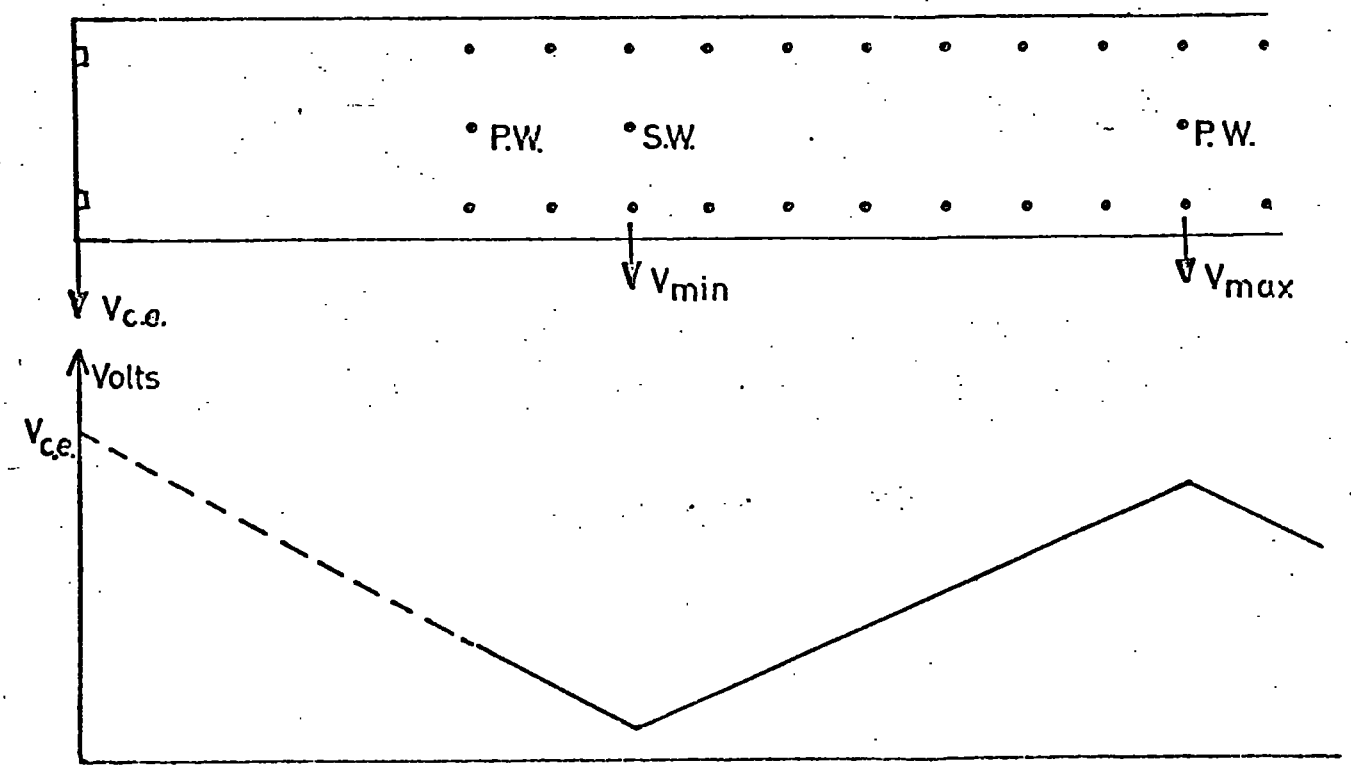

FIG 3.7(b) Modified Configuration

FIG. 3·8 FINAL VOLTAGE DISTRIBUTION TO CHAMBER

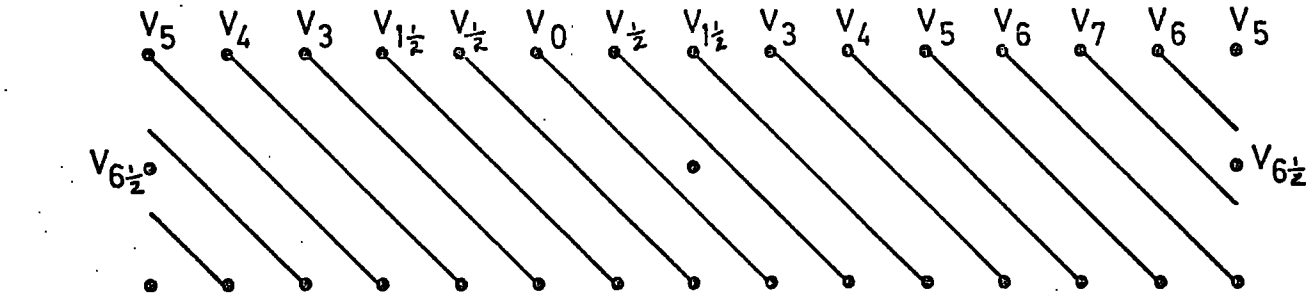

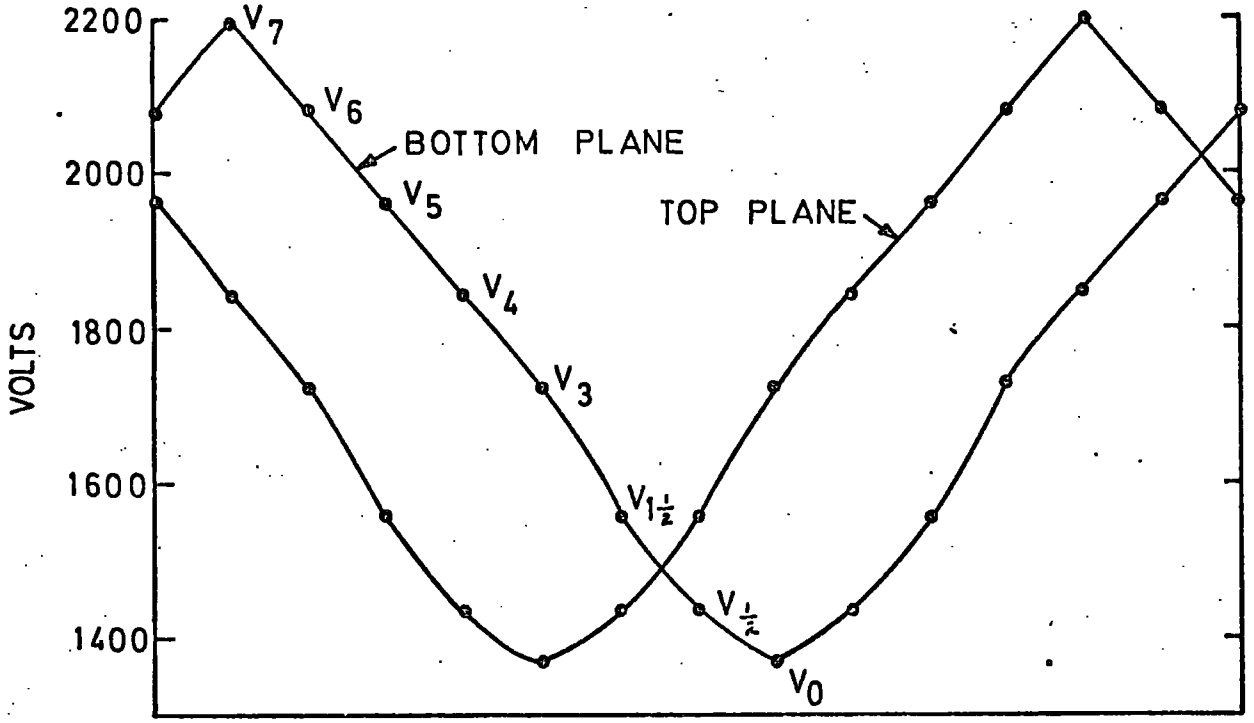

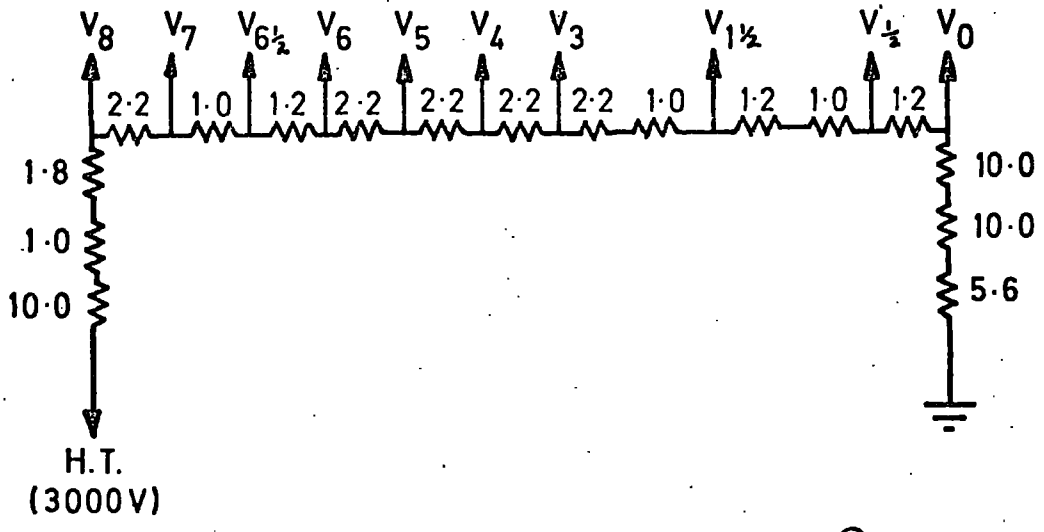

ALL RESISTOR VALUES IN MΩ

3.3.2 Electric Fields in Drift Chambers

The electric fields occurring in drift chambers on the application of various voltage configurations have been studied at CERN (6) using computer simulations. At Durham, a numerical relaxation technique has been used (7) to investigate the variations of electric potential in a Charpak type cell under different strengths of applied voltage gradient. This technique was applied to the wire potential configuration of figure 3.8 and the resultant equipotential map and electric field in the sense wire plane are shown in figure 3.9. The drift field is seen to be uniform over most of the cell, but increases rapidly at the sense wire. Such an increase in the avalanche region will be seen not to alter drastically the drift velocity of electrons in certain gases.

In order to counteract any radiation interference (eg. Suisse-Romande television transmission), the normal window material was replaced with aluminized Mylar, earthed on the outside, before final experimental installation. It has been shown (8) that the introduction of two such earthed planes, in the vicinity of a drift chamber cell, affects only marginally ($\sim 5\%$) the drift field.

Finally, it can be said that the magnitude of the drift field throughout most of the cell is close to the applied voltage gradient.

3.4 Gas Flow Systems

Many of the gases used in wire chambers are inflammable. For this reason and also to prevent back-diffusion of air into the system, leakages must be minimised. For small chambers, such as those discussed in this thesis, gas flow rates were low and pressures were only

FIG. 3·9 THE ELECTRIC DRIFT FIELD IN THE g-2 CHAMBERS.

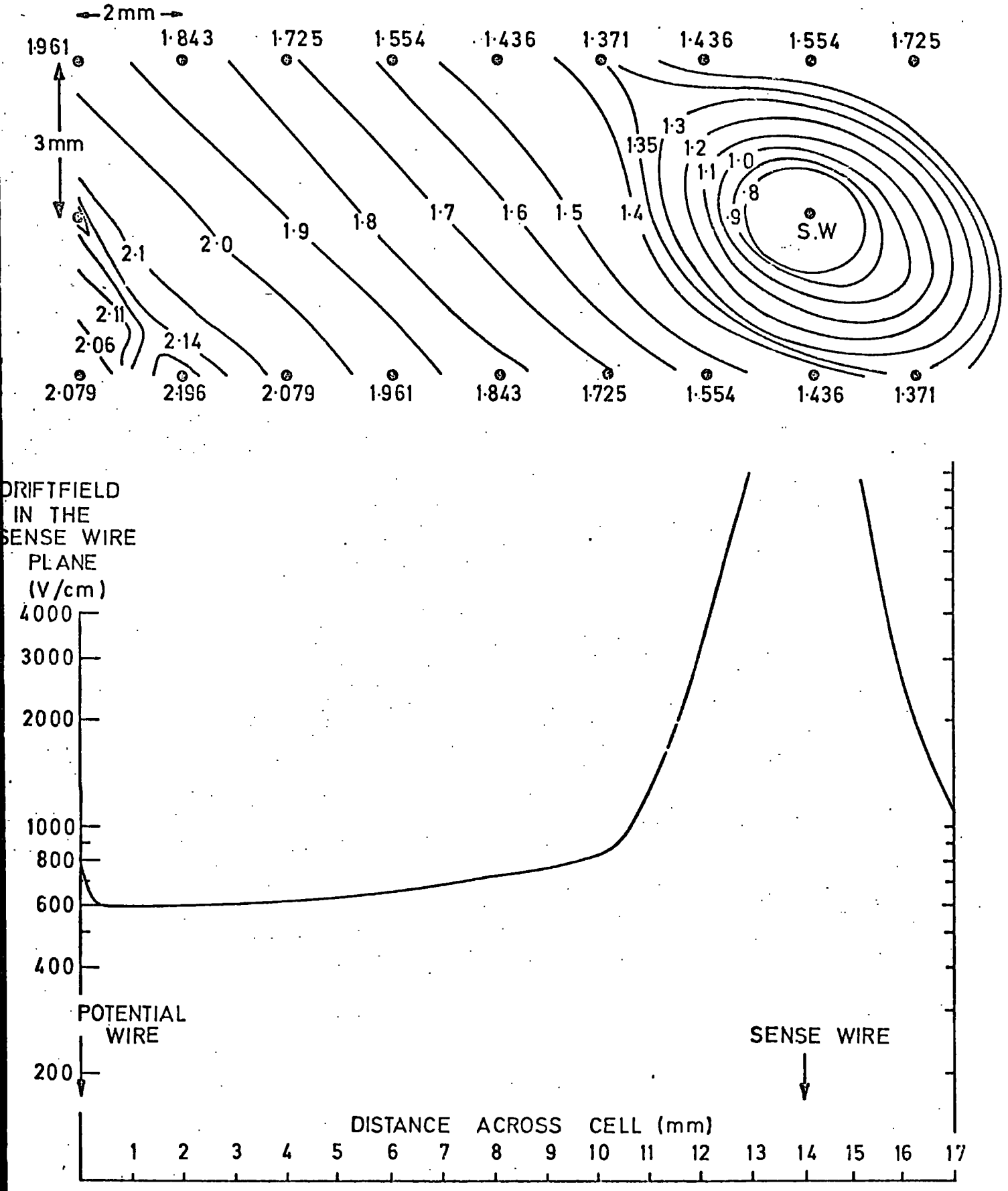

slightly above atmospheric. For the laboratory testing of gases, mixing was achieved using calibrated G.E.C.-Elliot Rotameter flowmeters, whereas for experimental work, premixed gas was always used.

3.5 Amplifiers for Drift Chambers.

Pulses from the g-2 chambers during normal operation are typically 5 mV into 50 Ω. These must be amplified to a convenient level for further electronic processing. The requirements of nuclear pulse amplifiers include (9) extremely linear (and usually high) gain; stability of operation and a high signal to noise ratio. They also serve to initially differentiate the pulse, thus preventing pulse overlapping and allowing operation at high rates; and to transform the impedance to a suitable value for matching with other units. Fast rise-times are desireable and in the case of drift chambers, electronic time slewing must be minimised.

By careful design (basically using a current amplifier of low input impedance), drift chamber preamplifiers can also be used to determine the second coordinate by the current division method.

The preamplifiers used in this work have been designed by Verweij at CERN (10). For early tests, a high input impedance (2 KΩ), 3-stage transistor amplifier, having a voltage gain of 20 and rise time (10 to 90% of maximum) of 2.5 ns was employed. The latest system included 64 channels of 20Ω input impedance transistor amplifiers, each with a voltage gain of 500 and rise time of 5.5 ns. For future experimental runs it is planned to change to integrated circuit-based preamplifier-trigger units in the form of octal N.I.M. modules (10).

3.6 Drift Time Measurement

A convenient method of recording the drift times occurring at a single sense wire is to use a time to amplitude converter (T.A.C.). The principle of this device is to allow, on the receipt of a start pulse (from a scintillator-P.M. tube say), a capacitor to charge up using a constant current source, and on the receipt of a stop pulse (from the sense wire), to turn off this source. Thus the voltage remaining on the capacitor is directly proportional to the elapsed time between start and stop pulses. Timing distributions can thus be obtained by recording T.A.C. output pulses with an amplitude to digital converter (A.D.C.), usually in the form of a pulse height analyser (P.H.A.).

For use with more than one sense wire, the T.A.C.-P.H.A. system can be compressed into a time to digital converter (T.D.C.) in the form of Lecroy Research Systems (L.R.S.) CAMAC units. Readout in this case is achieved by discharging the timing capacitor at a relatively slow rate and measuring the time to do so using a 40 MHz crystal clock; this time stretching technique is now used extensively in the drift chamber field (11). For one event, digitised times from many sense wires may be stored in a computer using a common start pulse.

The above two analogue time-recording techniques have been used extensively in the g-2 chamber work to date.

There have been developed several techniques of digital time measurement (12). The basic idea is to start recording clock train pulses on a scalar on receipt of the trigger, and to stop counting on receipt of the signal pulse. To achieve a suitable spatial resolution, a 2 ns separation of clock pulses is required, corresponding

to a clock frequency of 500 MHz. Such circuitry is expensive, but by employing a Vernier technique to interpolate between clock pulses (13), the use of 100 MHz scalars (available in M.E.C.L. III) is possible.

For drift time measurement when non-linear space-time relationships occur, automatic hardware compensation has been achieved by the use of a non-linear clock train (14).

It is intended to eventually install new, CERN-designed, drift time digitizers (D.T.D's) in the g-2 drift chamber system. These employ an inverse timing technique (stops preceeding starts) which eliminates the necessity of delaying many drift chamber wire channels to the same extent as the existing delay in the triggering shower counter. The time range covers 768 ns (1 ns bits) compared with the 512 ns of the L.R.S. T.D.C's, and the D.T.D's have the additional ability to process more than one hit per event on a single wire.

3.7 The Construction and Testing of the Production Chambers

After finalising the g-2 chamber design at Durham University, I.R.D. constructed eight such chambers under clean conditions. Close collaboration was maintained between Durham and I.R.D. in the form of cross-checking mechanical tolerances and sense wire positioning. Using a travelling microscope, the latter were determined with respect to the centre of a 0.1 mm wide fiducial line on a copper strip affixed to the main frame block. Thus, sense wire positions were known to better than ± 0.05 mm, and parallelism to within the accuracy of the measuring instrument was observed.

Rigorous electrical testing at Durham followed. This comprised checking the voltages on all H.T. wires using an electrostatic voltmeter and eliminating any breakdown caused by dust,

sharp solder points etc.; in this respect, G.C. Electronics "Corona Dope" was applied at the sense wire attachment regions.

Before final experimental installation, the pulse height-voltage characteristic (see chapter 4) of every cell was checked for uniformity.

References

1 J.M. Breare, R. Browell, K.A. Short, J. Webster. Durham University Internal Report, NI-74-7

2 G. Charpak, F. Sauli, W. Duinker. Nucl. Inst. Meth. 108 (1973) 613

3 K.A. Short. Durham University Internal Report, NI-72-13

4 J.M. Breare, K.A. Short, G.C. Smith, R.A. Cunningham. Proc. Int. Conf. Instrumentation for High Energy Physics, Frascati, (1973) 296

5 K.A. Short. Durham University Internal Report, NI-73-7

6 F. Bourgeois, J.P. Dufey. CERN NP Internal Report, 73-11

7 R. Browell, Ph.D. Thesis, University of Durham, in preparation

8 A. Wylie. CERN NP Internal Report, 74-7

9 A.B. Gillespie. Electronics for Nuclear Particle Analysis. (Ed. L.J. Herbst. Oxford University Press, 1970) Ch. 6

10 C. Engster, J.C. Tarlé, H. Verweij. CERN NP Internal Report, October 1973

11 C. Rubbia. CERN NP Internal Report, 73-1

12 H. Verweij. Proc. Int. Conf. Instrumentation for High Energy Physics, Frascati, (1973) 616

13 Discussed in: R. Browell, K.A. Short. Durham University Internal Report, NI-73-5, following discussion with H. Verweij.

14 B. Schürlein, W. Farr, H.W. Siebert, A.H. Walenta. Nucl. Inst. Meth. 114 (1974) 587

CHAPTER 4

THE LABORATORY TESTING AND SELECTION OF OPERATING PARAMETERS OF THE CHAMBERS

4.1 Introduction: Laboratory Test System (1)

This chapter describes the preparatory testing of the g-2 chambers, which was carried out using radioactive sources and cosmic rays, prior to using accelerator facilities. Emphasis is on measurements concerning electron drift in various gases and the selection of a suitable mixture for use in g-2. The system used for much of this work is shown in figure 4.1 and consisted of a narrowly collimated (0.25 mm) beam of ionizing particles which passed through the drift chamber and triggered a standard scintillator-photomultiplier-discriminator thus providing a zero-time start pulse for the timimg system. Timing was achieved using the T.A.C - P.H.A. method as described in section 3.6, stop pulses being provided by the chamber sense wire via a Verweij 2 KΩ input impedance preamplifier and a CERN Semra Benney shaper (discriminating at an input level of 10 mV). The ratio of the scalar readings (1:2) gave an estimate of efficiency which had to be corrected for P.M. noise and background radiation in this case.

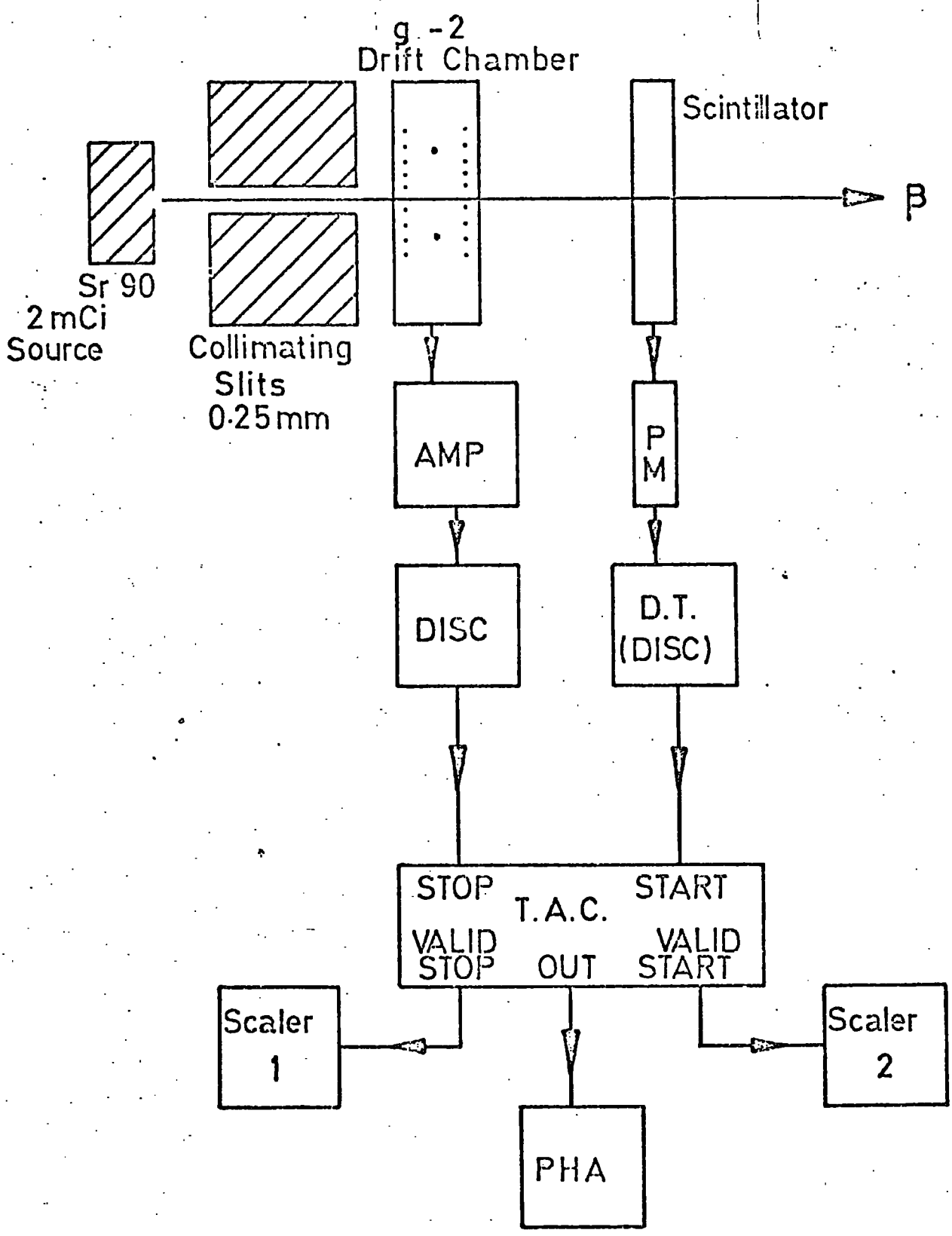

FIG 4.1 DRIFT TIME MEASUREMENT SYSTEM

The source used for timing tests was a 2 mCi Strontium 90 β-emitter providing particles of energy up to 2.27 MeV many of which were energetic enough to penetrate the amount of matter in front of the scintillator material. Because of the fine collimation, a high activity source was employed, necessitating much shielding and unfortunately producing a large amount of gamma-radiation (Bremstrahlung from the source-holder) which caused false starts.

The chamber could be moved between fixed runners to allow the beam to pass at various distances from a sense wire, and alignment in this direction to within 0.5 mm was achieved.

Such a system provides a useful drift chamber testing facility if an accelerator beam is not readily available and similar arrangements have been successfully employed elsewhere (2).

4.2 Pulse Height Measurements

Pulse formation occurs in the cylindrical field (as defined by equations 1.3 and 1.4) around the sense wire and it has been shown (3,4) that the amplification factor, A, for proportional wire systems follows a relationship of the form:-

$$A \propto \exp\left[V(V/V_c)^{\frac{1}{2}} - 1\right]^{\frac{1}{2}} \qquad (4.1)$$

where V is the basic accelerating potential ($\sim V_{MIN}$ for the g-2 drift chambers) and V_c is the ionization threshold.

Figure 4.2 shows the variation with high voltage of the most probable pulse height (measured on an oscilloscope) from the output of a high impedance Verweij amplifier connected to a g-2 sense wire. These results were taken using a Fe 55 X-ray source positioned a few

FIG. 4·2. PULSE HEIGHT-VOLTAGE CHARACTERISTICS OF g-2 CHAMBER CELL, (Argon(90)-Methane(10), Fe 55 x-ray source.)

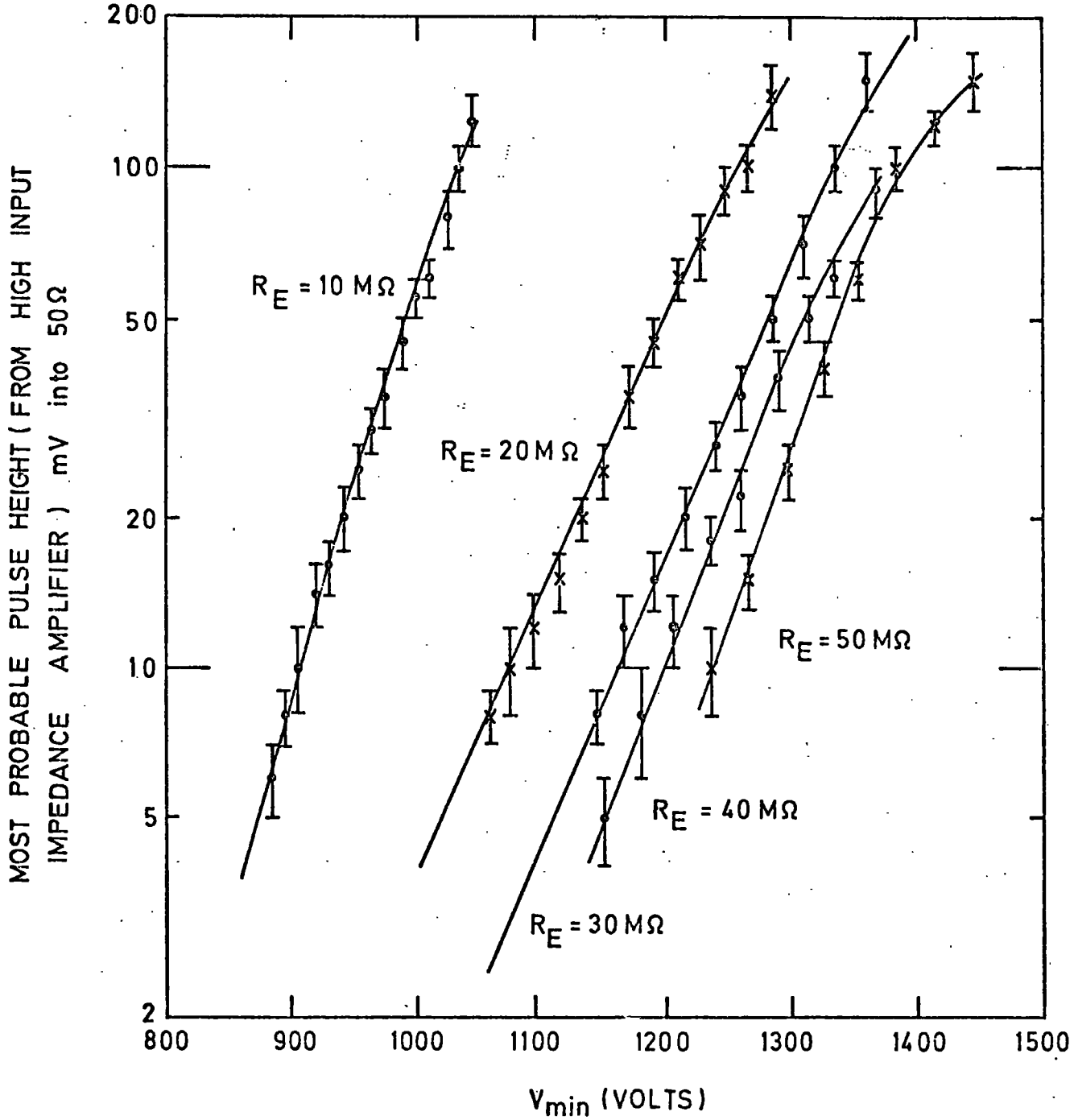

mm above the wire and straight lines on a logarithmic scale verify a variation of the form indicated in equation 4.1, the turnover at high voltages being attributed to the onset of space charge effects (data was collected into the breakdown region). As the value of R_E (figure 3.5) is decreased, producing a greater drift field per applied V_{MIN}, the value of V_{MIN} required to produce a particular pulse output decreases. This shows the adjustment of the accelerating field caused by a change in the graded field of a drift chamber ie. a strong drift field contributes significantly to the accelerating field. However, it must be noted that as the drift field is increased, chamber breakdown is more readily occurrent.

4.2.1 Pulse Heights from X-Ray Sources

By suitable electronic processing, the pulse height spectrum obtained from a Fe 55 source was displayed on a P.H.A.. Figure 4.3 shows the characteristic shape with the main peak due to the 5.9 KeV line and the smaller "escape peak" from the 2.9 KeV x-ray. The finite width of the 5.9 KeV line is due to the statistics of pulse formation during the avalanche process and the fluctuation in the initial ionization. If the assumption of pulse height proportionality with deposited energy is made, an energy resolution of 12% is observed by considering the starting point of the spectrum, this becomes 15% on considering an extrapolation from the gap between the two peaks. The observed resolution has probably been worsened by the spread in pulse heights due to the manifestation of x-rays in different parts of the chamber (see section 4.2.2)

Pulse height spectra were obtained for other x-ray sources and showed distinct peaks at various pulse heights depending on x-ray

FIG 4.3 Pulse Height Spectrum from Fe 55 X-rays

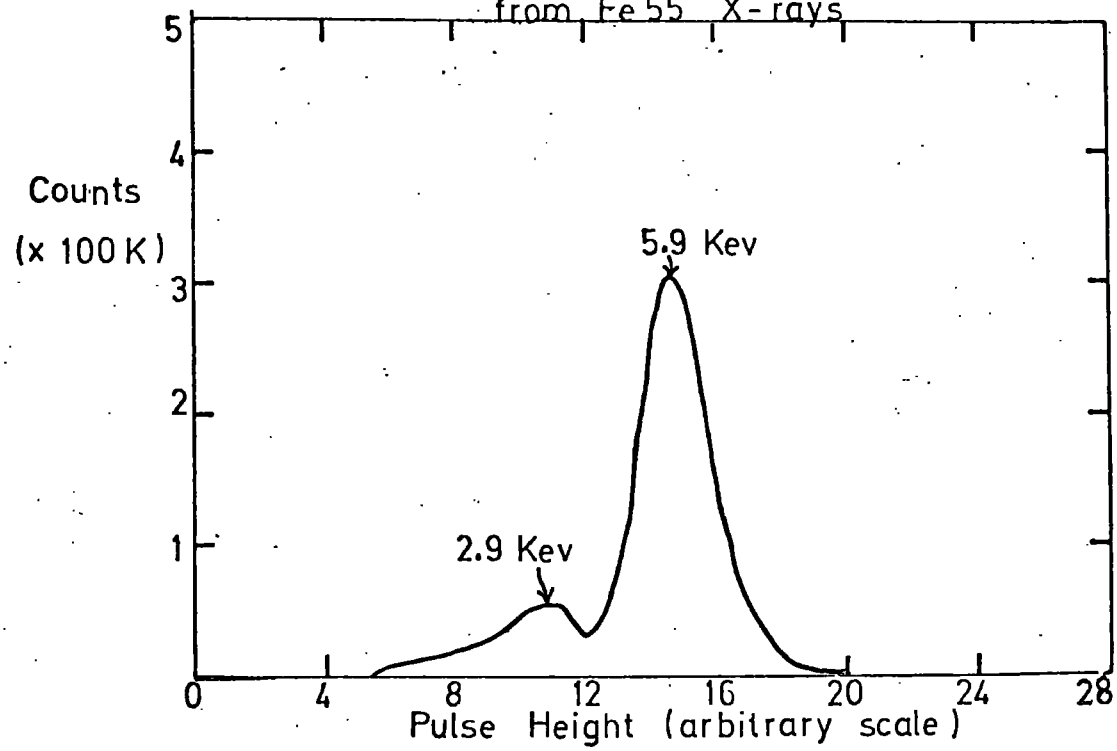

FIG 4.4 Most Probable Pulse Heights from Various X-ray Sources

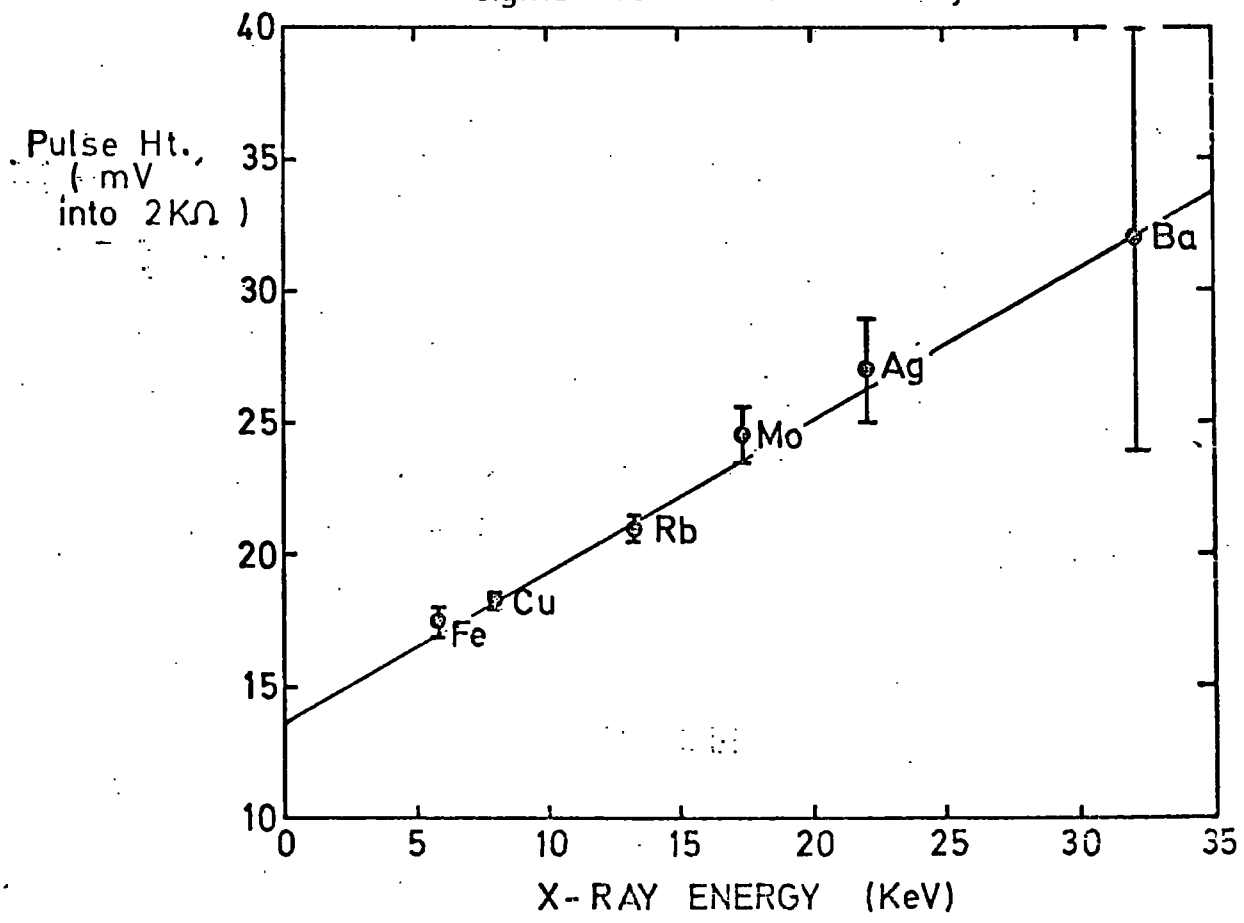

energy (5). In all cases, the Fe 55 peak was apparent due to primary source electrons impinging on the steel container as well as the relevant target metal; this could be eliminated to a large extent by increasing the source distance from the chamber thus allowing only the more energetic x-rays to materialise within a drift cell. The results are plotted in figure 4.4 and show an approximately linear variation of pulse height peak with x-ray energy.

The pulse height-voltage curves of Fe 55 x-rays and Sr 90 β-particles (not necessarily minimum ionizing) are compared in figure 4.5. The higher pulse heights for the β-source are a result of the greater energy deposited in the form of many primary ion pairs as electrons traverse or stop in the chamber, in comparison with the energy deposited by the single photoelectron produced by the x-rays. Once again the space charge effects at high fields can be seen.

4.2.2 Further Effects

The output pulse height at a particular voltage applied to a drift chamber is increased as the graded field is tilted to compensate for a magnetic field. This is a result of two effects: the increased field around the sense wire as the gap between any two equipotentials is decreased by $\sim$ cosine(tilt angle), and the higher voltage on the H.T. wires directly above and below the sense wire. The effect is shown in figure 4.6 where the x-ray pulse height is plotted against voltage for three different field tilts under otherwise similar conditions.

Using a Fe 55 source collimated with a 1 mm slit in perspex, the pulse height at various distances from the sense wire was investigated. Figure 4.7 shows a distinct and gradual deterioration

FIG 4.5 COMPARISON OF PULSE HEIGHTS FROM 5.9 KeV X-RAYS AND (UP TO) 2·27 MeV β-PARTICLES

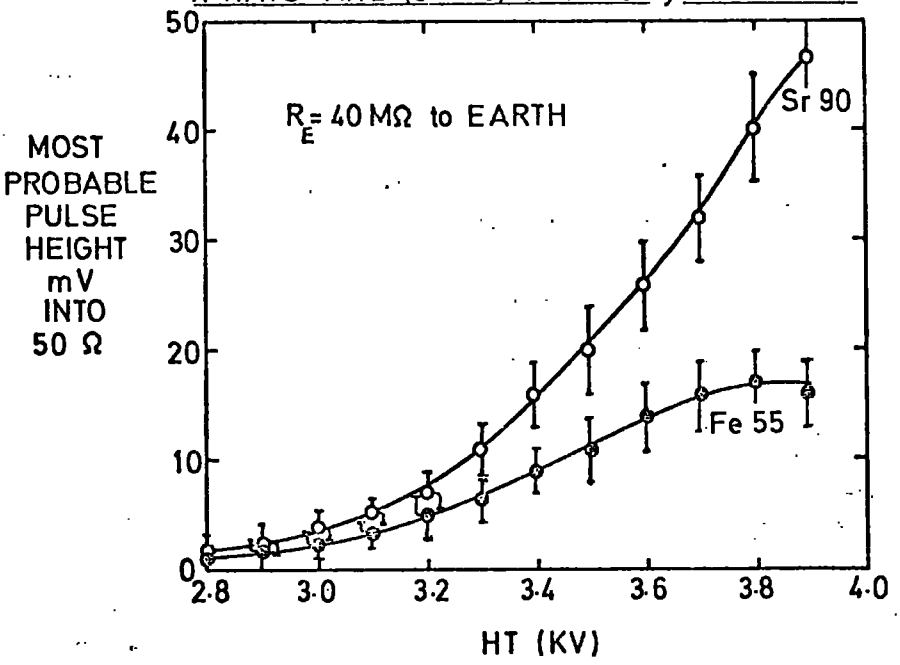

FIG. 4·6 MOST PROBABLE PULSE HEIGHT AS A FUNCTION OF HIGH VOLTAGE FOR VARIOUS TILTS OF ELECTRIC FIELD (Fe 55)

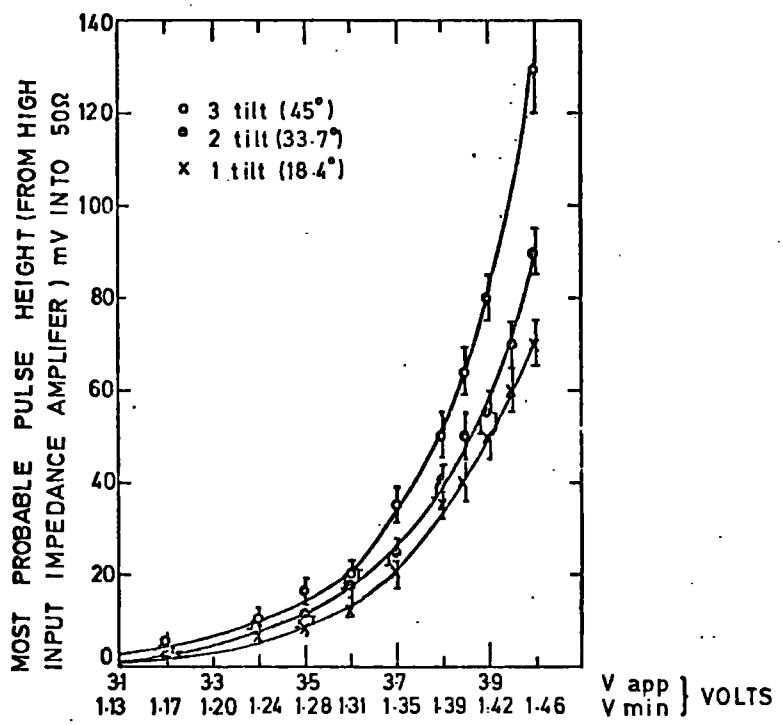

FIG. 4·7 PULSE HEIGHT VARIATION ACROSS DRIFT CELL (Fe 55)

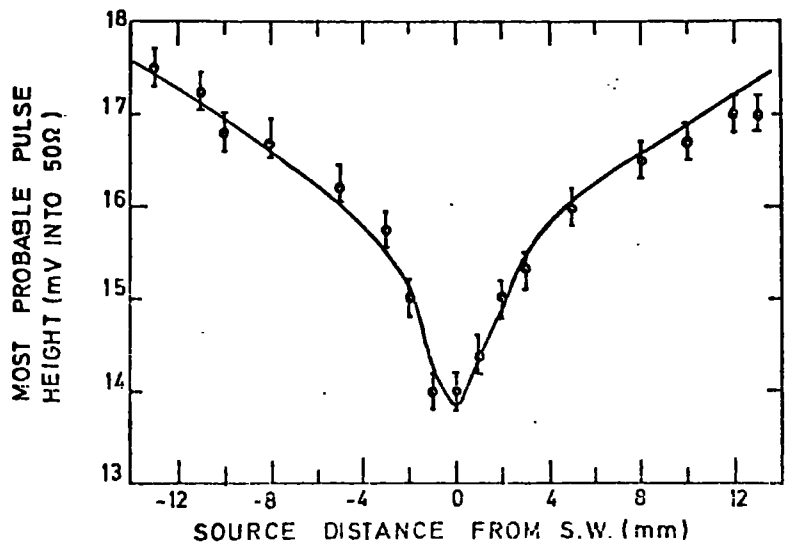

in pulse height towards the sense wire. This effect has since been observed by other workers (6) and has been attributed to a self limitation on gain caused by a slight assymetry of charges on the sense wire surface produced by the electric field structure of the chamber. Another possible explanation is that some gas multiplication may occur in the drift field, thus, less amplification is achieved as the sense wire is approached, resulting in the observed decrease in pulse height. (This explanation will certainly apply to the "avalanche region") For minimum ionizing particles which produce an ion trail along the whole track length, the effect is slightly enhanced by the spread of the electron swarm being greater (due to geometrical reasons) for tracks nearer the wire, thus causing a variation in pulse shape with distance from the wire. The pulse height dip effect is exaggerated in the differential pulse shaping of drift chamber amplifiers.

4.3 Efficiency Measurement

By careful shielding, the detecting surface area of the scintillator was reduced so that only those β-particles passing through a drift cell could trigger the system. Efficiencies of $> 90\%$ were obtained in this way, the inefficiency being attributed mainly to cosmic rays and γ-radiation from the source (plus a small amount of P.M. noise). The normalised efficiency-voltage curve obtained for a g-2 chamber is presented in figure 4.8 and shows the usual particle counter characteristics of an increase to a 100% plateau, ~ 125 V long in this case, after which breakdown occurred. This result was achieved using a gate width (T_W) of 1.0 μs, a discrimination level (V_d) of 100 mV at the output stage of the Verweij high impedance

FIG. 4.8 NORMALISED EFFICIENCY-VOLTAGE CURVE FOR g-2 DRIFT CHAMBER CELL

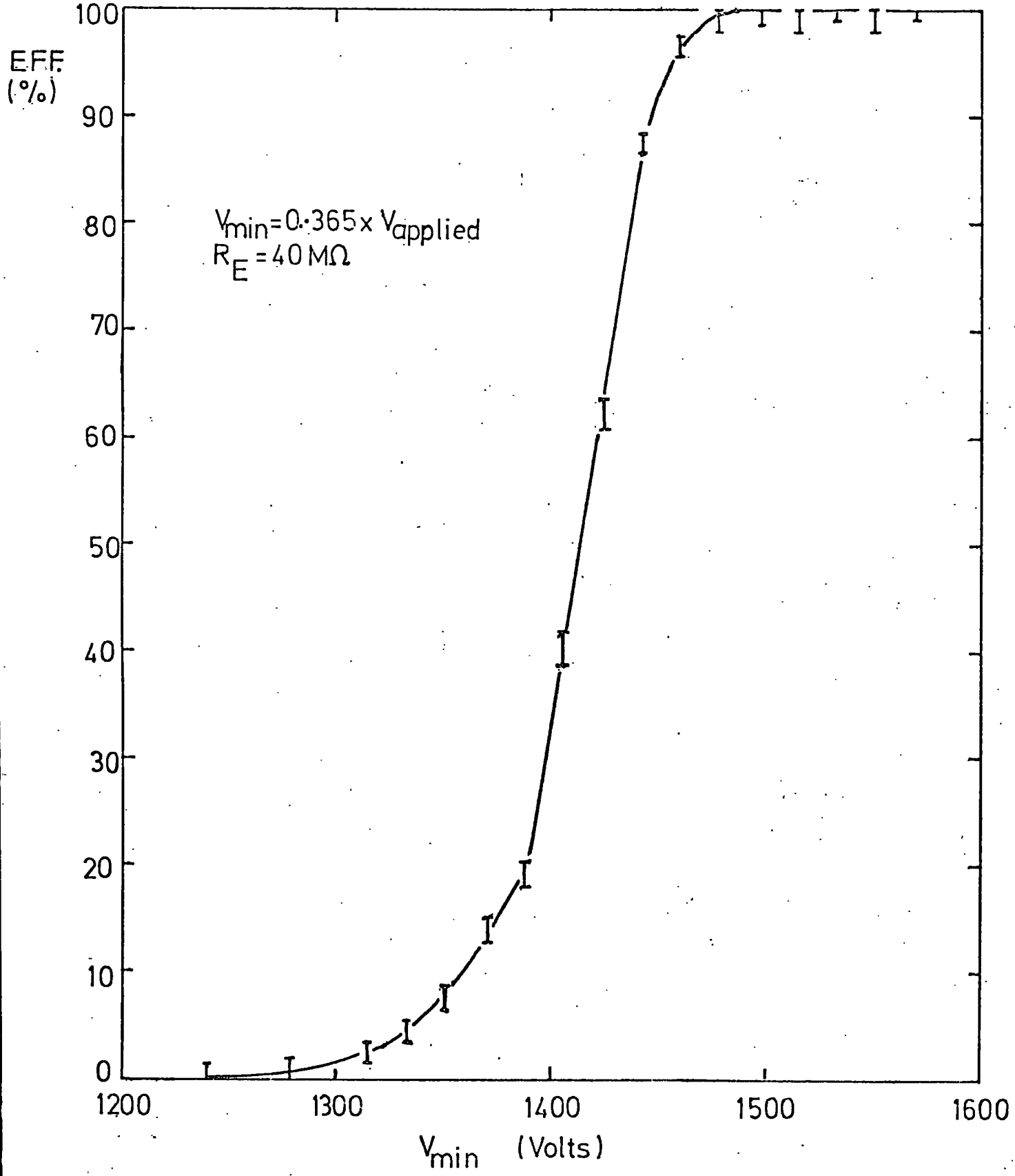

preamplifier, and a drift field of 602 V cm^{-1}.

The efficiency-voltage characteristic is a direct (statistical) result of the increase in pulse height with voltage as discussed in section 4.2 (compare figures 4.2 and 5.7) and is therefore a strong function of V_d. For drift chambers, T_W must be greater than the maximum drift time if the correct characteristic is to be obtained. A detailed discussion on the effects on efficiency of the parameters T_W, V_d and drift field forms part of another work (7). Further efficiency measurements will also be presented in chapter 5 and appendix 2.

4.4 Drift Time Measurement

By aligning the drift chamber so that the ionizing beam passed at known distances from the sense wire, drift time distributions throughout the cell could be obtained, examples for a drift field of 602 V cm^{-1} in Argon (90%) - Methane (10%) being shown in figure 4.9. Equal separations of peaks indicate a linear space-time relationship in the region of the chamber investigated and a horizontal scale calibration of 0.3 mm/channel is yielded. Thus typical distribution F.W.H.M's of $\sim$ 1.5 mm were obtained and the contributions to this dispersion will be discussed in section 4.6.

Drift times at various distances from the sense wire were obtained by observing the peak positions on the P.H.A. display. Figure 4.10 shows these variations for several drift fields in Argon (90%) - Methane (10%), where it is seen that linearity occurs over much of the cell except at low fields, and longer drift times are associated with higher fields for this particular gas mixture. Also for a distance of up to 4 mm on either side of the sense wire, the

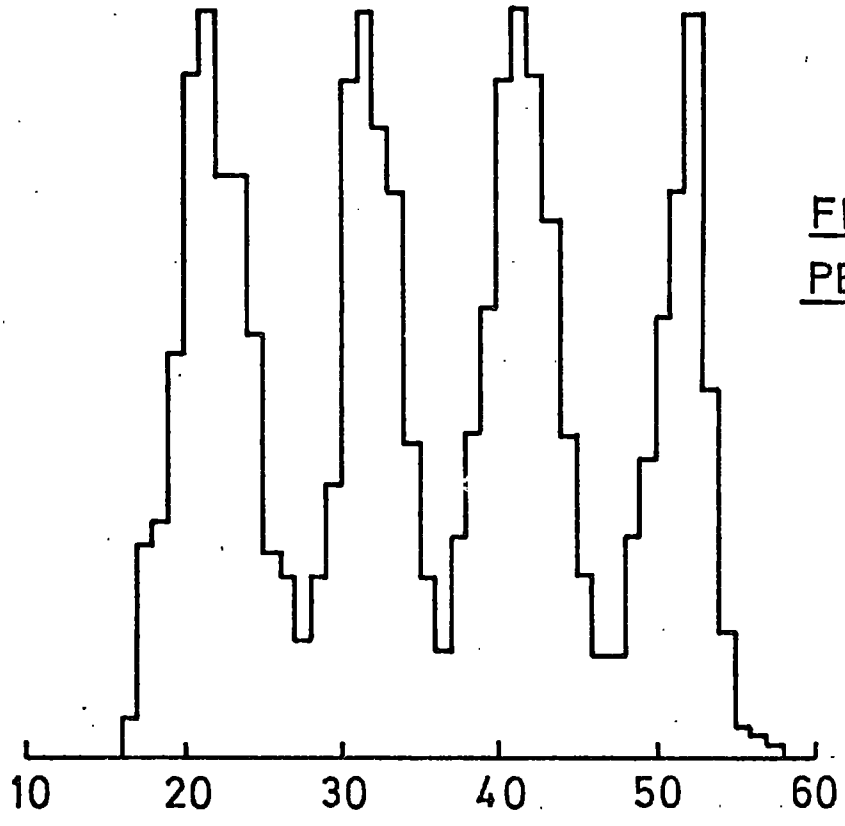

FIG. 4.9 a
PEAKS~3mm APART

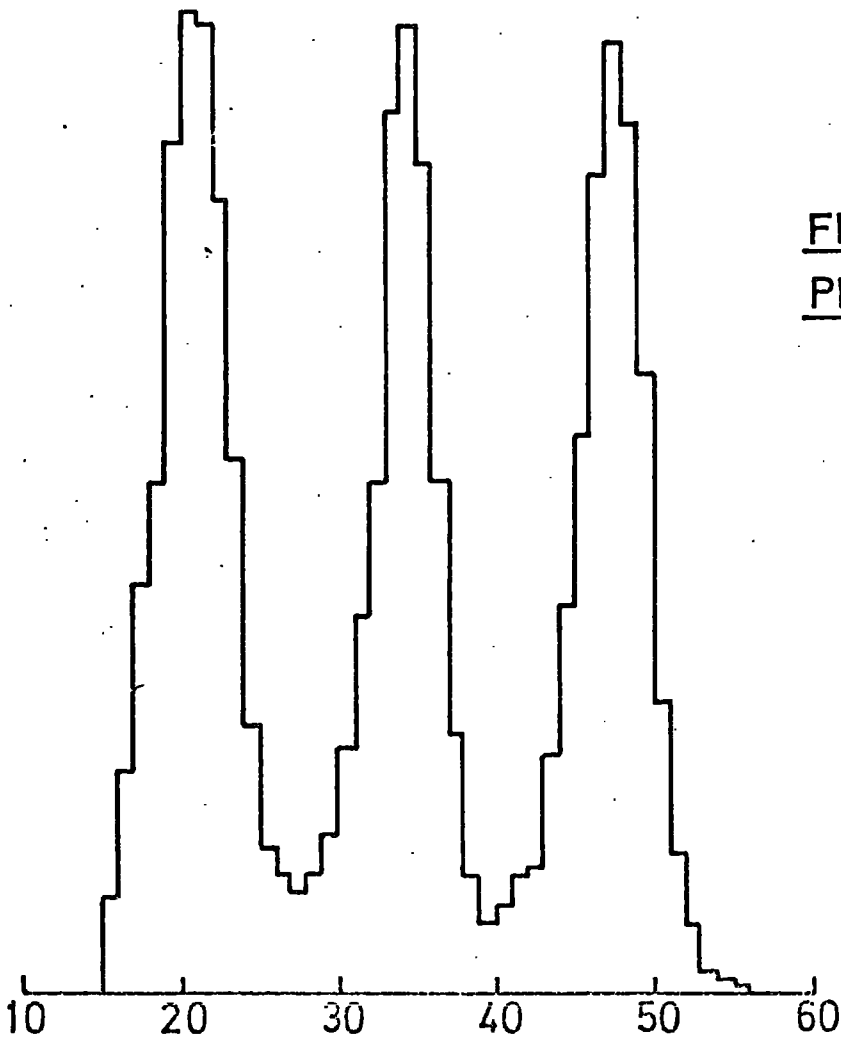

FIG. 4.9 b
PEAKS~4mm APART

FIG 4.10 DRIFT TIMES ACROSS CELL

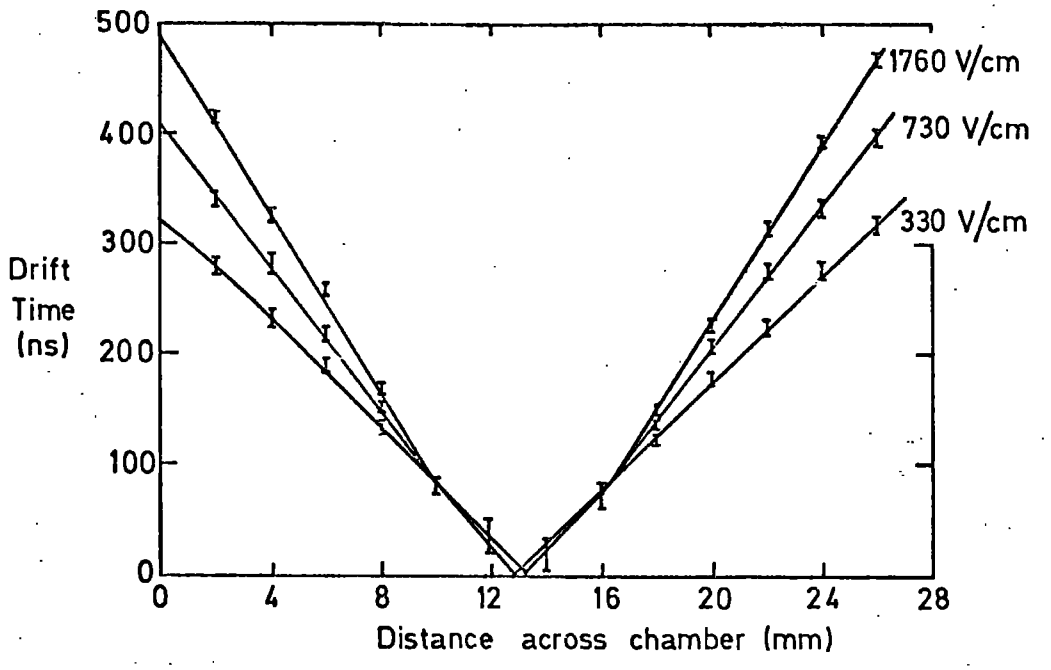

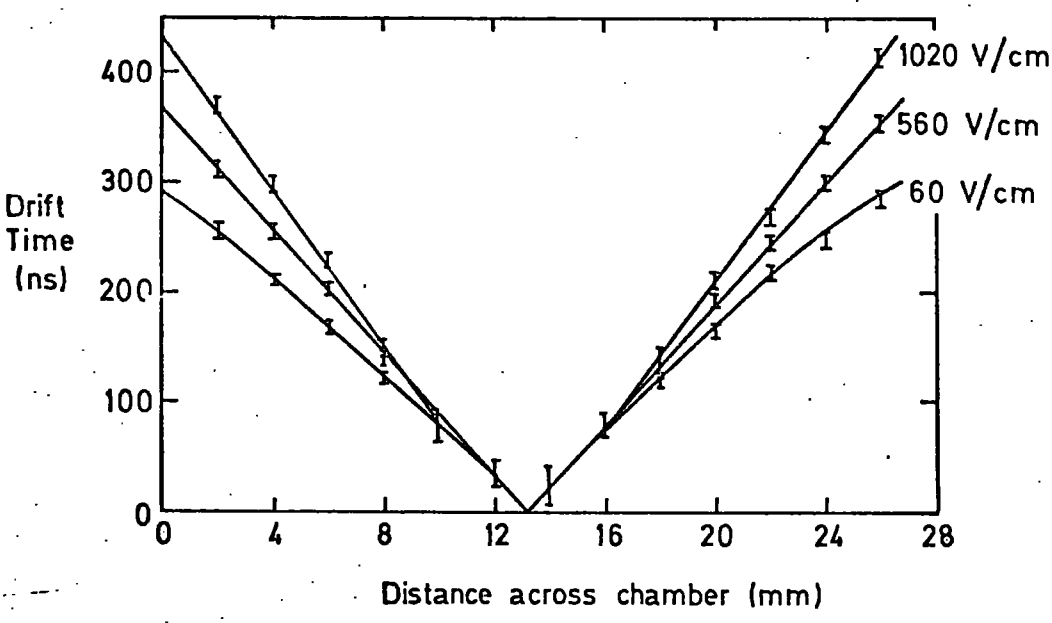

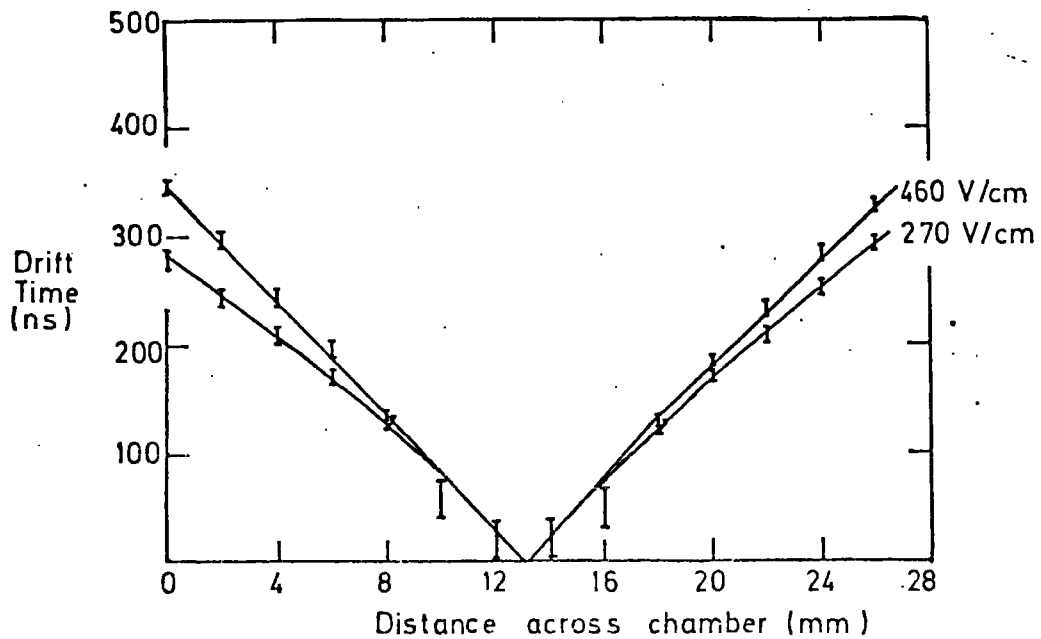

drift velocity is independent of the applied drift field, as in this region, electrons are drifting in the much stronger avalanche field.

4.5 Drift Velocity Measurement

The results of figure 4.10 indicate that the drift velocity of electrons in a gas is a direct function of electric drift field, hence, an extensive series of measurements for various gases and field values was performed with the following aims:-

a) to select a suitable gas mixture for use in the g-2 chambers while obtaining information concerning electron drift processes.

b) to investigate the diffusion of electrons in gases also with a view to selecting a suitable gas mixture.

c) to measure drift velocities in an operational chamber, at fields within the practical range up to 2 KV, rather than in a specially prepared system, (usually, such investigations are carried out at low fields; a region where more interesting physical effects occur) and to compare the resulting curve shapes with existing data.

The gradients in the uniform field regions of the space-time relationships of figure 4.10 were measured and hence the drift velocity variation with electric field was determined, this being presented together with an eye fit to the data in figure 4.11. Also in this figure are shown the early results of English and Hanna (9) for the same gas which indicate reasonable agreement at low fields and good agreement at higher fields, and the more recent theoretical prediction of Palladino and Sadoulet (10) which exhibits a sharper peak in the curve but at the same electric field value as that experimentally determined.

FIG. 4·11 DRIFT VELOCITY OF ELECTRONS IN ARGON (90%) METHANE (10%)

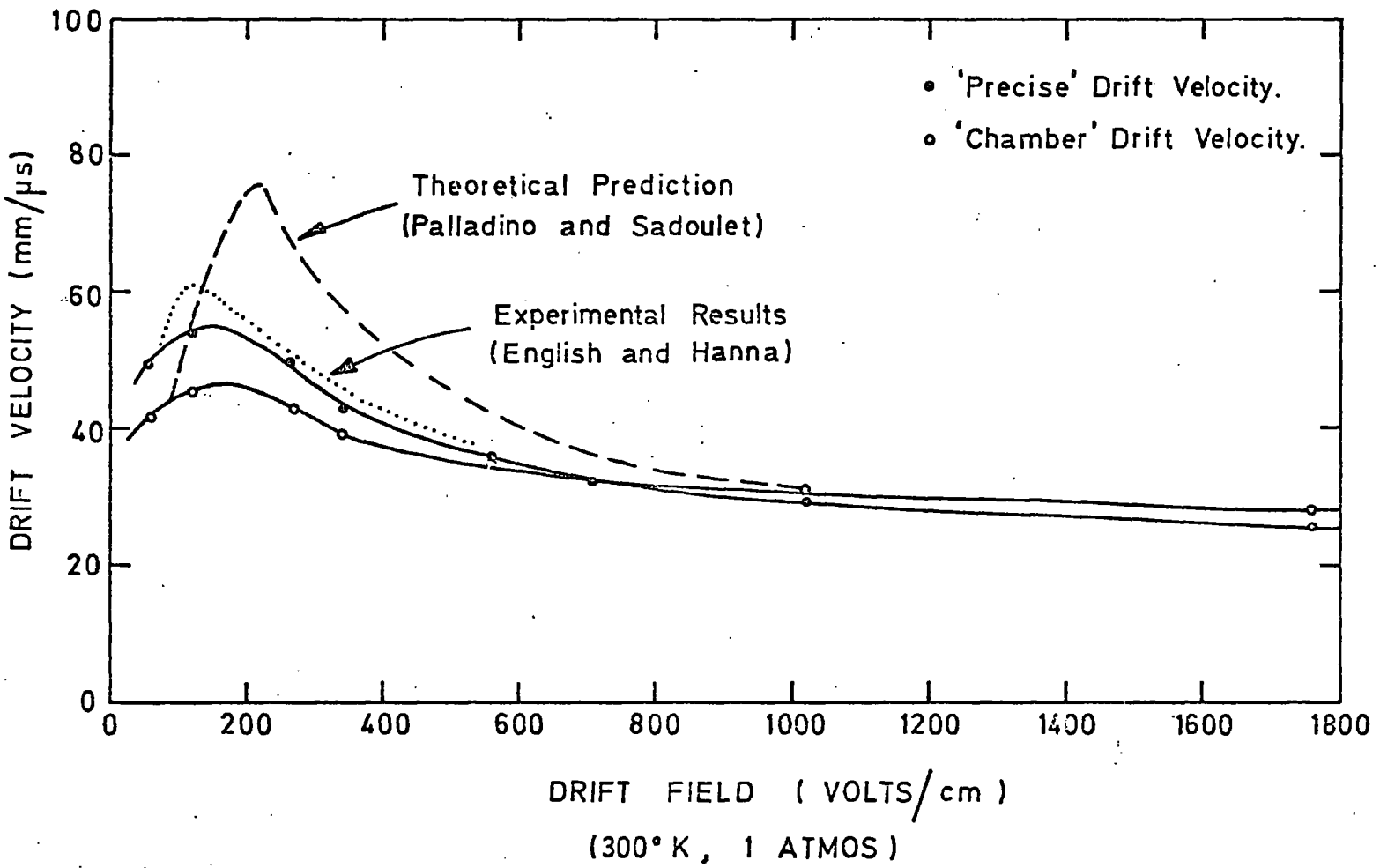

For measurement of drift velocity in different gases, in order to reduce the laborious work involved in determining distance-time gradients, and hence increase the number of gas mixtures tested, a method involving only one reading at each value of electric field was employed. This could be achieved in either of two ways:-

Observing the cut-off edge of the assymetrical distribution obtained in the proximity of the field wire (figure 4.12(a)) yields a value of maximum drift time (ie. the time to drift 14 mm in this case).

A novel method of determining the time to drift 10 mm was discovered. When the collimating slit was aligned at a position 10 mm from the sense wire, the resulting time distribution was found to have a slight trough in the centre (figure 4.12(b)) due to the "shadow" of the fifth H.T. wire from that directly above the sense wire. Thus the position of the minimum of this trough represented, in this case, the time to drift (10.3 ± 0.2)mm as determined using a travelling telescope.

The latter method was in fact used for these investigations. However, the drift velocity is not necessarily uniform over the whole of the 10 mm drift space for reasons evident from section 4.4 and hence the results following will refer to the "chamber drift velocity", this being defined by the above technique. "Chamber velocity" illustrates the correct forms of drift velocity variation with electric field and hence fulfills the objectives a), b) and c) without yielding absolutely correct values. An example of the variation of this quantity with field is also plotted in figure 4.11 for Argon(90)-Methane(10).

FIG 4.12(a) DRIFT TIME SPECTRUM AT THE END OF A CHAMBER CELL SHOWING A SHARP CUTOFF (ARGON (90) - METHANE (10)) (horizontal scale : 11 ns / channel)

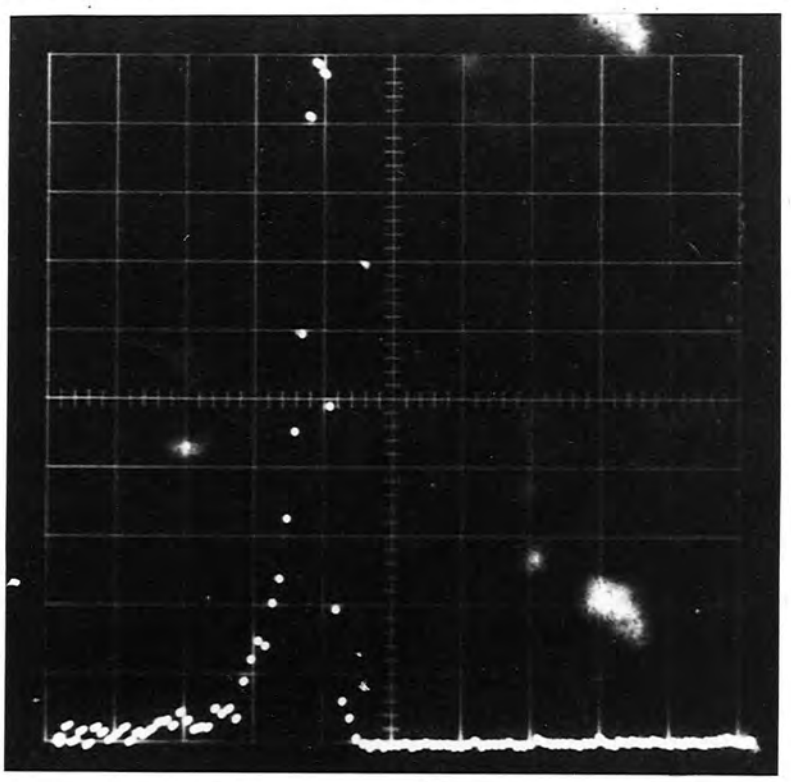

FIG 4.12(b) DRIFT TIME SPECTRUM FOR THE COLLIMATED SOURCE 10 mm FROM THE SENSE WIRE SHOWING THE H.T. WIRE "SHADOW" (ARGON (84) ISOBUTANE (16)) (horizontal scale : 3·5 ns/channel)

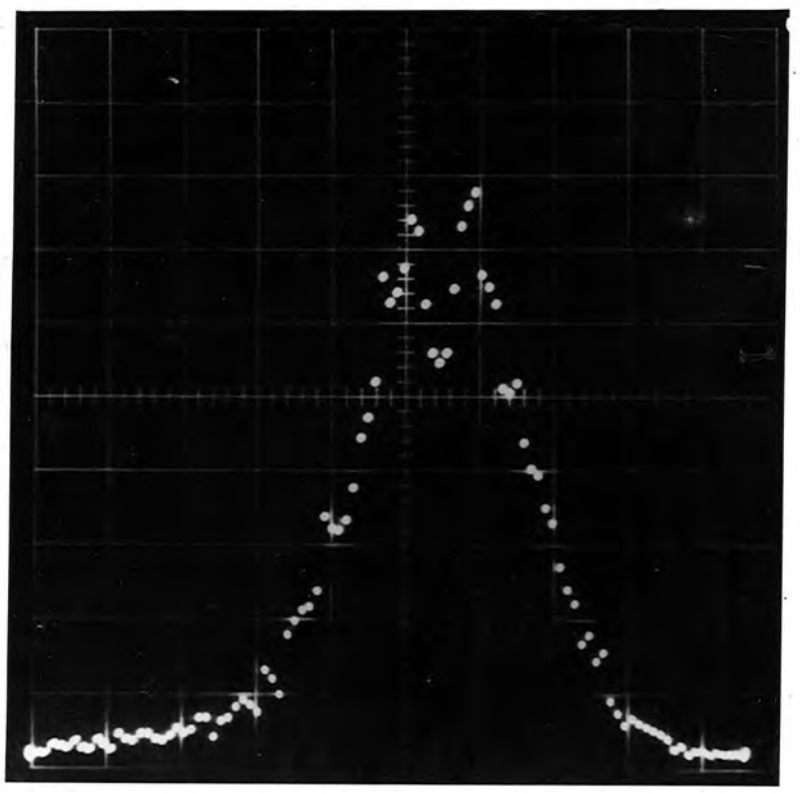

4.5.1 Drift Velocities in Various Gas Mixtures

The drift velocities for various Argon-Methane mixtures are shown in figure 4.13. (Errors in these and following curves are of the order ± 1.1 mmμs^{-1} and are omitted from the figures for clarity.) For Methane concentrations up to 10%, relatively low drift velocities are observed with large variation at low fields and small variation at high fields ($<10\%$ above 800 V cm^{-1}) tending towards a saturation plateau in this region. The effect of the Methane is to increase drift velocity at a rate of between 1.5 and 2 mmμs^{-1} per additional 1%, Methane itself supporting a high drift velocity of the order 130 mmμs^{-1} as indicated in figure 4.13 . For Methane levels below 3% spurious breakdown occurred at most operating voltages. The Argon-Methane and pure Methane results measured in the drift chamber show reasonable agreement with previously determined curves (9, 11).

Figure 4.14 shows the results for Argon-Isobutane mixtures. Peaks in these curves at low field values are not as pronounced as for Argon-Methane and, at high fields, increasing isobutane content increases drift velocity at the rate of ~ 1 mmμs^{-1} per 1%. For high Isobutane content ($>25\%$) a tendancy for drift velocity to steadily increase with increasing field is shown and reasonable saturation plateaus ($<8\%$ variation above 800 V cm^{-1}) are observed. Also in this figure are shown the results of Charpak et al. (12) for the commonly-used Argon(75)-Isobutane(25) mixture. The variations of all curves agree well with results since published (13) but values of the latter are $\sim 15\%$ lower, discrepancies being attributed to the measuring technique.

As the Argon-Methane curves tend to fall towards plateaus from 200 V cm^{-1} and the Argon-Isobutane curves tend to rise to their

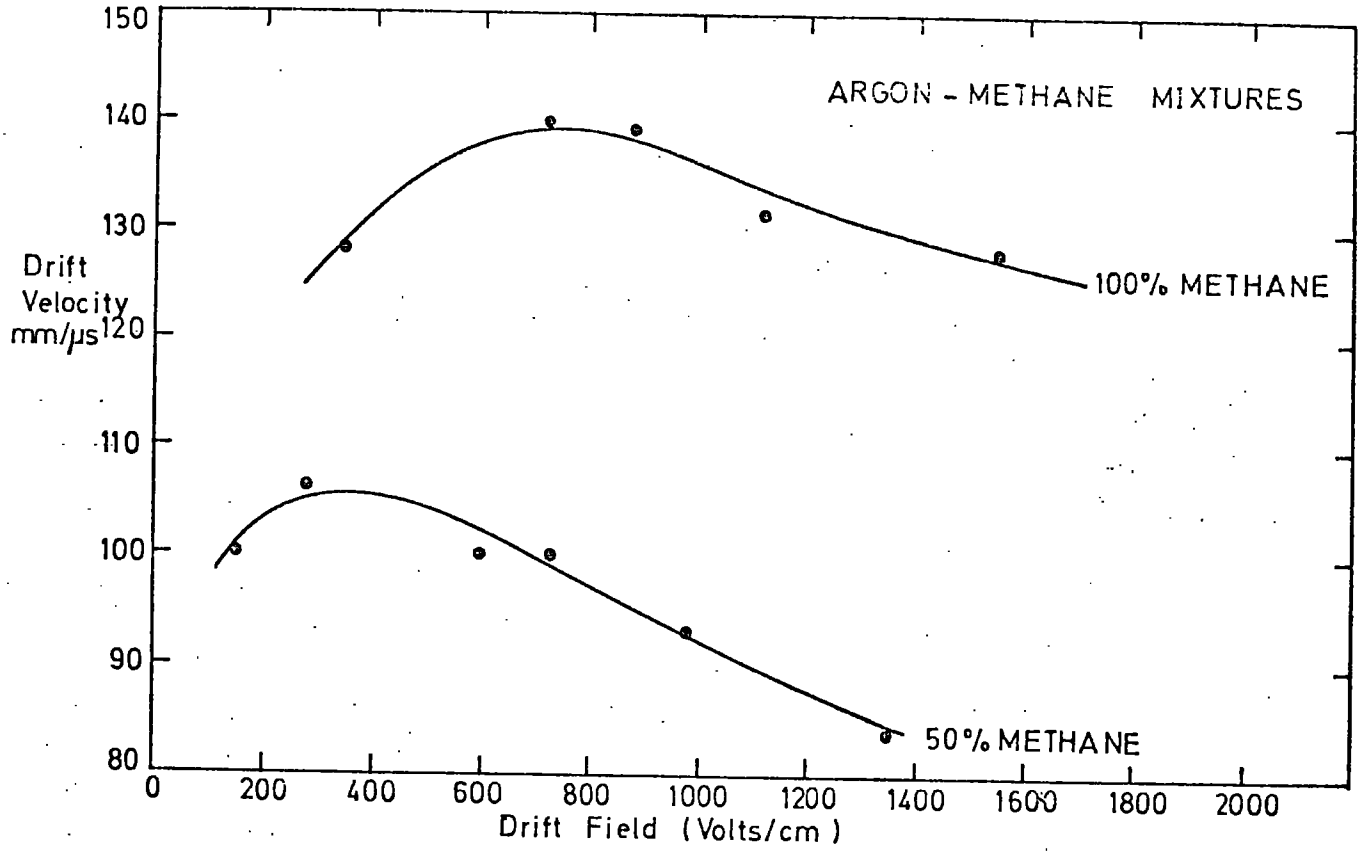
ARGON - METHANE MIXTURES
100% METHANE
50% METHANE
Drift Velocity mm/μs
Drift Field (Volts/cm)
150
140
130
120
110
100
90
80
0
200
400
600
800
1000
1200
1400
1600
1800
2000

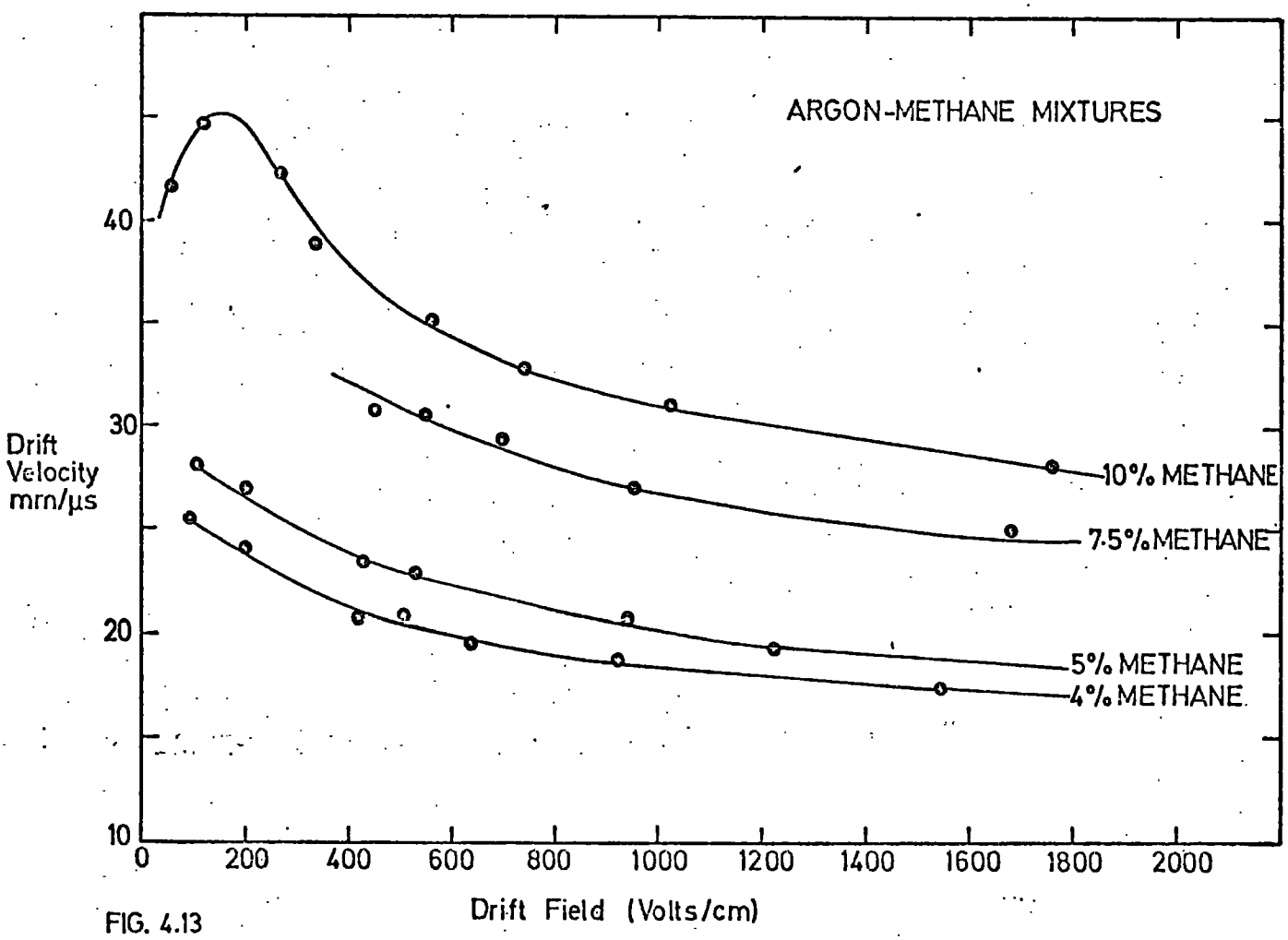
ARGON-METHANE MIXTURES
10% METHANE
7·5% METHANE
5% METHANE
4% METHANE
Drift Velocity mm/μs
Drift Field (Volts/cm)
40
30
20
10
0
200
400
600
800
1000
1200
1400
1600
1800
2000

FIG. 4.13

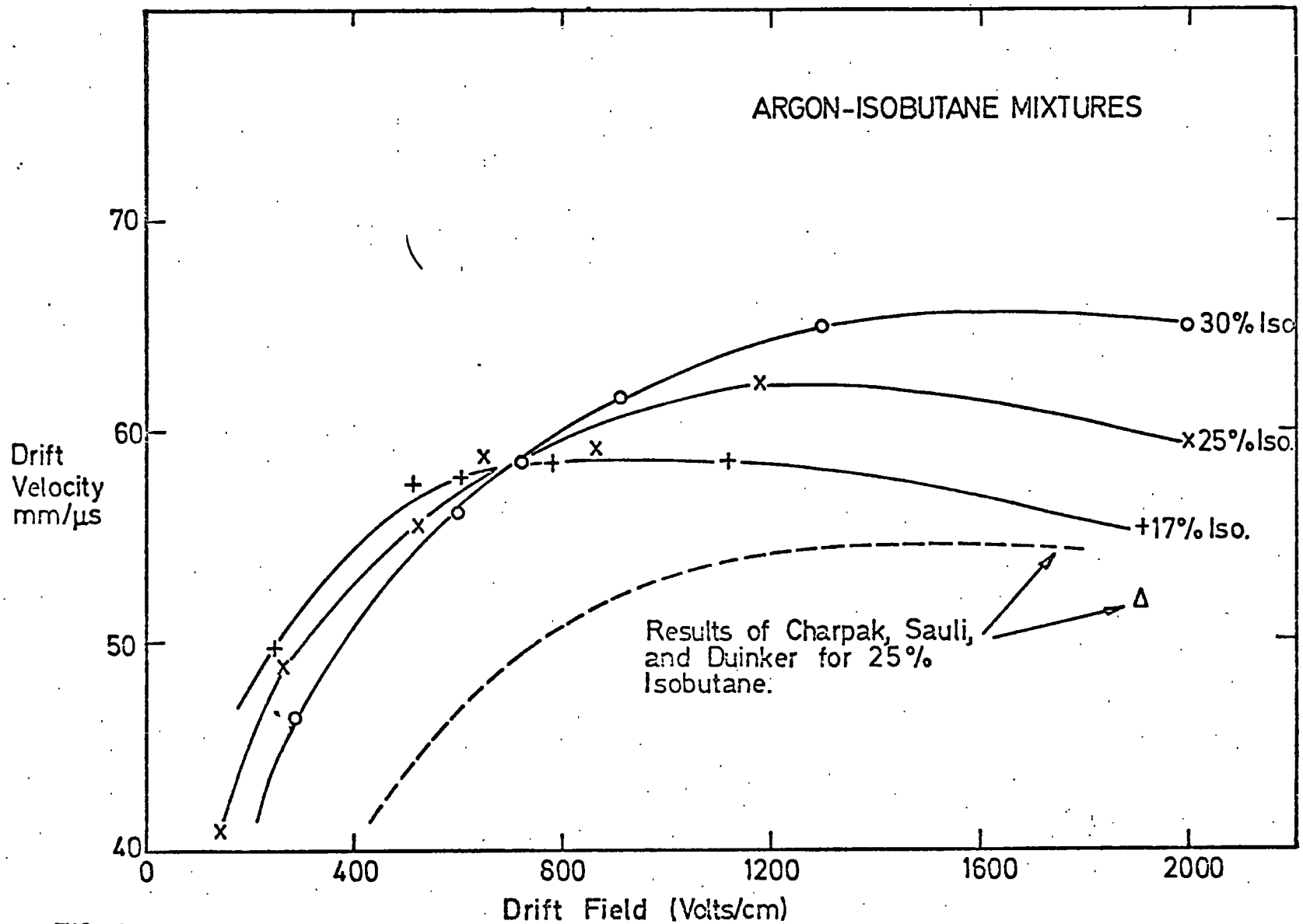
ARGON-ISOBUTANE MIXTURES
70
60
50
40
Drift
Velocity
mm/μs
0
400
800
1200
1600
2000
Drift Field (Volts/cm)
30% Iso
25% Iso.
17% Iso.
Results of Charpak, Sauli,
and Duinker for 25%
Isobutane.

FIG. 4.14

plateaus, it was decided to investigate mixtures of the three gases with the aim of achieving a good drift velocity saturation with electric field. Figure 4.15 indicates that the drift velocity curves for Argon-Isobutane-Methane mixtures follow predictable trends. Low content Isobutane mixtures show similar characteristics to Argon-Methane but for a given plateau level the drift velocity variation with field is slightly less for the former. At higher Isobutane concentrations, the curves look more like those of Argon-Isobutane but with better plateaus, excellent saturation properties being exhibited by Argon(67.5)-Isobutane(25)-Methane(7.5) and Argon(59.5)-Isobutane(34)-Methane(6.5) mixtures. Hence it can be said that the addition of a small amount of Methane to one of the common Argon-Isobutane mixtures produces favourable drift velocity characteristics for drift chambers.

Figure 4.16 shows a comparison between the different mixtures mentioned above with the addition of curves for two more gases. Argon(80)-Carbon Dioxide(20), a popular proportional counter gas (14), exhibits a steep rise as electric field is increased and is therefore unsuitable for normal drift chamber operation. However, it is suggested that such a mixture may prove useful when the effects of small variations in field configurations (eg. earthed windows) are to be investigated. An attempt to produce a saturation plateau at low fields by the replacement in this mixture of 8% Argon with Methane was unsuccessful as a similar characteristic was obtained. Attempts were also made to use pure Argon in a drift chamber but spontaneous breakdown prevented the collection of any useful data. The Argon curve of figure 4.16 is taken from experimental measurements by English and Hanna (9).

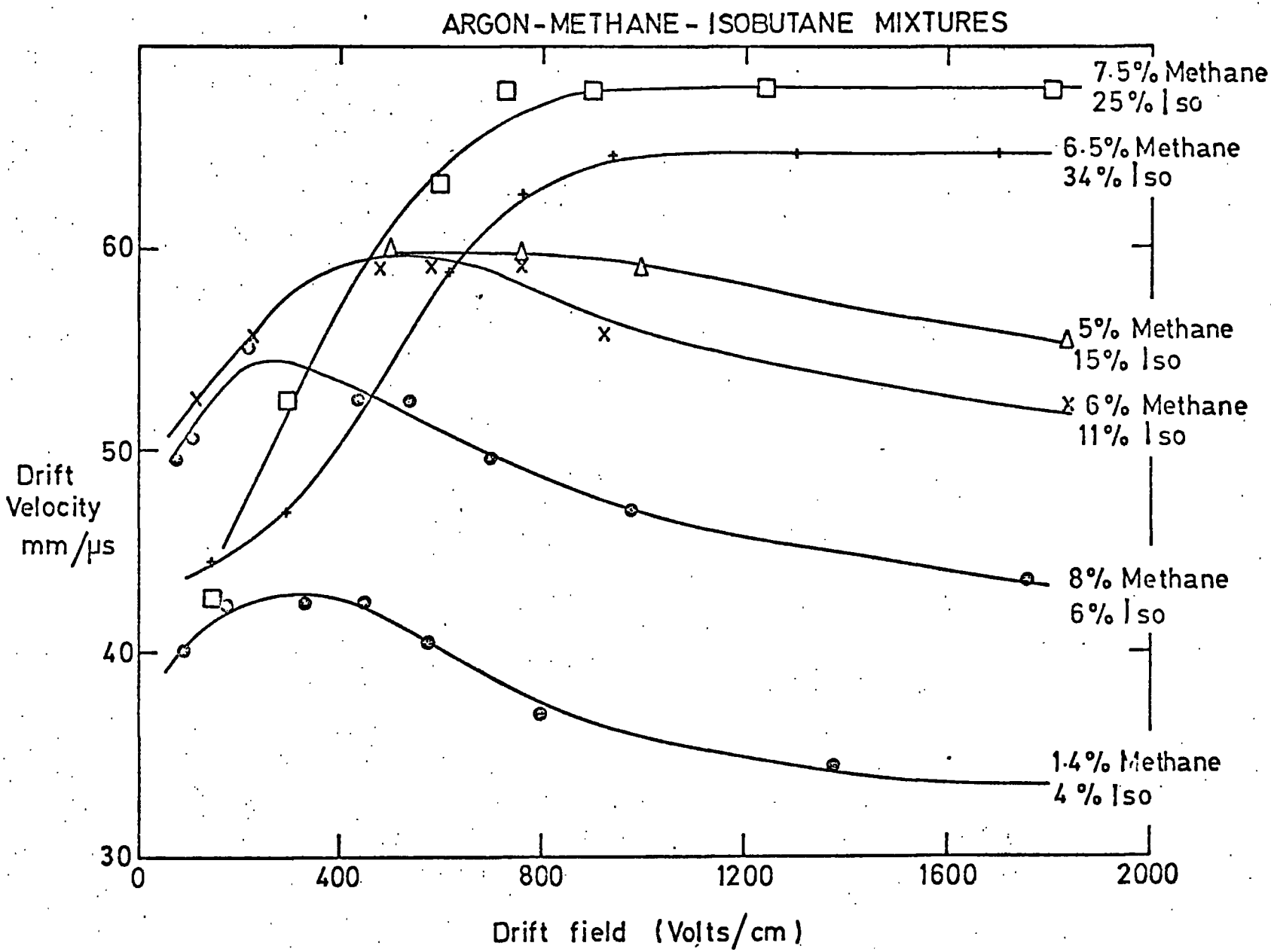
ARGON-METHANE-ISOBUTANE MIXTURES
7·5% Methane
25% Iso
6·5% Methane
34% Iso
5% Methane
15% Iso
6% Methane
11% Iso
8% Methane
6% Iso
1·4% Methane
4% Iso
Drift
Velocity
mm/μs
60
50
40
30
0
400
800
1200
1600
2000
Drift field (Volts/cm)

FIG. 4.15

FIG 4.16 : COMPARISON OF DRIFT VELOCITIES

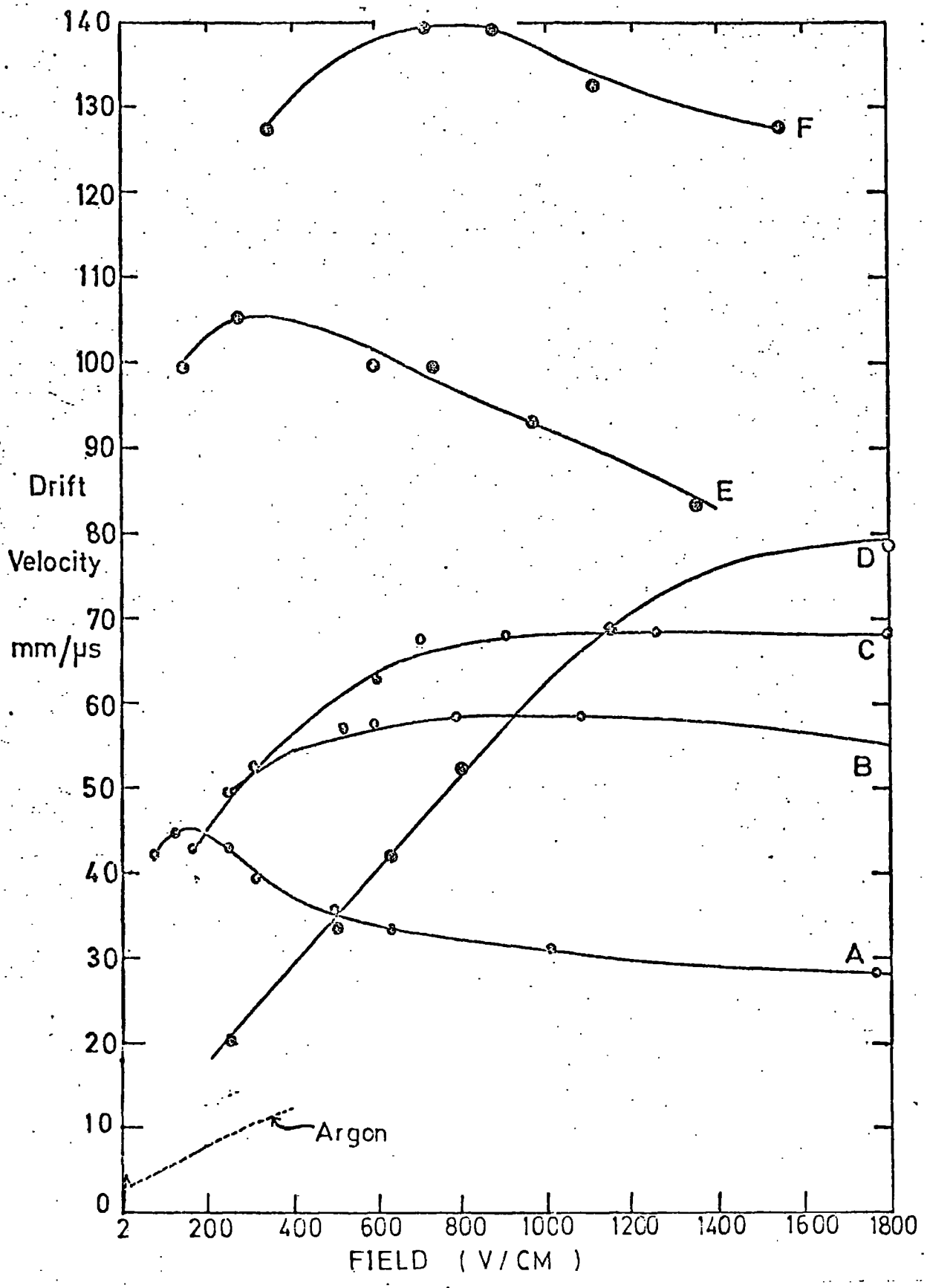

A - Argon - methane (90/10)

B - Argon - isobutane (83/17)

C - Argon - methane - isobutane (87.5/7.5/25)

D Argon - CO_2 (80/20) and Argon - methane - CO_2 (72/8/20)

E - Argon - methane (50/50)

F - Methane

Other gases which have been used in drift chambers are pure Ethylene (15) and a "magic gas" (13, 16) where the addition of a small quantity of Methylal to the normal Argon-Isobutane mixture prevents breakdown and the polymerization of Isobutane without modifying the drift velocity behaviour.

4.5.2 Explanation of Results

The drift velocity, w, and characteristic energy, ϵ_K (see section 1.3.2), of drifting electrons obey increasing power laws in electric field, E, (10), thus for a constant elastic collision cross section, σ_E, the electron drift velocity tends to increase with increasing field.

However, in Argon, for example, σ_E is a strong function of electron energy, ϵ $(= \frac{1}{2} m_e V^2)$ where V is the electron thermal velocity, as seen in figure 4.17, exhibiting a Ramsauer minimum (10, 17) at 0.3 eV. Thus for $\epsilon_K < 0.3$ eV, w will increase rapidly with E in this gas. As σ_E rises when $\epsilon_K > 0.3$ eV, the increase in energy lost per collision will reduce drastically (to an almost constant level) the rate of increase of w with E. After 11.5 eV, a fairly steep rise in w with E is resumed; theory and experimental results agree extremely well in this case (18).

In general, for large values of E, an electron accelerated in a viscous medium quickly attains a stable drift velocity as the energy gained between collisions with gas molecules is counter-balanced by that lost in the collision. The rise in σ_E with E for organic gases cannot account wholly for the latter process and rotational and vibrational excitation must be included to explain the saturation of drift velocity at high fields (10).

FIG 4.17

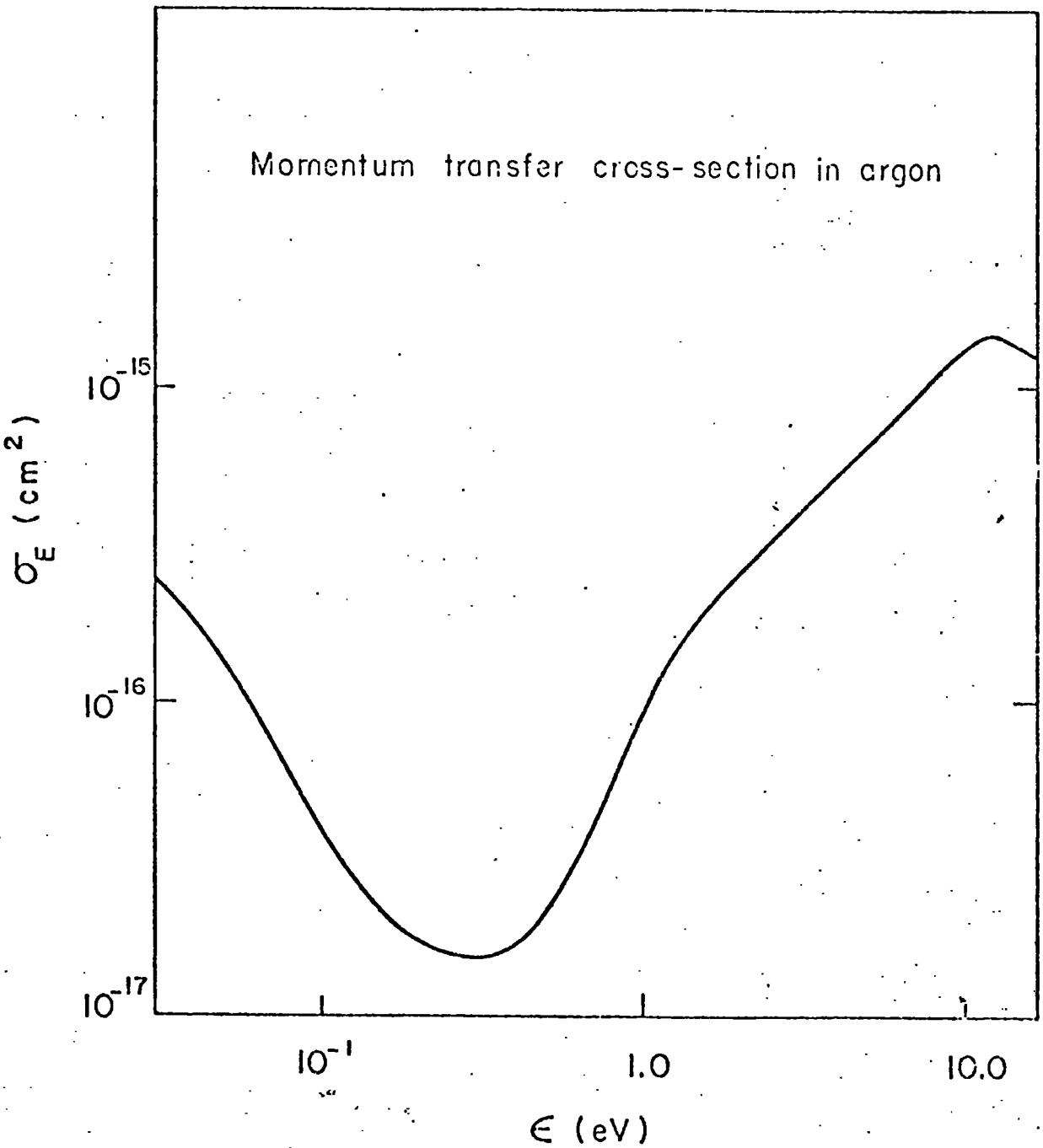
Momentum transfer cross-section in argon
10^{-15}
10^{-16}
10^{-17}
σ_E (cm^2)
10^{-1}
1.0
10.0
ϵ (eV)

In the same manner as for the Argon drift velocity curve, the behaviour of the Argon-Methane and Argon-Isobutane curves at low values of E can be accounted for by considering the resultant σ_E / ϵ variations when the gases are mixed. The variation of σ_E for organic gases is complex and not well known at low energies, however, by postulation of a flat cross section for Isobutane at energies below 1 eV, which results in a partial filling of the Ramsauer dip, the Argon-Isobutane variation has been successfully predicted (10). The theoretical variation calculated for Argon-Methane by the same workers does not agree as well with experiment (see figure 4.11). A rapid fall-off in cross section for Carbon Dioxide is known to occur, this explaining the drift velocity increase observed for the Argon-Carbon Dioxide mixture.

The different drift velocity magnitudes in gases are the result of the different mean free paths involved. The latter depends on the molecular structure and its increase effects a drift velocity increase.

4.5.3 The Selection of a Gas Mixture for the g-2 Chambers

The main requirement for a drift chamber gas is stability of drift velocity with electric field in order to produce linear space-time relationships throughout each drift region. From the results presented in section 4.5.1, this condition is seen to occur for Argon-Methane (in most proportions), Argon-Isobutane and Argon-Isobutane-Methane mixtures (providing the Isobutane content is high enough in the latter two) and providing the electric field at all points in the chamber is high enough ie. $\gtrsim 800$ V cm^{-1}. For resolution tests etc., where the regular field regions of the drift spaces are

involved, work at much lower fields is possible for these particular mixtures.

For short drift lengths, as in the g-2 chambers, a low drift velocity is advantageous as a larger range of times will be produced. (For very long drift spaces, a fast gas such as Methane may be beneficial to allow the use of commercial timing electronics). The low Methane content Argon-Methane mixtures tested show favourable results concerning this property.

The mixtures above compare similarly in their stability properties with gas composition and, in this respect, it is convenient (and cheap) to use a standard gas mixture (eg Argon(75)-Isobutane(25)). Argon(90)-Methane(10) was found to be an extremely cheap, premixed industrial gas, and reproducible results without any deterioration in chamber performance have been yielded from this mixture throughout this work.

The good behaviour of the selected gas in magnetic fields is desireable, and it will be observed in chapter 6 that the drift velocity saturation property of Argon(90)-Methane(10) is improved in magnetic fields up to 15 KGauss, allowing successful drift chamber operation at electric fields $\gtrsim 600$ V cm^{-1}.

An important aspect of gas selection (especially for large drift spaces) is the diffusion of the drifting electron swarm in the gas. This will be discussed in section 4.6 where it is shown that diffusion problems were greater for the Isobutane mixtures tested than for those containing Methane even in the small drift spaces of the g-2 chambers.

The gas mixture eventually chosen was Argon(90)-Methane(10) which was used for most of the work presented in this thesis, and, in

addition to the properties mentioned above, this mixture exhibited satisfactory gas gain characteristics without causing any damage to the chamber wires, as is the requirement of most wire discharge counters. Finally, it must be added that the gas mixture chosen is not necessarily the best drift chamber gas available, but has been found to be satisfactory to the particular requirements of this project. Argon-Isobutane mixtures are popular at CERN, while the search for an ideal gas still continues.

4.6 Spatial Resolution

In order to ascertain that most of the observed peak width in these laboratory tests was due to the severe multiple Coulomb scattering of the low energy source particles, the variation of the F.W.H.M's of the time spectra, as the sense wire to collimating slit distance (d of figure 4.18) was altered, was investigated. This was done for a drift field of 602 V cm^{-1} in Argon(90)-Methane(10).

The main contributions to the width are: the geometrical dispersion (x_g) indicated in figure 4.18 and the multiple scattering (mostly in air) which produces an apparent radius of curvature (r) for the particle of:-

$$r = 0.9\ R\ (M/m_e Z)^{\frac{1}{2}} \qquad (4.2)$$

over the first half of the range (R). In this case, $Z \simeq 7.4$ for air and $M \equiv m_e$ the electron mass. This expression produces a sideways displacement of $\sim d^2/0.662R$ and on including the forementioned geometrical factor, the expected displacement (X mm) is given by:-

FIG 4.18 : GEOMETRICAL CONTRIBUTION TO WIDTHS OF DRIFT TIME DISTRIBUTIONS

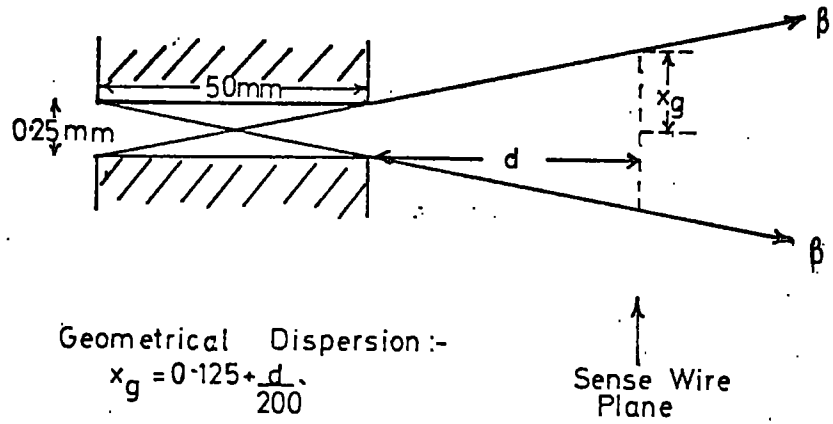

Geometrical Dispersion :-

$$x_g = 0{\cdot}125 + \frac{d}{200}$$

FIG 4.19 : VARIATION OF F.W.H.M. OF PEAKS WITH DISTANCE FROM SLIT

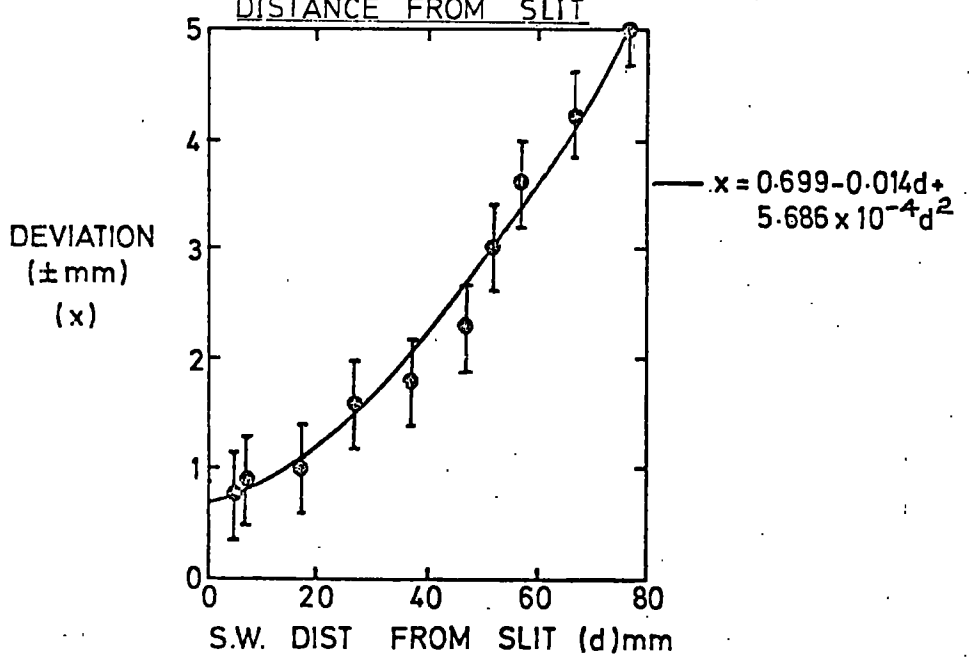

FIG 4.20 : COMPARISON WITH SCATTERING OF VARIOUS-ENERGY ELECTRONS

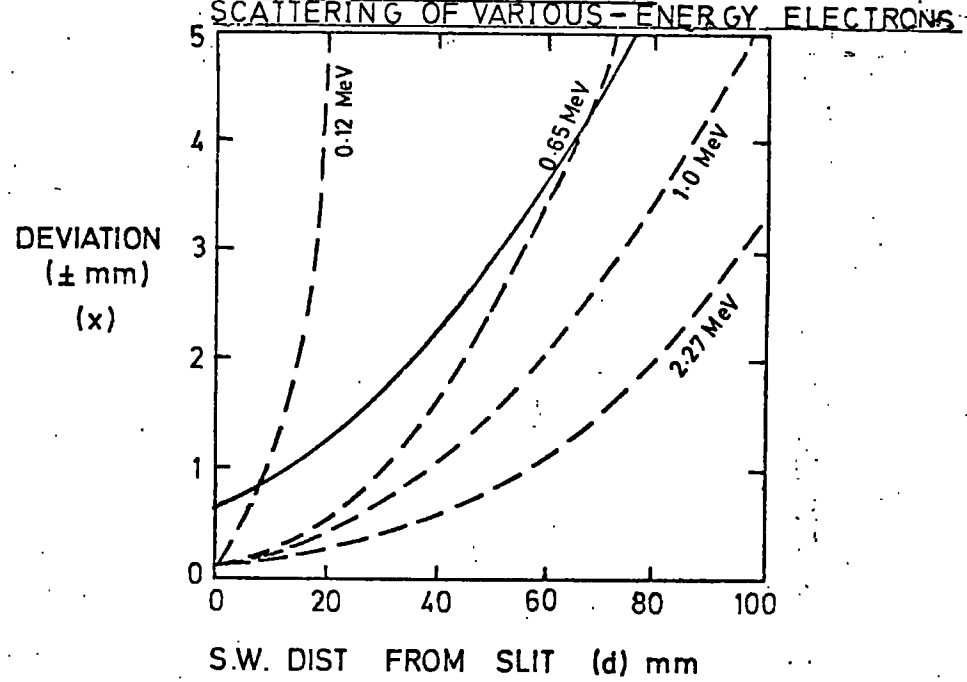

$$X = 0.125 + \frac{d}{200} + \frac{d^2}{0.662R} \qquad (4.3)$$

Figure 4.19 shows the variation of F.W.H.M. with d, the line being a least squares fit to the function $X = a_0 + a_1 d + a_2 d^2$. Figure 4.20 compares the fit to the predicted scattering curves for electrons of energy up to 2.27 MeV (the cut off for the Sr90 spectrum). An extrapolation of the fit to d = 0 should yield a deviation corresponding to the slit width, however the failure to produce this result implies extra scattering which will certainly occur from the sides of the slit and is difficult to account for in these calculations. Extra contributions to the peak width are scattering in the air within the 50 mm long slit and from chamber wires and windows, plus the genuine timing jitter occurrent in the drift process itself. (The latter will be discussed in the next section.)

On normalising the fit at d = 0, a curve of similar form to the theoretical variations is obtained, whose mean value of R (determined from equation 4.3) corresponds to a particle of energy 0.8 MeV, which is a reasonable result on considering the β-spectrum from Sr90

Hence, the typical spatial resolutions observed ($\sim \pm$ 0.7 mm) using the system of figure 4.1, can be attributed mainly to the multiple scattering of the beam, and to measure the intrinsic resolution accurately, a high energy particle beam must be employed.

4.6.1 Diffusion and Other Contributions to the Time Spread

For this system, the following contributions (additional to the spread of the collimated beam) to the peak widths are present:-

a) Fluctuations in the primary ionization (statistical and dependent on energy) and initial track thickness (significant at low incident particle energies).

b) The diffusion of the electron swarm in the gas.

c) The mechanical alignment of the sense wire and its parallelism with the collimating slit.

d) Fluctuations in the H.T. voltage and gas composition.

e) Electronic processing and time measurement.

f) Random stops from γ's and cosmic rays.

a) and b) depend on the gas composition, c) and d) were limited as far as possible and little further control could be exercised over e) and f). As b) is a significant factor and instrumental in the choice of gas, diffusion will now be briefly discussed.

Equation 1.2 can be rewritten in terms of drift velocity, w:-

$$\sigma_X = \sqrt{2DX/w} \qquad (4.4)$$

D/w is high for Argon but can be reduced by the addition of an organic gas which effectively cools the electrons (reduces ϵ_K). Thus, for a particular beam position, any variation in peak width with gas composition must be due to the different values of diffusion, σ_X, produced.

This result is presented qualitatively in figure 4.21 for three of the gas mixtures tested. The variation of peak width with electric field shows a form similar to that of the data collected together by Rice-Evans (18), and can be explained in terms of equation 4.4 (ie. variation of w and ϵ_K with E). The Argon-Methane curve shows

FIG 4.21 Variation of Peak Width with Field

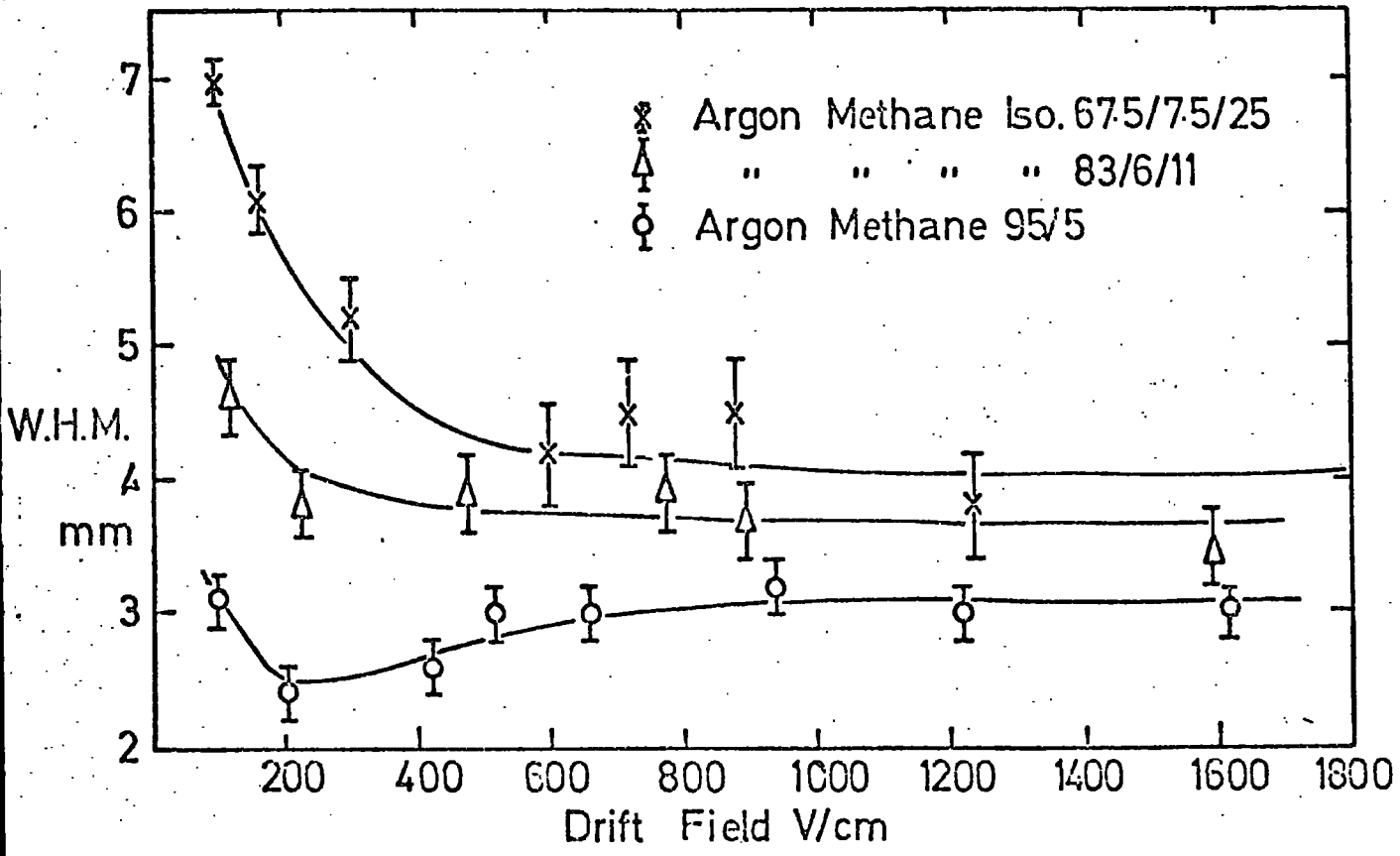

FIG 4.22 Variation of Peak Width with Drift Time

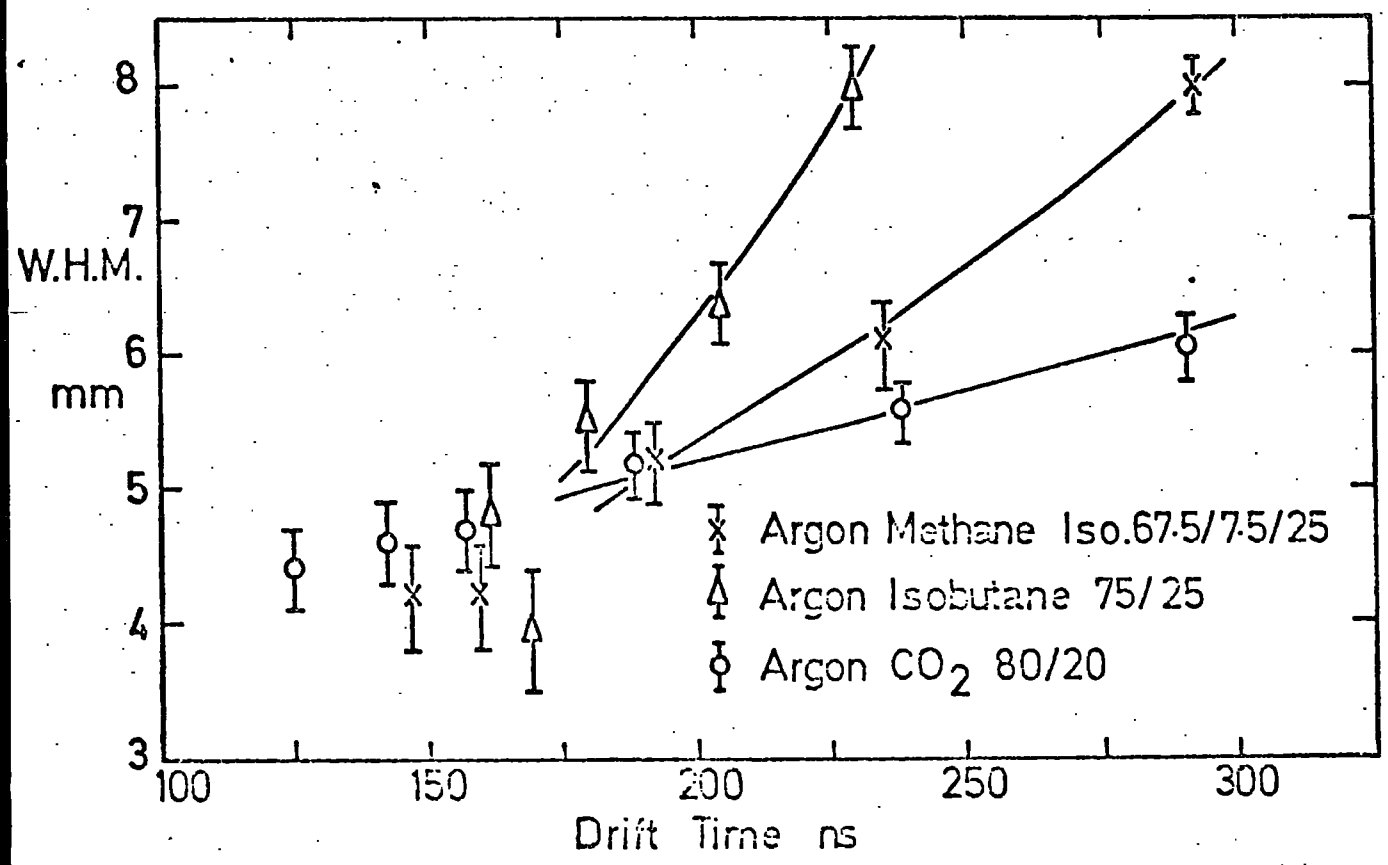

resolution typical of mixtures containing up to 10% Methane and in this respect is more suited to drift chambers than Argon-Isobutane. Equation 4.4 also implies that diffusion is proportional to $\sqrt{\text{time}}$ which is verified by a plot of peak width against drift time for three gases in figure 4.22. The diffusion with drift distance was found to be very small for Argon-Methane, this effect being swamped by the scattering in this system.

It should also be mentioned that the diffusion is partially responsible for the pulse shape at the sense wire and, as such, electronics should be designed to be sensitive to a few electrons (one if possible) in order to reduce the jitter caused by spread in rise times. The timing precision could be improved by detecting always the centroid of the swarm but this would require more sophisticated discrimination techniques than those normally employed.

4.7 Cosmic Ray Tests

A useful method of monitoring drift velocity throughout a cell is to use cosmic radiation (C.R.) (mainly high energy muons and electrons at sea level (20)) as a trigger source. Since the C.R. flux (dN/dx) over a drift chamber is essentially uniform, the distribution of drift times (dN/dt) measures directly the drift velocity (V_D) of the electrons as a function of total drift time ie.:-

$$\frac{dN}{dt} = \frac{dN}{dx} \cdot \frac{dx}{dt} \propto V_D(t) \qquad (4.5)$$

Figure 4.23 shows the results of two 70 hour exposures to C.R. of one horizontally-positioned cell of a g-2 chamber, the start

FIG. 4-23 DRIFT TIME DISTRIBUTIONS FROM COSMIC RAYS

a) DRIFT FIELD = 465 $V cm^{-1}$

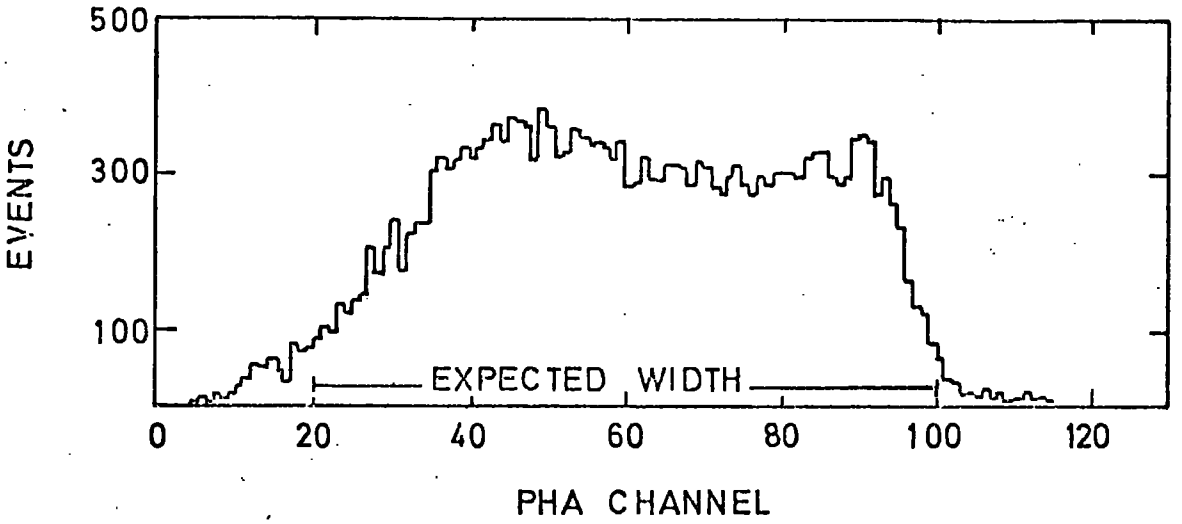

b) DRIFT FIELD = 593 $V cm^{-1}$

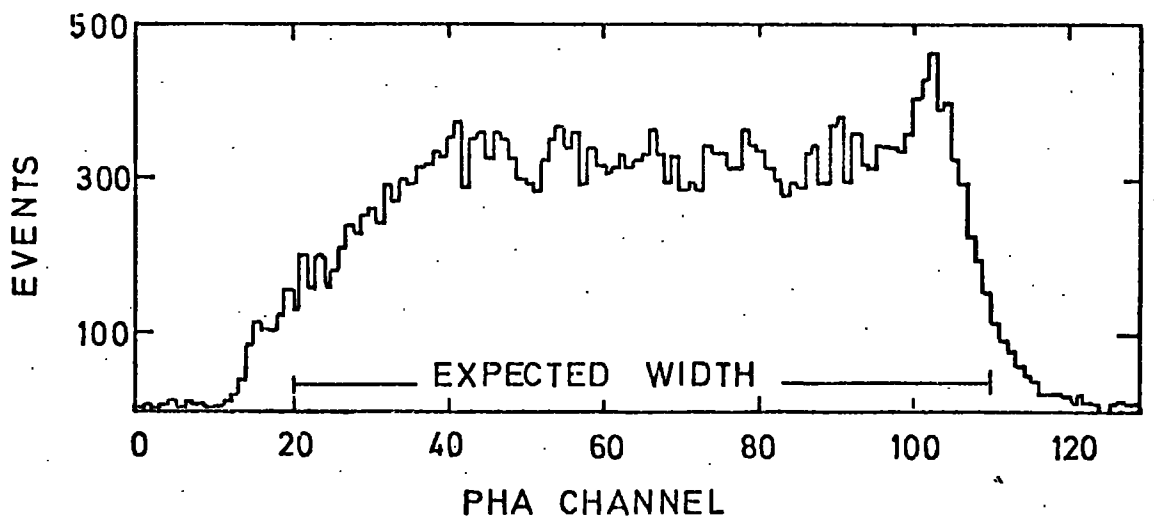

HORIZONTAL SCALE: 4·375 ns/CHANNEL

signals provided by a vertical scintillator telescope (ie. one scintillator above and one below the chamber, covering the whole cell area). Reasonably flat-topped distributions were obtained indicating uniform efficiency (also implying linear gain) and uniform drift velocity over most of the cell.

The spectra cut off edges were not as steep as initially expected and the following explanations are offered: At the field wire end of the distribution, this is probably due to the geometrical effect of angled tracks (13) which produces longer drift lengths, the cosine^2 angular distribution for cosmic rays (20) causing the gradual slope. The sloping edges of the spectra at short times are probably due to an inefficiency around the sense wire (see section 5.5.1) together with the low drift velocities of electrons in the high fields of this same region biasing the spectra towards slightly higher times. This latter effect may also be responsible for the slight peak observed at the beginning of the plateau (plus the fact that any random chamber pulses are likely to originate in the sense wire region). The peak at the other end of the plateau is probably due to field emission from the potential wire.

From previous measurements (figure 4.11) maximum drift times of 359 ns and 378 ns were predicted for fields of 465 Vcm^{-1} and 593 Vcm^{-1} respectively, these times representing well the distribution widths as indicated in figure 4.22.

This C.R. technique has been of importance in the testing of large experimental drift chambers (21).

4.8 Tests on the Curved End

The feasibility of creating a useful drift field in the

curved end region was first investigated using the small test chamber mentioned in section 3.1. Two extra H.T. wires were introduced into the chamber at a voltage 614 V greater than and at a distance 10 mm from the potential wire of one end of the cell (which supported a drift field of 602 Vcm^{-1}). Outside the other end of the cell, two curved electrodes constructed from 0.75 mm diameter tinned copper wire were connected at a distance of 4 mm from the potential wire, the curvature extending to a maximum distance of 10 mm from the cell; these were maintained at a voltage 614 V greater than that of the potential wire, thus producing drift fields between 614 and 1535 $V\ cm^{-1}$. The wire configurations are schematically illustrated in figure 4.24 where the results of a normal drift time-distance scan are presented. Linearity was observed outside the normal cell for both simulated curved end electrode configurations.

Figures 4.25 and 4.26 show the space-time relationships obtained for the prototype and production curved ends respectively, reasonable drift time linearity being recorded in the latter case, but the observation of sensitivity to the end of the chamber was not possible due to the absorption of the beam by the glC window supports.

These tests have shown that electrons can be drifted successfully in distorted shape electric fields thus allowing the curved end region of the g-2 chambers to be sensitive to traversing ionizing particles. The absolute efficiency in this region was difficult to measure due to the geometrical shape involved, and the resolution was at the most a factor of two worse than for the normal cell. The purpose of the curved end region is to provide some degree of sensitivity to electrons near the storage tank in the g-2 experiment and, although the performance of this region as a drift

FIG 4.24 DRIFT TIMES IN SIMULATED CURVED ENDS

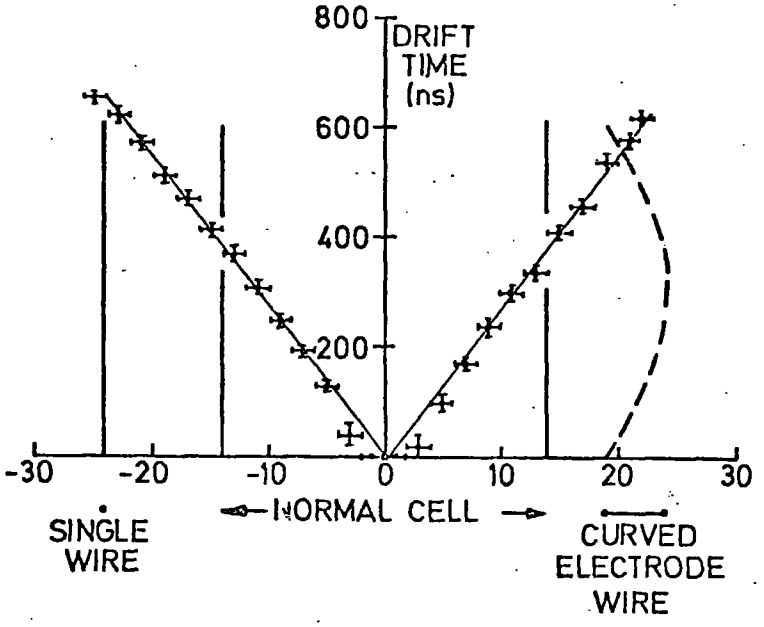

FIG. 4·25. DRIFT TIMES IN THE PROTOTYPE CURVED END.

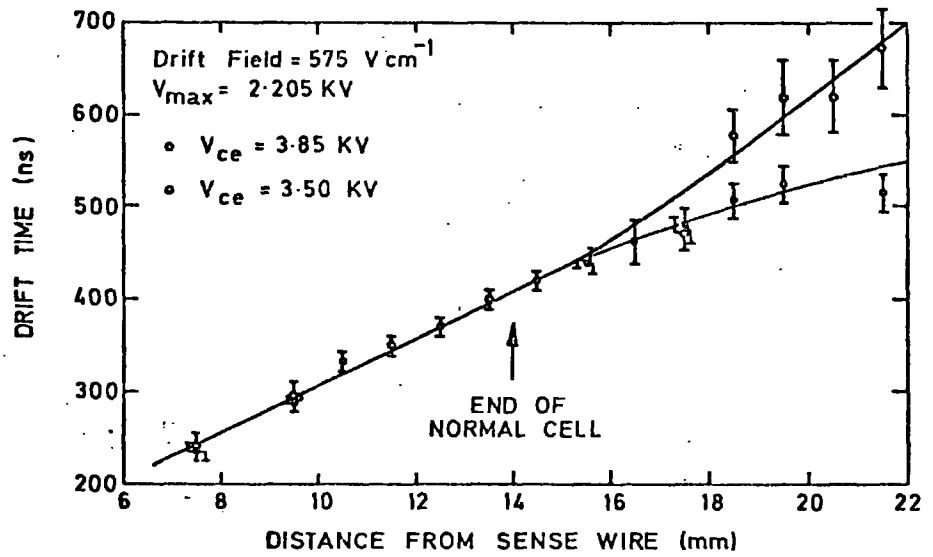

FIG. 4·26. DRIFT TIME VS. DISTANCE IN FINAL (TILTED) DRIFT FIELD SHOWING DRIFT TIMES IN CURVED END.

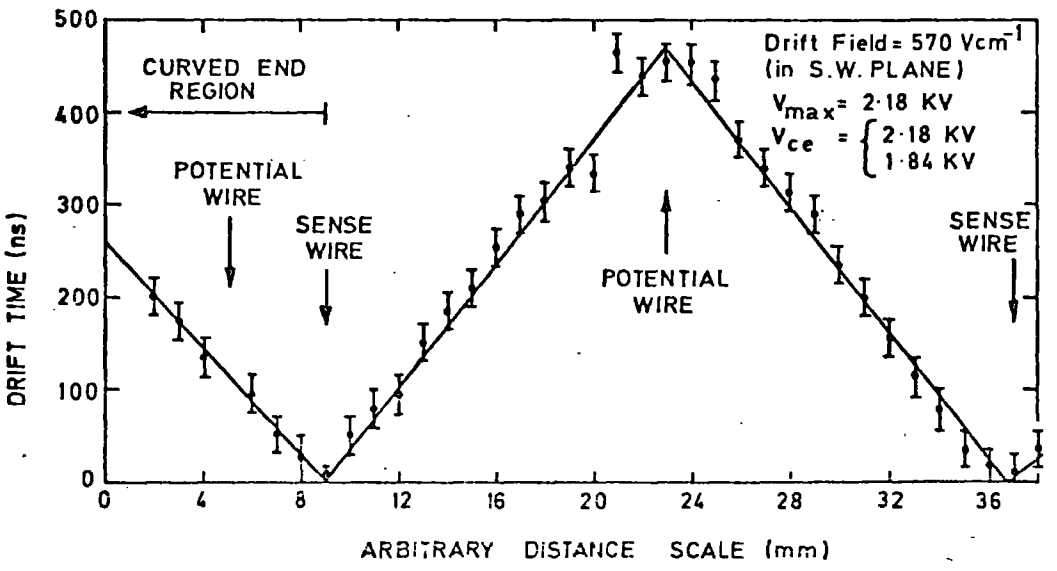

space is naturally not as good as that of the normal cell, results were nevertheless encouraging.

4.9 Other Parameters

The observed drift times in tilted electric fields are affected by the flow-line trajectories followed by the electrons. The operation of drift chambers in this mode (B = 0) is normally not of great significance and as such, discussion is left until chapter 6 where the similar situation of low B values is encountered, and results for B = 0 are presented in appendix 2. As well as the investigation of the curved end region, figure 4.26 also shows the space time relation across the final field configuration (45^{o} tilt of electric field) to be approximately linear.

Angled tracks are important in drift chambers. Consider the various trajectories of an infinitely narrow beam passing a fixed point in the sense wire plane as in figure 4.27, where the quantities l and d are defined. P and Q are the points where the semicircle, centre A and radius l/2 intersect the bottom H.T. plane. It is easy to see that for the beam intersecting this plane outside PQ (or for all tracks when $d \leq l/2$) the closest approach distance (X) of a track to the sense wire is given by:-

$$X = l \cos\Theta \qquad (4.6)$$

where Θ is the angle of the beam. For intersection between P and Q we have:-

$$X = \sqrt{l^2 + d^2\sec^2\Theta - 2ld \tan\Theta} \qquad (4.7)$$

FIG. 4.27 Construction for angled tracks

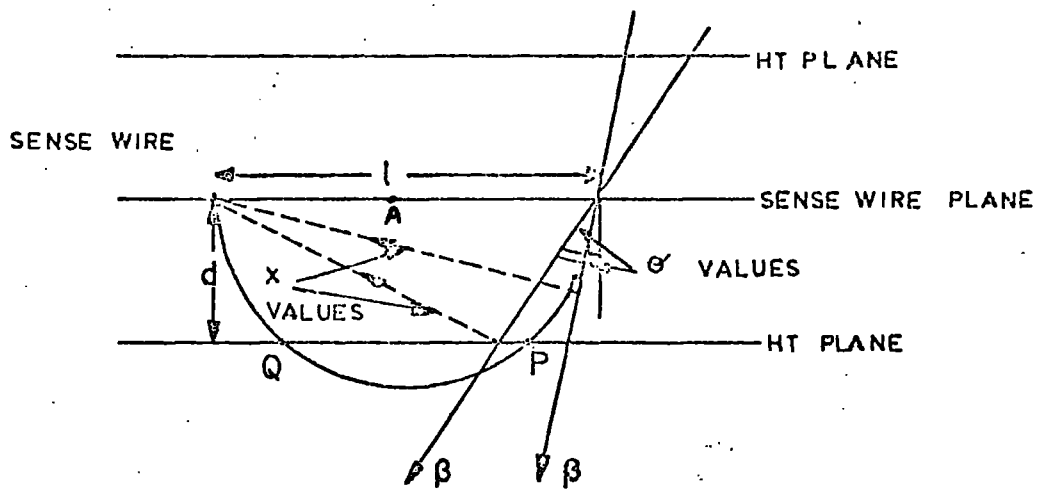

FIG. 4.28 Drift time distribution for various track angles (horizontal scale: 4.375 ns/channel)

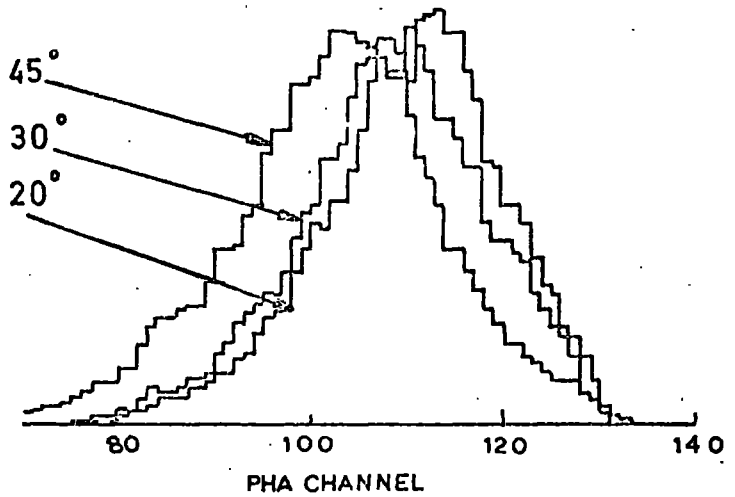

FIG. 4.29 Drift time Vs' track angle (vertical scale: 8.75 ns/channel)

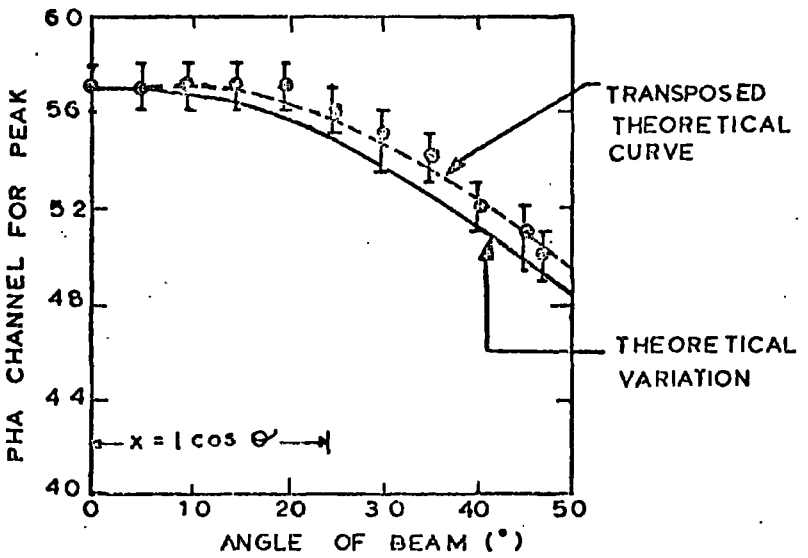

As an example, the system of figure 4.1 was arranged so that the chamber could be rotated about a point 8 mm from the sense wire, (ie. l = 8, d = 3) and the beam passed through this point. The time distributions obtained for various values of Θ are shown in figure 4.28 and indicate the expected movement towards shorter drift times as Θ increases. Figure 4.29 shows the experimental variation of drift time with angles up to 47^{o} and the estimated curve from equations 4.6 and 4.7. The discrepancy is most certainly due to the flow-line trajectories followed rather than the direct paths (a transposed theoretical curve fitting the data well), thus the angle effect is reduced in practice. Also, no serious deterioration in resolution with angle has been observed (1).

Since this work, extensive data on angled trajectories has been published (12), and although the above example has not considered the effect of varying l, it has been illustrated that angle effects will be minimal for g-2 electron tracks.

The multitrack resolution and depreciation in pulse height and efficiency at high particle rates has been studied at CERN (6) and is a significant aspect of drift chamber operation in high energy physics. However, no attempt to pursue this work has been made in this project as this is not a problem in g-2.

4.10 Conclusion

The prototype chambers have been successfully operated in source and cosmic ray tests and the capabilities of a test system designed for a laboratory have been investigated. Resolutions of the order ± 0.7 mm have been observed with most of the spread accounted for in the multiple Coulomb scattering of source electrons.

A mixture of 90% Argon and 10% Methane has been chosen as a working gas for the final g-2 chambers, this showing favourable properties of pulse height, efficiency, diffusion and magnitude and stability of drift velocity.

An applied drift field of 600 Vcm^{-1} (~850 Vcm^{-1} on considering the final field tilt) has been chosen as a satisfactory parameter regarding space-time linearity, saturation of drift velocity and good gain, without any appreciable breakdown or need for excessive voltages. Pulse height and efficiency tests have enabled the complete final design of the H.T. parameters.

Discrimination levels compromising between the requirements of sensitivity to one drift electron and the reduction of noise have been selected, these corresponding to a threshold at ~7% of the signal maximum.

A brief investigation into angled tracks has been made and the curved end region has been successfully made a sensitive drift space.

Finally, the drift velocity characteristics of a selection of gases have been measured and explanations have been offered for any effects apparent during these tests.

References

1 R. Browell, K.A. Short. Durham University Internal Report, NI-74-2

2 J.E. Bateman, J.F. Connolly. Rutherford Laboratory Internal Report, RL/75/044, February 1975

3 M.E. Rose, S.A. Korff. Phys. Rev. 59 (1941) 850

4 G.A. Erskine. Nucl. Inst. Meth. 105 (1972) 565

5 Radiochemical Centre Handbook. 1974/5 35

6 A. Breskin, G. Charpak, F. Sauli, M. Atkinson, G. Schultz. Nucl. Inst. Meth. 124 (1975) 189

7 R. Browell. Ph.D. Thesis, University of Durham, in preparation

8 R. Browell, K.A. Short. Durham University Internal Report, NI-74-3

9 W.N. English, G.C. Hanna. Canadian Journal of Physics, 31 (1953) 768

10 V. Palladino, B. Sadoulet. Lawrence Berkeley Laboratory Internal Report, LBL-3070 (1974)

11 G.S. Hurst, J.A. Stockdale, L.B. O'Kelly. Journal Chem. Phys. 38 (1963) 2572

12 G. Charpak. Proc. Int. Conf. Instrumentation for High Energy Physics, Dubna, (1970), 227

13 A. Breskin, G. Charpak, B. Gabioud, F. Sauli, N. Trautner, W. Duinker, G. Schultz. Nucl. Inst. Meth. 119 (1974) 9

14 R. Bouclier, G. Charpak, Z. Dimkovski, G.Fischer, F. Sauli. Nucl. Inst. Meth. 88 (1970) 149

15 A.H. Walenta, J. Heintze, B. Schürlein. Nucl. Inst. Meth. 92 (1971) 373

16 G. Charpak, G. Fischer, A. Minten, L. Neumann, F. Sauli, G. Flügge, C. Gottfried, R. Tirler. Nucl. Inst. Meth. 97 (1971) 377

17 E.W. McDaniel. Collision Phenomena in Ionized Gases, (J. Wiley) 1964, Ch. 4

18 G. Charpak. Proceedings of the Workshop on Research Goals for Cosmic Ray Astrophysics in the 1980's, Frascati, 1974

19 P. Rice-Evans. Spark, Streamer, Proportional and Drift Chambers, (Richelieu Press) 1974, Ch. 10

20 A.W. Wolfendale. Cosmic Rays, (Newnes) 1963

21 D.C. Cheng, W.A. Kozanecci, R.L. Piccioni, C. Rubbia, L.R. Sulak, H.J. Weedon, J. Whittaker. Nucl. Inst. Meth. 117 (1975) 157

CHAPTER 5

THE OPERATION OF DRIFT CHAMBERS IN AN ACCELERATOR BEAM

5.1 Introduction

This chapter describes the operation and performance of the g-2 drift chambers in the Daresbury Laboratory e^+ test beam. The main aims were to study chamber efficiency and resolution under various conditions of incident particle energy and external magnetic field strength.

Simple, straight-line track reconstruction in up to four chambers was carried out and the reproducibility of drift time measurements in Argon-Methane was investigated. Also, from these tests, information on the beam profile was forthcoming, such an exercise being useful as this is similar to the main function of the storage ring system.

5.2 The NINA Test Beam (1, 2)

The Daresbury test beam is a low intensity positron beam having a cross sectional spread in the experimental area of up to ~ 25 cm^2 and an available energy range up to 5 GeV with a spread of $\sim 1\%$ at any setting above say 1 GeV.

Positrons may be produced in two ways:-

a) Use of a "beam bump"; a pulsed magnet is used to deflect part of the hard core of the main circulating electron beam through a collimator and onto a tungsten target once every 60 cycles or more (a cycle occurring every 20 ms). Such an extraction occurs at the beginning of an accelerating cycle and hence only positron energies of up to $\sim$40% of "NINA" energy are obtainable. The advantage of this method is that high and controllable fluxes are obtained.

b) Parasitic extraction: this method involves allowing electrons at the edge of the circulating beam to impinge on the target after the main beam has been targeted elsewhere, advantages here being that the main user is not disturbed and energies up to almost maximum beam energy can be obtained.

After extraction by one of the above methods, the target produces a photon beam which is cleaned of charged particles and incident on a second target which produces e^+ e^- pairs (see figure 5.1). A momentum selection system comprising a H10 bending magnet and momentum slits follows. After this double conversion process, the resulting positron beam is channelled into the experimental area.

Most of the drift chamber tests were completed using the parasitic mode as only one event per extraction pulse could be obtained using beam bump and, for high fluxes, misrelated stops could occur.

5.3 Experimental Arrangements

The results presented in this chapter were taken over three Daresbury cycles, using a different system in each according to the availability of drift chambers at the time. Each system will now be described as this will indicate the type of testing which can be

IG 5.1 The Daresbury e^+ Testbeam Line and Drift Chamber Array

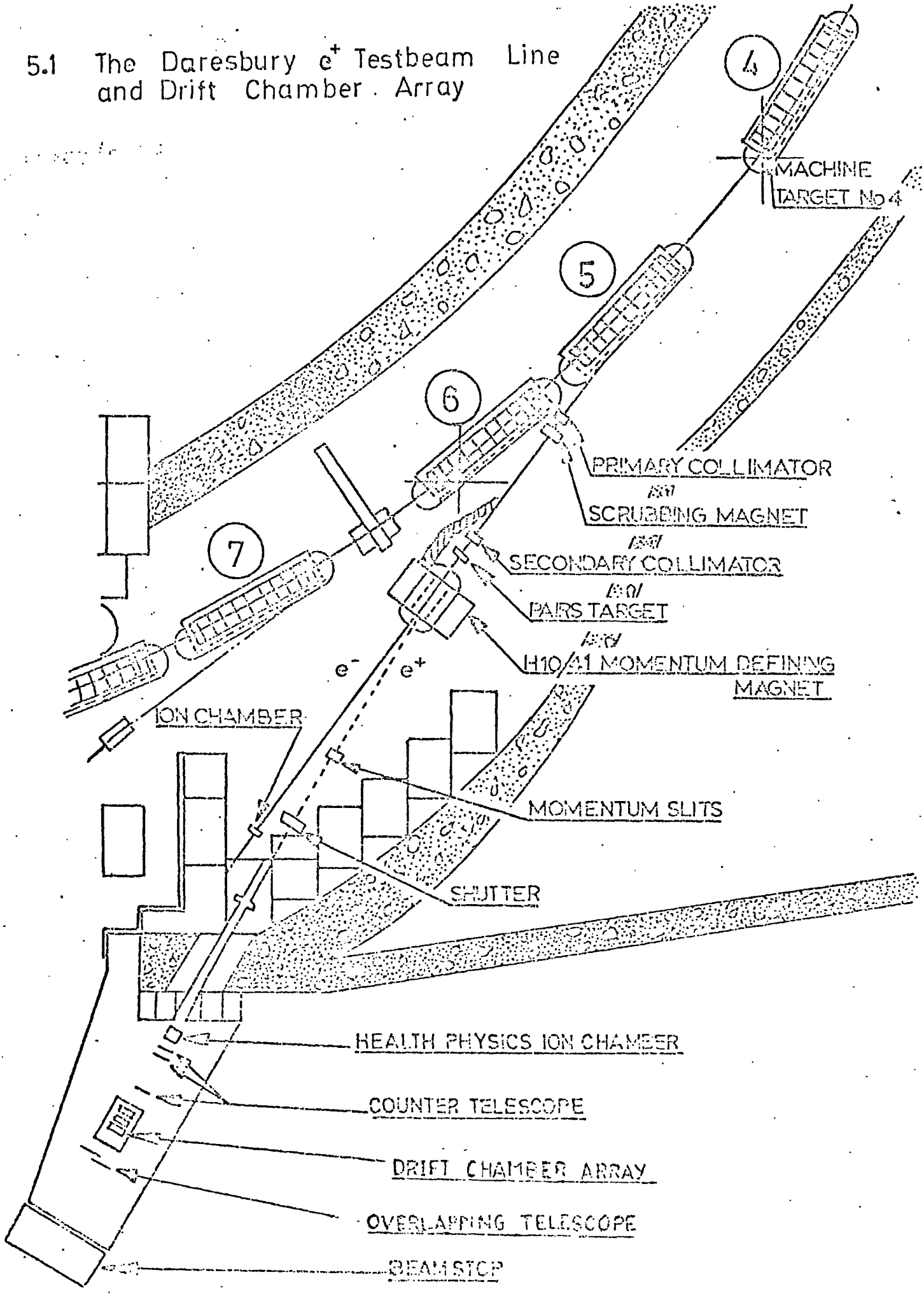

carried out, prior to installation in an experiment, using an accelerator facility and a limited number of chambers.

5.3.1 System 1

This system employed only the first prototype chamber with two finely-overlapped scintillators as an event trigger. Drift time measurement was achieved using a T.A.C. and P.H.A. as in the Durham tests and the data acquisition system is shown in figure 5.2, an event being signified by S1, S2, S3, S4 for example. Thus a beam as narrow as the overlap (a) of scintillators S3 and S4 can be selected and it is this value which is the limiting factor in resolution determination, in this case mainly due to the non-parallelism of the scintillator edges. The setting up and alignment of this system has been documented in detail (3) and it was eventually found that a best resolution of $\pm$ 0.4 mm was possible.

Such an arrangement is, however, useful for measuring variation in resolution with energy, and is ideal for efficiency and drift velocity measurements.

5.3.2 System 2

This system comprised three prototype chambers mounted on a rigid baseplate and carefully aligned using a system of fiducials and a theodolite. The alignment method, gas and electrical supply systems are described elsewhere (4), and the experimental arrangement is shown in figure 5.3. Note that different high voltage supply values were involved, this being due to the different resistor network configurations of the various prototypes. However, resultant variations in drift velocity were estimated to be less than 0.39% (4).

FIG. 5.2 : Data Acquisition System for One Chamber (System 1)

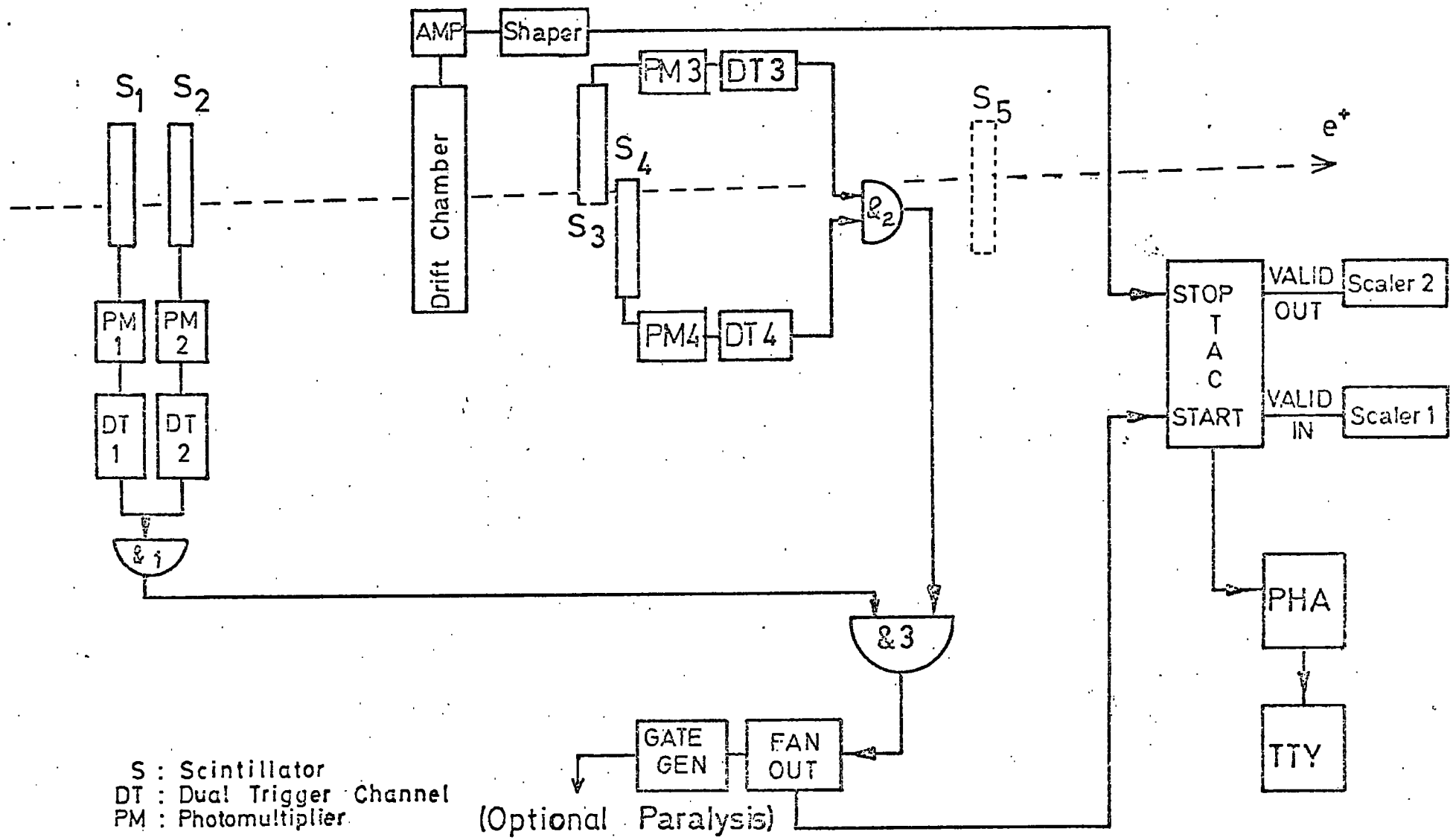

S : Scintillator
DT : Dual Trigger Channel
PM : Photomultiplier

FIG. 5.3 EXPERIMENTAL ARRANGEMENT FOR 3 CHAMBERS (SYSTEM 2)

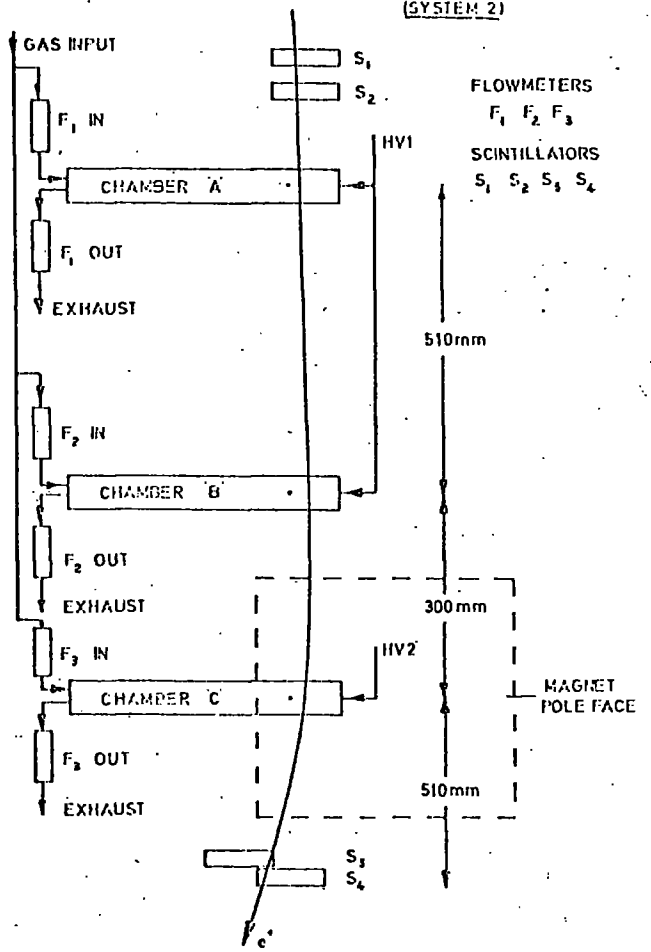

FIG. 5.4 DATA ACQUISITION SYSTEM (SYSTEM 2)

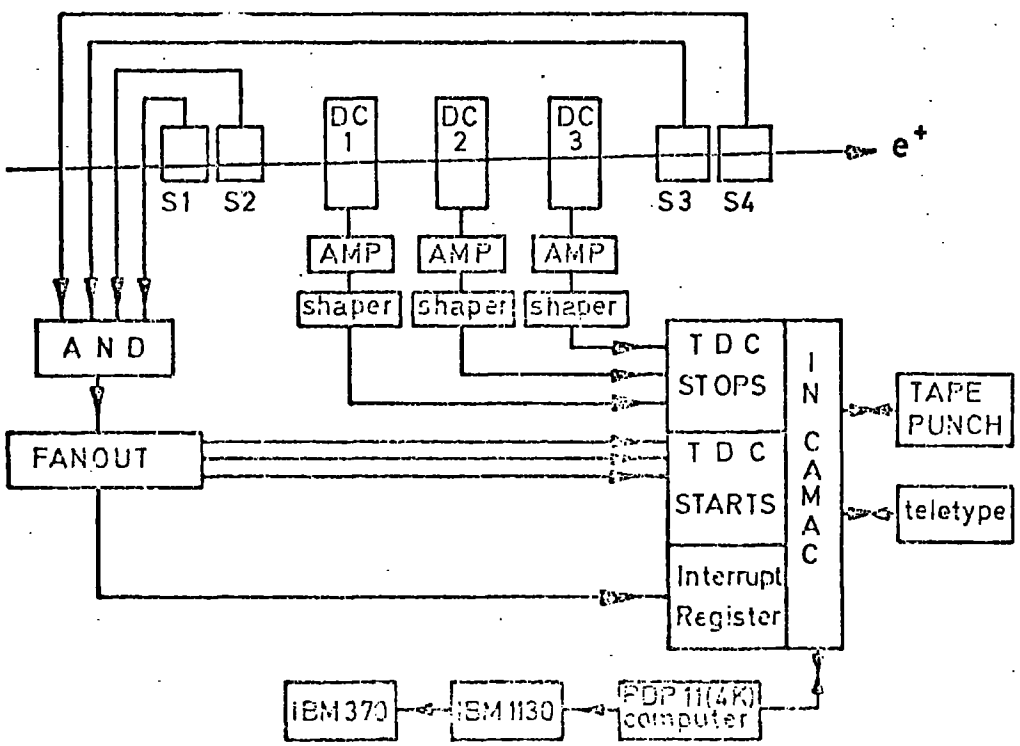

The left-right ambiguity was reduced by careful telescope alignment.

Figure 5.4 shows the data acquisition system used. Timing was achieved by a Lecroy quad T.D.C. unit in CAMAC, starts being provided by a scintillator telescope (which also provided an interrupt signal to initialise the CAMAC) and stops by shaped drift chamber pulses. Data acquisition was controlled by a programme written in CAT 11 language (a modified form of BASIC developed at Daresbury) and stored in a PDP 11 (4K) computer, the method of doing this being set out in figure 5.5. Data blocks were transferred to an IBM 1800 and then to an IBM 370 computer where initial online analysis was carried out using a FORTRAN IV programme and storage onto magnetic tape achieved (4).

The main objectives of the tests performed using this system were to determine the resolution of the chambers and to observe qualitatively their operation in a magnetic field. Due to availability of electronics, one cell in each chamber was used.

The magnetic field was provided by a C 13.5 electromagnet, manufactured by Lintott Engineering Co. Ltd. and was capable of producing fields up to 8 KGauss. A Hall probe field map at a current of 375 Amps is shown in figure 5.6 (a) and represented graphically in figure 5.6 (b). It can thus be seen that the connected sense wire of the chamber between the magnet pole pieces was in a position of reasonably uniform field.

5.3.3 System 3

The final system consisted of four production model chambers, with the aims of checking spatial resolutions and performance of all cells before installation at CERN. The mechanical support system was

FIG.5.5 COMPUTER FLOW DIAGRAM (SYSTEM 2)

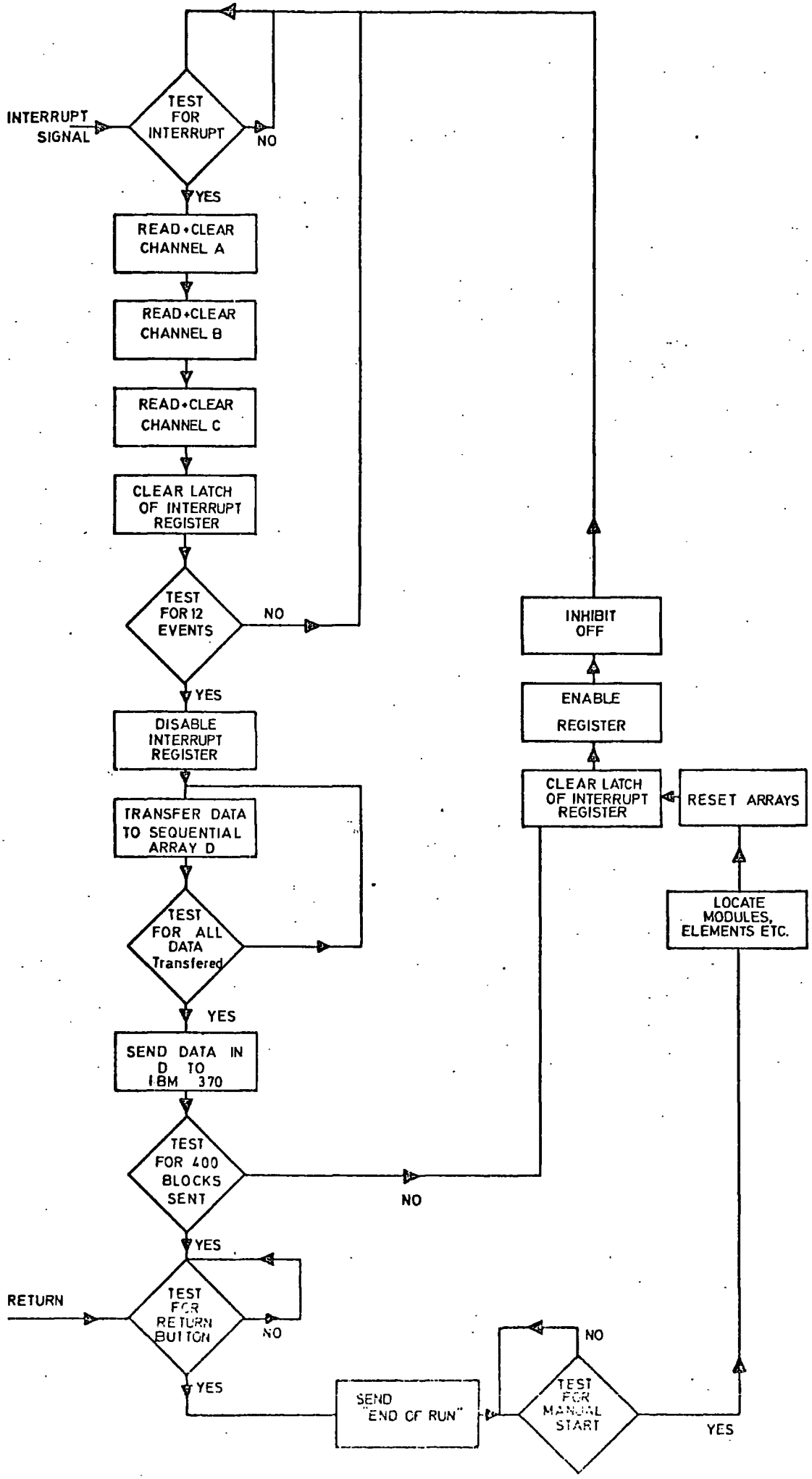

FIG.5.6a FIELD MAP

BACK OF MAGNET	A	B	C	D	E	F	G
1	1·7	2·8	2·9	2·7	2·0	1·3	0·5
2	3·6	5·4	5·9	5·5	4·2	2·2	0·8
3	5·2	7·2	7·6	7·4	5·8	2·8	1·1
4	5·8	7·6	7·8	7·6	6·1	3·1	1·2
5	5·5	7·0	7·7	7·4	5·8	2·9	1·1
6	4·2	5·9	6·3	6·1	4·6	2·3	0·9
7	2·0	2·9	3·3	3·1	2·4	1·2	0·5
8	0·7	1·2	1·3	1·2	1·0	0·6	0·3
9	0·2	0·4	0·5	0·4	0·3	0·2	0·1
10	0·0	0·1	0·2	0·2	0·1	0·1	0·0
11	0·0	0·0	0·0	0·0	0·0	0·0	0·0

Pole face perimeter

Position of SW

SCALE : 5 cm

CURRENT : 375 Amps

FIELD VALUES IN KGAUSS

e^+

FIG.5.6b MAGNETIC FIELD VS POSITION

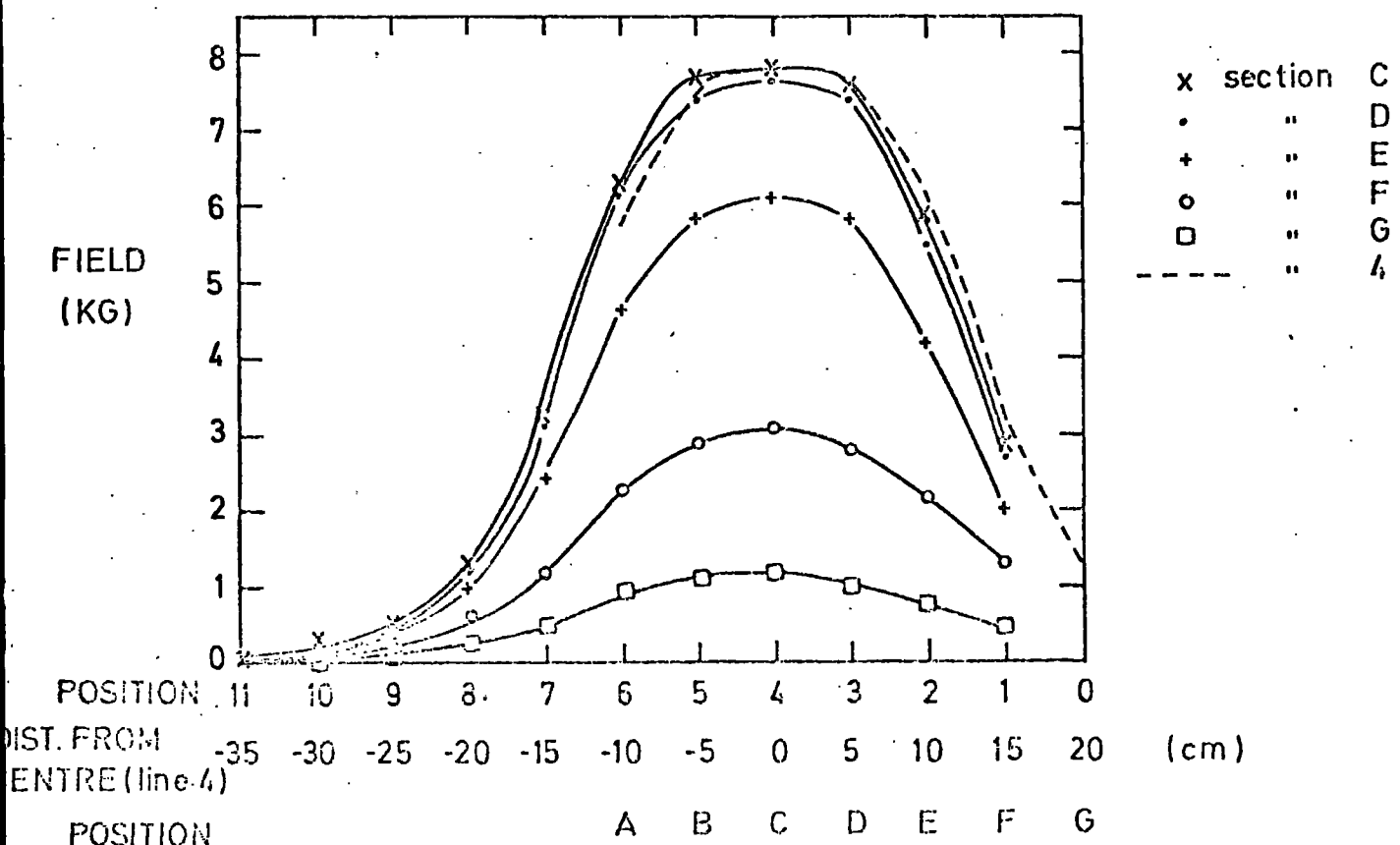

built and the electronic processing system was designed to simulate as closely as possible the intended g-2 drift chamber system, and the left-right ambiguity could be resolved in this case by staggering alternate chambers by a half cell width. The data acquisition was similar to that of system 2 with the following modifications:-

32 channels of Lecroy discriminator and T.D.C. (octal units) were connected.

The acquisition programme was written in PAL 11 (a modified form of ASSEMBLER) and stored in an 8K PDP 11.

Event blocks were larger and the system of writing data to magnetic tape was improved.

5.3.4 Additional Remarks

In all systems, chamber pulse amplification was achieved using Verweij-designed circuits as previously mentioned and logic processing was by means of E.G. and G. modular electronics.

Timing units were calibrated using a system comprising a pulse generator, variable delays and a P.H.A. and, where applicable, software corrections were applied to the data. Careful matching of cable lengths was ensured for all systems. The gas was, in all cases, premixed Argon (90) Methane (10) mixture with flow through the chambers in a parallel sense, as indicated in figure 5.3 for example.

For systems 2 and 3 the applied drift field was kept at $\sim 600\ Vcm^{-1}$

5.4 Experimental Procedure and Analysis

For system 1, drift time distributions were obtained on a P.H.A. as in chapter 4 and data was transferred to a teletype for

hand analysis. Various efficiency measurements were recorded using a 1.0 μs gate provided by the T.A.C., an efficiency being determined from the ratio scalar 2 reading : scalar 1 reading in figure 5.2. These are discussed shortly.

For systems 2 and 3, digitized drift times were stored on magnetic tape for various configurations of geometrical positioning, positron energy and values of electric and magnetic fields. Run lengths were typically of size 8,000 events for system 2 and 30,000 events for system 3 and, after consideration of various inefficiencies, some 2 million positron tracks were collected in this manner. Again, chamber efficiencies could easily be monitored.

Final data analysis was carried out on the Daresbury IBM 370 and the Durham IBM 360 computers using programmes written in FORTRAN IV.

5.5 Experimental Results

5.5.1 Efficiency Measurements

Using system 1, the ratio S3, S4, C : S3, S4 yields an approximation of chamber efficiency and, in this way, the efficiency versus H.T. voltage applied to the chamber was investigated. Figure 5.7 shows this variation for several values of final resistance (R_E) to earth in the prototype resistor chain described previously. High efficiency is obtained at a lower V_{MIN} value as the drift field is increased (R_E-value decreased), this being in accordance with the pulse height curves of figure 4.2. These measurements were made for a scintillator overlap of 10 mm and a beam energy of 600 MeV.

Note that the plateau level is $\sim$ 85%. The reason this is not 100% is clearly shown in figure 5.8, where efficiency is plotted

FIG 5.7 EFFICIENCY (UNNORMALIZED) VS VOLTAGE.

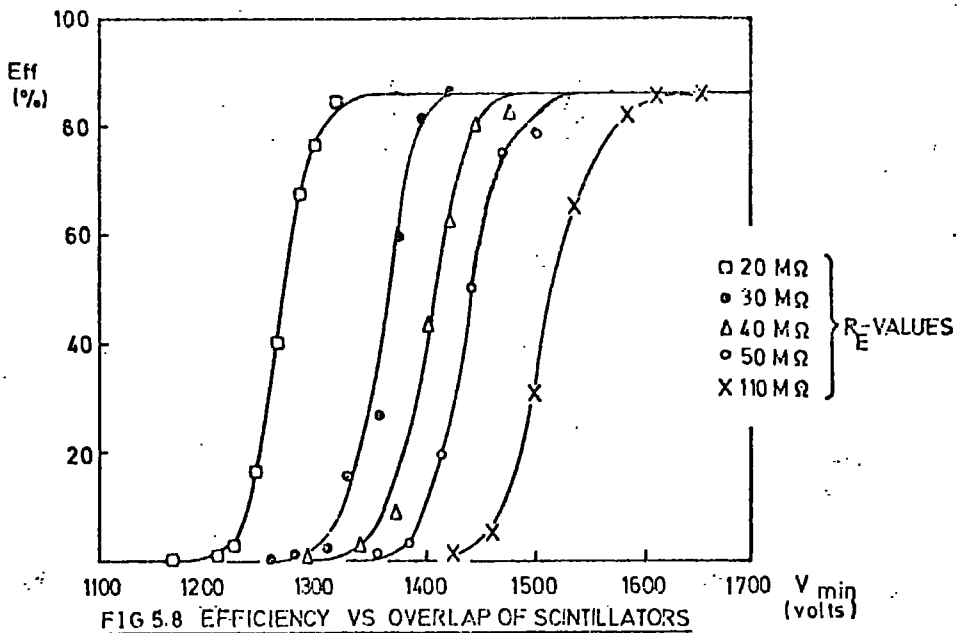

FIG 5.8 EFFICIENCY VS OVERLAP OF SCINTILLATORS

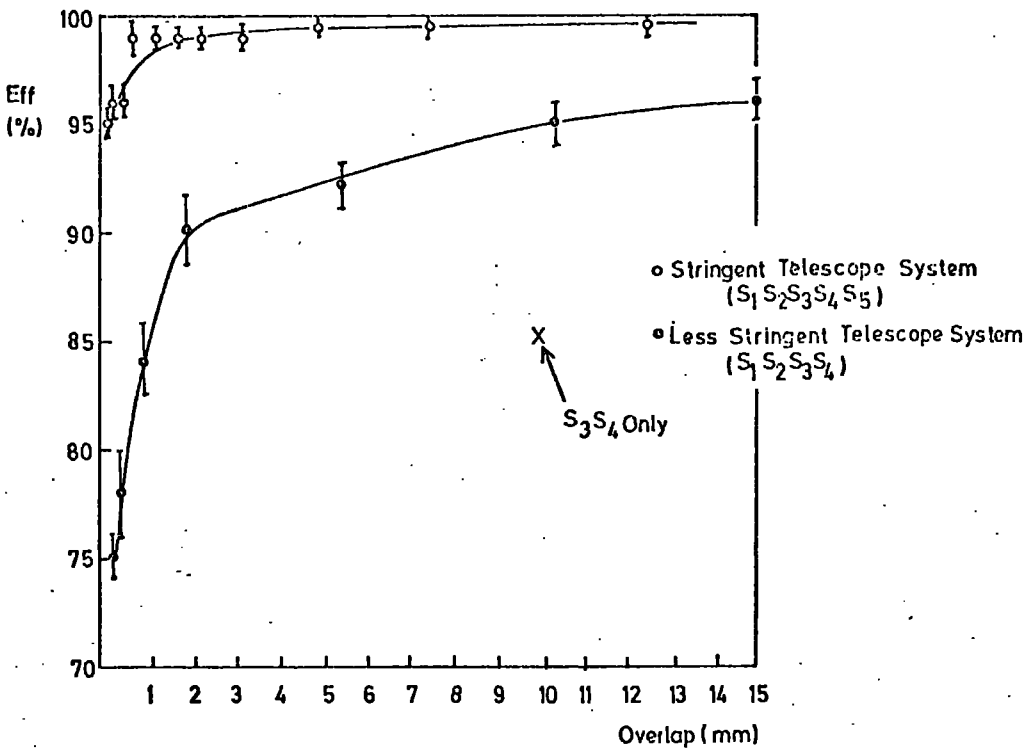

FIG 5.9 EFFICIENCY SCAN ACROSS SENSE WIRE

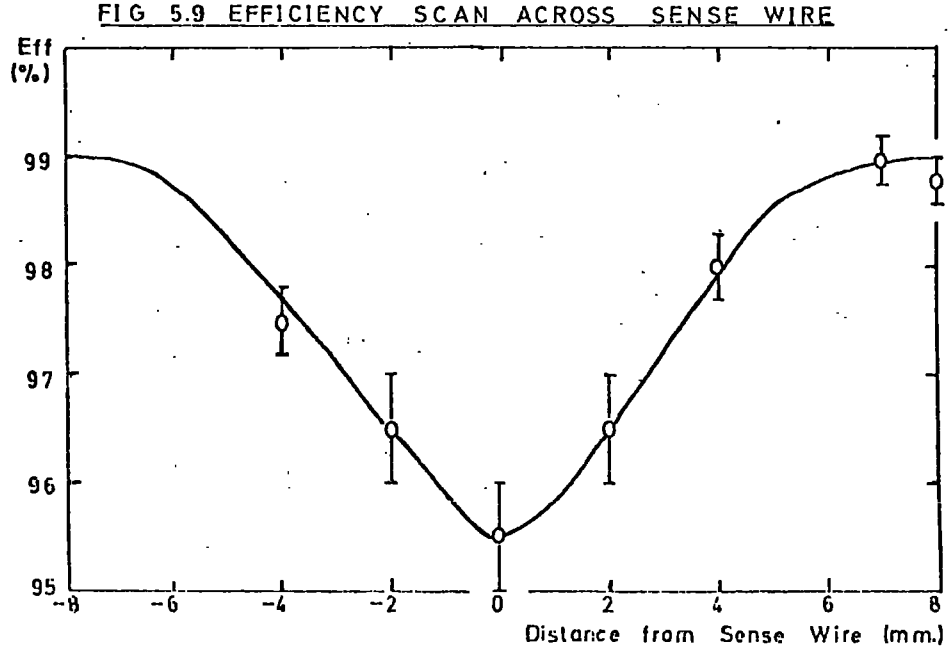

against overlap, a, for different telescope systems. Noise pulses, scattered particles and showers can lead to random triggers, these effects being reduced by a stringent telescope system. For events triggered by S1, S2, S3, S4, S5 (where S5 was a scintillator placed downstream of S4) efficiencies of $>99.5\%$ were recorded (R_E = 30 MΩ, V_{MIN} = 1.403 KV). The efficiency fall-off at low values of a can be attributed to the greater significance of false starts at low event rates.

Figure 5.9 shows the results of scanning a 2 mm overlap across the centre of a cell and measuring efficiency at 2 mm intervals. The efficiency starts to fall at 6 mm on either side of the sense wire and reaches a minimum, of value 3.5% below the plateau, at the wire. This will be due mainly to the decrease in output pulse height towards the sense wire as already explained in chapter 4, thus causing an increase in the statistical number of pulses failing to cross the discriminator threshold. The effect will be enhanced by the finite width of the overlap. Note that the plateau value is only 99% because of the small overlap width in this case (see figure 5.8). This efficiency dip is small enough not to affect seriously the chamber performance.

Efficiencies were monitored by a programme during runs with systems 2 and 3 and were found to be mostly $>90\%$, also, efficiency decreases were observed with increasing event rate. This has been found by other workers (5, 6) and is another pulse height decrease effect, this time due to positive ion build up and subsequent avalanche paralysis. As the event rates in the g-2 experiment will be extremely low, such effects are not discussed in detail in this thesis.

Note that the previous two inefficiency effects are

indirectly sensitive to pulse discrimination level and hence can be minimised by increasing amplifier signal to noise ratio thus allowing lower thresholds to be set.

5.5.2 Drift Velocity Measurements

There are several ways of measuring drift velocity using a high energy particle beam:-

The easiest, but crudest method is to allow triggering particles to pass through the whole of a chamber cell, thus building up a square-edged time distribution (as observed previously using cosmic rays) of which the width represents the maximum drift time. Hence a direct transformation to drift velocity can be made if linearity is assumed. This is the method which in fact will be used for final calibration in the muon storage ring.

A similar method to the laboratory technique described in chapter 4 can easily be applied using the overlapping scintillator system. Figure 5.10 shows the timing distributions obtained for various distances from the sense wire of the centre of a 0.25 mm overlap. Clear peaks of F.W.H.M. $\sim$ 35 ns are observed with a noise table of width (440 $\pm$ 30)ns representing in this case the maximum drift time, that is to say, a drift velocity of (31 $\pm$ 3)mm μs^{-1}. This result was achieved with a drift field of 756 V cm^{-1} for which previous calibration has yielded a drift velocity of (33.0 $\pm$ 0.5)mm μs^{-1}.

Figure 5.11 shows the space-time characteristic obtained by scanning a 2 mm overlap between a sense wire and cell boundary when the drift field was as above. The gradient yields a drift velocity value of (33.4 $\pm$ 1.4)mm μs^{-1}, comparing favourably with the

FIG 5.10 DRIFT TIME DISTRIBUTIONS FROM SYSTEM 1
(distances from sense wire shown)

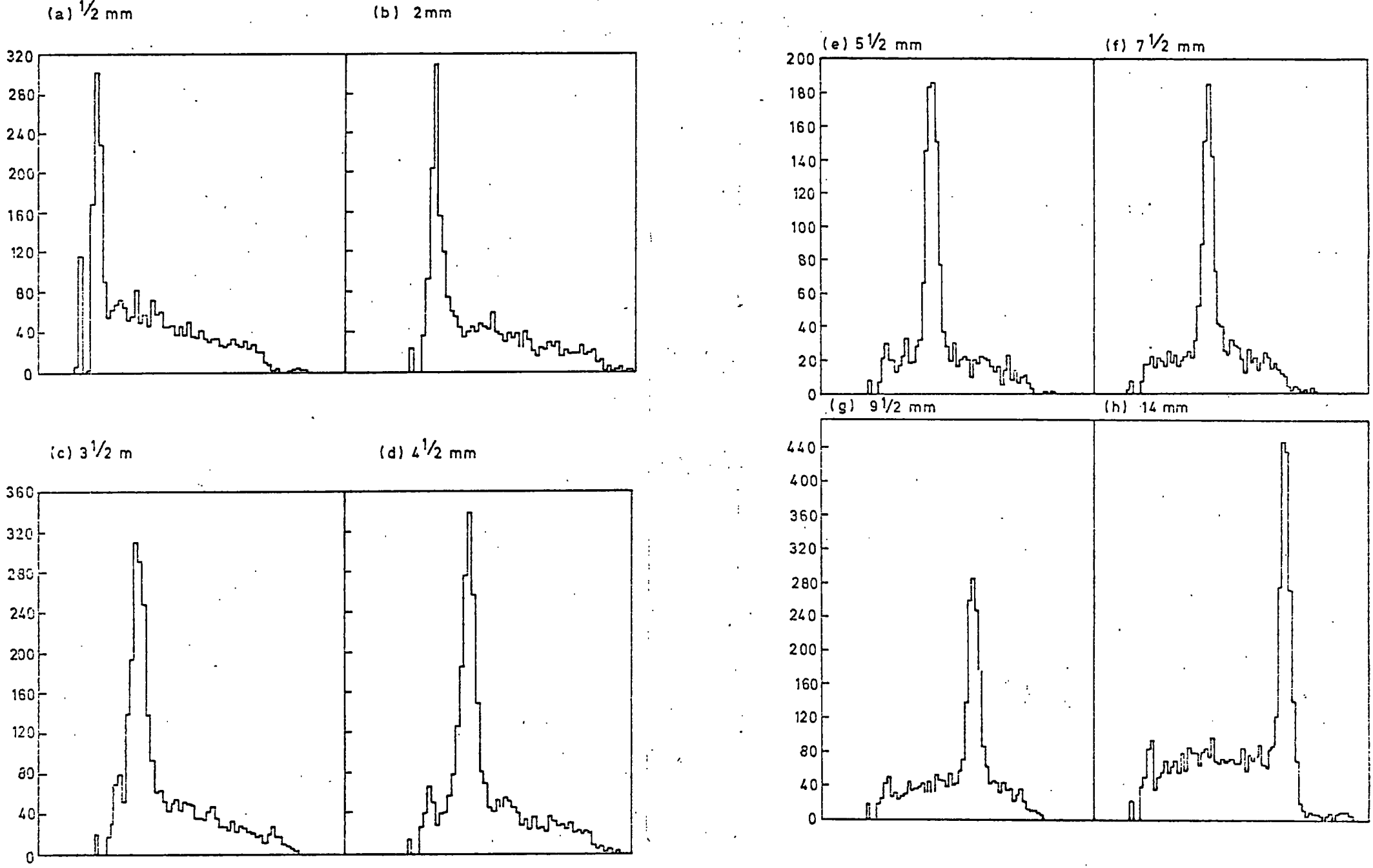

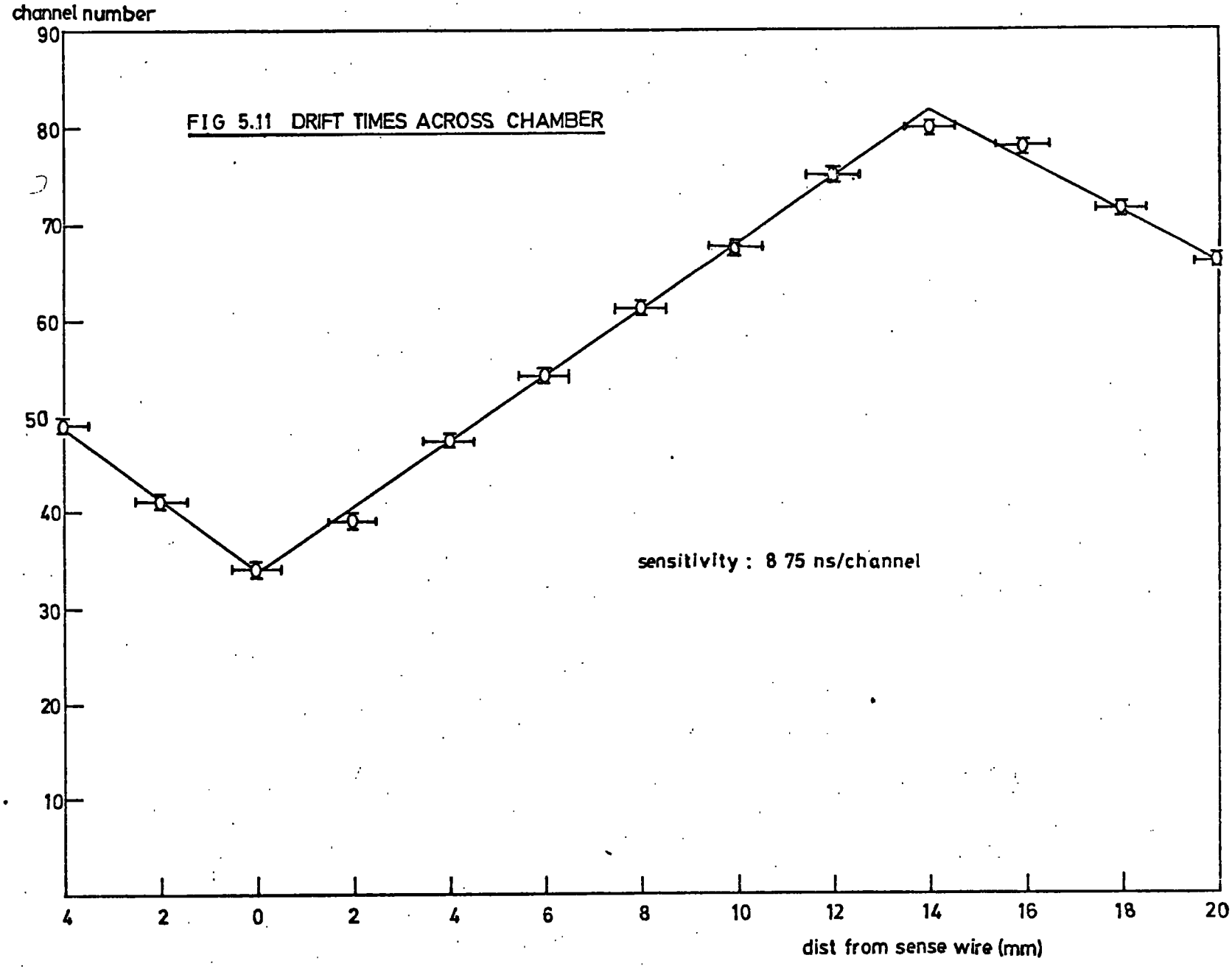
channel number
90
80
70
60
50
40
30
20
10
FIG 5.11 DRIFT TIMES ACROSS CHAMBER
sensitivity : 8 75 ns/channel
4
2
0
2
4
6
8
10
12
14
16
18
20
dist from sense wire (mm)

laboratory-determined value.

Returning to the first idea of measuring cutoff edges in timing spectra, the overlapping scintillator system provides another convenient method of drift velocity measurement; that is, to vary the overlap width and measure the observed time spectrum width. Examples of such distributions are shown in figure 5.12 and the estimated widths are plotted in figure 5.13. The line represents the values predicted from a previous knowledge of drift velocity, again showing the reproducibility of such results.

The maximum drift time can be measured using three, equally separated chambers alternately staggered by a half cell width as shown in figure 5.14. This quantity (T) given by :-

$$T = (T_1 + T_3 + 2T_2)/2 \qquad (5.1)$$

was histogrammed and produced a distribution of FWHM 30 ns (68% of data lying between ± 17.5 ns) and peaking at (373 ± 25)ns (the error also taking into account photomultiplier delay) as observed in figure 5.15. Thus, an estimate of drift velocity of (37.5 ± 2.5)mm μs^{-1} was yielded, to be compared with a previous value of (35.5 ± 0.5) at this particular field.

Figure 5.16 shows the method employed by Charpak et al. (5) to measure drift velocity for various electric and magnetic field configurations. This method involves electronically selecting, using drift chambers, two narrow, parallel beams, and passing these through the centre of the drift space of a chamber undergoing test. Drift times from the latter appear as two distinct distributions, the separation of the peaks permitting a measurement of drift velocity.

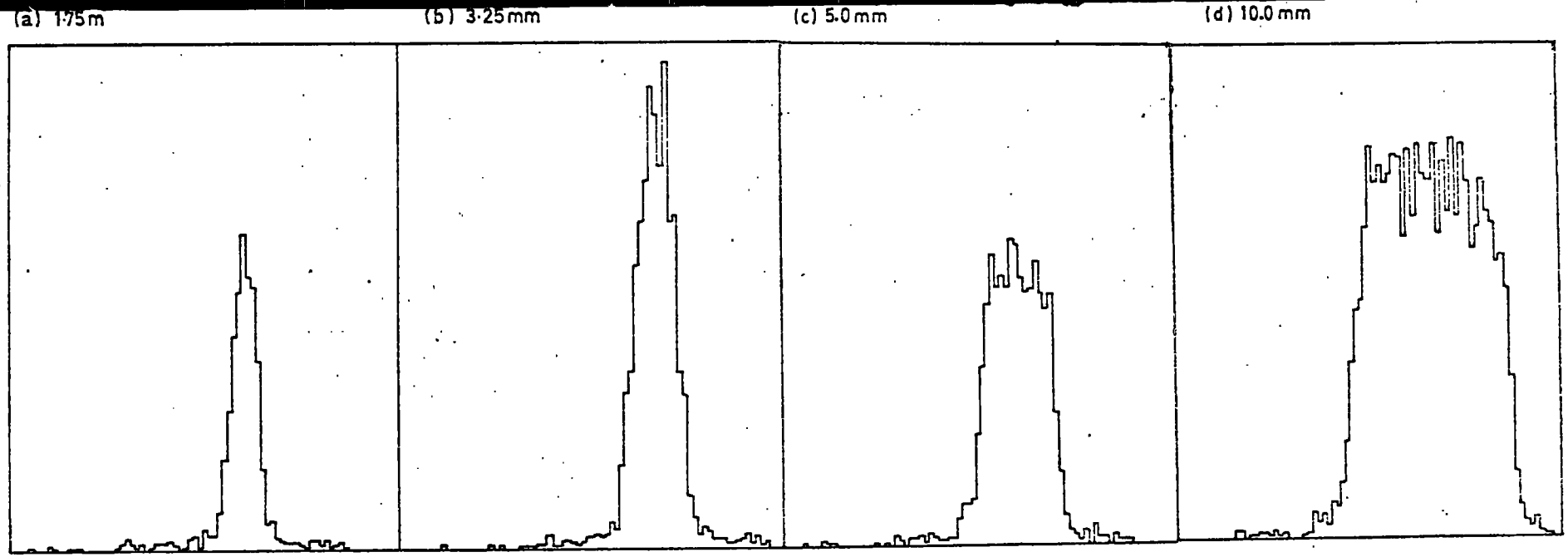

FIG 5.13 Width of distribution VS overlap set.

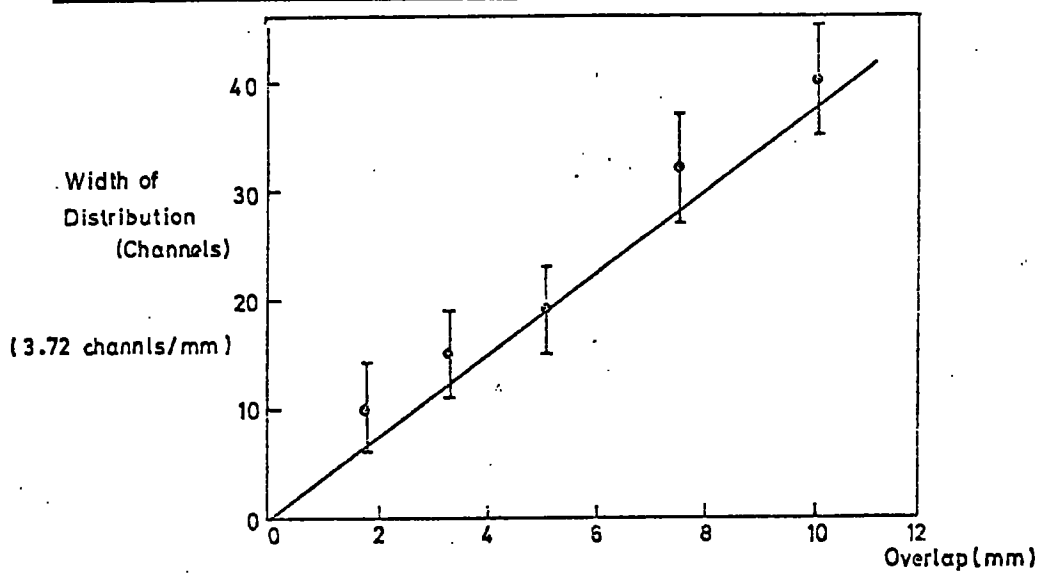

FIG 5.14 ARRANGEMENT FOR MEASURING MAXIMUM DRIFT TIME (T)

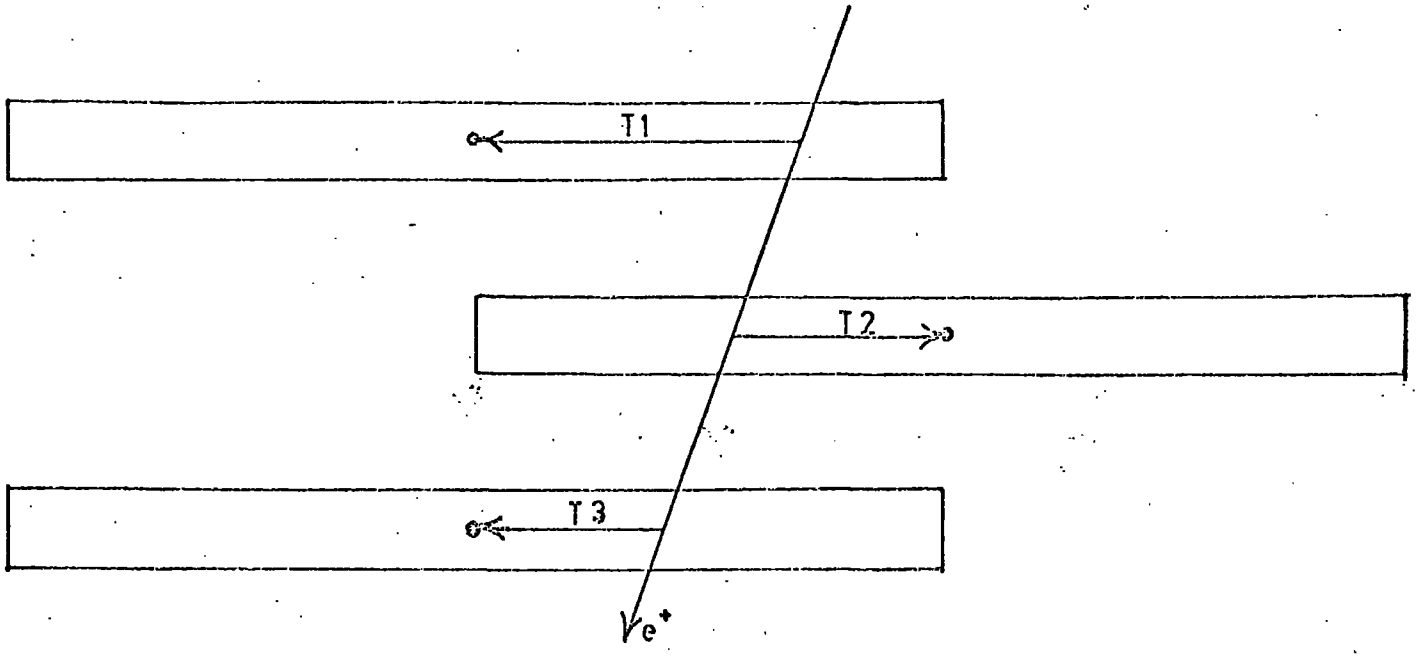

FIG 5.15 DISTRIBUTION OF MAXIMUM DRIFT TIMES

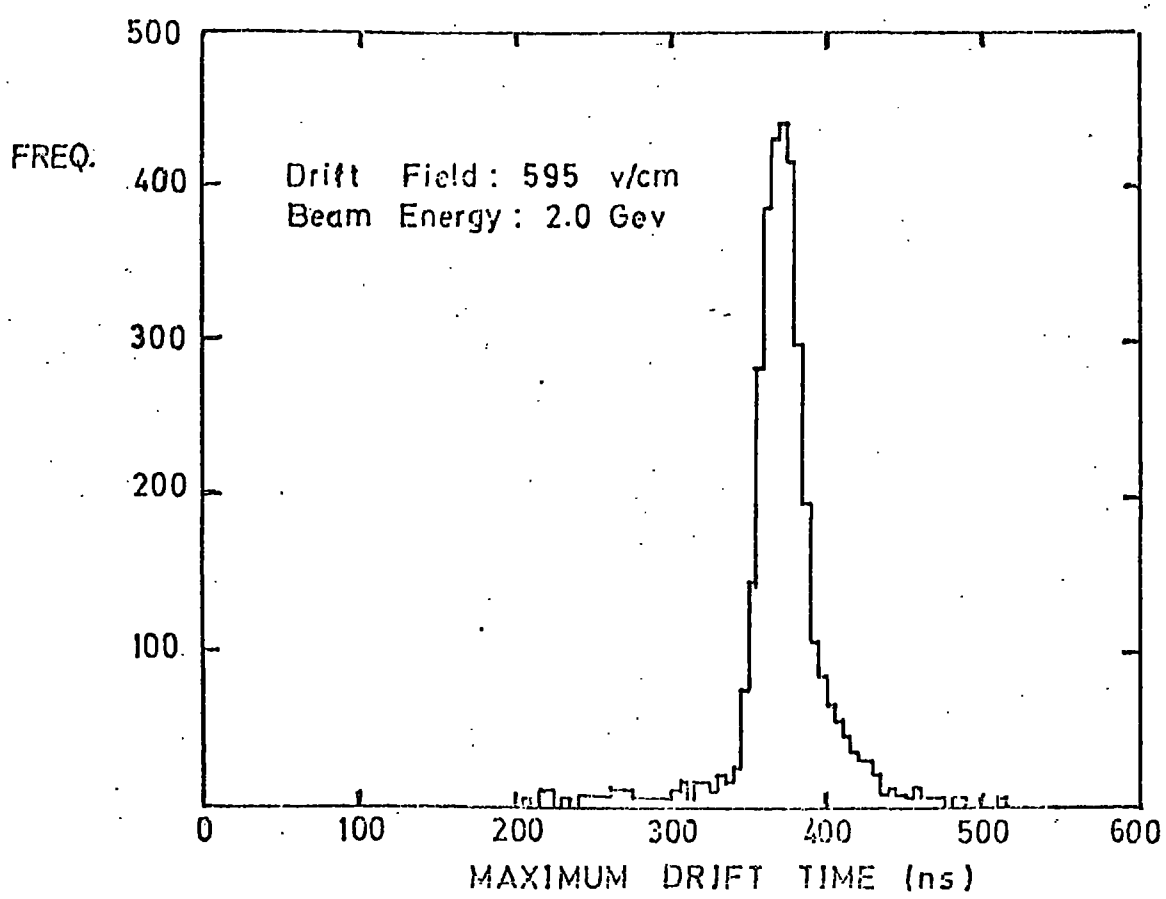

FIG 5.16 Drift Velocity
Measuring System (Charpak)

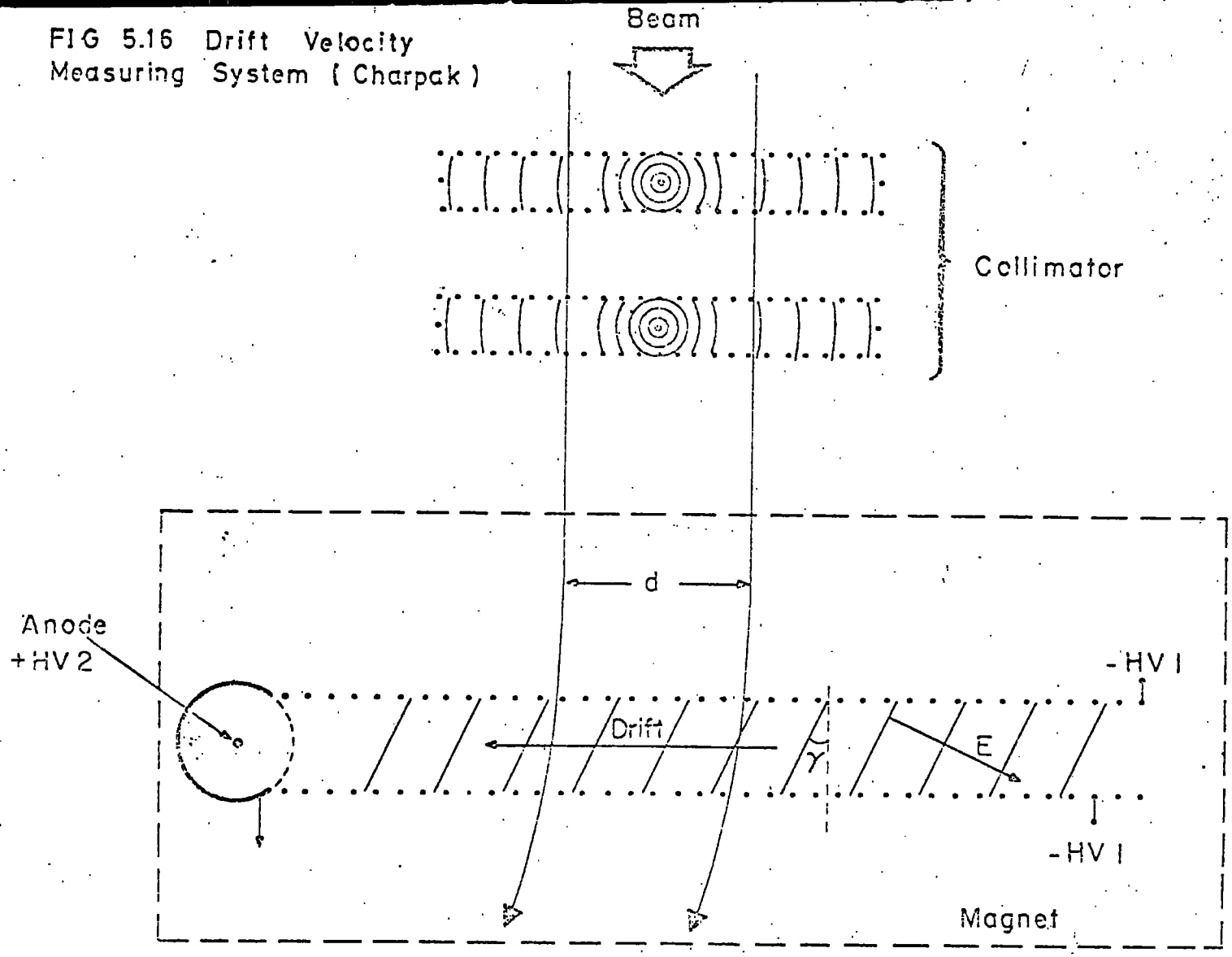

5.5.3 Resolution Measurements

As already indicated, system 1 is limited in resolution measurement, yet is useful for investigating variations in this quantity with, for example, beam energy, as shown in figure 5.17. Here the F.W.H.M. of drift time histograms, obtained with a 0.25 mm overlap, are plotted as a function of positron energy. The Coulomb scattering of positrons (from scintillators, air molecules etc.) causes a dispersion in the timing distributions at energies below 800 MeV in this case; above this level the effect becomes minimal. (It must also be noted that at energies below 1 GeV, the test beam is not as "clean" as for higher energies.) The line is an eye fit to the data and follows something like the expected $(\text{energy})^{-1}$ variation. Such results indicate that for precise resolution measurement, the working energy range is $\gtrsim$ 1 GeV. This figure can also be taken as a useful guide to a suitable energy threshold required for the chambers during the g-2 run.

To measure, with precision, the resolution of drift chambers, three or more chambers are required. One method is to determine, using three chambers, the time deviations (assumed equal) of each of the "hit positions" from the best straight line; this method is illustrated in figure 5.18. The geometry yields a value for deviation ($\Delta \simeq \Delta\cos\theta$) of :-

$$\Delta = \frac{t_2 - t_3}{2} + \frac{r}{2(r+1)}.(t_3 - t_1) \qquad (5.2)$$

where r is defined as the ratio l_1/l_2 and t_1, t_2, t_3 are the measured drift times.

FIG 5.17 RESOLUTION IN DRIFT CHAMBER VS BEAM ENERGY. (SYSTEM 1)

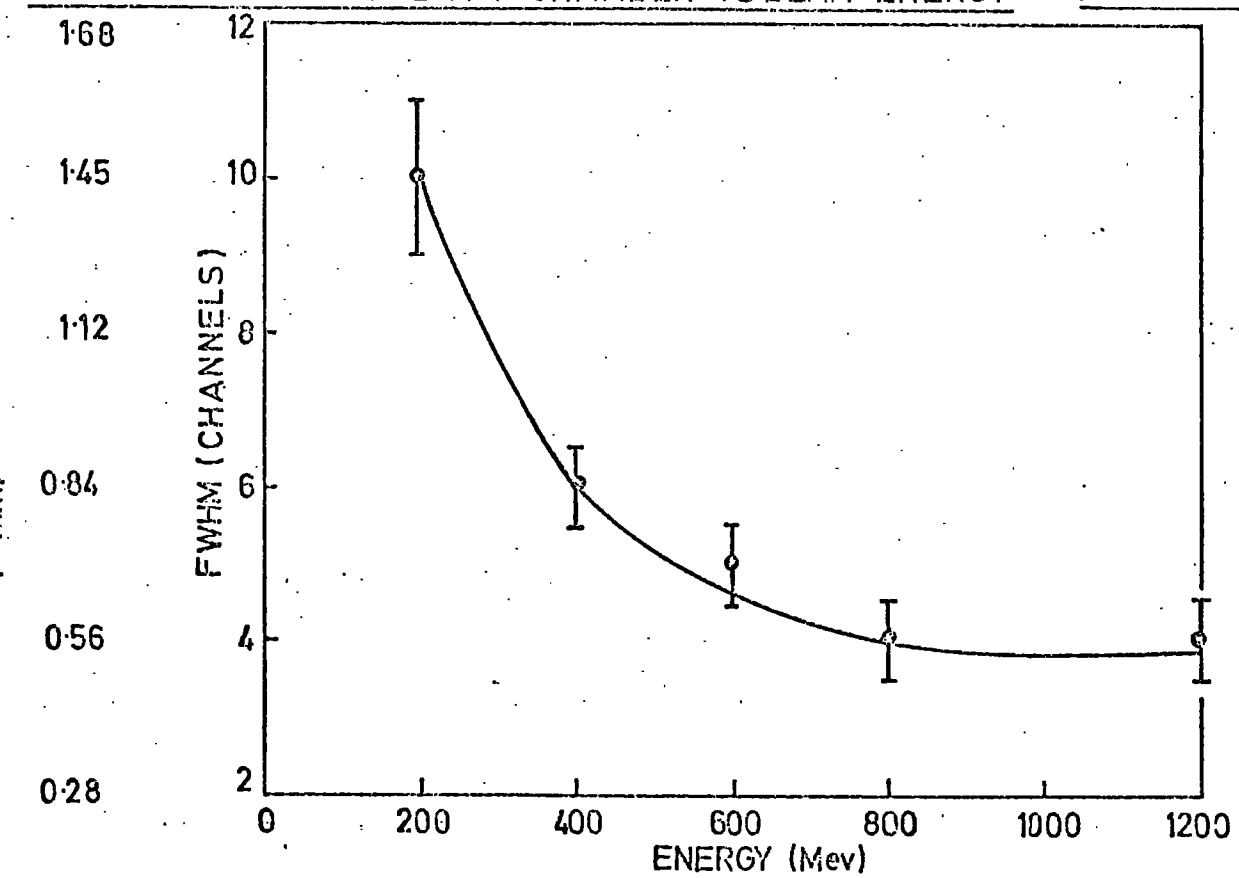

FIG 5.18 TRAJECTORY FITTING DIAGRAM

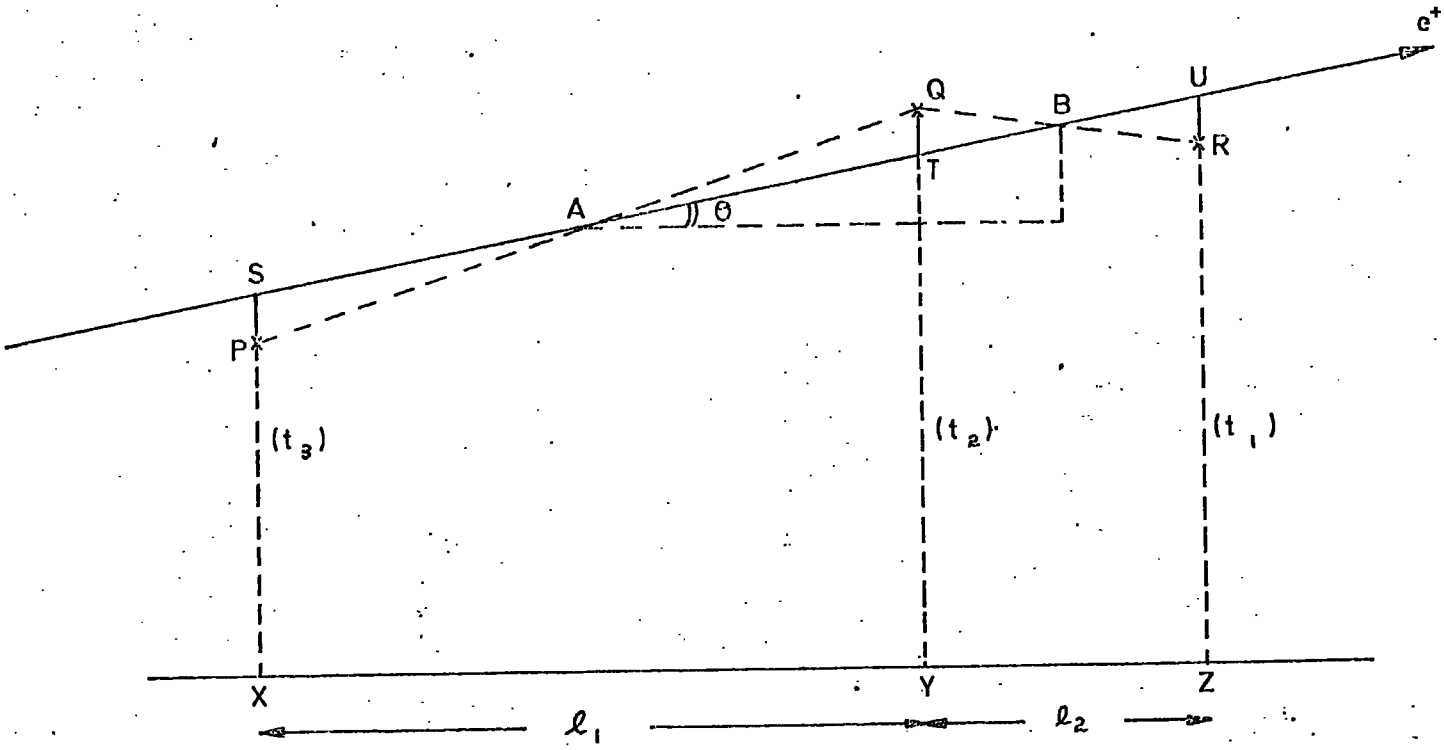

FIG. 5.19 Deviation Histogram

(2·5 GeV)

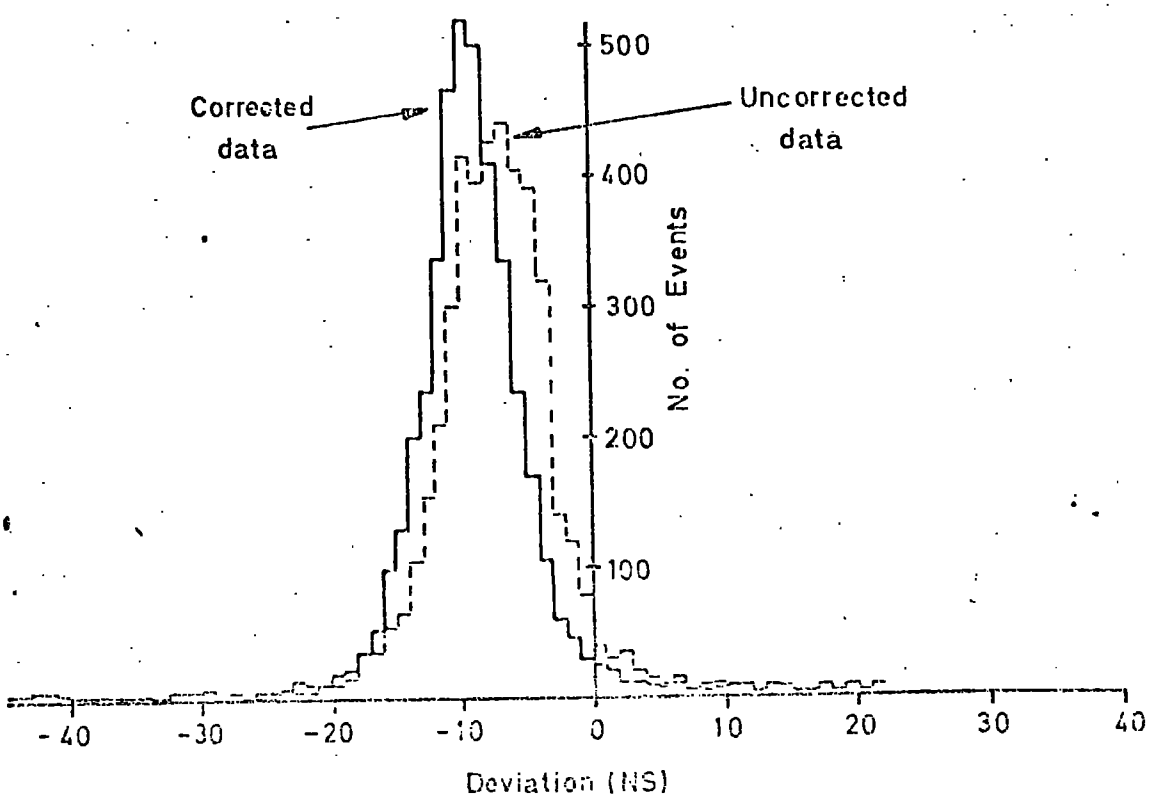

Figure 5.19 shows a typical deviation histogram obtained in the above manner using system 2 with a drift field of ~ 600 V cm^{-1}. The shift of the peak from the origin was attributed to slight wire misalignment for this particular run, and peaks could be shifted in a predictable way by addition of known-value delay cables (4). The difference between the distribution constructed from raw data and that corrected for T.D.C. errors is also indicated. At this stage, a F.W.H.M. of $\sim \pm 3.5$ ns suggests a good spatial resolution of between 0.1 and 0.2 mm.

Deviation histograms were obtained for various beam energies up to 2.0 GeV and are presented in figure 5.20. To compare these distributions, the histograms were broken down into the amounts of data lying between certain resolutions; this analysis is shown in figure 5.21. Figure (a) indicates clearly the effect of energy change on the histograms, and shows, for instance, that for a sufficiently high energy (2 GeV) approximately 90% of the data is contained within $\pm$ 7 ns (that is $\sim \pm 0.25$ mm). From the lines A, B and C (representing resolutions of $\pm$ 0.1, $\pm$ 0.2 and $\pm$ 0.3 mm respectively), figure (b) showing the amount of data lying within a given spatial resolution, versus energy, was derived. Once again, the multiple scattering factor causes a significant depreciation in resolution below $\sim$ 1 GeV. In the best cases, over 60% of data lie within $\pm$ 0.1 mm.

Using the same technique, a systematic check on all cell channels was carried out for three aligned production model chambers and satisfactory deviation histograms were obtained throughout.

Using four alternately staggered chambers as illustrated in figure 5.22, and inserting a value for drift velocity, a least squares fit to a straight line was applied to the data. Thus the spatial

FIG 5.20 DEVIATION HISTOGRAMS FOR DIFFERENT BEAM ENERGIES

(Nanosecond Binwidths)

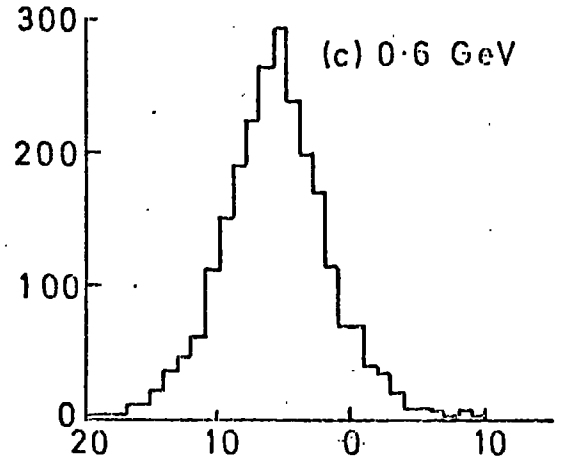

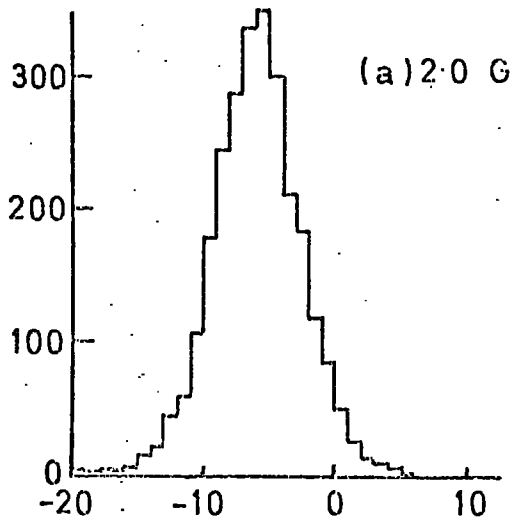

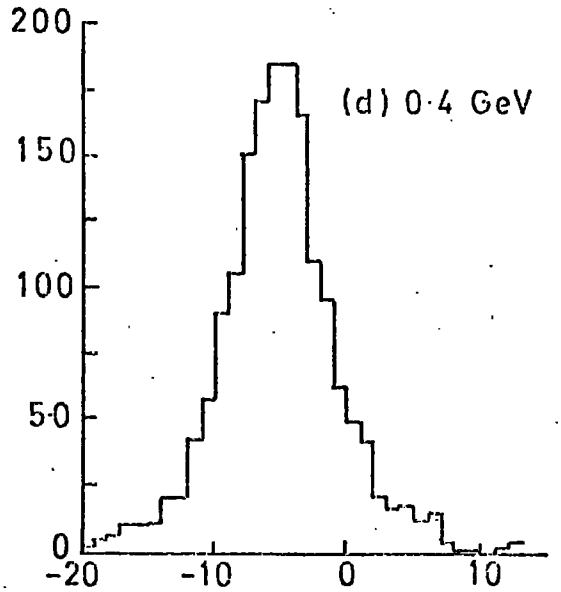

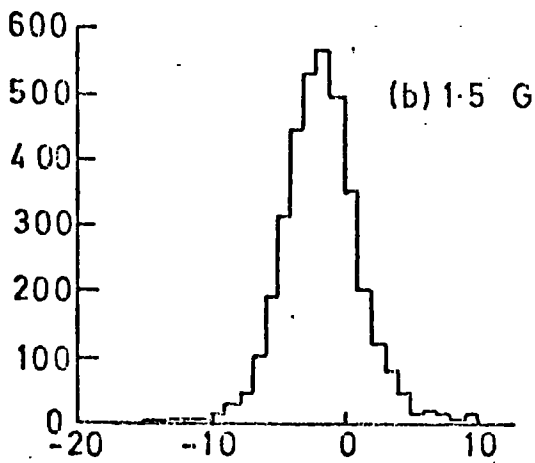

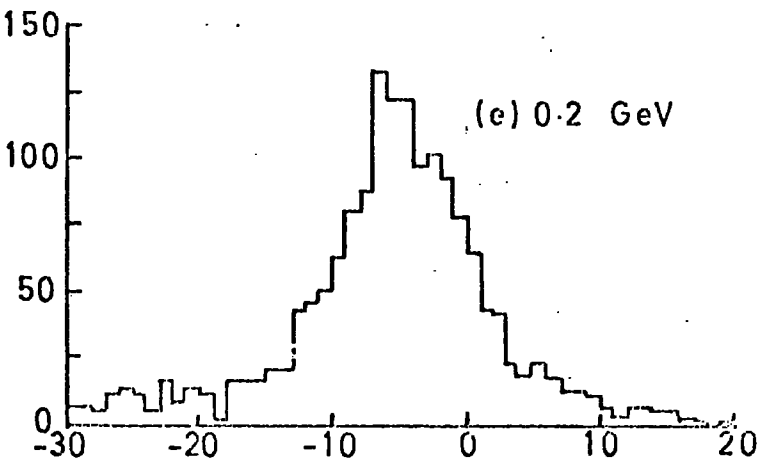

FIG.5.21(a) Amount of data within given resolution — various energies of beam.

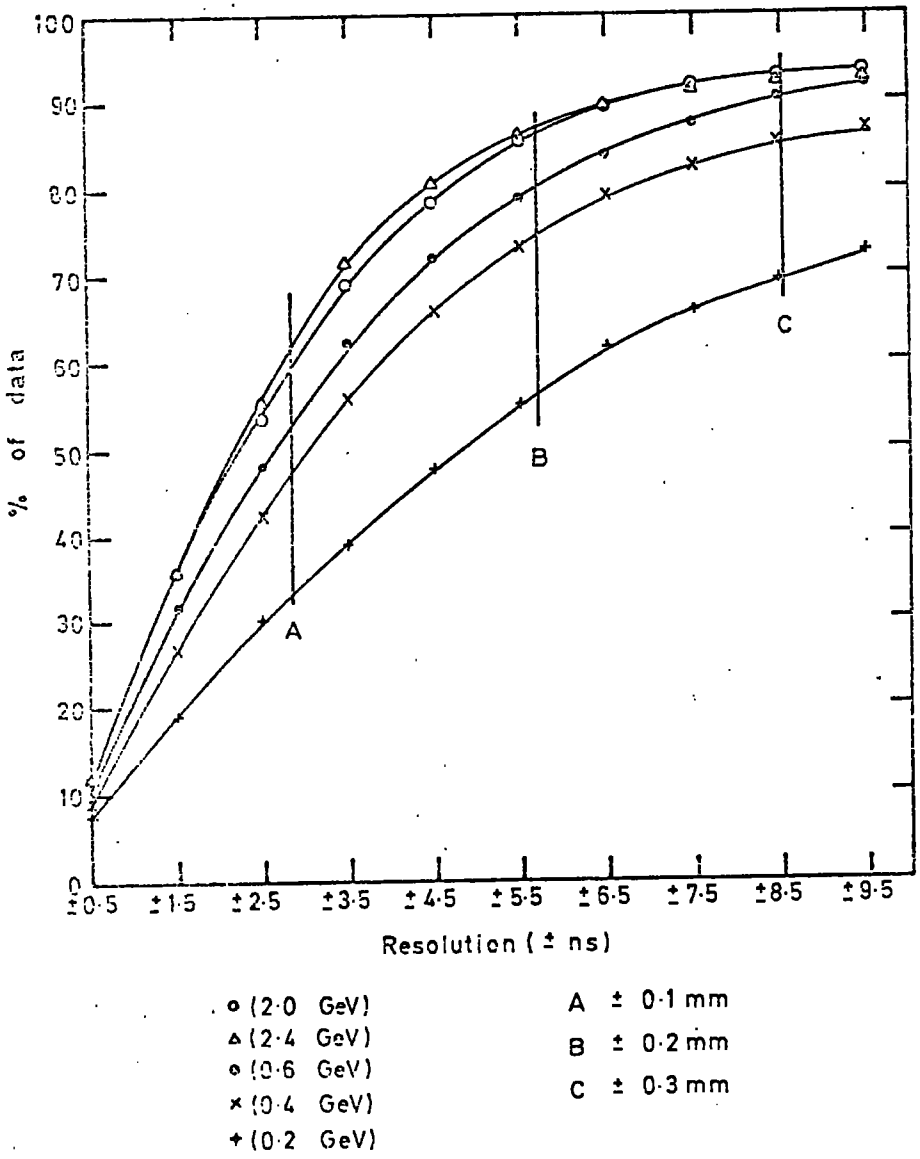

FIG. 5 21(b) Amount of data within given spatial resolution vs energy of beam.

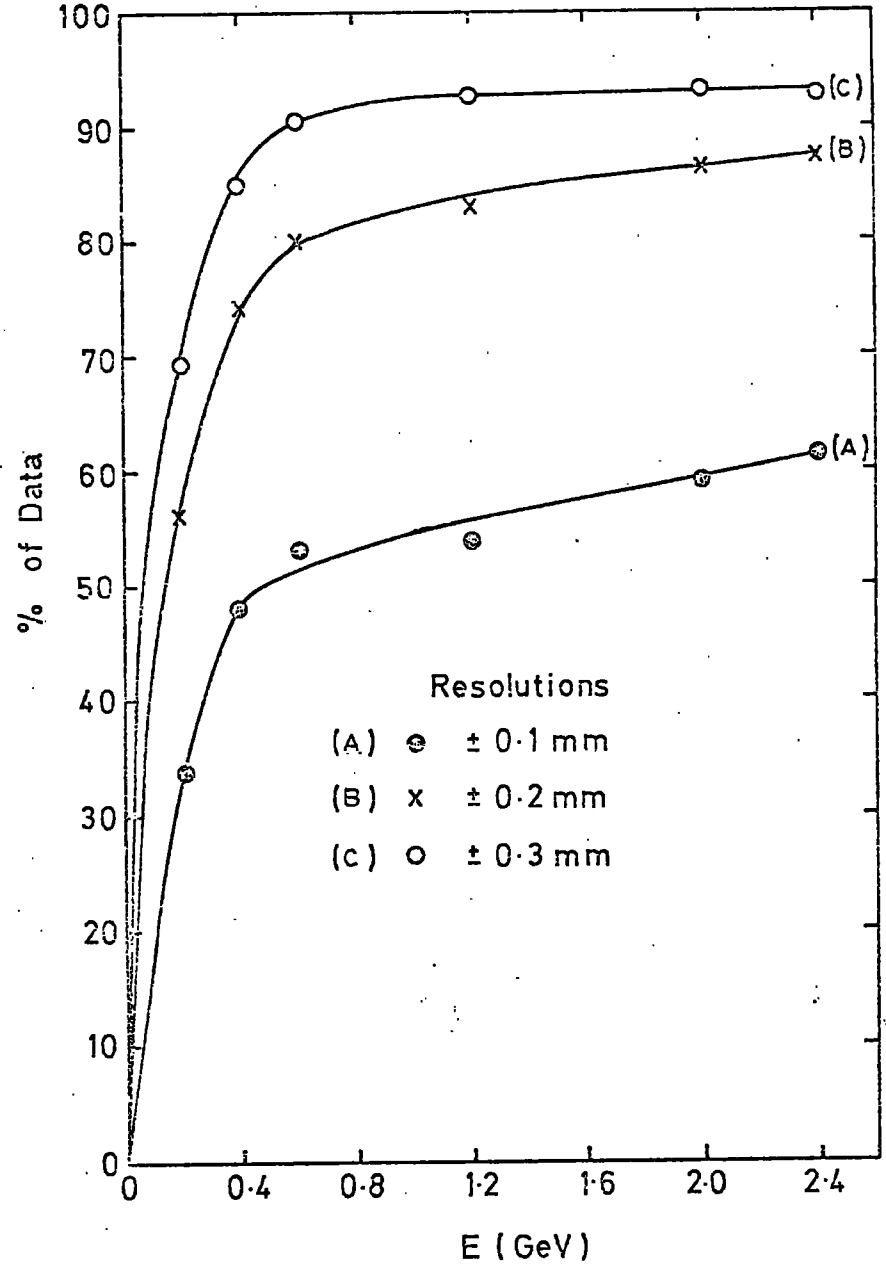

FIG 5.22 RESOLUTION MEASURING SYSTEM USING FOUR CHAMBERS

(a) Curved End Run
(b) Normal Cell Run

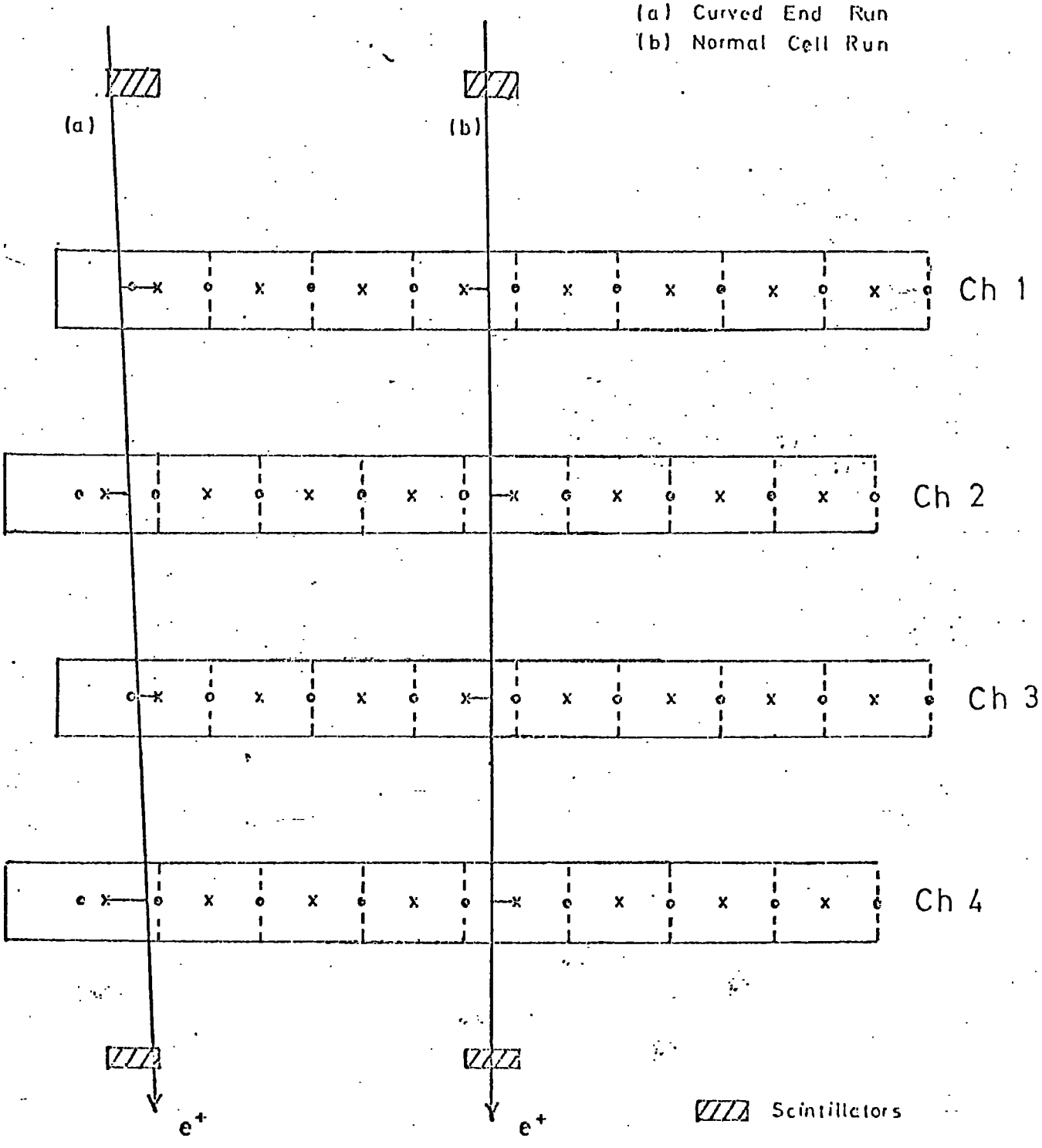

deviations S_1, S_2, S_3 and S_4, between the experimental and theoretical hit points, for each chamber were calculated and used to determine a value of standard deviation (S) using the formula:-

$$S^2 = \left(\sum_{n=1}^{4} S_n^2 \right) / 4 \qquad (5.3)$$

Figure 5.23 shows the results of processing one run in this way. The individual chamber deviation distributions are seen to be off centre due to mechanical system misalignment and yield a standard deviation histogram peaking at ~ 0.9 mm. By inserting relevant software adjustments, the peaks were centralised, a process which automatically improved the quality of the individual deviation distributions and reduced the standard deviation peak position to 0.15 mm (figure 5.24). Such a technique stresses the need of careful chamber alignment and surveying in the actual g-2 system.

Figure 5.25 shows the results of applying the same method to a run in which two curved end half-cells (as indicated in figure 5.22) were included. The standard deviation distribution in this case peaks at 0.3 mm, a result which is encouraging in view of the electric field distortion in the curved end region.

5.5.4 Operation and Resolution in a Magnetic Field

The straight line fit method illustrated in figure 5.18 was used to make a qualitative investigation of the behaviour of one drift chamber (C of figure 5.3) in a magnetic field. This method is valid for a monochromatic beam and uniform magnetic field as the deflection of all particles will be the same. Such analysis produces two peaks

FIG. 6.23

UNCORRECTED LEAST SQUARES FIT HISTOGRAMS

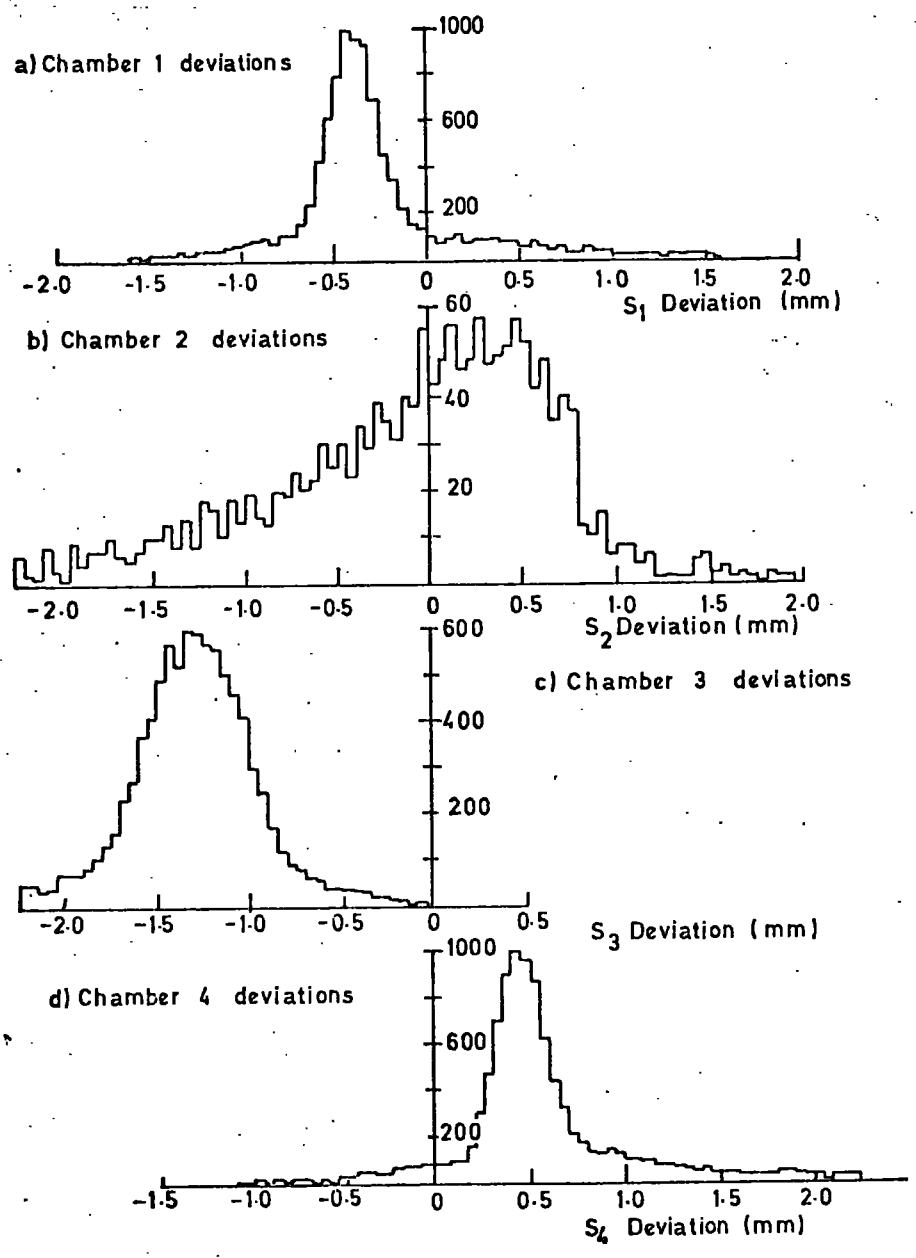

e) Distribution of standard deviation.

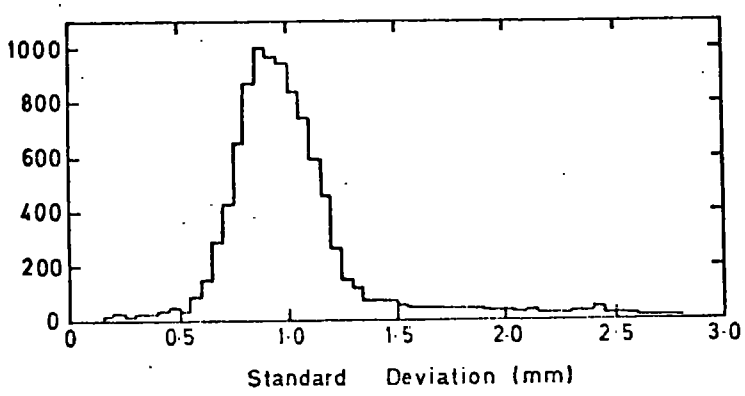

FIG.5.24 CORRECTED LEAST SQUARES FIT HISTOGRAMS.

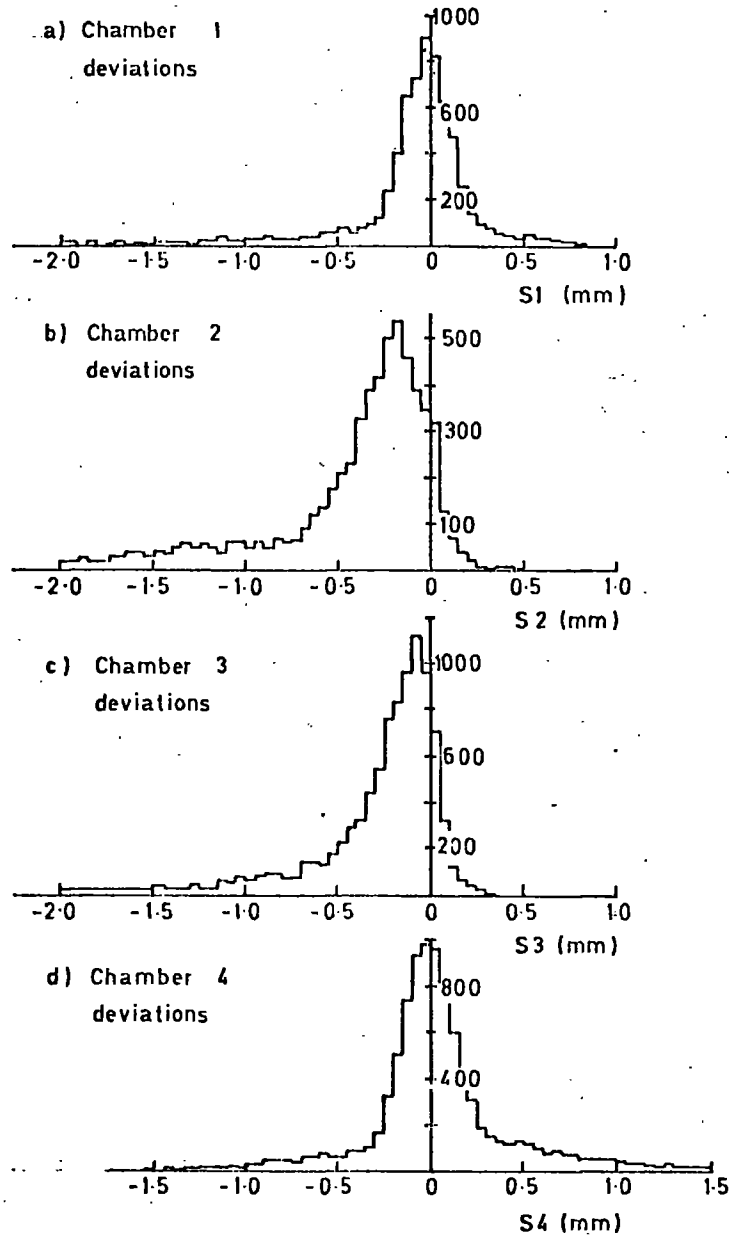

e) Distribution of standard deviation.

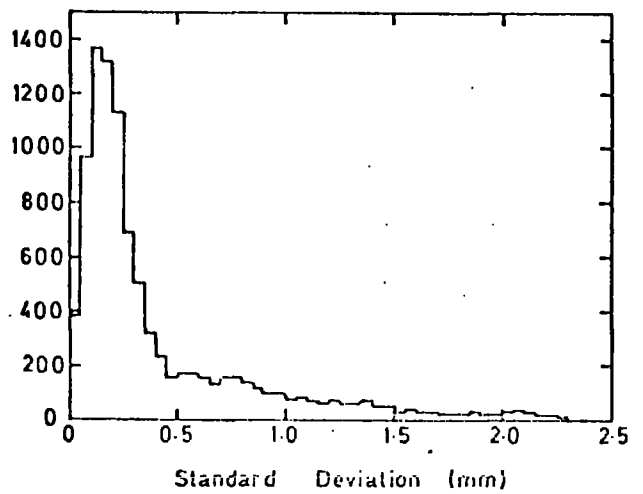

FIG.5.25 CORRECTED LEAST SQUARES FOR CURVED END RUN.

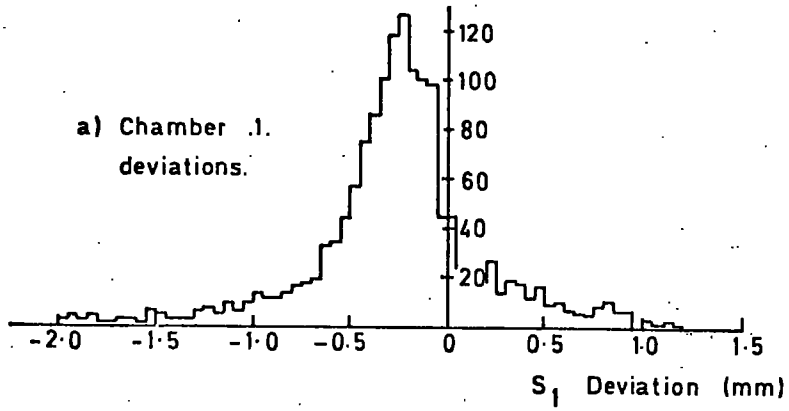

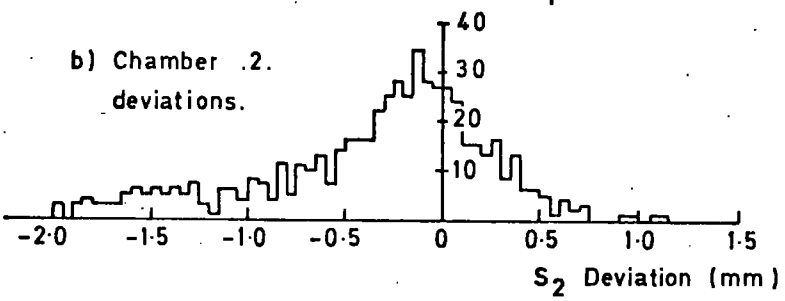

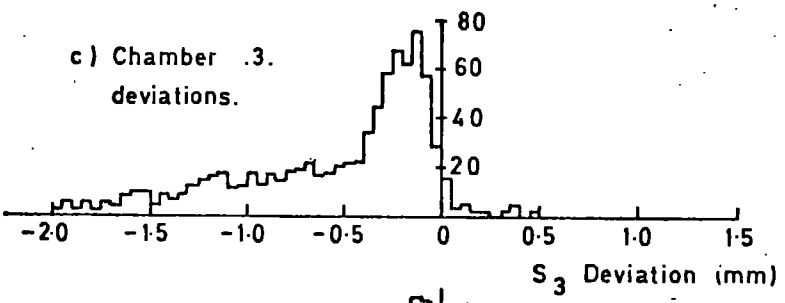

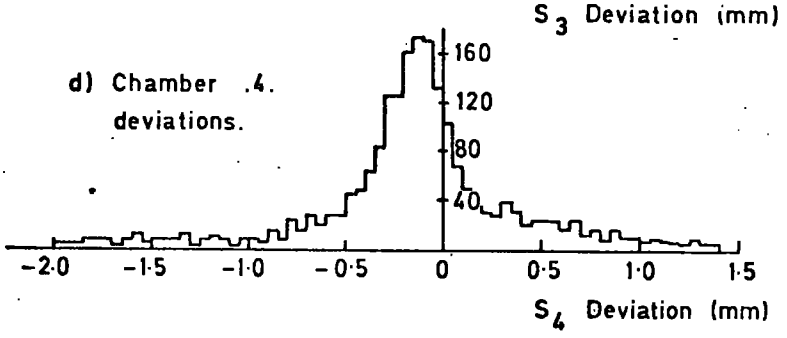

e) Distribution of standard deviation.

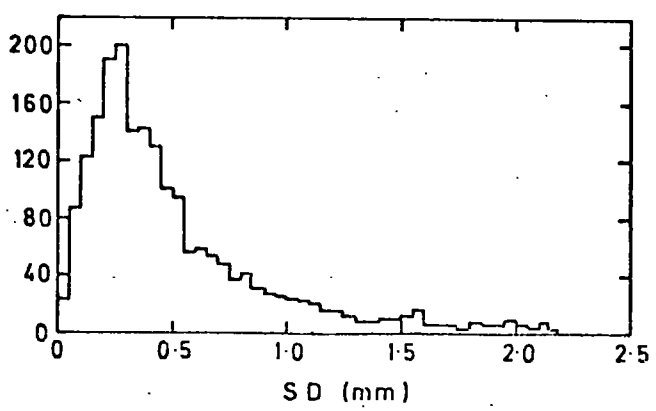

as seen in figure 5.26 where the effect of varying the distance (movement in the same direction as the drift planes) of the overlapping scintillators from a fixed position (A) is shown. The two peaks are due to the deflection of positrons to either side of the sense wire, their spatial separation representing twice the deflection. The varying height of the respective peaks in figure 5.26 is due to the different ratio of particles being collected, and for investigation of resolution, the telescope can be positioned so as to predominantly select one peak. These results were taken for a magnetic field (B) of 7.5 KGauss, a compensating electric field tilt of 2 H.T. wire spacings and a beam energy of 2.0 GeV. Already a F.W.H.M. comparable to the B = 0 case is observable.

Figure 5.27 shows three deviation histograms obtained under the above conditions but for different beam energies. Here any change in peak separation is due entirely to different particle deflections. Separations of (25, 21 and 19 ± 4)ns for 2, 3.5 and 4 GeV respectively indicate the correct order of deflection as determined by classical equations.

Figure 5.28 shows the effect of varying magnetic field at an energy of 2.0 GeV and with suitable telescope positioning. As the three runs for these results were consecutive, any change in peak position is due to different particle deflections and also any change in drift velocity with magnetic field. As these two effects act in the same sense, that is, drift velocity generally decreases as B increases, thus extending drift times in a similar manner to increasing the deflection, the small peak movement observed (up to 3 ns) indicates that drift velocity fluctuations with magnetic field are small for this particular electric field value (600 V cm^{-1} in the

FIG.5.26 DEVIATION HISTOGRAMS IN MAGNETIC FIELD (7·5 K.GAUSS) DIFFERENT DISTANCES OF SCINTILLATOR FROM "POSN. A" SHOWN.

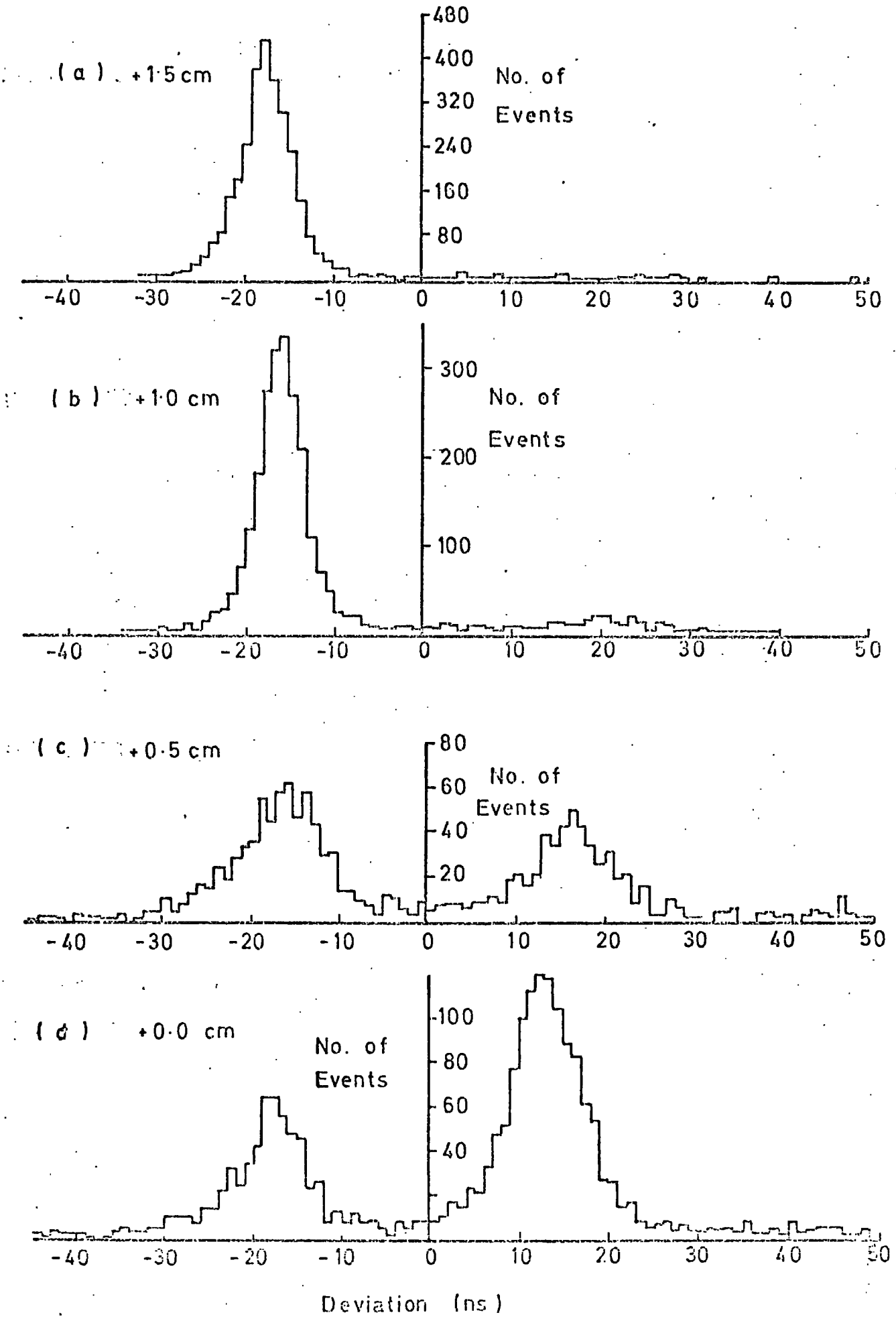

FIG. 5.27 Deviation Histograms For Different Beam Energies in a Magnetic Field of 7·5 K.Gauss

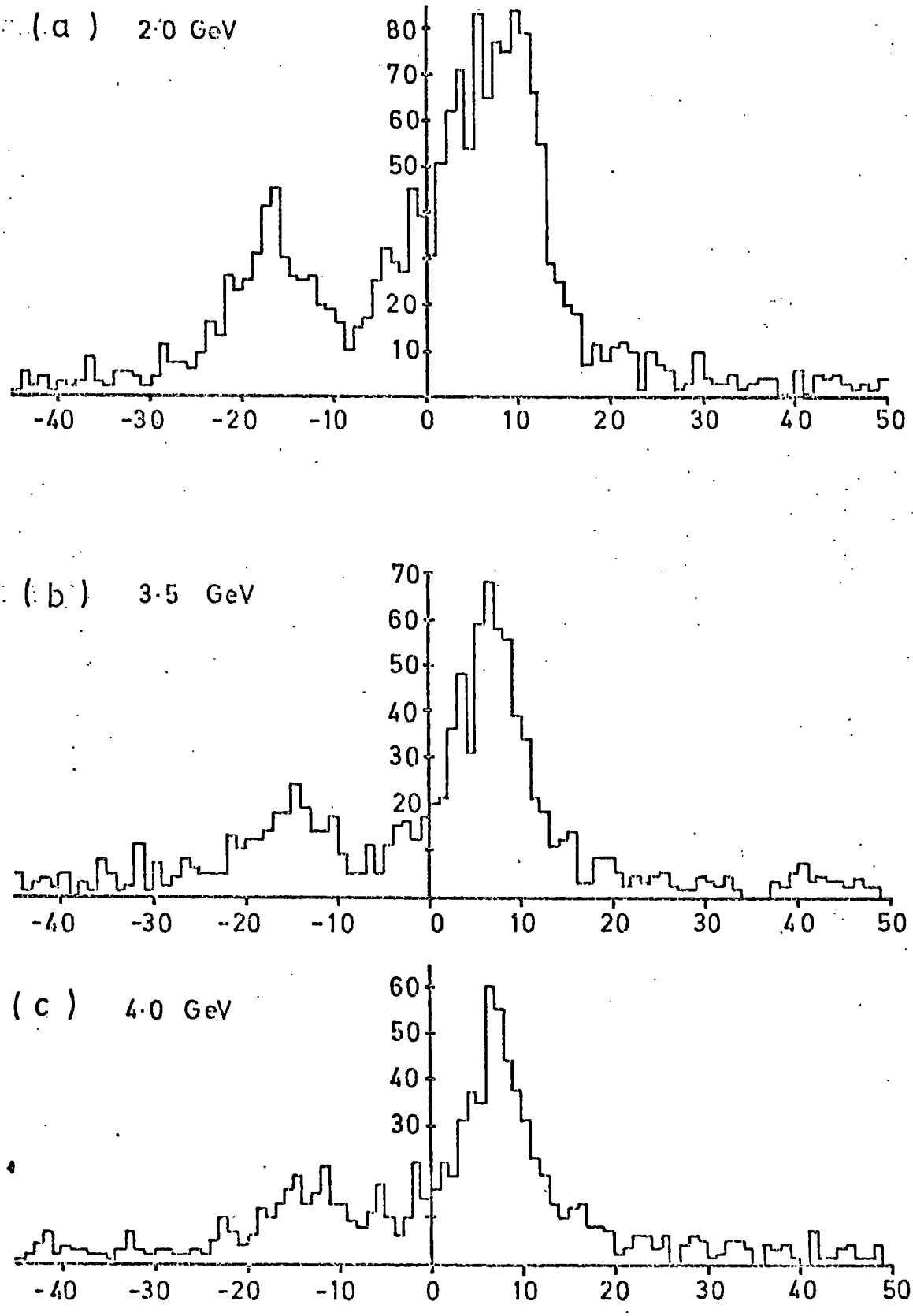

FIG. 5.20 Deviation Histograms in thr
different magnetic fields (E = 2·0 Ge

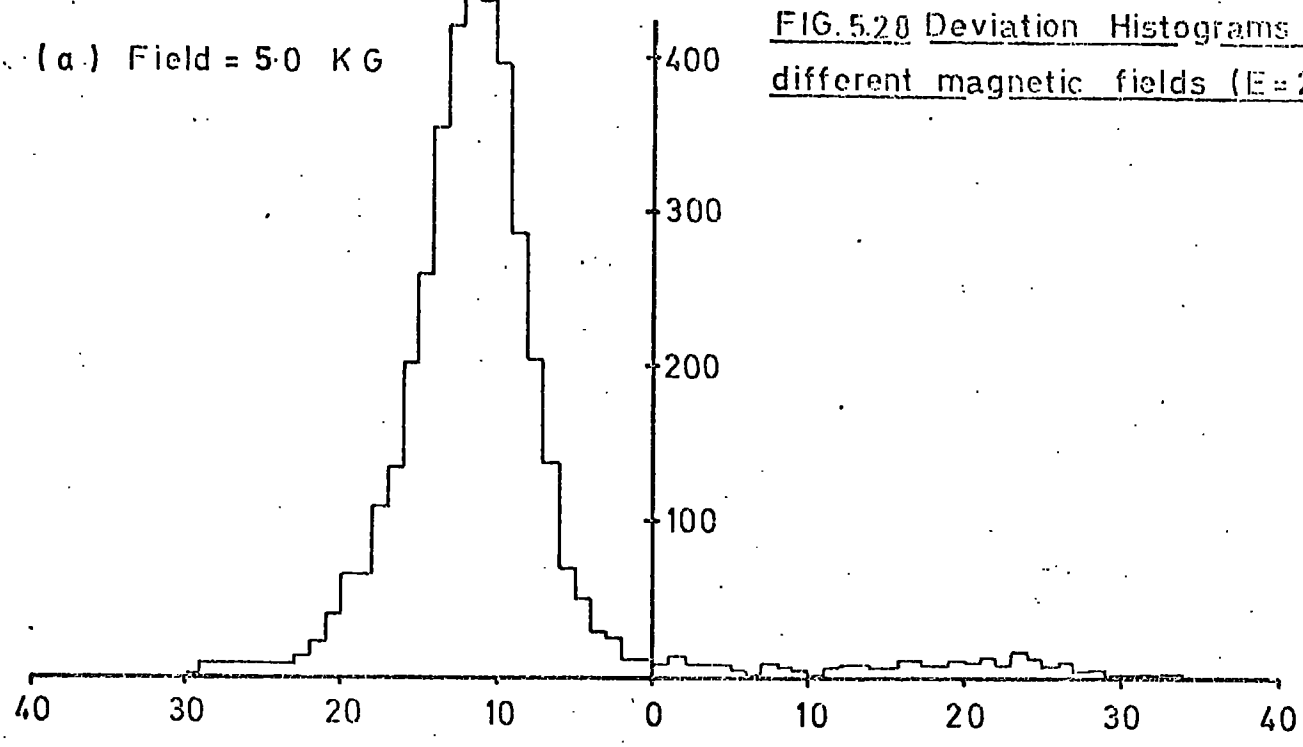

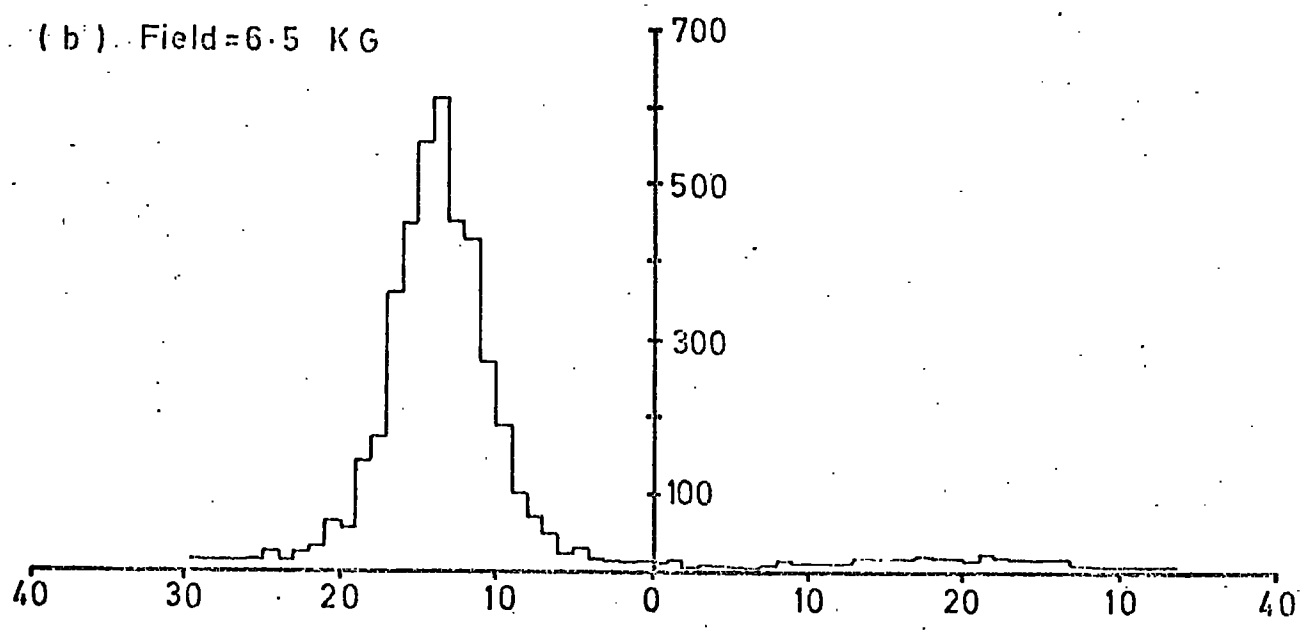

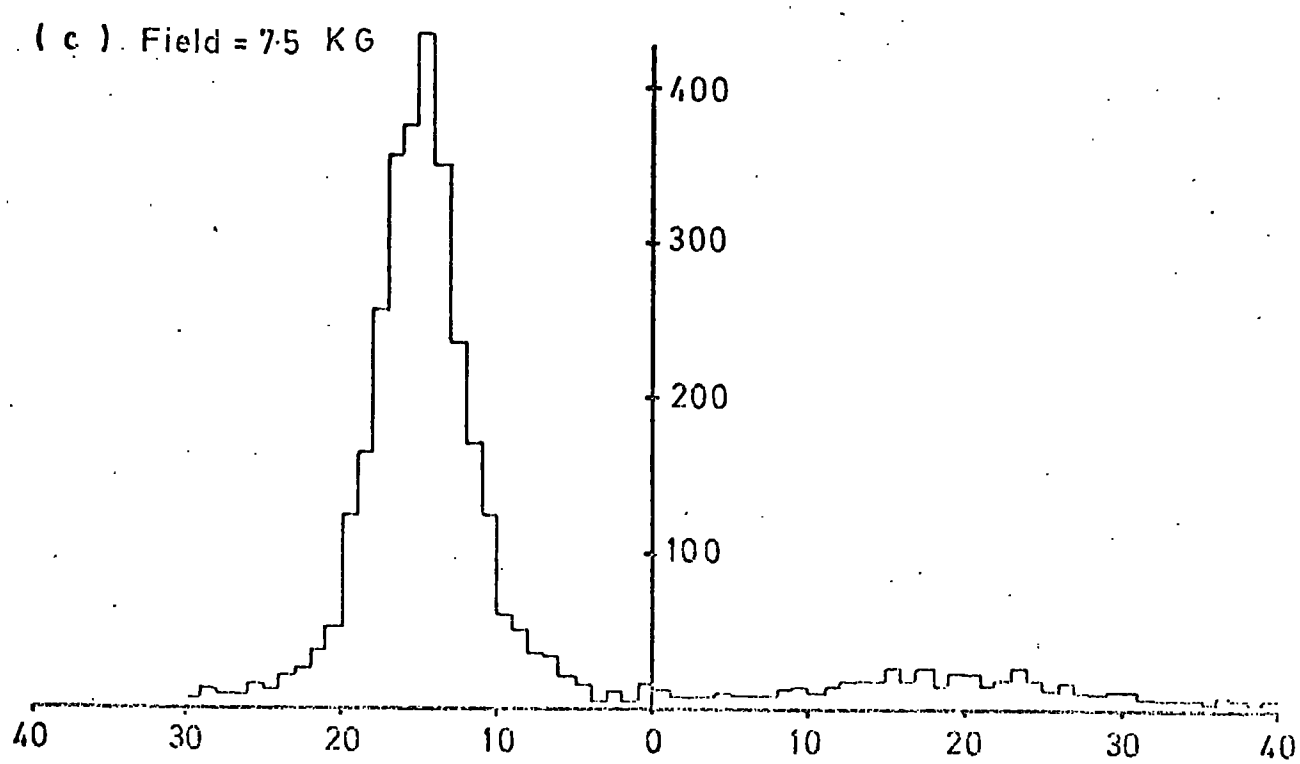

drift plane). This will be verified in the next chapter. Also from this figure it is evident that the distribution width narrows as 7.5 KGauss is approached, showing a "2-tilt" compensation to be correct for this field value. The very slight deterioration of resolution as magnetic field is reduced can be attributed to the more diverse flow lines followed by drifting electrons.

Continuing the investigation of correct compensation for magnetic field, figure 5.29 shows the deviation histograms obtained for various electric field tilts in a 7.5 KGauss magnetic field using 2 GeV particles. As tilts further away from the best estimation of 2 H.T. wire spacings were encountered, a slight widening of the histograms was observed. However, even when compensating in the wrong direction (tilt of -1) a good histogram is produced as seen in figure 5.29 (d).

Another interesting effect forthcoming from these results is the reduction in peak deviation as the compensation becomes closer to the correct value. This effect is due to the increase in drift lengths produced by incorrect compensation, particularly at low electric fields (a full discussion is presented in chapter 6), plus a small contribution from the increase in drift velocity with electric field at this particular magnetic field (see figure 6.3).

In conclusion, for magnetic fields up to 7.5 KGauss, F.W.H.M's of deviation distributions in the range 6 to 11 ns have been obtained, meaning a spatial resolution of better than ± 0.3 mm in all cases. It must, however, be remembered that only one chamber was positioned in the magnetic field to yield these results.

5.5.5 Final Comments on Resolution

To state exactly a figure for resolution is difficult;

FIG.5.29 Deviation Histograms In a Magnetic Field of 7·5 K Gauss.

(Electric Field Compensations shown)

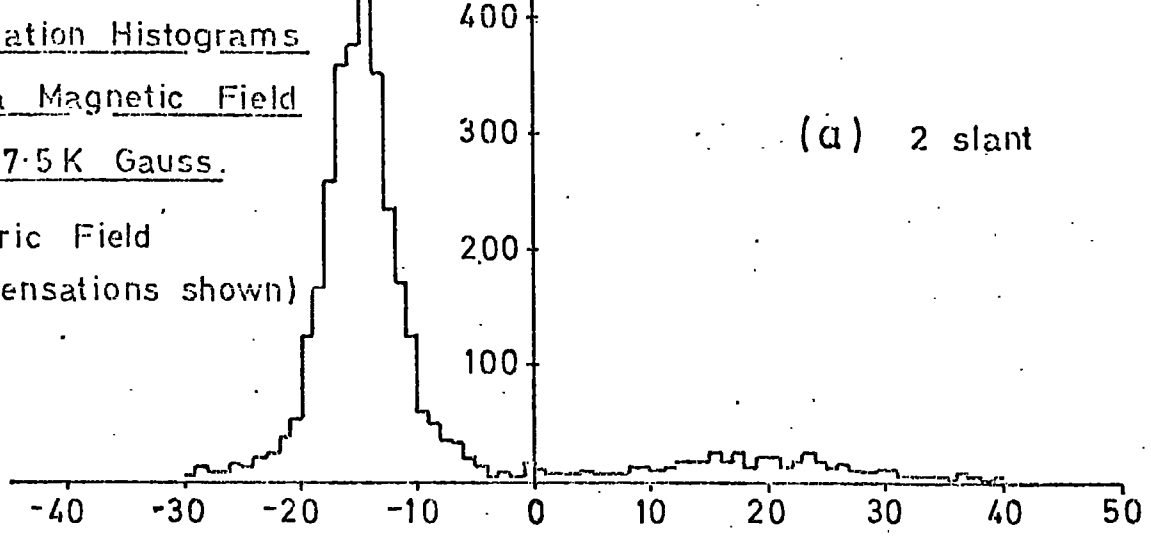

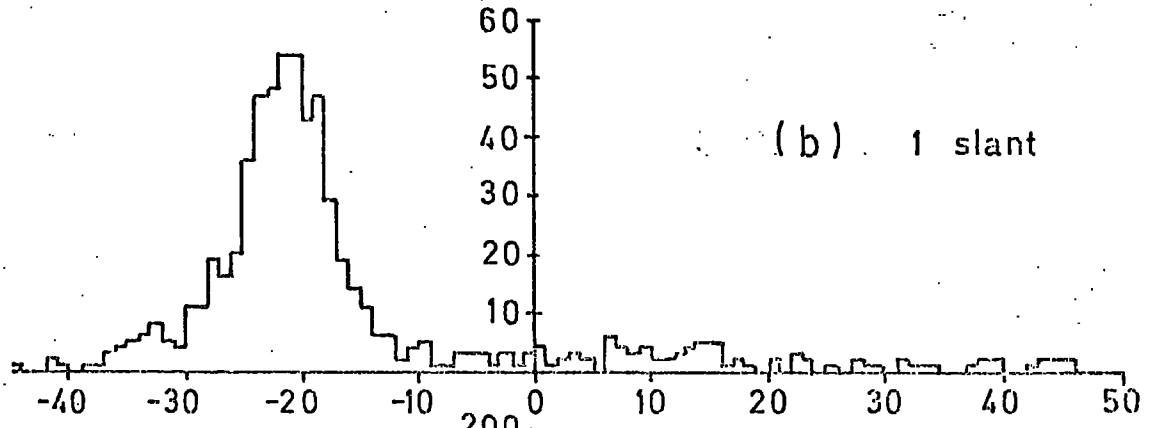

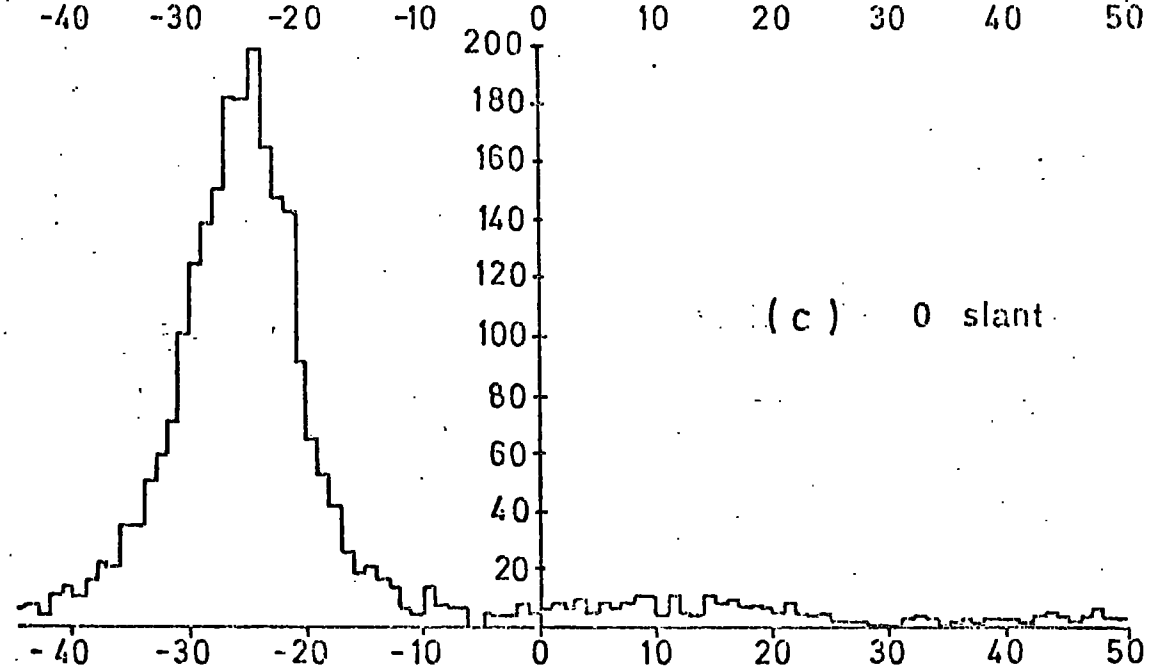

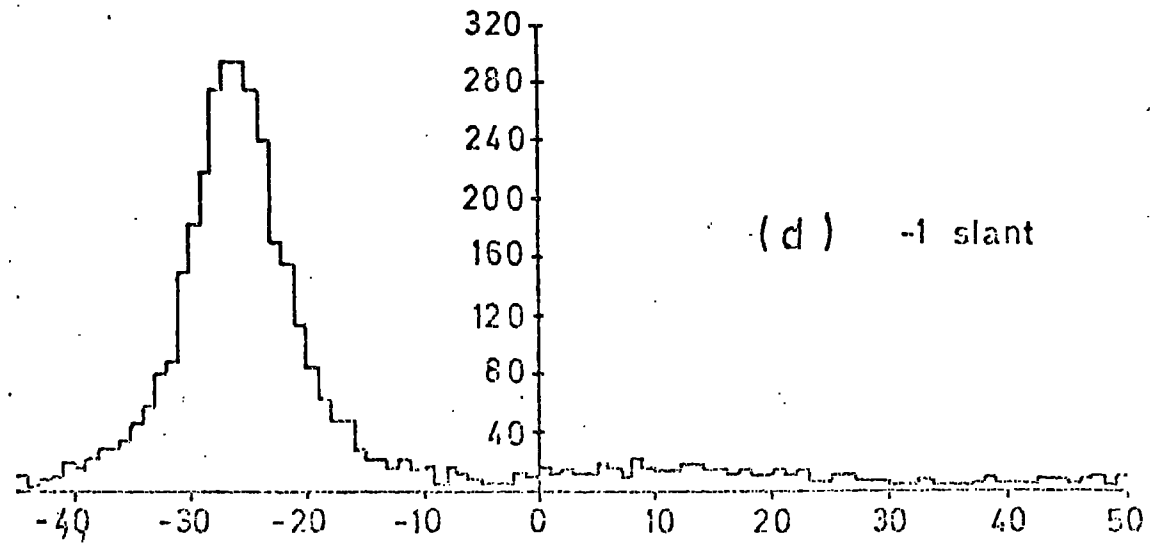

however, estimates can be made in the following ways (the errors occurring due to judgement and binning techniques):-

Method	Resolution (± mm)			
	Normal Cell	Prototype Curved End	Production Curved End	Normal Cell In Mag. Field
FWHM of Three-Point Deviation Histogram	0.12 ± 0.03	0.3 ± 0.1	0.25 ± 0.03	0.12 ± 0.03
Section of above Distribution Containing 68% of Data	0.11 ± 0.03	0.25 ± 0.03	0.21 ± 0.03	0.13 ± 0.03
FWHM of Best Deviation Histo-grams Obtained by Least Squares Method	0.175 ± 0.03		0.25 ± 0.03	
Section of above Distribution Containing 68% of Data	0.175 ± 0.03		0.425 ± 0.03	
Peak Position of Least Squares Standard Deviation Distribution	0.15 ± 0.05		0.3 ± 0.05	

NB 1 68% of data usually defines ±one standard deviation for a normal distribution.

NB 2 The production curved end figures are improved by the fact that normal half-cells will also contribute to the results for these runs. Similarly, the measurement system reduces any deterioration of deviation histograms for magnetic field runs.

Figure 5.30 shows a comparison between various runs in the form of a breakdown of the three-point deviation histogram as in figure 5.21 (a), one peak being selected for magnetic field cases.

Finally, on observing deviation histograms for various time-windows in the central of three chambers (that is to say for various parts of the cell), no appreciable deterioration was apparent (4).

5.5.6 Beam Profile Measurements

Figure 5.31 ((a) to (d)) shows the beam profile observed at each of the four chambers arranged as in figure 5.22 with equal spacings of 76 mm between them. For each track, a straight line was fitted to the three downstream chambers (geometry as in figure 5.18) and projected upstream to predict the hit point at the first chamber. Thus a predicted beam profile at this chamber could be constructed (figure 5.31 (e)) comparing favourably with that directly observed. Figure 5.31 (f) shows the distribution of differences between the observed and predicted points and has a F.W.H.M. of 1.5 mm agreeing with the error magnitude of ± 0.5 mm obtained by leverage in such a reconstruction.

The reconstruction was also done for an increased distance (555 mm) between chambers 1 and 2, and the observed and predicted profiles are shown in figure 5.32. This time the error distribution

FIG 5.30 Amount of data within given resolution - comparison of various experimental conditions.

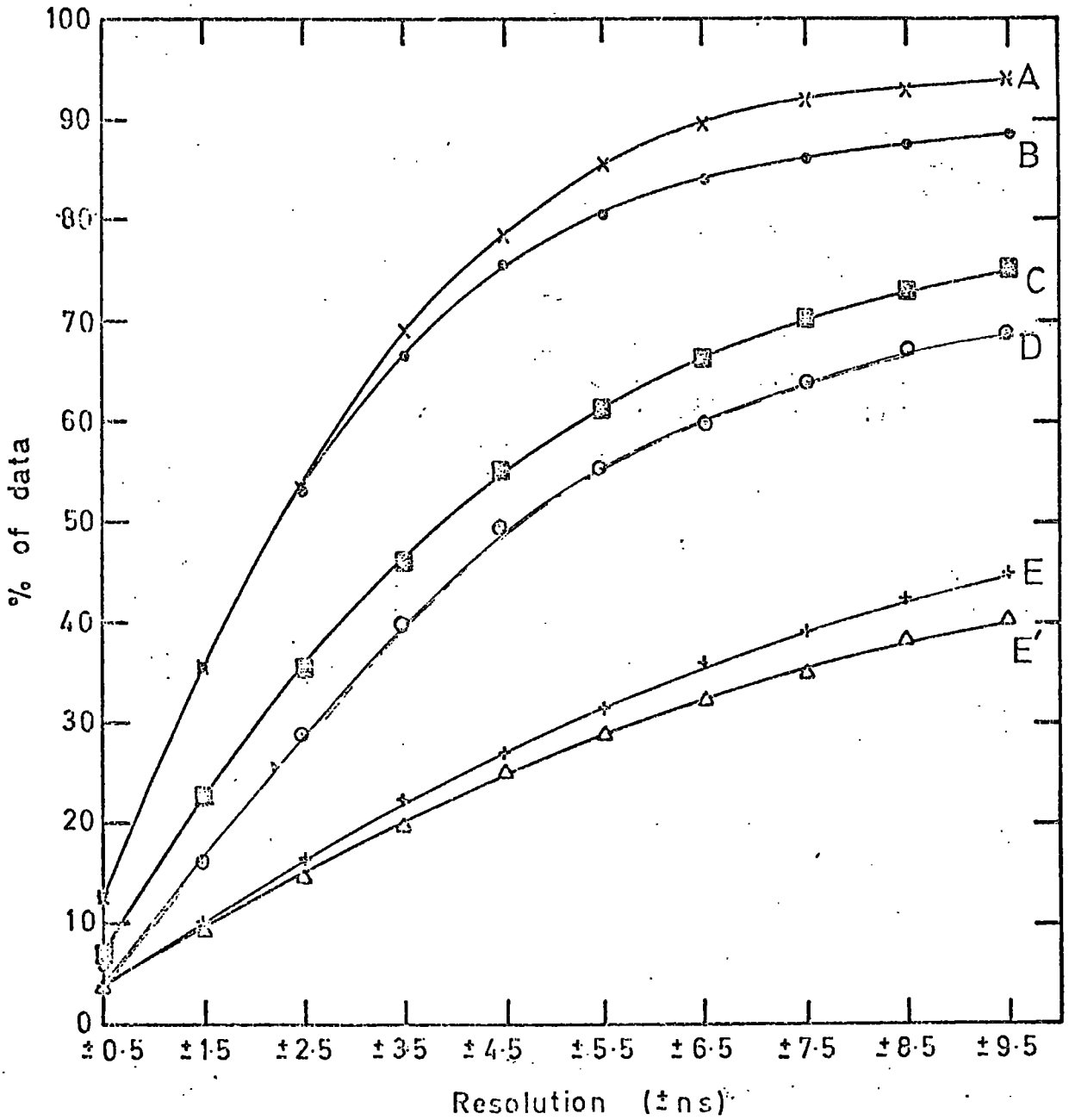

A × 2.0 Gev no Magnetic Field
B • "GOOD" Conditions for Magnetic Field Run
C ▪ "ADVERSE" Conditions for Magnetic Field Run
D o Production Model Curved End
E + (and E' ▵) Prototype Curved End

FIG.5.31 BEAM PROFILES AT DRIFT CHAMBERS.
(Equaly spaced 76 mm apart)

a) Profile at chamber .1.

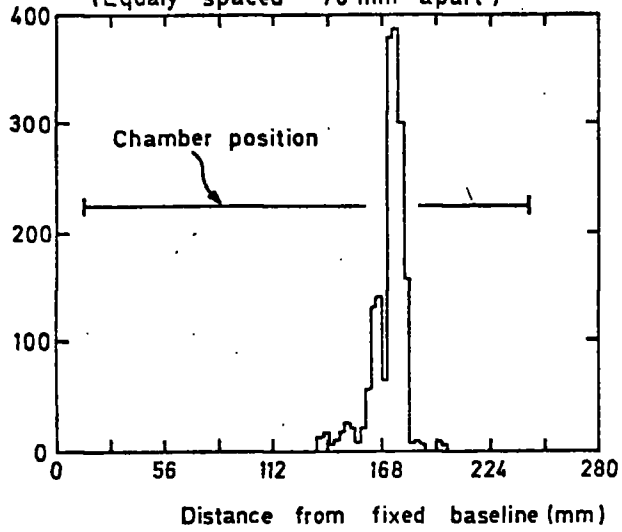

b) Profile at chamber .2.

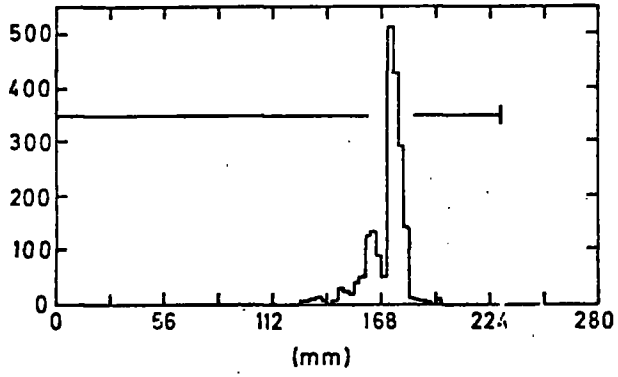

c) Profile at chamber .3.

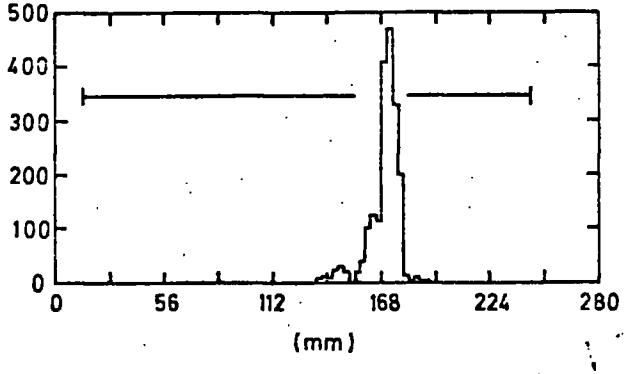

d) Profile at chamber .4.

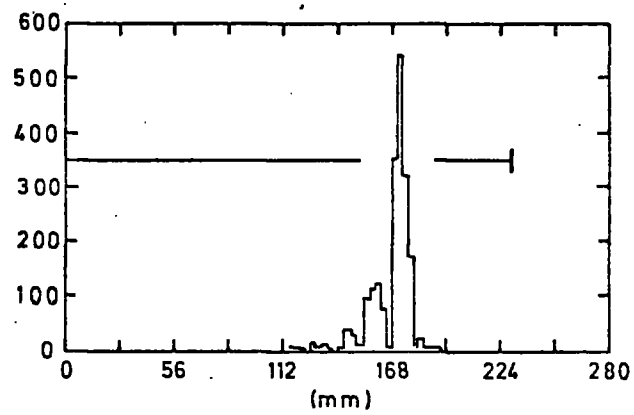

e) Predicted profile at chamber .1.

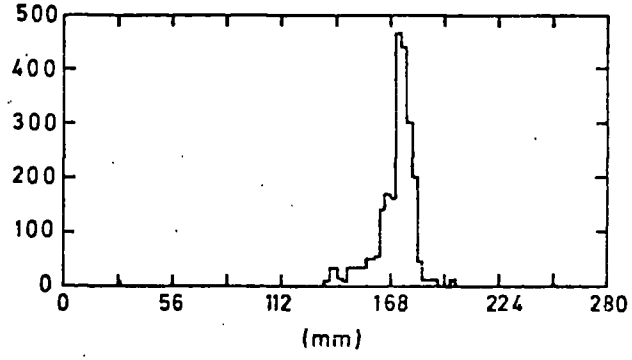

f) Deviations between observed and predicted hits at chamber .1.

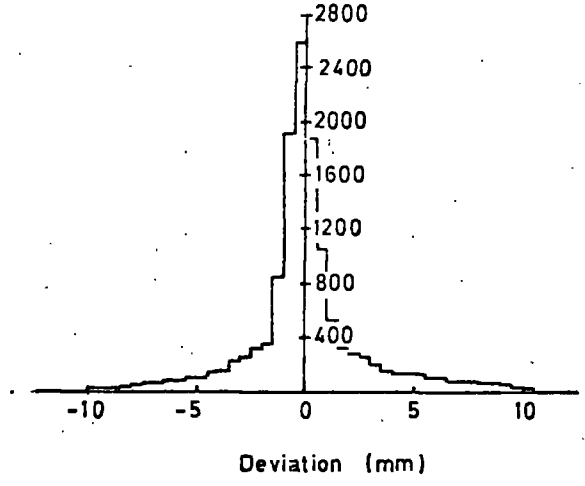

FIG. 5.32 BEAM PROFILES.

(Chambers 1 and 2 555 mm. apart, separation of other chambers 76 mm)

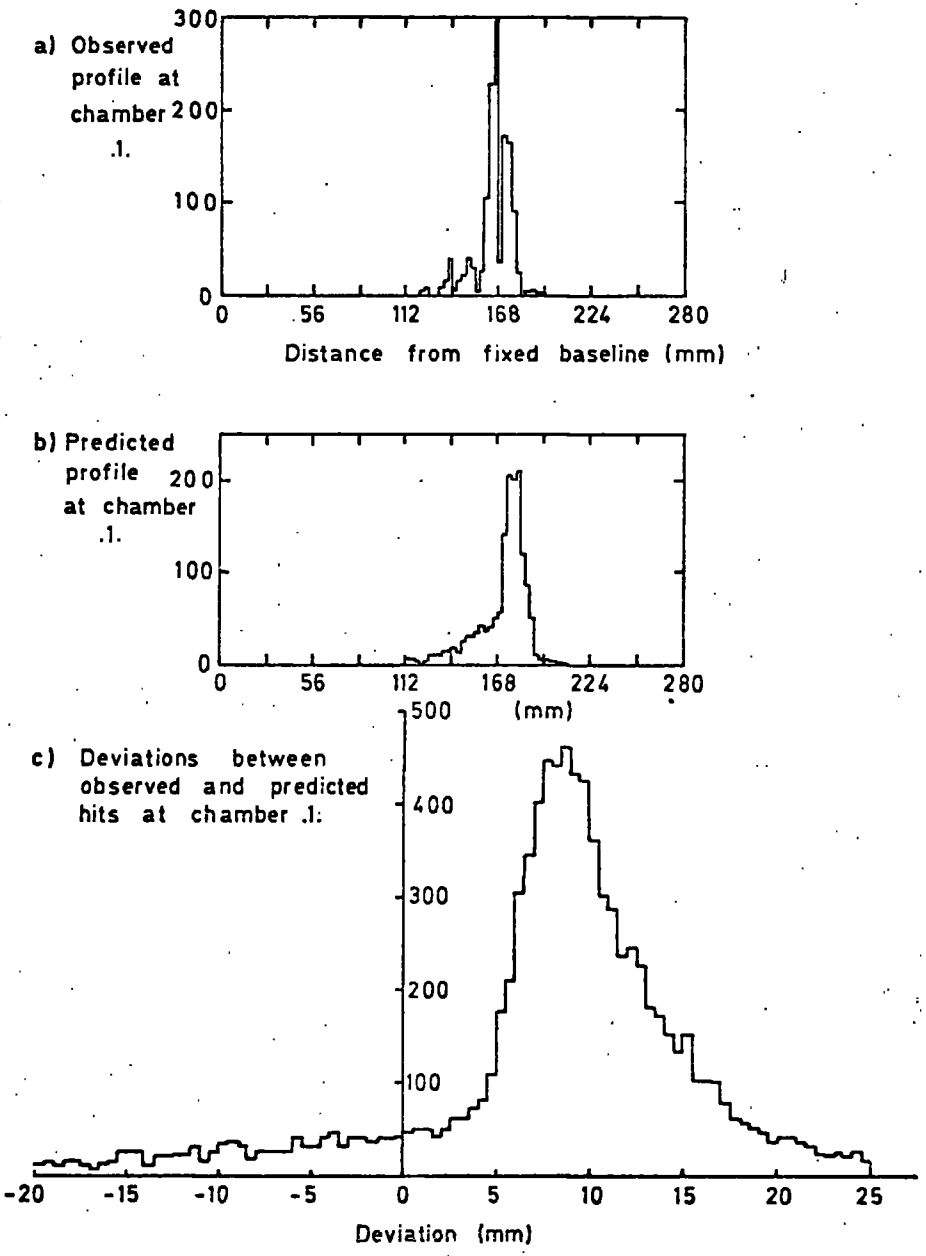

has a F.W.H.M. of 7 mm which is higher than the expected ± 2 mm for this geometry.

On considering leverage, profile reconstruction will certainly be more accurate for circular and parabolic fits as will be the requirements of the g-2 system.

5.5.7 Other Measurements

For linear track reconstruction using three points (figure 5.18), the angle (Θ) is given by:-

$$\tan\Theta = \frac{(t_3 - t_1)}{(l_1 + l_2)} \cdot V_D \qquad (5.4)$$

where V_D is the relevant drift velocity.

On plotting the distributions of Θ obtained for various energies as in figure 5.33, the desireability of working at energies above 1 GeV is again apparent as spread in the distributions due to Coulomb scattering occurs below this value. The angular acceptance of the system for these results was $\pm 1^o$ and most distributions lie well within this range, the angular dispersion of the beam at high energies being 0.2^o F.W.H.M.

An investigation was made of the showering effect of material placed in the beam as this would indicate any such difficulty to be expected during a g-2 run.

By observing the frequency of hits on each cell of an array of four drift chambers, the shower shapes could be observed for

FIG. 5.33 Angular Distibutions For Different Energies.(Binwidth of $\frac{1}{10}^{\circ}$)

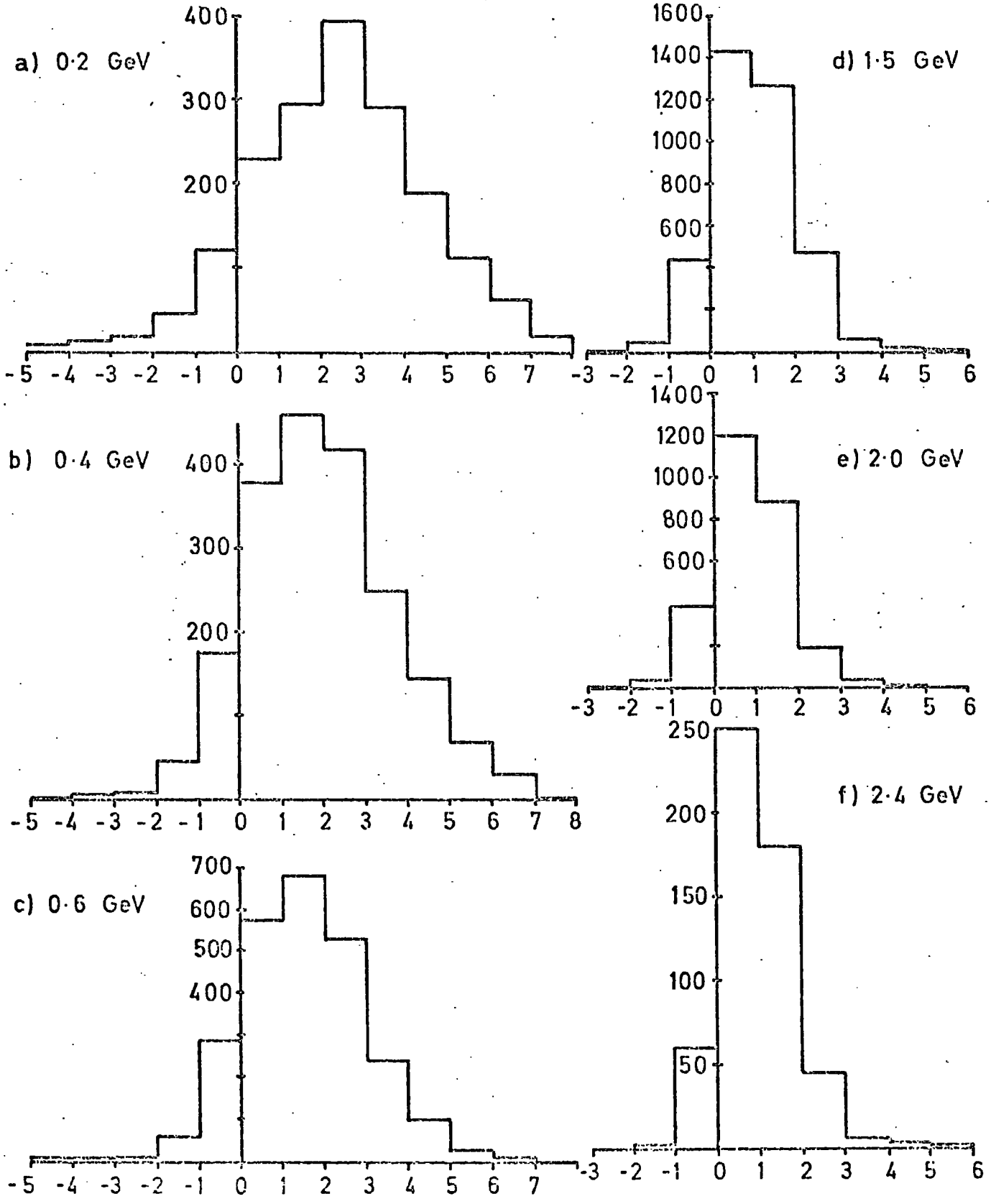

various thicknesses of lead placed on the downstream side of chamber 1 at a distance of ~550 mm from chamber 2. These results were taken for a beam energy of 2 GeV and are represented in figure 5.34 where it can be seen that distinct showers are formed after the insertion of a few mm of lead.

For 2 GeV electrons emerging from the centre of the g-2 storage tank it was calculated that typically 2 g cm^2 of material would be traversed on considering the 0.8 mm thick Titanium wall and 5 g cm^2 for the 3 mm Aluminium wall. The purpose of this brief investigation was solely to provide a crude estimate of the differences to be expected for the different wall thicknesses to be encountered in early g-2 runs, and, in this respect, figure 5.34 indicates that the Aluminium wall should produce significantly more showering and scattering of electrons than the thin wall.

5.6 Conclusion

The g-2 drift chambers have been successfully operated in the Daresbury test beam with equally good performance of prototype and production models. Efficiencies of almost 100% have been obtained and previous laboratory measurements of drift velocity in Argon-Methane have been satisfactorily reproduced by several methods.

System resolutions of the order 0.1 to 0.2 mm have been observed with no serious deterioration in a 7.5 KGauss magnetic field (providing correct electric field compensation is applied) and only a factor of 2 or 3 worse for curved end regions.

The encouraging results obtained on drift velocities, resolutions and efficiencies (even in the presence of magnetic fields and incorrect electric field compensation) can be attributed to the

FIG. 5.34 SHOWER PROFILES IN DRIFT CHAMBERS

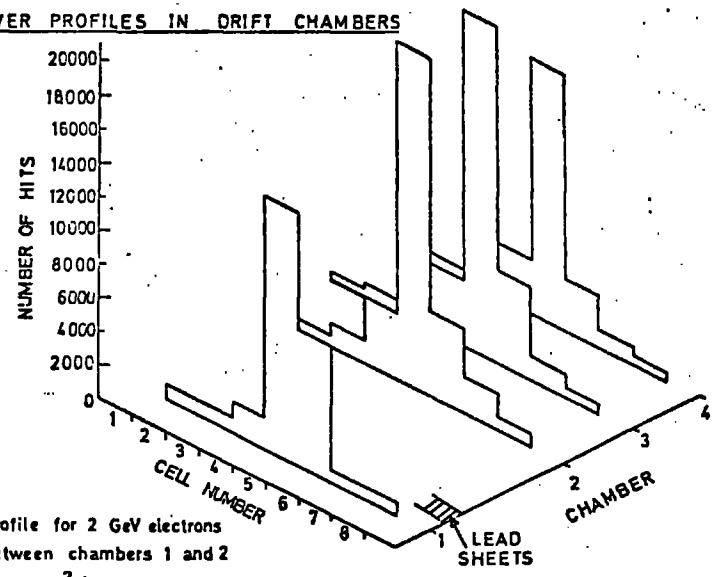

FIG. (a)
Electron shower profile for 2 GeV electrons
3mm of lead between chambers 1 and 2
(3.4 gm cm^2)

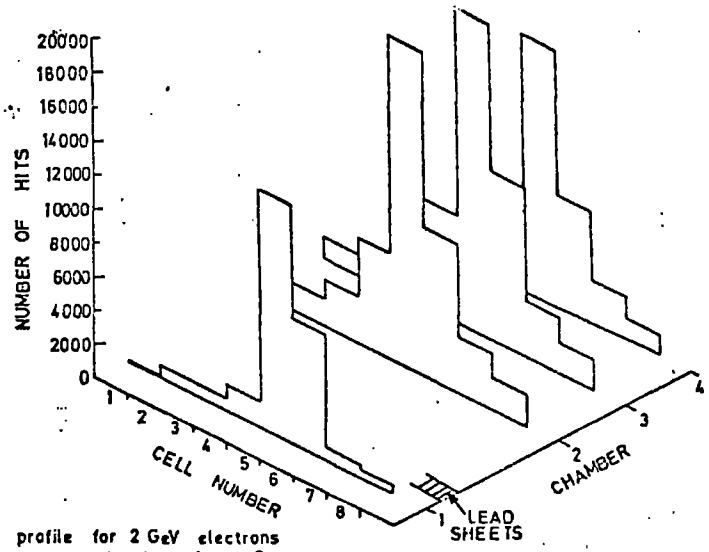

FIG. (b)
Electron shower profile for 2 GeV electrons
6mm of lead between chambers 1 and 2
(6.8 gm cm^2)

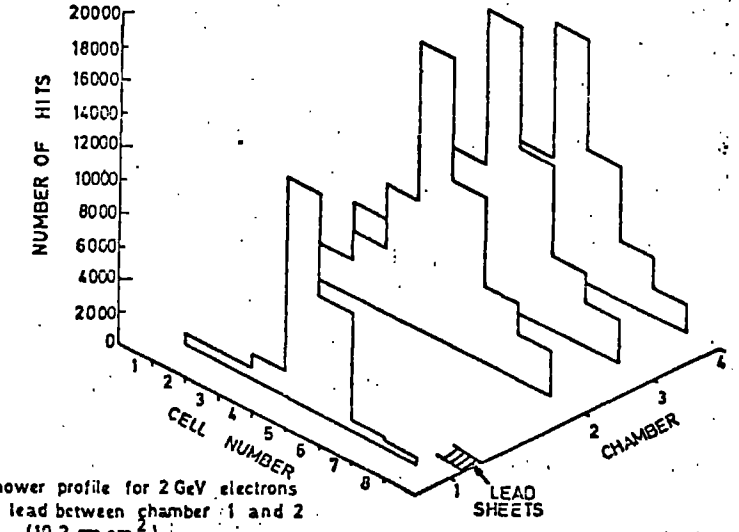

FIG. (c)
Electron shower profile for 2 GeV electrons
9mm of lead between chamber 1 and 2
(10.2 gm cm^2)

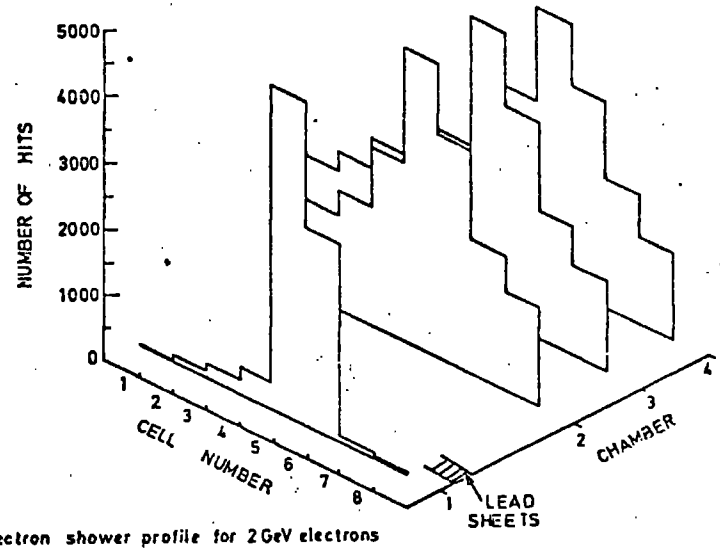

FIG. (d)
Electron shower profile for 2 GeV electrons
25mm of lead between chamber 1 and 2
(28.0 gm cm^2)

small drift distances ($\lesssim 14$ mm) in question. For larger distances, serious problems would occur in these respects, in particular concerning efficiency in magnetic fields.

A working energy threshold level of 1 GeV has been shown to be suitable for the g-2 array and the possible benefits of the thin wall section of the g-2 muon storage tank have been illustrated.

References

1 T.W. Aitken. Daresbury Laboratory Technical Memorandum. DNPL/TM 70, September 1970

2 D.J. Thomson. Daresbury Laboratory Internal Report. June 1972

3 J.M. Breare, R. Browell, K.A. Short. Durham University Internal Report, NI-74-5

4 J.M. Breare, R. Browell, K.A. Short. Durham University Internal Report, NI-75-1

5 A. Breskin, G. Charpak, F. Sauli, M. Atkinson, G. Schultz. Nucl. Inst. Meth. 124 (1975) 189

6 J.E. Bateman, J.F. Connolly. Rutherford Laboratory Internal Report, RL/75/044 February 1975

CHAPTER 6

THE OPERATION OF DRIFT CHAMBERS IN MAGNETIC FIELDS

6.1 Theoretical Considerations of Drift Chambers in Magnetic Fields

6.1.1 Basic Considerations

It is a commonly known fact that the motion of drifting electrons will be affected by a strong external magnetic field. This effect is of maximum importance to drift chambers for a component of the field (B) parallel to the wire direction, in which case, the electrons tend to be swept away from the sense wire plane and possibly completely out of the chamber. Thus, this geometrical motion alone will affect drastically the observed drift times and efficiency of the device. (It will be seen later in this chapter that the presence of a magnetic field also affects the actual drift velocity).

A neat method of correcting such an undesireable electron motion has been realised by Charpak et al. (1); that is, to tilt the equipotential lines in the chamber by the amount necessary to balance the electric field and Lorenz forces in such a way as to produce a resultant electron motion in the sense wire plane. The correct angle of electric field tilt is given by:-

$$\alpha = \arctan\left(\frac{BW}{E_o}\right) \qquad (6.1)$$

where α is shown in figure 6.1, W is the drift velocity and E_o is the electric field towards the sense wire. Such a configuration is easily achieved in a chamber of the Charpak design (as in the g-2 chamber case).

Having described a basic magnetic field compensation mechanism, it is now necessary to discuss the effect of such crossed fields on the drift velocity and angle of the electrons. As in the case where B = 0, it is the collision processes which are important, and, to this end, the classical theory of electron motion in such an environment has been considered by Palladino and Sadoulet (2, 3). A simpler theory has been presented in the early work of Townsend (4) and sucessfully applied to the explanation of recent results by Charpak et al. (5). The purpose of this chapter is essentially to apply this theory to the Argon-Methane gas used in the g-2 chambers, and to develop a simple model which takes into consideration a non-uniform magnetic field of flux up to 15 KGauss.

6.1.2 Classical Theory of Electron Drift

For electrons in an electric field and no external magnetic field, the drift velocity can reasonably be expressed as:-

$$W_o = k \frac{eE}{m} \tau \qquad (6.2)$$

where τ is the mean free time between collisions (assuming here that

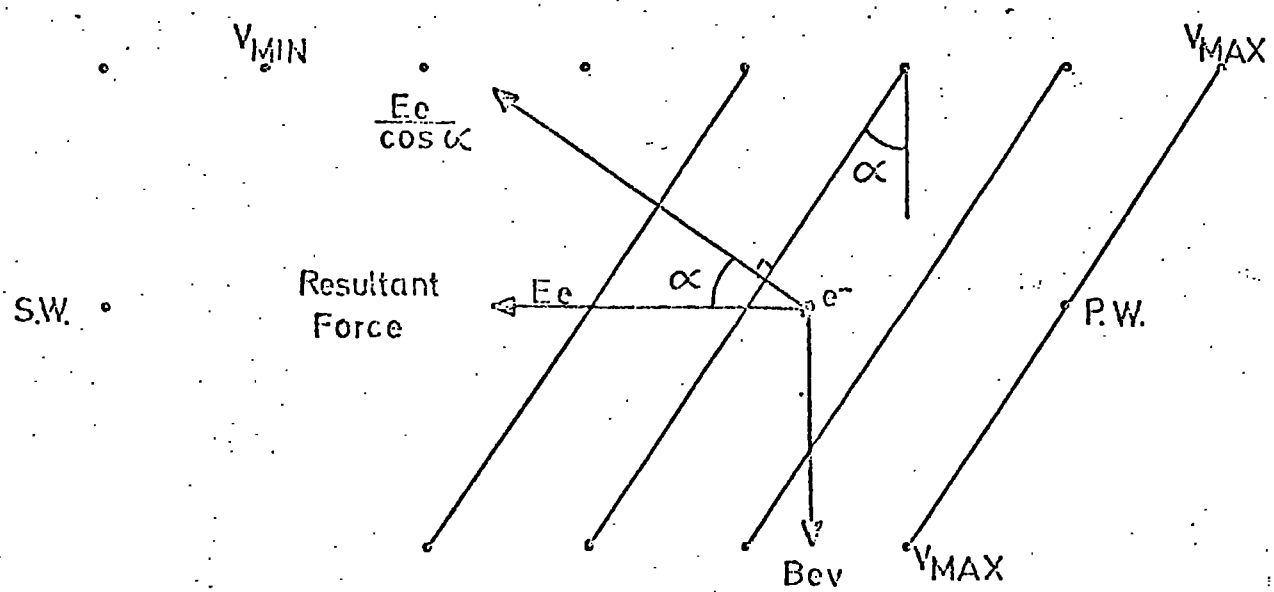

FIG 6.1 Method of Compensating for a Magnetic Field

$\tau(E,B) = \tau(E,B = 0)$), and k is a constant derived from some assumed velocity distribution of the swarm; a value of k = 0.75 as pertaining to the Maxwellian distribution (6) will be used in the model, as good fits have been obtained by other workers (5) with this value.

In the presence of a magnetic flux, B, the drift velocity becomes (4):-

$$W_B = k \frac{E}{B} \frac{\omega\tau}{\sqrt{1+\omega^2\tau^2}} \qquad (6.3)$$

where ω = eB/m, the Larmor frequency of electrons. Hence it can be seen that the modification of drift velocity due to the introduction of a magnetic field is given by:-

$$W_B = W_o \left[1 + \left(\frac{BW_o}{kE}\right)^2\right]^{-\frac{1}{2}} \qquad (6.4)$$

The angle of drift of electrons in orthogonal magnetic and electric fields is given by:-

$$\theta(E,B) = \arctan(\omega\tau) \qquad (6.5)$$

a result which has been experimentally verified by Charpak (5) using a special drift chamber. On considering this expression, inspection of equation 6.3 now yields:-

$$W_B = k \frac{E}{B} \sin\theta(E,B) \qquad (6.6)$$

For drift chambers with adjustable electric fields, one further important consideration is that only discrete angles of tilt (γ) may be realised; in the g-2 chambers these being 18.4^{o}, 33.7^{o}, 45^{o} and 53.1^{o}, corresponding to relative displacement of voltages on opposite H.T. planes of ± 1, ± 2, ± 3 and ± 4 wire spacings respectively. Hence, for given E and B values, it may be that Θ (the correct angle for drift to be in the sense wire plane) cannot possibly be reproduced exactly, thus causing the initial drift direction to be at a slight angle to the normal drift plane. Because of this, the measured drift velocity (derived from the time taken to cover a known distance) will be observed as:-

$$W_{//} = W_B \cos(\gamma - \Theta) \qquad (6.7)$$

Notice that the value of Θ is similar to the previously expressed angle, α, (equation 6.1), but in fact represents a better model. It must also be mentioned that E in the above expressions refers to the electric field orthogonal to the lines of force and is of value $E_o/\cos\gamma$.

6.1.3 Application of the Theory to Experimental Results

A complete set of drift velocity data, including variations due to magnetic and electric field strengths has been collected at a CERN test beam (5,7). These results were taken mainly for Argon-Isobutane gas mixtures and were found to agree quite well with the variation predicted by the classical theory presented here. An almost perfect fit was obtained for drift velocity and angle variations with magnetic field in an electric field of 500 V cm^{-1}, but slight

discrepancies were apparent for 1000V cm^{-1}. This is because the method of deriving expressions 6.3 and 6.5 does not include the fact that electron energy and collision cross section are functions of E; hence the model is better for low electric field values.

Reasonable agreement between experiment and theory has also been established (8) in the case of Argon-Methane gas mixtures.

6.2 Application of the Theory to Argon-Methane.

Using equation 6.4 with k = 0.75, the values of drift velocity in Argon (90) - Methane (10) were calculated for various values of E and B. The zero magnetic field drift velocity, W_o, is a function of electric field, and values were extracted from the experimentally determined drift velocity curve previously shown in figure 4.11. Hence starting with a set of experimental values, the theoretical behaviour of electrons in various magnetic fields has been investigated for electric fields up to 1000 V cm^{-1}. This variation is shown in figure 6.2, indicating a tendancy for the drift velocity to decrease as magnetic field increases. For fields in the 15 KGauss region, a convenient levelling off of these curves is displayed, which means that fluctuations in magnetic field in this region do not seriously alter drift velocity.

A tendancy towards a plateau can also be observed in figure 6.3 where drift velocity variation with electric field is plotted for several magnetic field values up to 15 KGauss. Saturation is complete in all cases at a field of around 1000 V cm^{-1}.

Figure 6.4 shows the variation of drift angle with magnetic field for various values of electric field; in other words, the required angle of electric field tilt to exactly compensate for

FIG 6·2

DRIFT VELOCITY Vs MAGNETIC FIELD FOR VARIOUS ELECTRIC FIELDS

(Ar (90) : CH_4 (10))

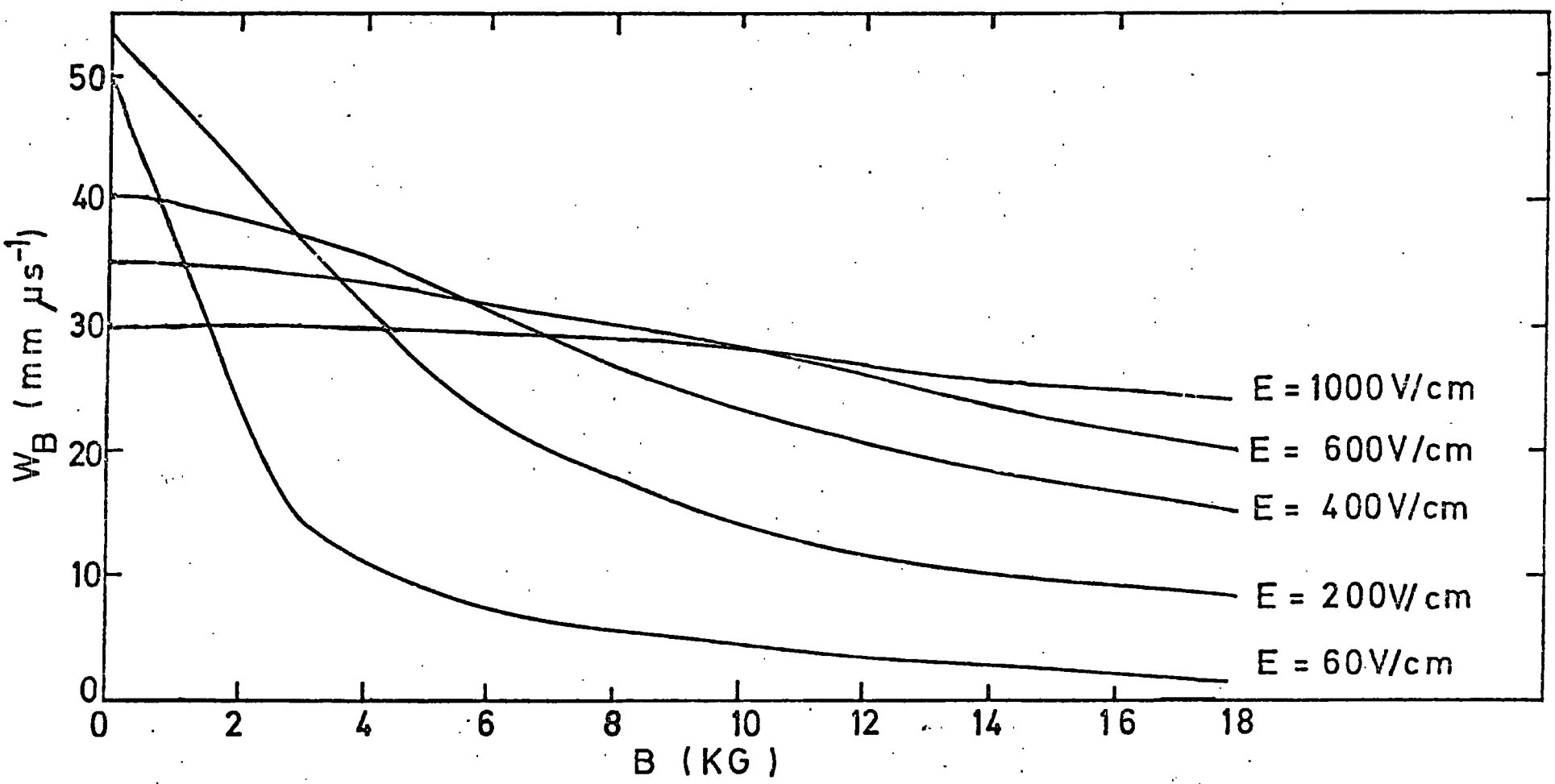

FIG. 6·3 DRIFT VELOCITY V_s ELECTRIC FIELD FOR VARIOUS MAGNETIC FIELDS. (Ar (90) : CH_4 (10))

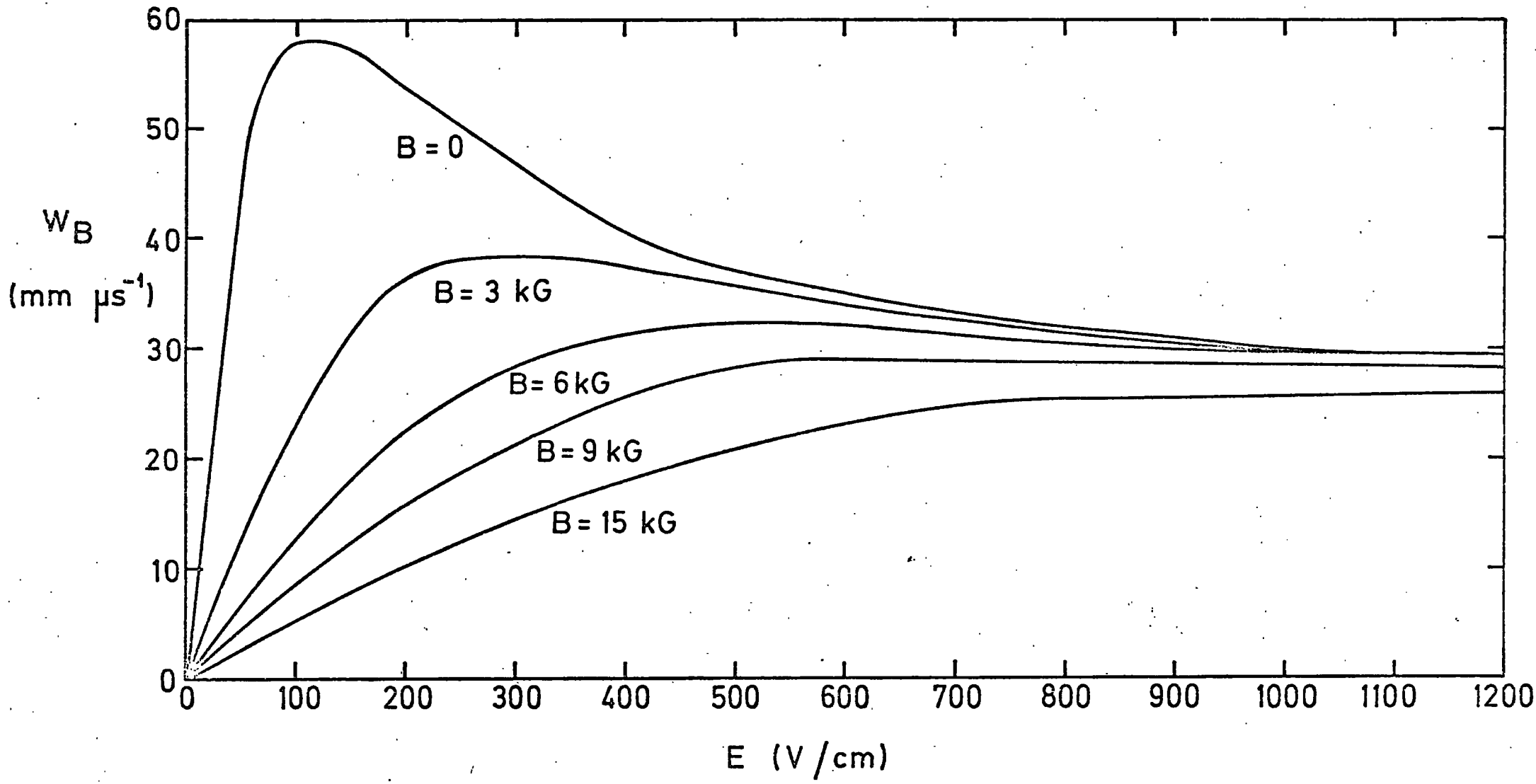

FIG. 6·4 ANGLE OF ELECTRON DRIFT (θ) IN ORTHOGONAL MAGNETIC AND ELECTRIC FIELDS: θ Vs. MAGNETIC FIELD FOR VARIOUS ELECTRIC FIELDS. (Ar (90): CH_4 (10))

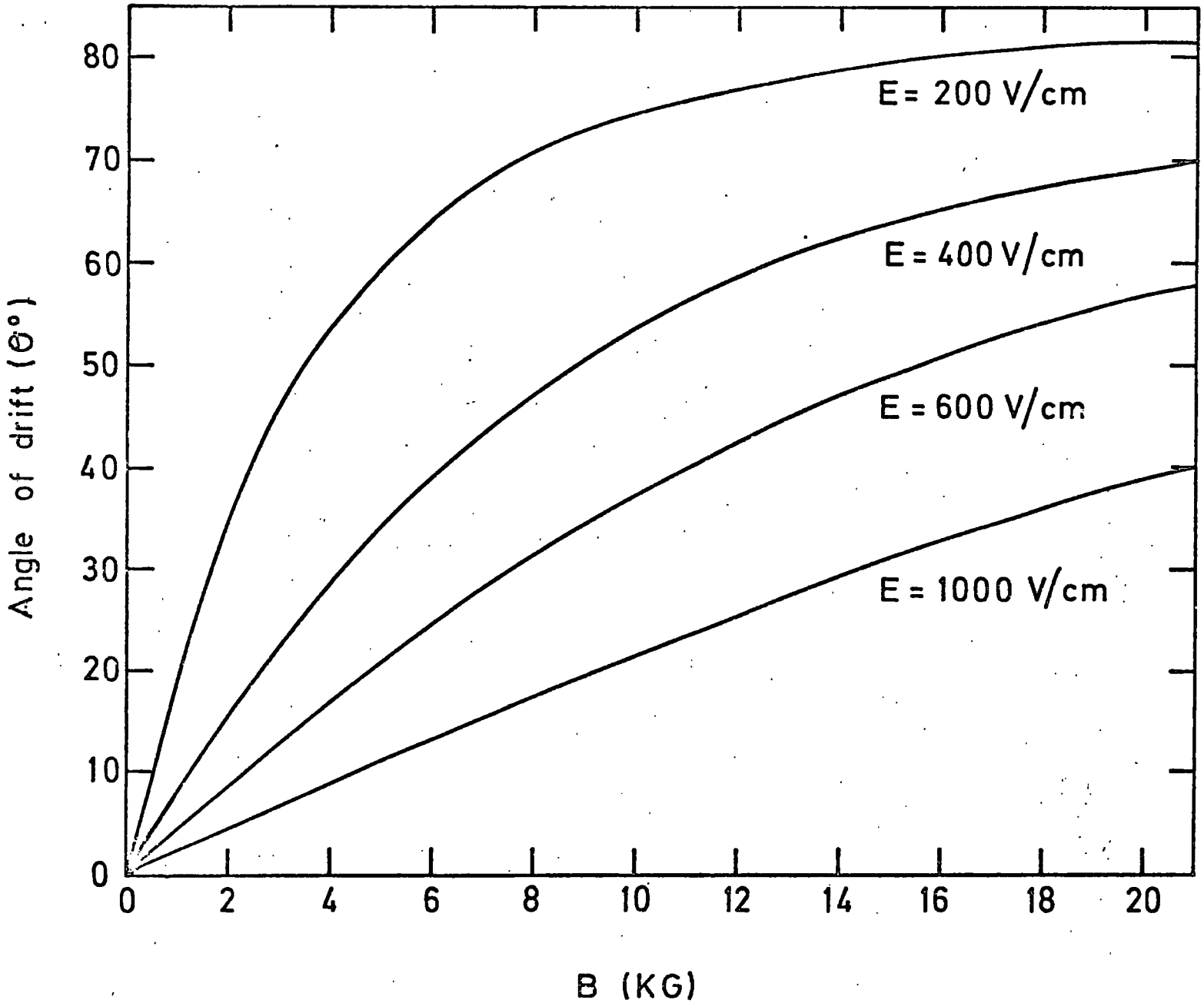

the magnetic field effect. The tangent variation indicated in equation 6.5 means that the Θ-value is more critical for lower magnetic fields; however, this is offset by the fact that the flow-line trajectories of electron swarms due to the actual field in a drift cell (see for example figure 3.9) overrides the effect of small magnetic fields. This has been experimentally observed (7) in the operation of drift chambers in leakage fields of bending magnets. As expected, larger electric fields necessitate smaller tilting angles.

6.2.1 Example

The magnitude of magnetic fields usually encountered in high energy physics is of the order 15 KGauss; consider then, a cell of a g-2 chamber operating in such a field. Inserting known values into the cruder model equation, 6.1, indicates a necessary field tilt of $\sim 41^{\circ}$, hence consider a tilt of 3 H.T. wire spacings, that is $\gamma = 45^{\circ}$. E_0 in this case is ~ 600 V cm^{-1} giving a value of $E \sim 850$ V cm^{-1} at which field the drift velocity should be about on the saturation part of the curve. (This is certainly true for B = 15 KGauss as seen from figure 6.3)

Equations 6.2 and 6.5 now give the required angle of tilt to be $\sim 37^{\circ}$, meaning that in this case γ and Θ differ by 8°.

The variation of the observed drift velocity given by equation 6.7 is plotted as a function of magnetic field in figure 6.5, where it is also compared with the actual drift velocity of electrons in the gas. The two curves approach each other, touch at B = 20 KGauss and move apart as B is increased further; that is to say that such an electric field configuration in a g-2 chamber as described above would compensate exactly for a 20 KGauss field. The usual

FIG 6.5

THEORETICAL VARIATION OF DRIFT VELOCITIES WITH MAGNETIC FIELD

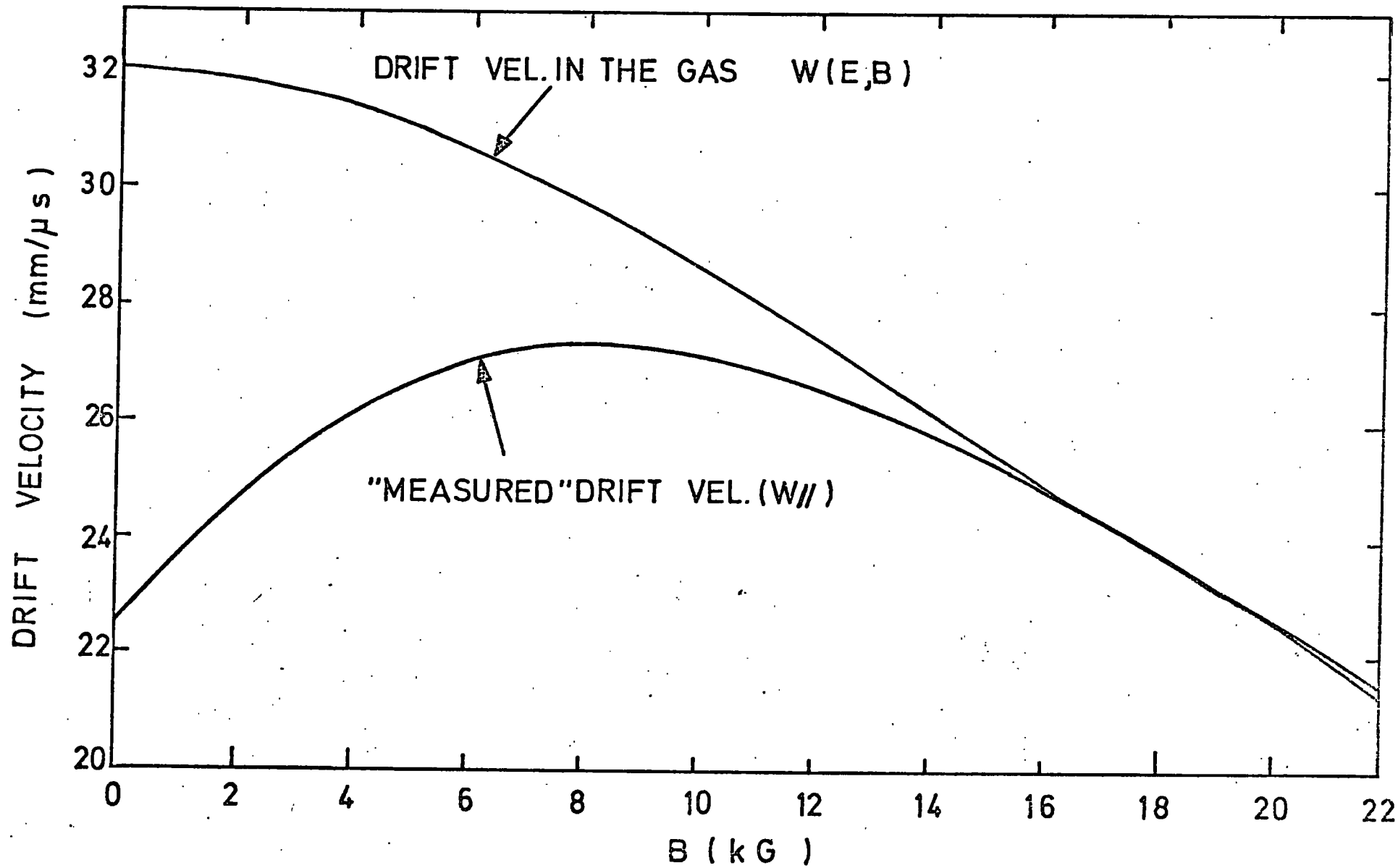

decrease of actual drift velocity with magnetic field is once again apparent whereas the observed drift velocity reaches a maximum value at $\sim$ 8 KGauss because of the additional cosine modification. This presents another convenient property (as will be seen in the next section) of there being less variation in observed drift velocity than in actual drift velocity as the magnetic field varies up to 16 KGauss.

With this in mind, the next section deals with the application of such a model to a real case in which a strong magnetic field varying between 5 and 15 KGauss is encountered.

6.3 A Proposed Method to Compensate for a Non-Uniform, Strong Magnetic Field

6.3.1 The g-2 Magnetic Field

The magnetic field between the pole pieces of a g-2 magnet block is known to 1 ppm. This is shaped at the edges of the pole faces for reasons discussed previously in section 2.4. Outside this region is the leakage flux common to all such C-magnets. Figure 6.6 is a plot of the magnetic flux against radial distance on a median plane and shows a marked variation in B across the length of the drift chamber superimposed on the diagram. Notice that the radial field variation is slightly different for the block-centre and block-corner cases; for convenience, the calculations following will be done using only the block-centre field; bearing in mind that some software modifications may eventually be required. Electric field compensation for up to 14.745 KGauss will be required.

FIG. 6.6

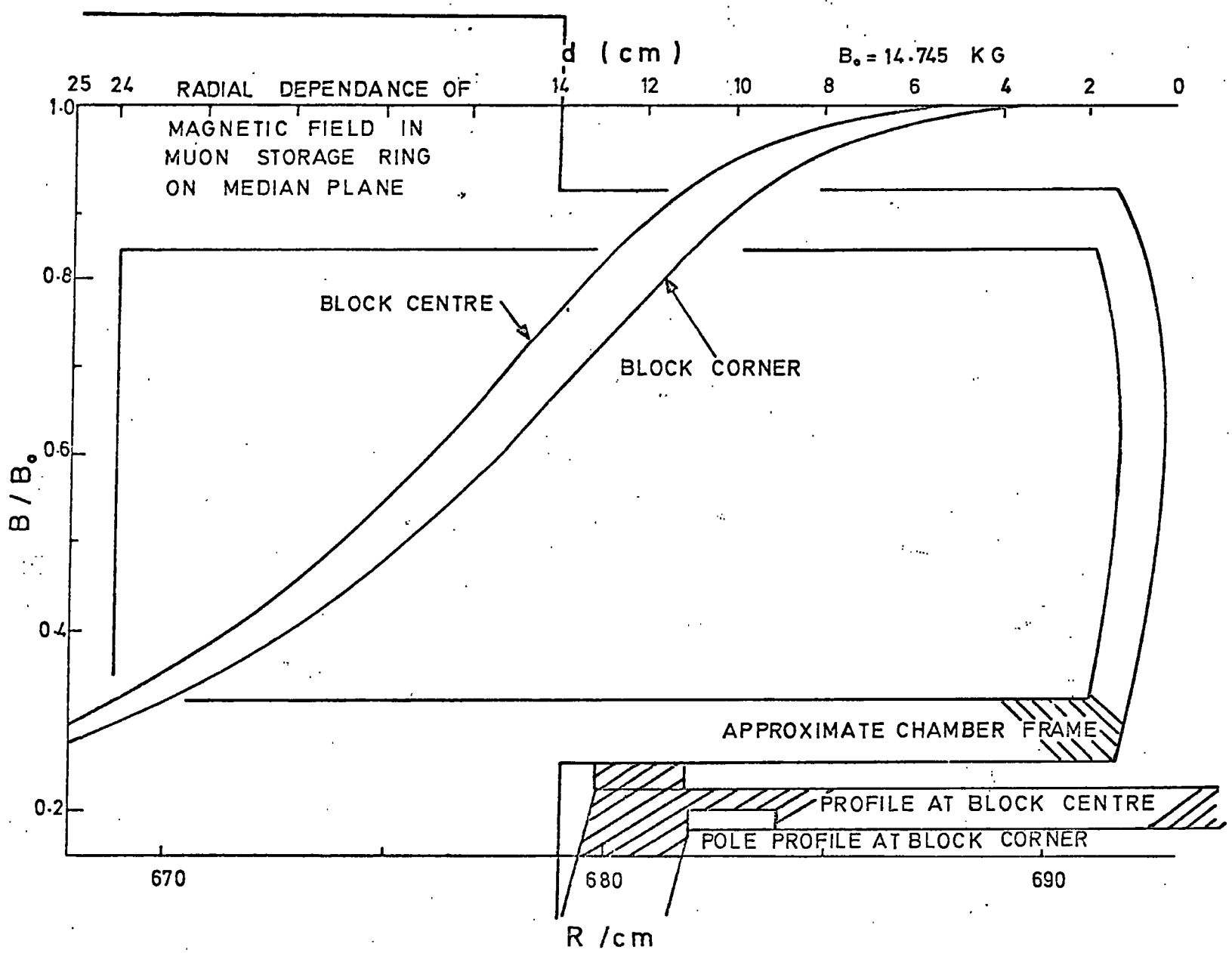
d (cm)
B_0 = 14.745 KG
25 24
14 12 10 8 6 4 2 0
RADIAL DEPENDANCE OF
MAGNETIC FIELD IN
MUON STORAGE RING
ON MEDIAN PLANE
1.0
0.8
0.6
0.4
0.2
B / B_0
BLOCK CENTRE
BLOCK CORNER
APPROXIMATE CHAMBER FRAME
PROFILE AT BLOCK CENTRE
POLE PROFILE AT BLOCK CORNER
670
680
690
R /cm

6.3.2 Initial Compensating Mechanism Proposals

A series of calculations was performed to estimate the voltage on each H.T. wire to produce at each point on the sense wire plane an electric field to compensate exactly for the Lorenz force. This idea was dismissed because of the large number of resistors and leads required and the complicated nature of the fields thus produced.

The next attempt was to have different electric field tilts in the chamber, that is to vary the angle of the electric field in three distinct regions of the chamber according to the average magnetic field strength in each region. This method would certainly restore the otherwise depleted chamber efficiency and, indeed, first tests in the g-2 storage ring (9) were done with the innermost two cells having an electric field tilt of 3 H.T. wire spacings, the next three cells having 2 and the final three cells 1. However, a varying-tilt system such as this can lead to complicated drift velocity variations as will be evident from the next section.

6.3.3 Theoretical Examination of Various Electric Field Configurations

To choose the best electric field tilt (or combination of tilts) to provide compensation for the g-2 magnetic field, and, at the same time, produce a manageable drift velocity variation along the length of the chamber, the classical theory was applied to various field configurations in the following way:-

Knowing the value of E, W_o can be found from figure 4.11, and thus the theoretical drift angle ($\Theta(E,B)$) can be determined by combining equations 6.2 and 6.5. This value can then be used to find the drift velocity in the gas ($W(E,B)$) from equation 6.6 which can then be converted to observed drift velocity ($W_{//}$) using equation

6.7. If this process is repeated at mm. distance increments from the vacuum tank wall, that is to insert the radial distance variations of B and E into the above expressions, the observed drift velocity variation along the length of the chamber can be determined.

Figure 6.7 shows the variation of drift velocity in the gas with radial distance from the vacuum tank wall, as derived by the above method, for several electric field tilt configurations (E_o=600 Vcm^{-1}). As would be expected, smooth curves with W(E,B) increasing with distance from the tank wall are yielded for constant electric field tilts. For the varying tilt cases, sharp velocity discontinuities are observed. This does not seem likely in practice but laboratory tests on tilted electric fields at B = 0 have shown strong drift time variations at cell boundaries (appendix 2). Hence it was decided to continue work only for constant tilts of 2, 3 and 4 wire spacings (tilts of < 2 and > 4 would almost certainly lead to a reduction in efficiency in the 14.745 KGauss region which is the most important detecting area).

For the values of γ obtained from the above three tilts, the variation with distance of the initial direction of the electron swarm could be estimated. Figure 6.8 shows this variation $|(\gamma - \Theta)|$ for each case and also indicates how reasonable a compensation each tilt produces over the full length of the chamber. As γ increases, E also increases and hence Θ decreases. For the particular values of γ chosen here, this leads to $(\gamma - \Theta)$ being finite in all cases except at a radial distance inwards of 148 mm., where exact compensation for the magnetic field at that point occurs for a tilt of 2 spacings. In fact it is this field tilt which produces the smallest deviations of $(\gamma - \Theta)$ from zero. The fact that $|(\gamma - \Theta)|$ is initially of a similar value for the 2 and 3 tilt cases is simply because the under-

FIG. 6·7 (a) PREDICTED DRIFT VELOCITY "IN THE GAS" V_S DIST. FROM VAC. TANK WALL. (g-2 FIELD)

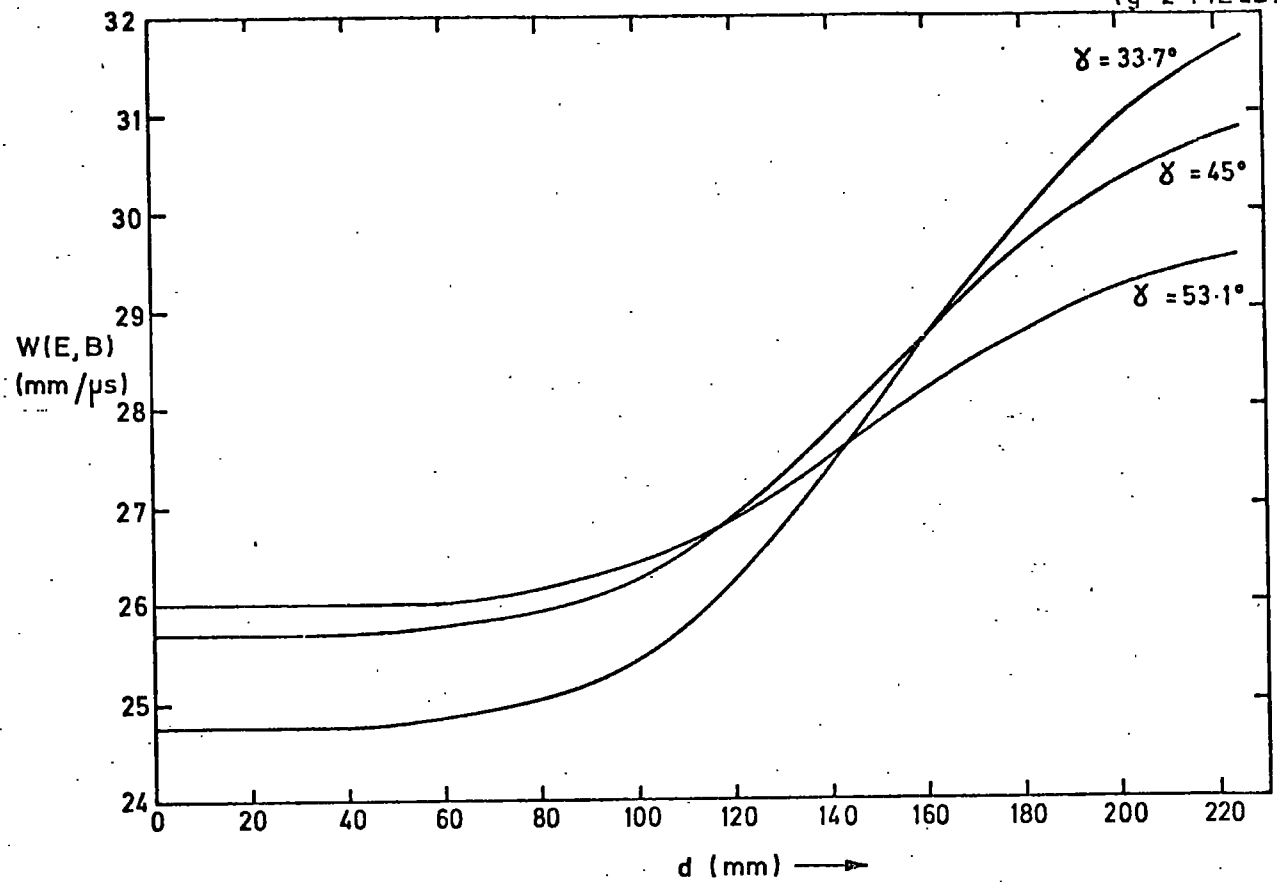

FIG. 6·7 (b)

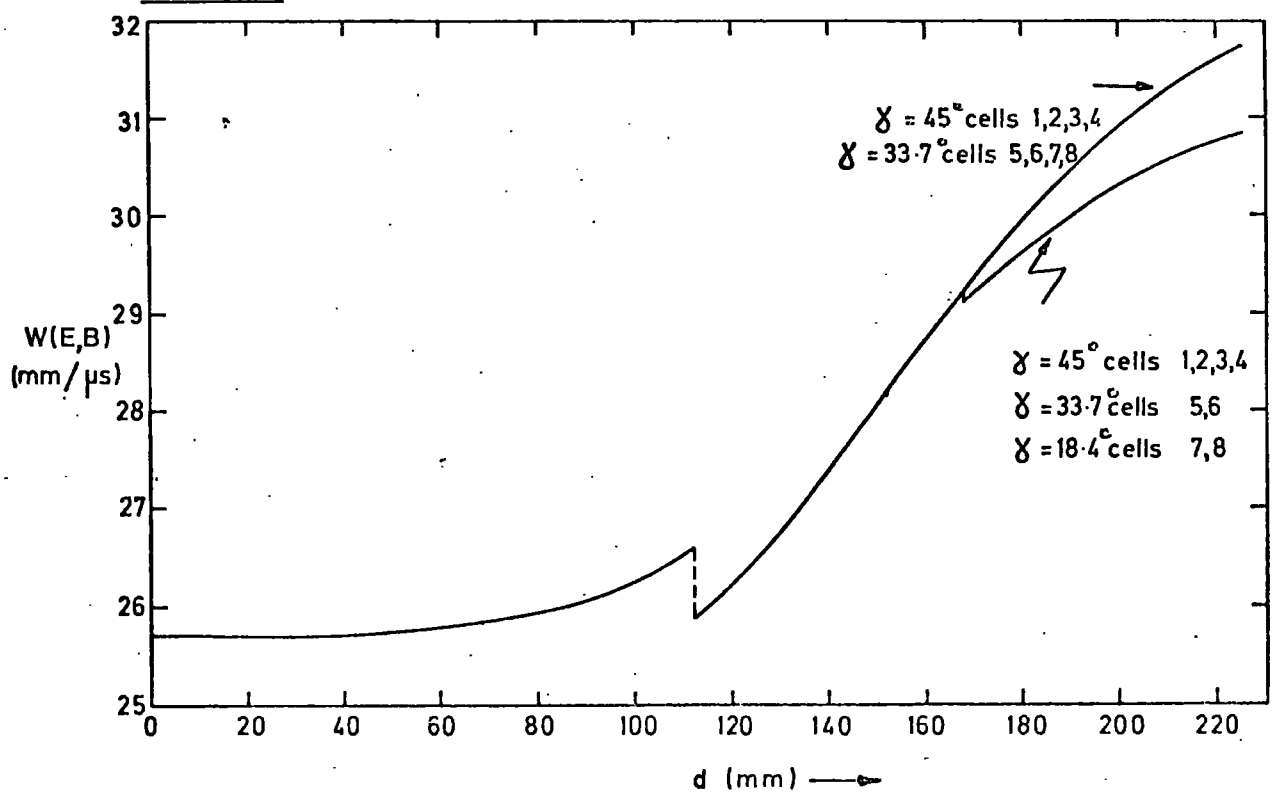

FIG. 6·8

DIFFERENCE BETWEEN DRIFT ANGLE AND ANGLE OF TILT OF ELECTRIC FIELD Vs' DISTANCE FROM VACUUM TANK WALL

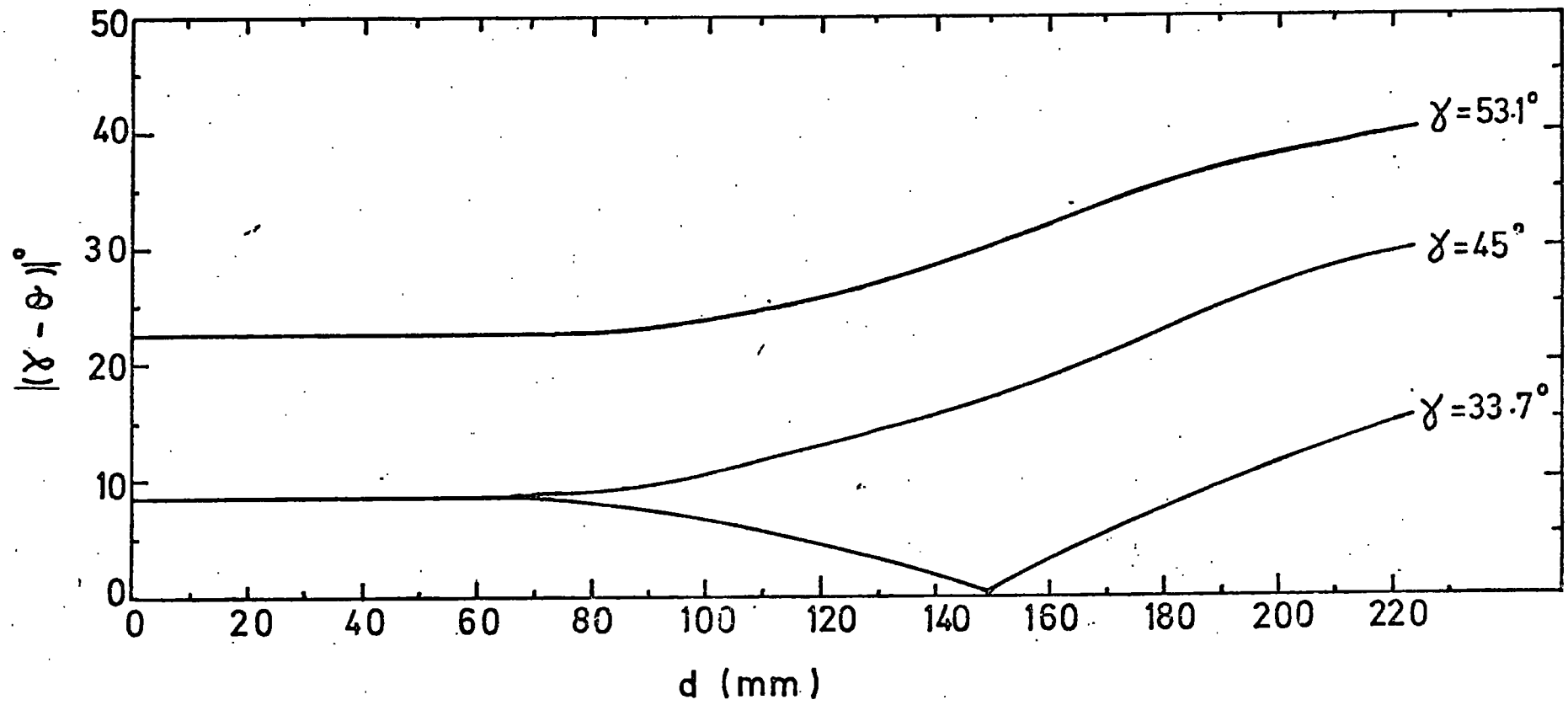

compensation produced by the former tilt happens to equal the over-compensation of the latter.

The most important property of the value of tilt set is shown in figure 6.9, that is, the radial distance variation of observed drift velocities. It is desireable to keep the variation of $W_{//}$ as small as possible and this is best manifested for a tilt of 3 spacings ($\gamma = 45^{o}$). For this value, the curve shown in figure 6.7 modified by the relevant curve of figure 6.8 produces a variation in $W_{//}$ between 25.45 and 27.30 mm. μs^{-1} only; that is to say that although W(E,B) is increasing with radial distance inwards (due to B decreasing), this is offset to a large extent by γ becoming further away from the desired compensation angle, θ, thus causing cosine$(\gamma-\theta)$ to decrease in equation 6.7.

(Although the electron swarm will eventually follow flow lines which are not necessarily straight, the $(\gamma-\theta)$ variation will basically mean longer drift paths as distance from the tank wall increases and hence smaller observed drift velocities.)

6.3.4 Final Choice of Compensating Mechanism

For the detection of primary tracks, that is, those where the electron detected in the drift chambers is the one that triggers the shower counter, the most important chamber detecting area is that which overlaps the g-2 counter sensitive area. A significant part of this area is in a region of almost uniform magnetic field, as can be seen from the field variation in figure 6.6, and many of the decay electrons will be detected in this region.

For maximum chamber efficiency in this, the most important detection zone, it is obvious that $(\gamma-\theta)$ must be as small as

FIG. 6.9

PREDICTED DRIFT VELOCITY Vs' DISTANCE FROM VACUUM TANK WALL
(g - 2 FIELD)

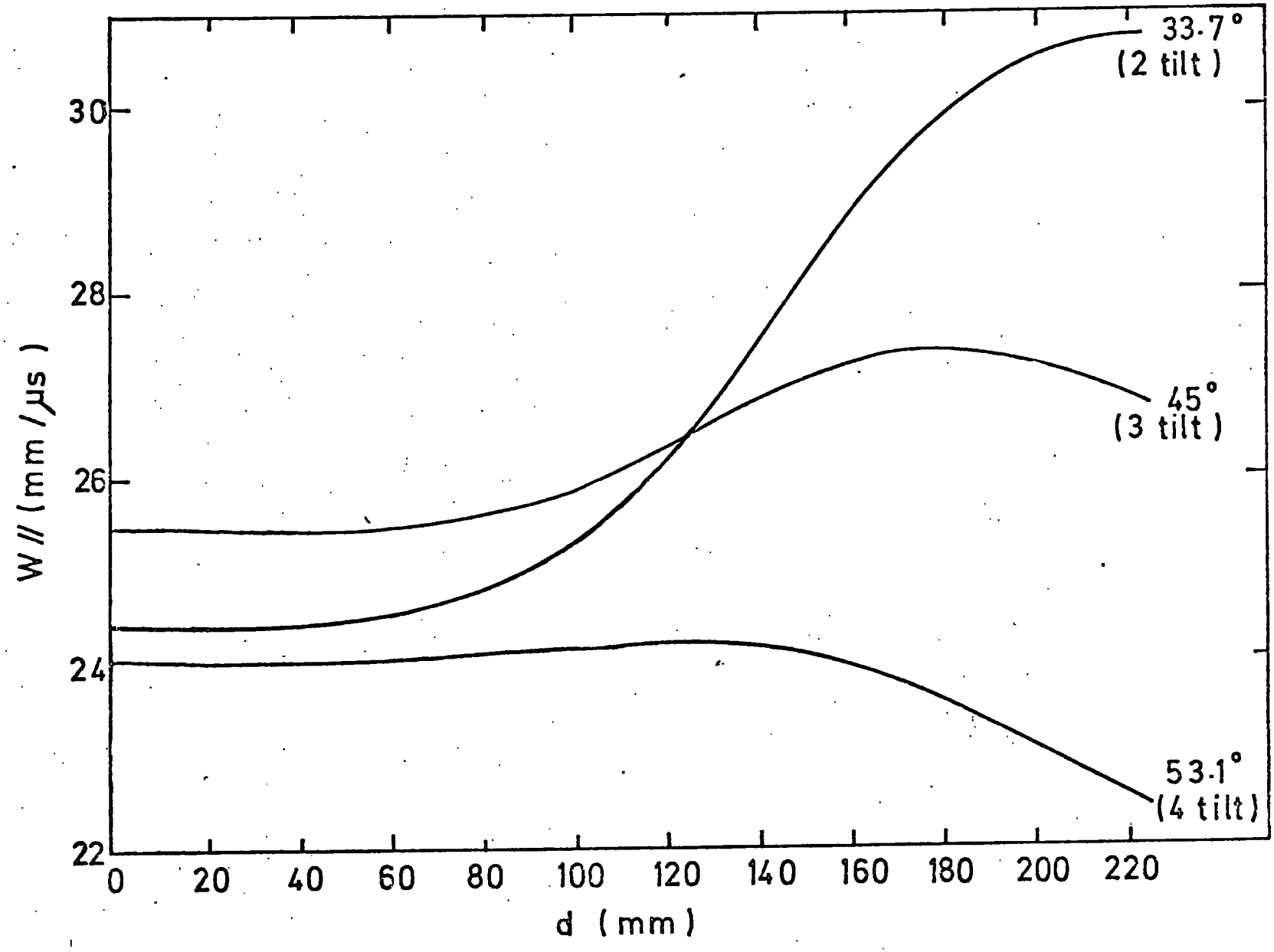

possible, from figure 6.8 this value is a minimum for the 2 and 3 tilt cases ($|(\gamma - \theta)| = 8.7^{\circ}$ and 8.4° respectively). The fact that outside this region, the variation of $(\gamma - \theta)$ is smaller for two tilts is overridden by the much flatter $W_{//}$ versus d curve presented by 3 tilts in figure 6.9

Points also to be taken into consideration are:-

The value of E manifesting from 3 tilts is more favourable than that of 2 tilts as regards drift velocity stability, and, the lower drift velocities for 2 and 4 tilts present many drift times outside the ranges of normal digital timing devices.

On considering such factors, it is apparent that tilting the electric field by 3 H.T. wire spacings ie. 45° provides in a simple way the most suitable compensation mechanism for the g-2 magnetic field; a reasonably small observed drift velocity variation being produced at the expense of inheriting some degree of inefficiency in the region of low magnetic field (for efficiency measurements with slanted electric fields in no magnetic field see appendix 2).

Using the above chosen compensating mechanism, a drift time to radial distance calibration curve was derived for all cells. This is shown in figure 6.10, the values being obtained by approximating figure 6.9 to a series of straight lines (that is, assuming constant drift velocity over half a cell width, such an approximation leading to maximum errors in timing of the order 0.5%, that is, under 0.07 mm over the maximum drift distance).

Those values lying outside a normal TDC range (512 ns) are indicated.

FIG. 6·10

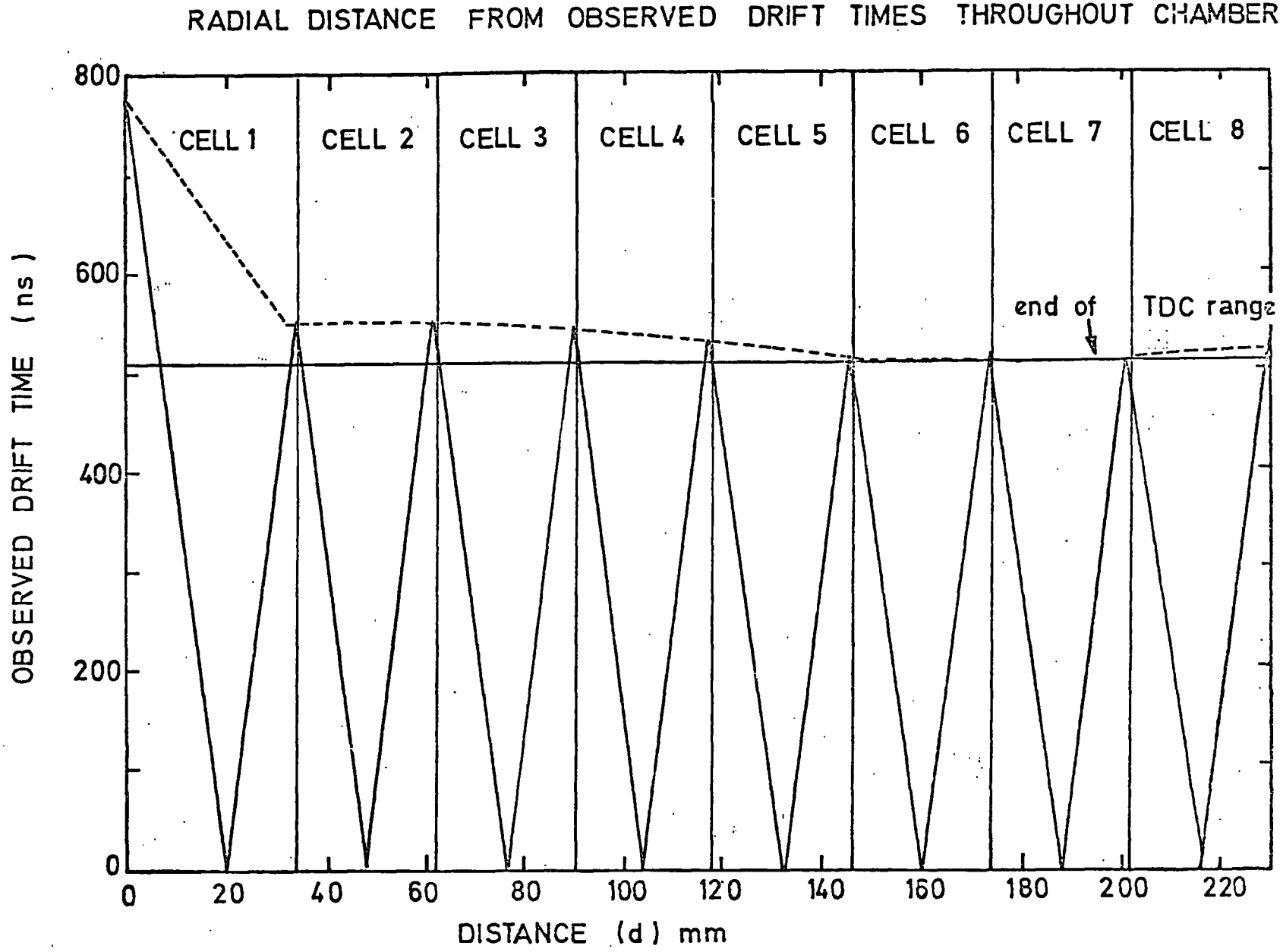

6.3.5 Criticism of Model and Concluding Remarks

The value of the constant k has been chosen arbitrarily to define a Maxwellian velocity distribution. This is most certainly not the case for the drifting electron swarm, however such a fit to the experimental results of Charpak (5) encourage such a choice. Several calculations were done for Argon-Methane using k = 0.81 (a Druyvesteyn distribution (6)) but have not been used in this current work.

The main fault with the model is the assumption of a constant electric field experienced by the swarm. This is invalidated firstly by the field pattern occurring in the chambers (see chapter 3) and secondly by the flow line trajectories of electrons. Also, in this respect, the model gives no firm drift time predictions for the curved end region which must be assumed to exhibit similar drift velocity characteristics to the normal side of the first cell in the chamber. The reasonable assumption is made that values of E acting on the swarm are always high enough to be on the saturation part of the drift velocity curve.

Initially, for simplicity in the data analysis, linearity of $W_{//}$ will be assumed across each cell half-width. Better estimates should however be obtained after complete experimental drift time calibration. In this respect, reasonable drift velocity calibration for the chambers in their experimental locations will be automatically forthcoming from the track data, that is, by observing the cut off points of drift time distributions for each cell. Such results will give an indication of the validity of the model described here and are presented with the rest of the initial drift chamber data from g-2 in the following chapter.

References

1 G. Charpak, F. Sauli, W. Duinker. Nucl. Inst. Meth. 108 (1973) 613

2 V. Palladino, B. Sadoulet. Lawrence Berkeley Laboratory Internal Report, LBL-3013 (1974)

3 V. Palladino, B. Sadoulet. Lawrence Berkeley Laboratory Internal Report, LBL-3070 (1974)

4 J. Townsend. Electrons in Gases. Hutchinson's Scientific Publications, London, 1948

5 A. Breskin, G. Charpak, F. Sauli, M. Atkinson, G. Shultz. Nucl. Inst. Meth. 124 (1975) 189

6 L.B. Loeb. Basic Processes of Gaseous Electronics. University of California Press, (1961)

7 A. Breskin, G. Charpak, B. Gabioud, F. Sauli, N. Trautner, W. Duinker, G. Shultz. Nucl. Inst. Meth. 119 (1974) 9

8 R. Browell, Ph.D. Thesis, University of Durham, in preparation

9 J.M. Breare, R. Browell, K.A. Short. Durham University Internal Report, NI-74-6

CHAPTER 7

THE TRACK MEASURING SYSTEM IN THE g-2 MUON STORAGE RING

7.1 Introduction

Preceeding chapters have discussed in detail the development and properties of the g-2 drift chambers and the purpose of this chapter is to describe their installation in the muon storage ring at CERN. The operation of the chambers in this environment is studied using subsystems of the final track measuring array; the latter system, comprising eight M.W.D.C's and three M.W.P.C's, being now fully constructed. A satisfactory data acquisition system for the final drift chambers, independent of that of the main experiment, is described and initial results from this system are presented. This work has been carried out during three g-2 runs.

7.2 Initial Tests in the Storage Ring (1)

Initial investigations were made using one prototype drift chamber mounted on a rigid baseplate at a distance of ~330 mm upstream of counter 11. Argon(90)-Methane(10) gas, from a supply outside the storage ring, was flushed through the chamber, and a drift field of 580 V cm^{-1}, usually tilted by 2 H.T. wire spacings, was applied. Signal outputs were fed via 50 cm miniature coaxial cables (RG 174) to

low input impedance Verweij preamplifiers from which 32 metres of coaxial cable conducted the signals to triple shaper discriminator units in the control room.

7.2.1 Observations Prior to a g-2 Run

Radiative interference from Suisse Romande television transmission was picked up by the chamber sense wires and after amplification appeared as a A.M. $\leqslant 60$ mV noise level into $50\,\Omega$. The steel magnet blocks afforded no shielding against this pickup, however, earthed aluminized-mylar windows reduced this level to 20 mV maximum peak to peak.

Pulses from the chamber due to an Fe 55 X-ray source in the presence of the magnetic field were successfully observed in the control room and showed no observable deterioration after traversing the length of cable in question.

7.2.2 The "Initial Flash"

Figure 7.1 shows a simplified representation of the main part of a g-2 cycle. A capacitative pickup pulse, generated as protons from the synchrotron pass a fixed point in the g-2 beam line, provided the trigger to the main experiment. As the inflector was pulsed, on receipt of a pion bunch, a 10 μs long pulse train was observed in detector electronics. This was immediately followed by a high flux pion burst in the storage ring referred to as the "Initial Flash". The main experiment collected electron data from the shower counters for a time of 750 μs after the initial flash, a further disruptive noise source due to the electrostatic focussing electrodes being occurrent at 800 μs after the latter.

FIG 7.1 THE (SIMPLIFIED) g-2 CYCLE
(occuring once every 2 secs.)

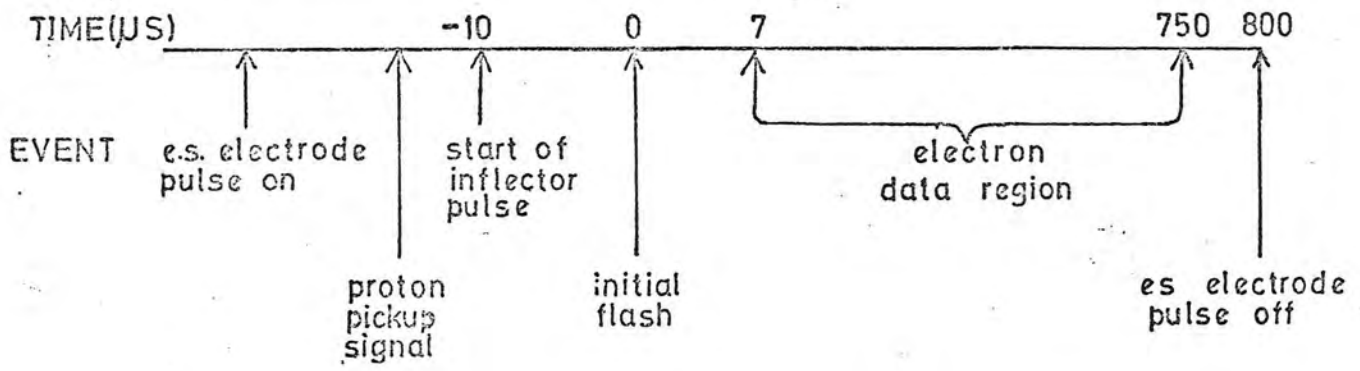

FIG 7.2 THE INITIAL FLASH PION PULSE
(200ns/cm , 200mv/cm)

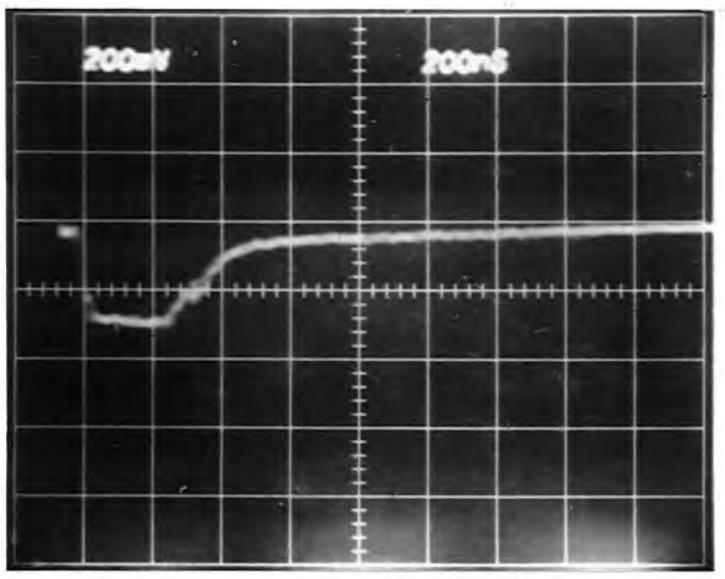

With the drift chambers operational, the initial flash appeared as a few hundred ns long pulse on the sense wire as exemplified in figure 7.2 (for cell 8 with no electric field tilt); an estimated 10^6 pions per chamber per flash causing electron swarms to drift from all parts of the cell.

Figure 7.3 compares the pulse height voltage characteristic, obtained for this pion pulse, to that from non-minimum ionizing Sr 90 electrons in the same cell. Saturation of the amplifier is reached at lower H.T. values for the former due to the massive ion flux involved.

7.2.3 Data Acquisition from One Chamber

Timing was achieved using a T.A.C.-P.H.A. system and in order to eliminate the noise sources described in the previous section, the T.A.C. "starts" from counter 11 were gated in for a period 7 to 707 μs after the initial flash using the system shown in figure 7.4 (t_D = 7μs, t_W = 700μs). Events were shifted onto the 1.0μs scale of the T.A.C. by the inclusion of delay cables in the drift chamber output channels and calibration of the timing system was achieved in the usual manner.

As the g-2 electron shower counter operates on the principle of output pulse height being proportional to energy deposited, by discriminating these pulses at various levels, data from electrons of greater than certain energies could be observed in the main experiment. By fanning out the electron pulse and using five discrimination levels, a series of five "pulse height bits" determined the energy of any electron to within $\sim \pm 0.25$ GeV. In a similar manner, by attenuating the relevant (drift chamber trigger) counter pulse before discriminating at a fixed level, an energy threshold for drift chamber

FIG.7·3. COMPARISON OF PULSE HEIGHT-VOLTAGE CURVES FOR PION PICKUP PULSE AND Sr 90 β-RAYS.

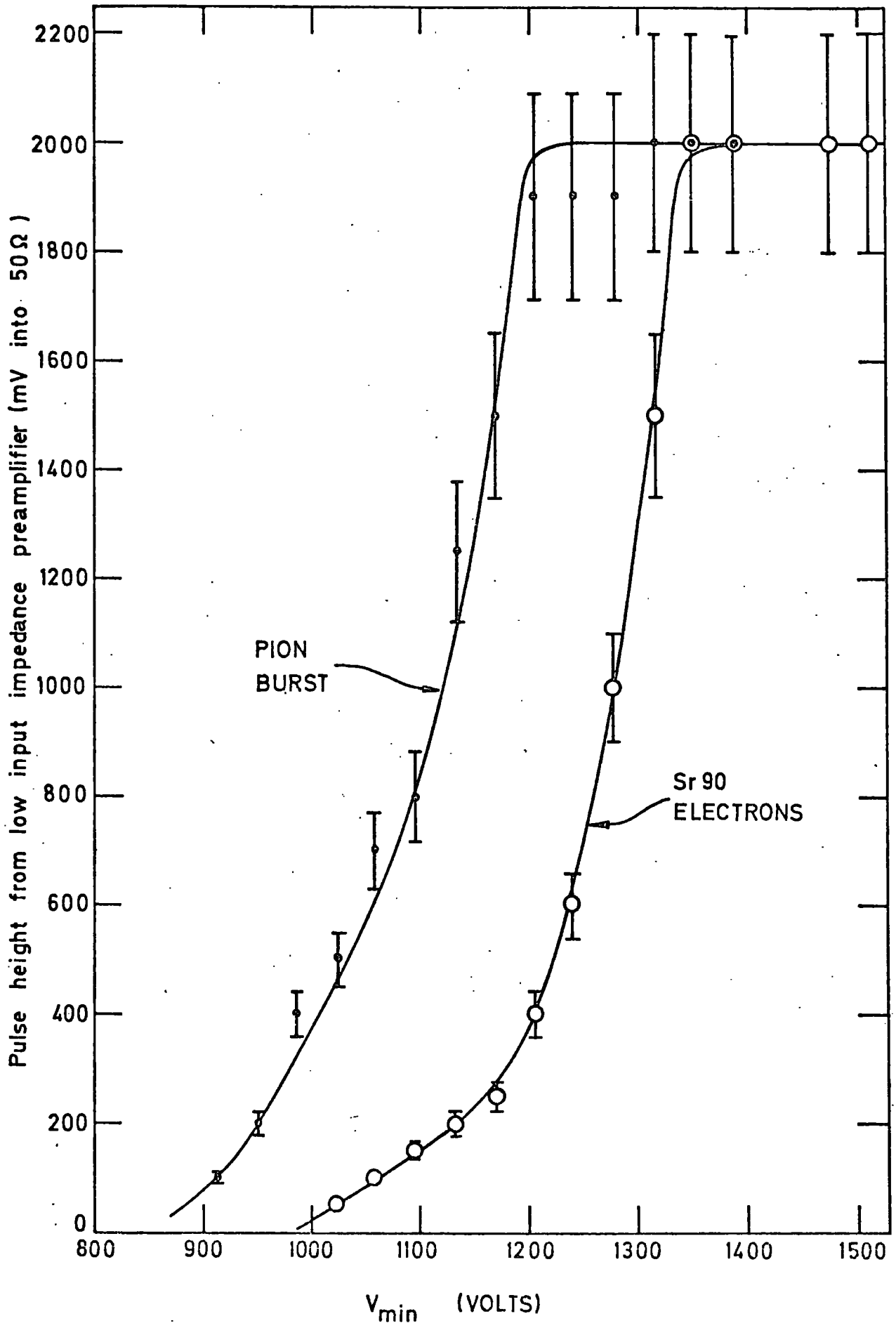

FIG 7.4 : THE EVENT GATE SYSTEM.

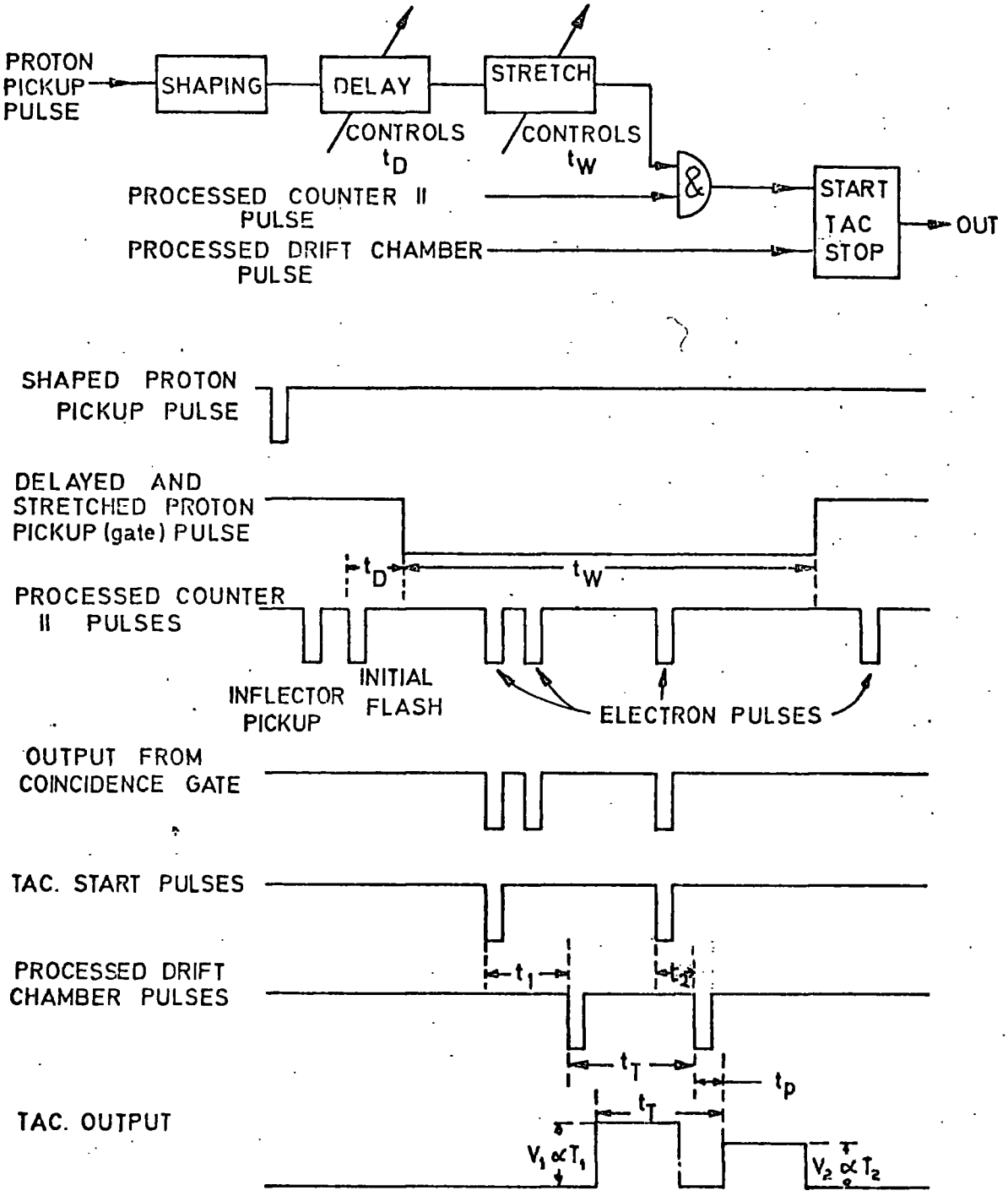

t_D = Delay between initial flash and start of gate.

t_W = Gate width.

t_1 , t_2 : Drift times

t_T : Separation time of events.

t_p : Processing time of TAC.

events could be set (figure 7.5).

Figure 7.6 shows the observed rate of gated counter 11 pulses as a function of attenuation. Comparing these rates with the count rates of the pulse height bits (as observed at the drift chamber electronics rack to eliminate any pulse height attenuation due to different cable lengths), as presented in figure 7.7, leads to the attenuation level-energy calibration curve of figure 7.8. For the collection of drift time data, a threshold of 1 GeV was usually set thus selecting forward decaying electrons in the muon rest frame and reducing the scattering factor as discussed in chapter 5. Note that certain changes in g-2 conditions (eg. number of injected bunches) necessitates a recalibration.

On collecting data from one cell with this system, event rates were typically 1 or 2 per minute.

7.2.4 Observations During a g-2 Run

Figure 7.9 shows the drift time distribution obtained when decay electrons traversed cell 5 of the chamber. A square edged spectrum is observed on top of a significant noise level, the latter being attributed to random T.A.C. starts and stops occurring frequently compared to the event rate (signal:noise $\simeq$ 1:1), and the width of the distribution is estimated to be (483 $\pm$ 21)ns. The observed detection efficiency of only ~5% can be attributed partly to geometrical collection areas and an electron flux decrease over the length of the drift chamber (further efficiency effects will be discussed in section 7.4.2).

On inserting the relevant parameters into the equations discussed in chapter 6 (the sense wire was ~165 mm from the tank wall

FIG. 7·5 THE ENERGY THRESHOLD SELECTION SYSTEM

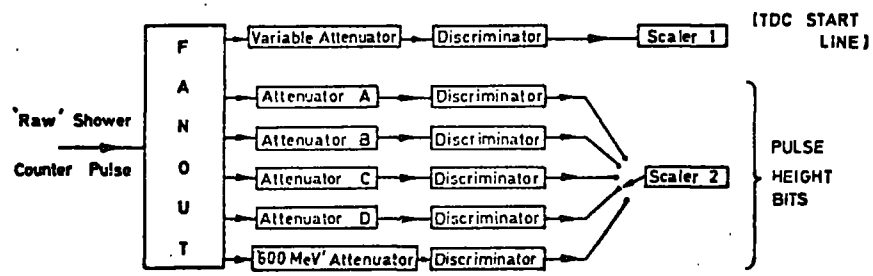

FIG. 7·6 COUNT RATE FROM SHOWER COUNTER VS ATTENUATION

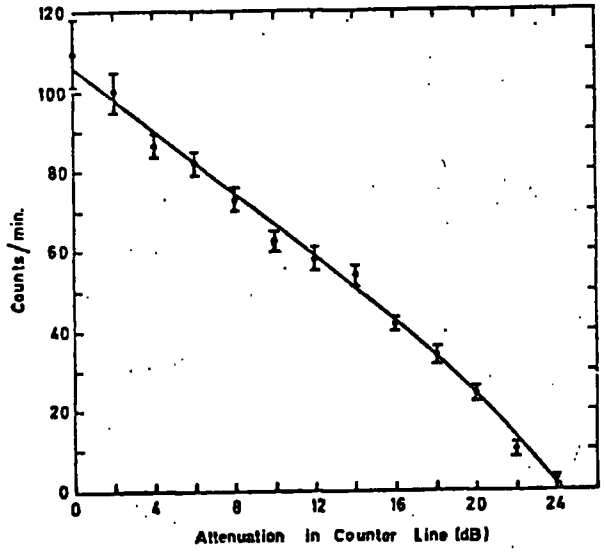

FIG. 7·7 "Pulse height bit" count rates.

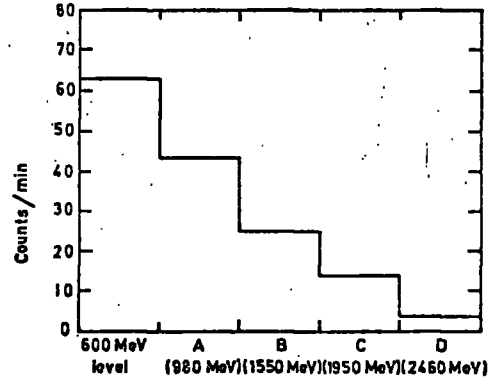

FIG. 7·8 Attenuation required for energy threshold.

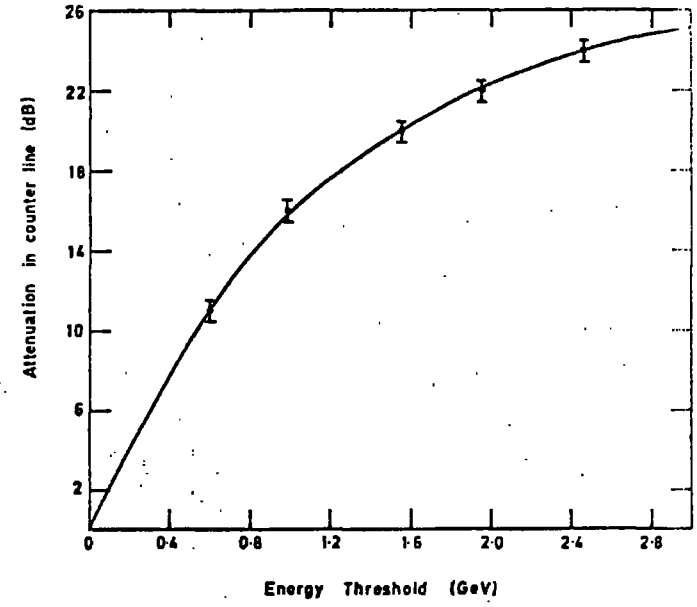

FIG 7.9 : DRIFT TIME DISTRIBUTION FROM CELL 5 IN g-2 STORAGE RING. (HORIZONTAL SCALE : 4·2 ns/channel)

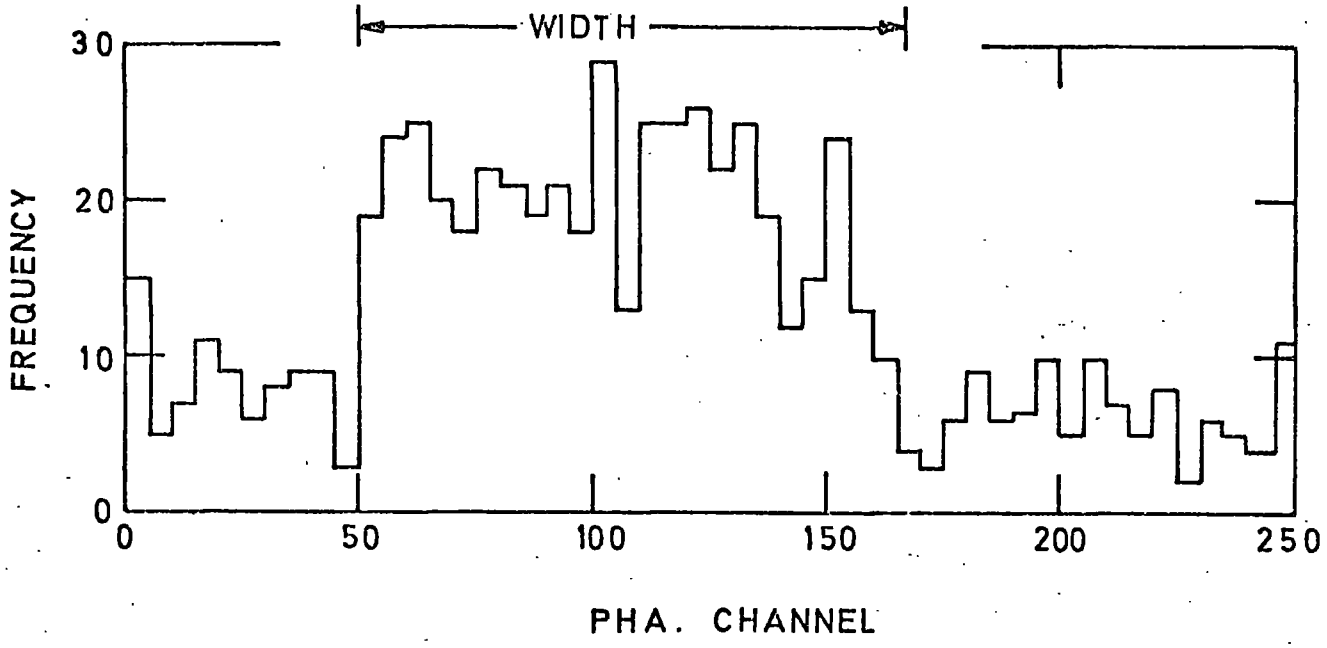

FIG 7.10 : DRIFT TIME DISTRIBUTION FROM CELL 1 (curved end cell) IN g-2 STORAGE RING (4·2 ns/channel)

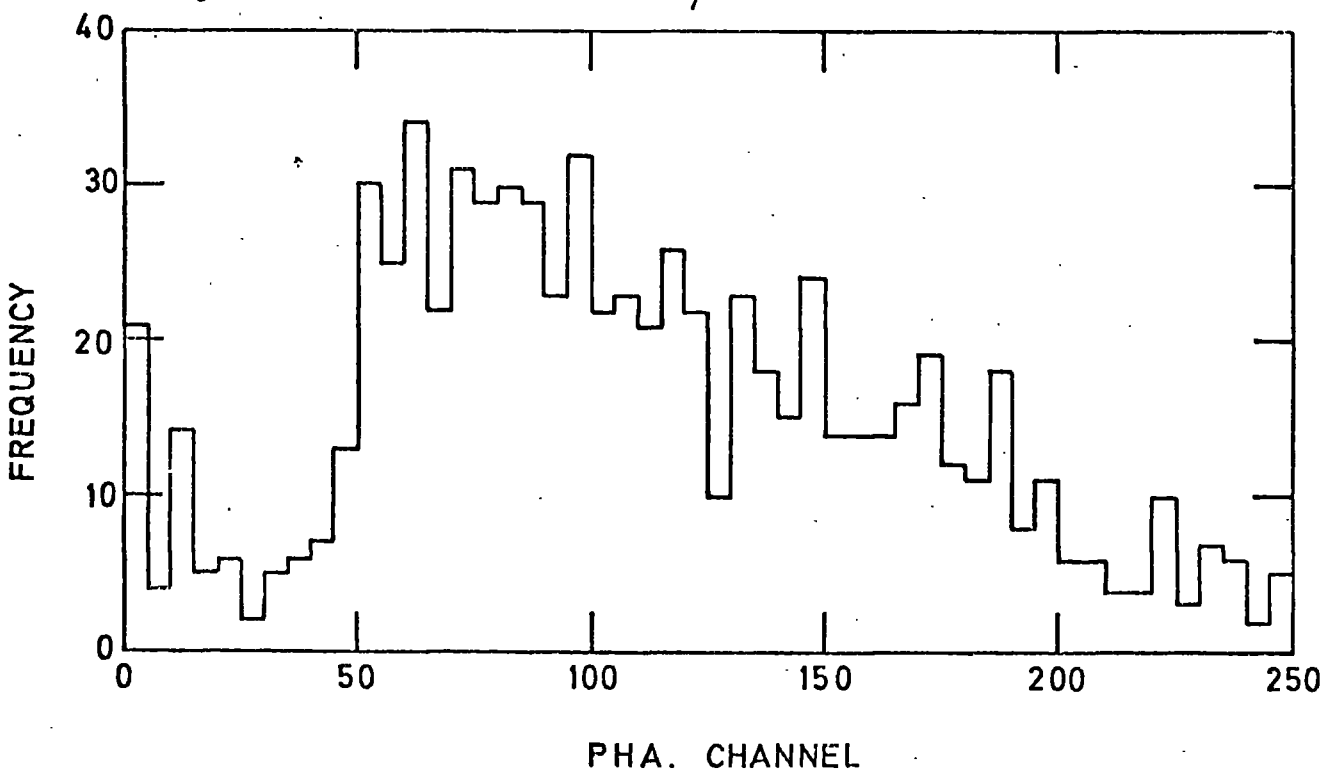

in this arrangement and therefore the magnetic field across cell 5 varied between 8.1 and 10.3 KGauss), $(\gamma - \theta)$ at the sense wire was estimated to be 2.76^{o} (compared to 3.5^{o} in figure 6.8 for the slightly higher drift field of 600 Vcm^{-1}) and $w_{//}$ was estimated to be (29.0 ± 2.5) mm μs^{-1} (equalling the value of figure 6.9) thus yielding a predicted distribution width of (483 ± 42)ns. Extremely good agreement between the observed performance and that predicted by the theory of chapter 6 is thus apparent from this data.

Similar drift time data were collected for cell 1 (which included the prototype curved end of figure 3.7(a)). Here a detection efficiency of ~10% was observed and the distribution obtained is shown in figure 7.10. The tail on the distribution is attributed to electrons traversing the curved end region which is thus seen to function as a drift space in the high magnetic field; the gradual fall off is probably due to a combination of the chamber geometry and inefficiency in this region.

7.2.5 Initial Track Observation

Using four drift chambers (three prototypes and one production model) separated by ~90 mm with the downstream chamber being ~120 mm from counter 11, electron data were collected from all cells using a data acquisition system including a small computer (to be described in section 7.3). At the time, the magnetic field compensating mechanism was one of variable electric field tilts throughout each chamber and decay electrons emerged from the vacuum tank through the 3 mm Aluminium alloy wall.

At a threshold of 1.3 GeV, ~85% of the event candidates (four chambers hit) collected exhibited more than one cell being hit

in at least one chamber. This suggested severe showering and scattering of electrons in the tank wall and made the deciphering of data difficult. Very few clean tracks were obtained, some of which are illustrated in figure 7.11, and no beam profile reconstruction was made due to insufficient data being collected. However, this work has proved, as expected, the importance of installing the thin wall section in the drift chamber region.

7.3 The Present Storage Ring Drift Chamber Array

Eight drift chambers are currently installed in the g-2 muon storage ring, a schematic plan diagram being illustrated in figure 7.12 where the positions of the M.W.P.C's of the array are also indicated. The chambers were mounted in adjustable cradles and carefully surveyed into position on the baseplate (2) ensuring verticality of sense wires, the spatial positions of the latter being determined to within 0.15 mm. Figures 7.13 (a) and (b) show the drift chambers in position between the pole pieces of magnet blocks 22 and 23 of the storage ring. Also featured in these photographs are: the thin wall section under vacuum, the gas flow control panel, the baseplate and cradle assembly, the preamplifier banks and the "up-down" scintillators of the dipole moment experiment. The drift field and compensating mechanism of all chambers were as described in section 3.3.1 and H.T. voltages were derived from a single, well calibrated Brandenburg 707R power supply.

7.3.1 The Data Acquisition System

Figure 7.14 shows the system used to collect and store data from the drift chambers. Pulse discrimination was achieved using

FIG 7.11 ELECTRON TRACKS IN FOUR CHAMBER SUBSYSTEM
(sense wire planes parallel)

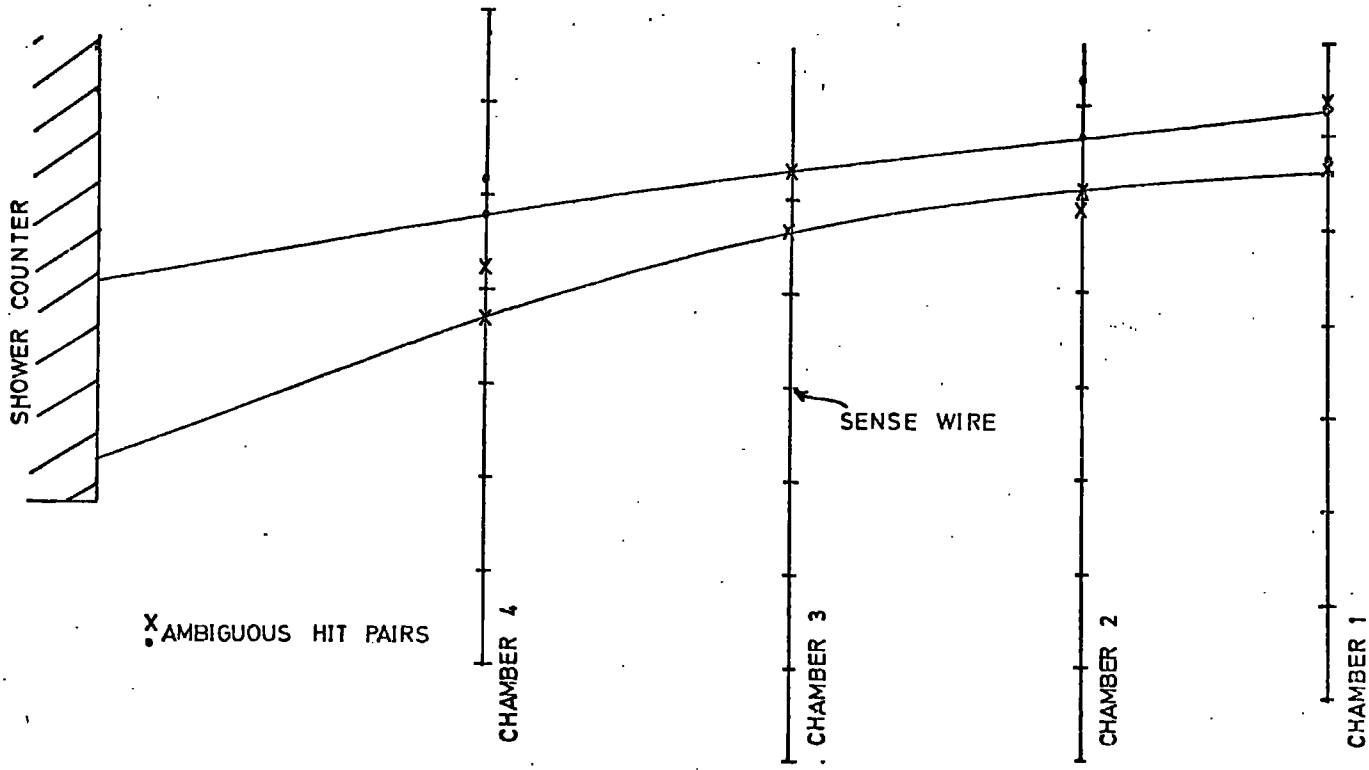

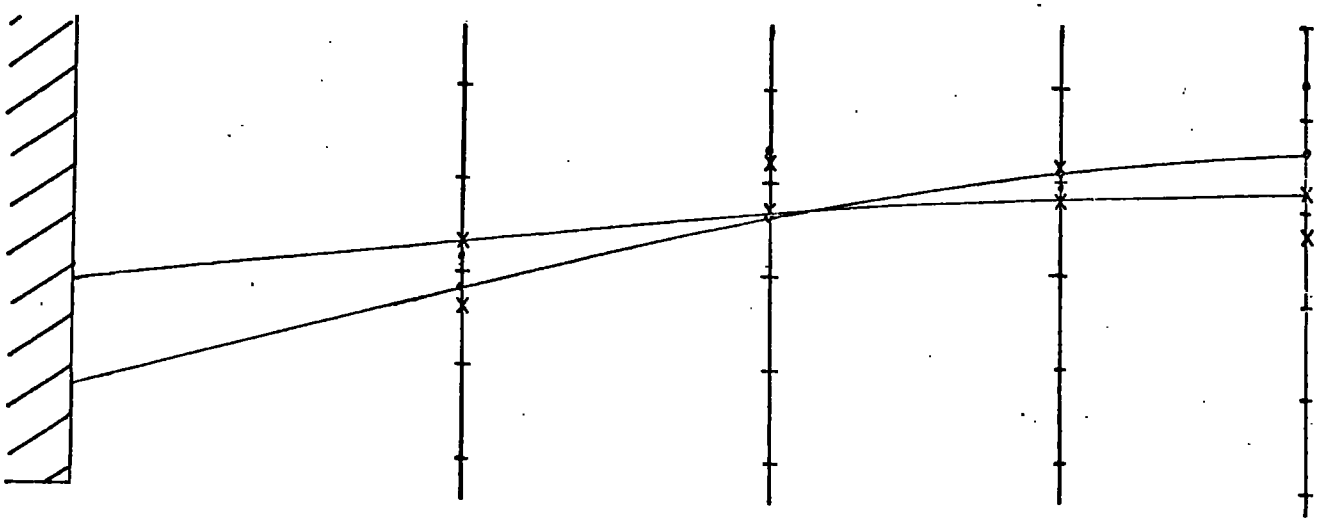

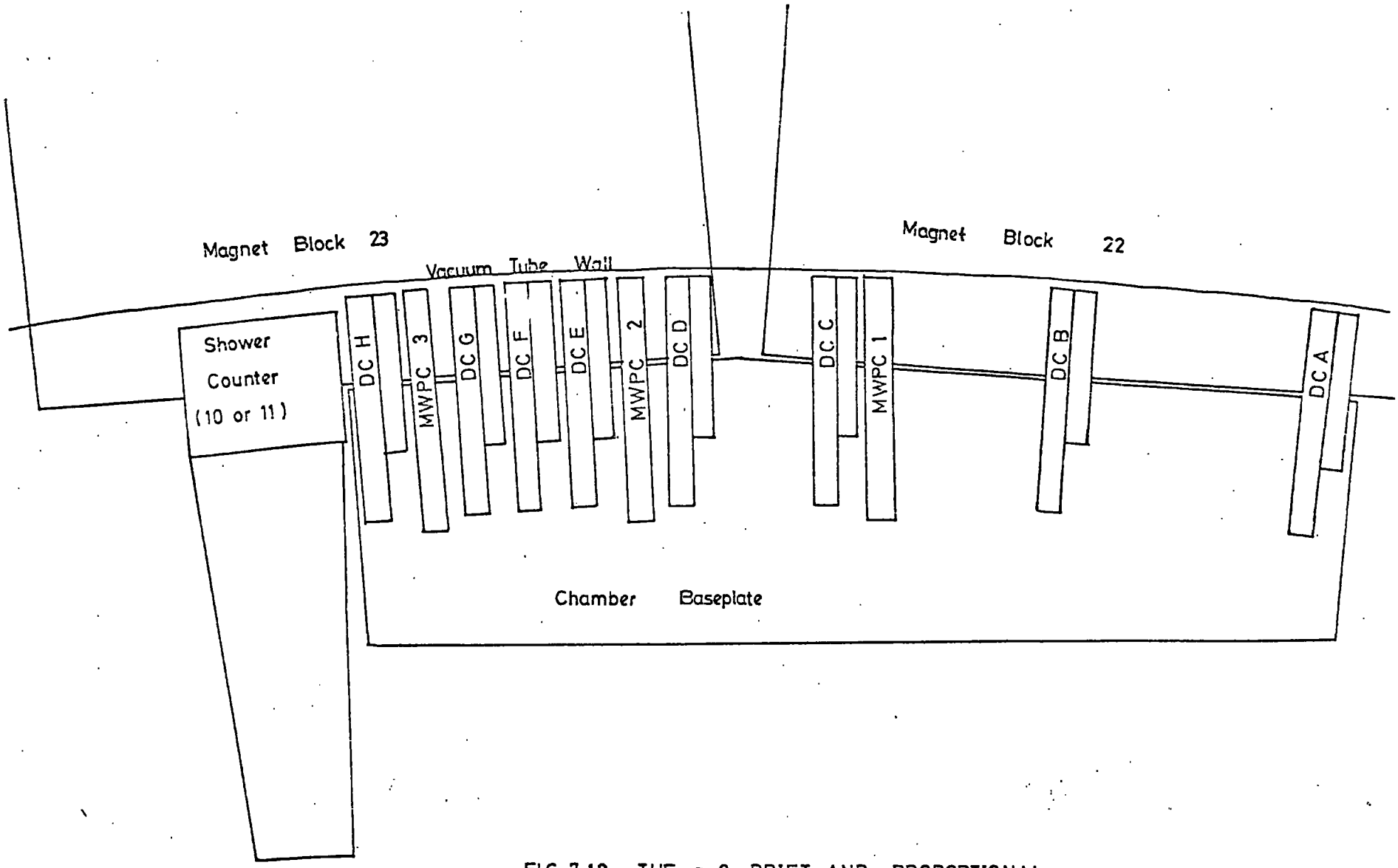

FIG 7.12 THE g-2 DRIFT AND PROPORTIONAL CHAMBER ARRAY

Lecroy octal NIM modules and timing was by Lecroy octal TDC units in CAMAC as previously described. Event gating and energy threshold selection were achieved by those methods discussed in section 7.2.3 and digitized drift times from the TDC's were stored in a Hewlett Packard 2100 (32K) computer. Other information collected in CAMAC included the event time (t_E) within the g-2 cycle (in fact the quantity ($t_D + t_W - t_E$) was stored), the pulse height code denoting the energy range for the event and an electric field fault message from the main experiment. The data acquisition programme took the form of a software package written in ASSEMBLER language and provided by CERN to specified requirements. Manual control over this programme could be achieved using a teletype visual display unit. An event block consisted of sixty 16-bit words including event labels and spare microscaler channels (breakdown monitors). These blocks, including only forty eight channels of TDC which were available at the time of the run, were transferred sequentially to magnetic tape, the low rate offering no problems to the system.

Online data analysis (low priority) was achieved using programmes written in BAMBI (a form of BASIC developed at CERN and including CAMAC commands and the facility to call FORTRAN subroutines) stored on punched paper tape.

The data acquisition system, including CAMAC electronics, the HP 2100 computer and ancilliaries, is shown in the photograph of figure 7.15.

7.3.2 Experimental Procedure

Data were written to magnetic tape during a g-2 data taking period; typically 5,000 events, collected at a rate of 10-20 per

FIG 7·13(a) THE MULTIWIRE DRIFT CHAMBER ARRAY IN THE g-2 MUON STORAGE RING WITH THE GAS FLOW CONTROL SYSTEM AND AMPLIFIERS

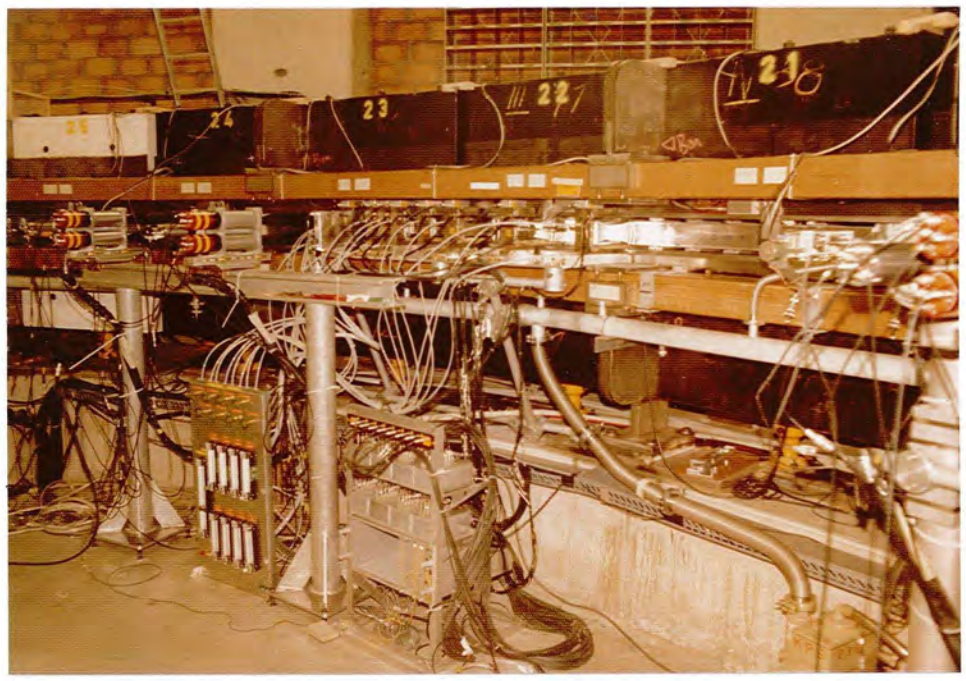

FIG 7.13(b) THE g-2 DRIFT CHAMBERS MOUNTED BETWEEN THE MAGNET POLE PIECES IN THE REGION OF THE THIN-WALLED VACUUM STORAGE TANK

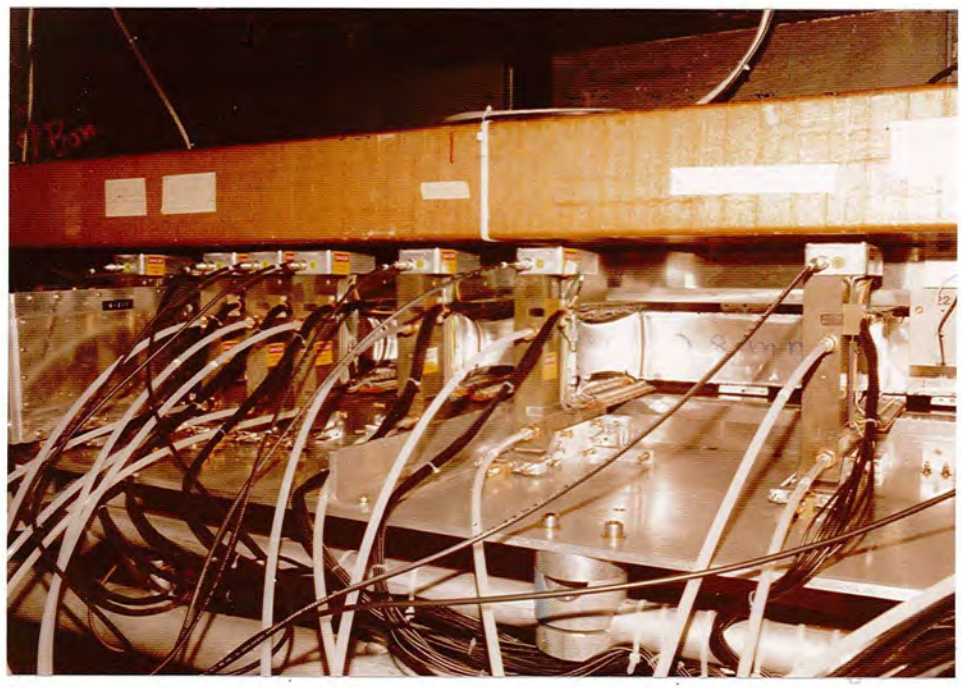

FIG. 7·14 THE DATA ACQUISITION SYSTEM

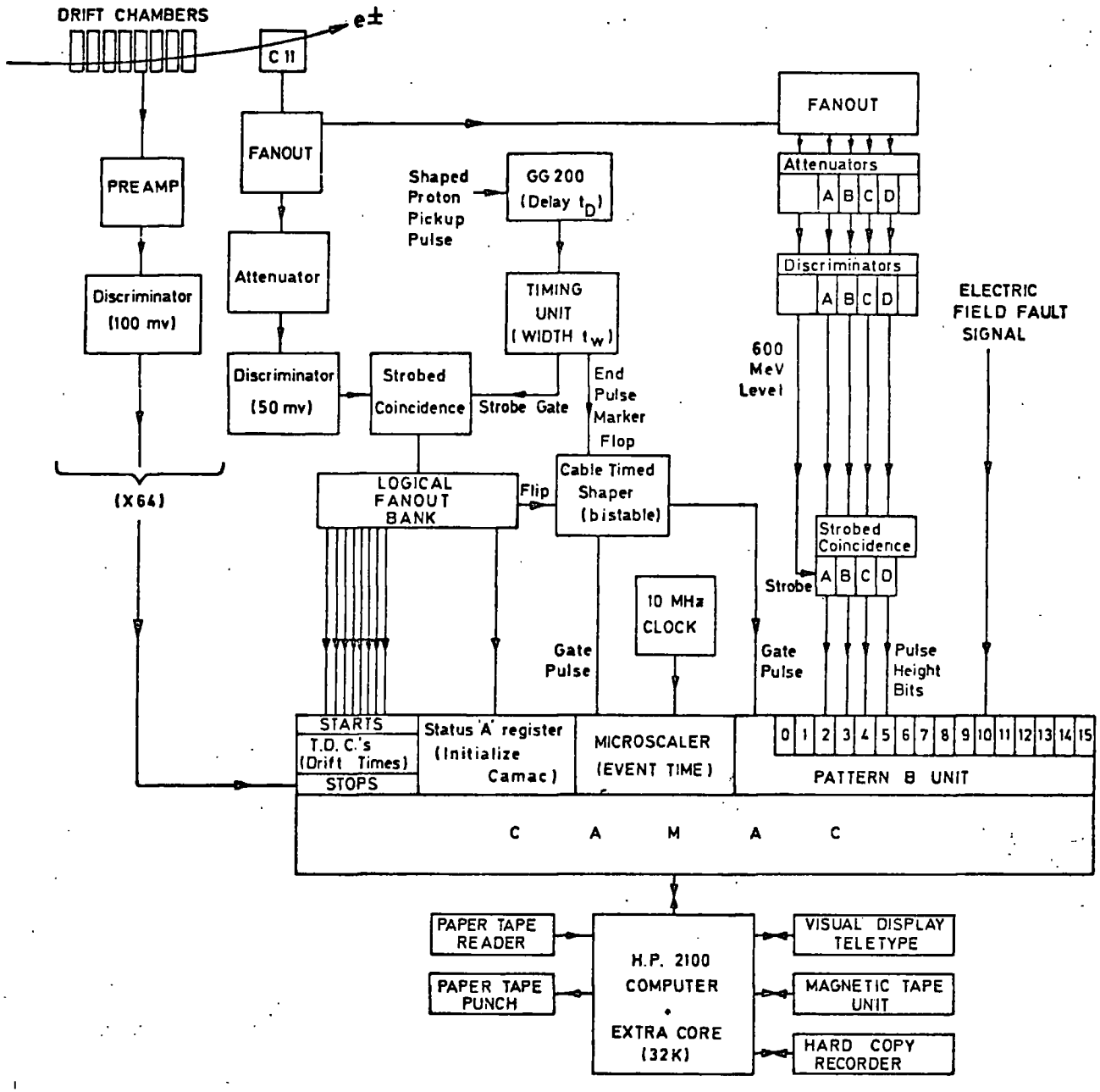

FIG 7.15 THE DATA ACQUISITION SYSTEM INCLUDING CAMAC ELECTRONICS AND A HP-2100 SMALL COMPUTER

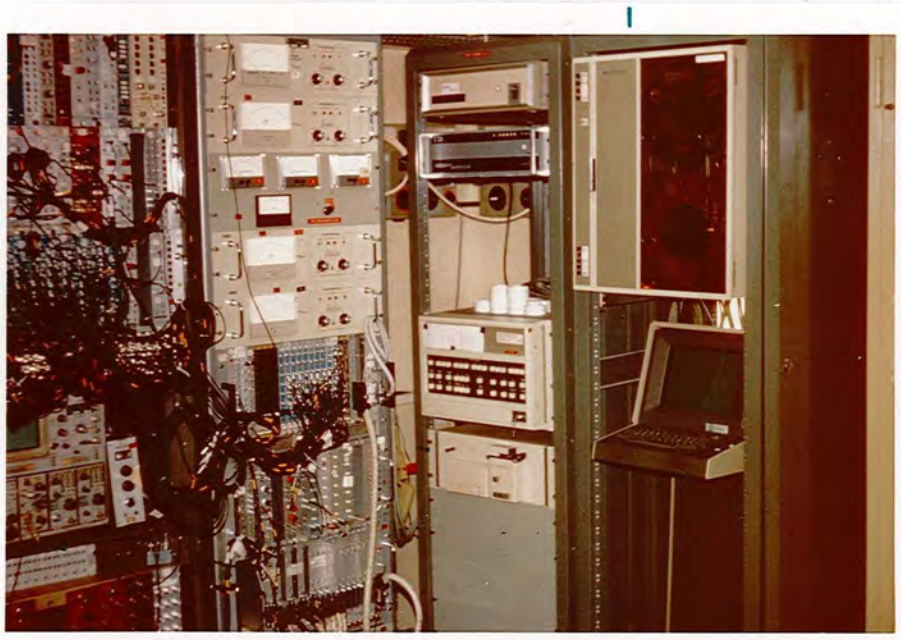

minute, constituting a drift chamber run. Parameters varied during this work were: the attenuation in the counter line (energy threshold), the gate delay (t_D) and the gate width (t_W).

Pulse height and event time information were available with only a limited amount of the data due to hardware problems, however, the effect of altering the energy threshold was clearly apparent on observing the values of the former using a simple display programme.

The performance of individual drift chamber cells was monitored regularly and a decrease in spurious pulse rate with running time was observed over the first few days of operation; this is in accordance with previous findings (3)

7.4 Initial Results

Using the online programmes, the data collected have been analysed in order to assess the performance of the chambers. The results obtained will now be discussed.

7.4.1 Drift Time Distributions

The drift time distributions of each cell (summed over six chambers) are presented in figure 7.16. The reason for extending the drift time bins up to only 500 ns was that to ensure the correct functioning of the CAMAC autoscan, some of the TDC's used had to be artificially stopped at a time <512 ns after receiving the start signal when no digitized time was present. 500 ns was chosen to represent the overflow bit (safely below 512 ns) and the time jitter in the logic system providing this stop pulse caused the fall off in counts observable for the final bin.

In all cells, the distributions extend over the full time

FIG 7.16 DRIFT TIME DISTRIBUTIONS FROM CHAMBERS POSITIONED IN STORAGE RING

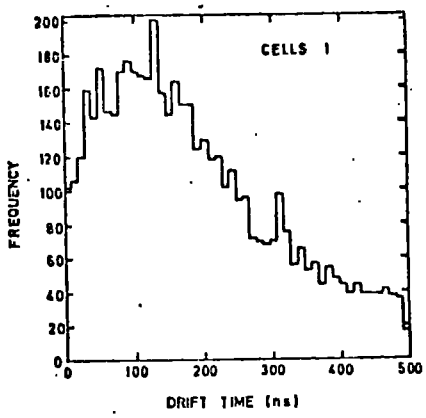

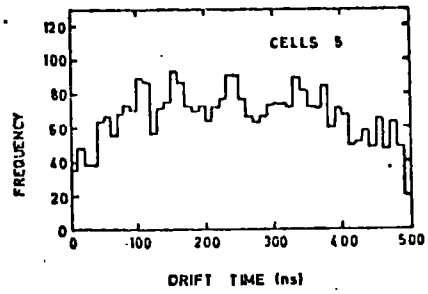

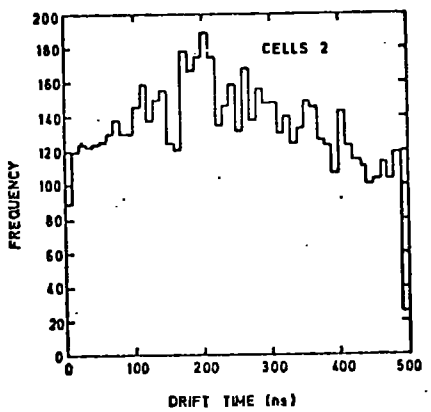

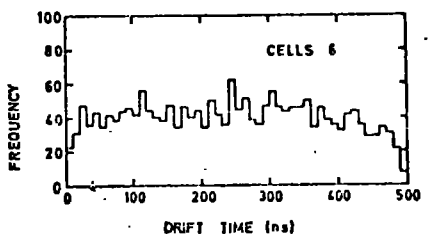

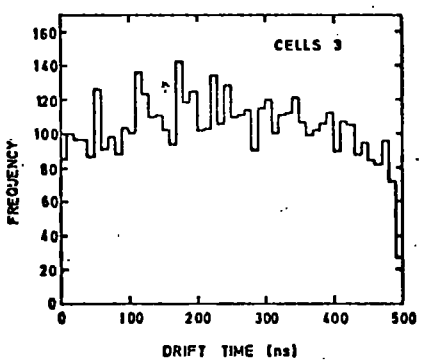

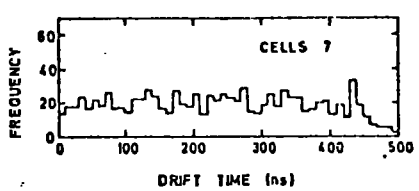

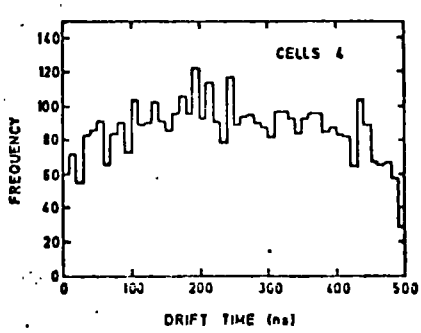

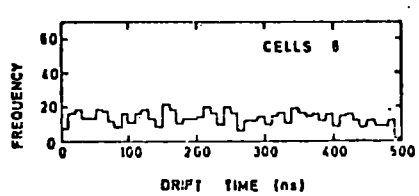

range of the TDC's, with some suggestion of a fall off at high times for cells 6 and 7. This is in agreement with the theory presented in chapter 6 (see figure 6.10) and illustrates the extension of drift times in the magnetic field; however, no rigorous calibrations were possible with the electronics used. The distribution from cell 1 again illustrates the geometrical effect of the curved end drift space.

The plateaus of the distributions are slightly curved, which may reflect the form of electron intensity reduction with radial distance inwards (a linear fall off would produce a flat-topped distribution on consideration of the contributions from each half of the cell). An estimate of the electron flux variation was made from figure 7.16 and is shown in figure 7.17. Another contribution to the plateau curvatures may be slight inefficiencies in the sense wire and potential wire regions as discussed in various parts of this thesis.

7.4.2 Efficiency Measurements

Using chambers F and H and the shower counter as a trigger (effectively a 500 ns gate), the efficiency of chamber G was investigated. Figure 7.18 shows this quantity as a function of the delay (t_D) of a 400 μs wide event gate and the electron energy threshold (due to the short length of cable between the counter and the attenuator for this particular system, 31 dB $\simeq$ 1.8 GeV and 19 dB $\simeq$ 0.8 GeV). Maximum efficiencies were of the order 80% due to the slightly inefficient zones created at the cell centres and ends (as discussed in this thesis), dead regions due to the TDC time range being exceeded in some cells and spurious triggers from the telescope (enhanced by the fact that all cells of a chamber were used to provide the event trigger, thus a true electron event was not neccessarily

FIG. 7·17. VARIATION OF ELECTRON INTENSITY WITH RADIAL DISTANCE

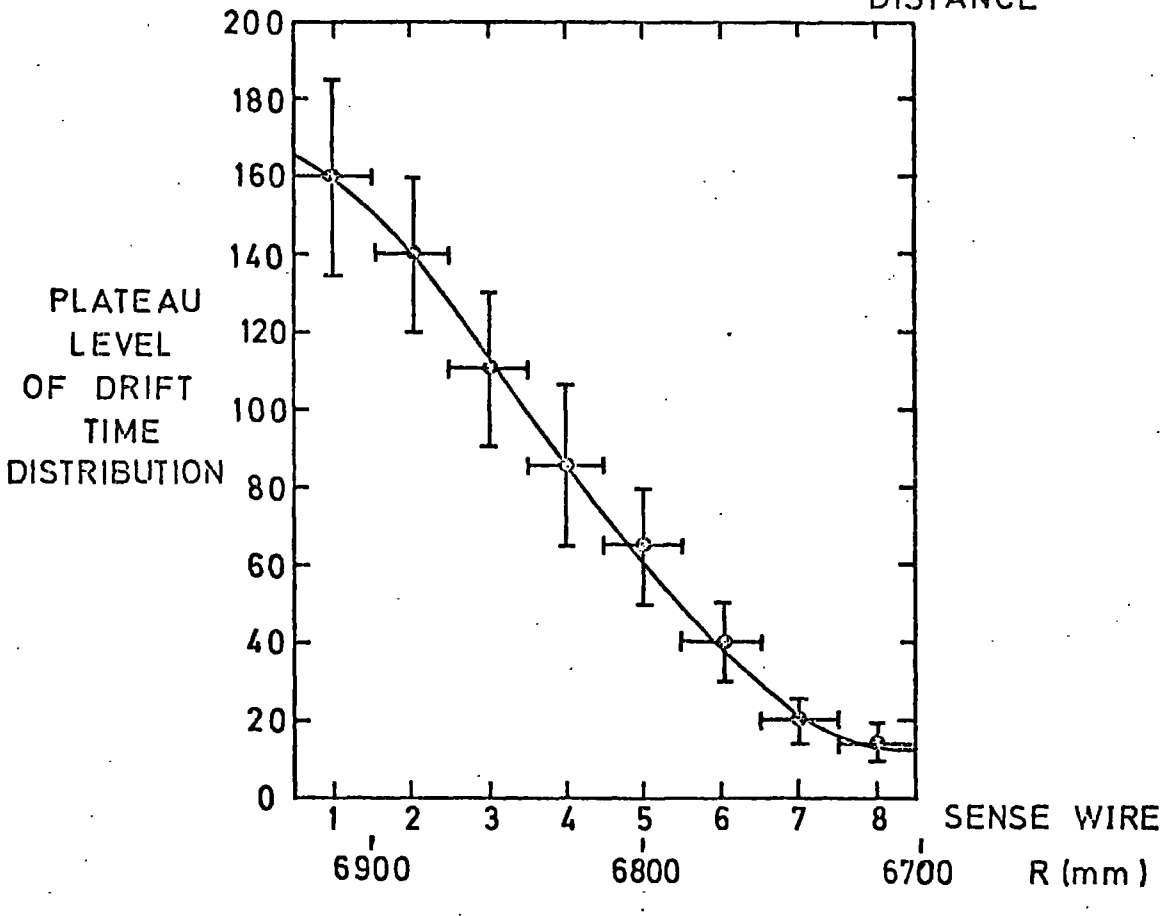

FIG. 7·18 CHAMBER EFFICIENCY AS A FUNCTION OF DELAY OF EVENT GATE WITHIN THE g-2 CYCLE

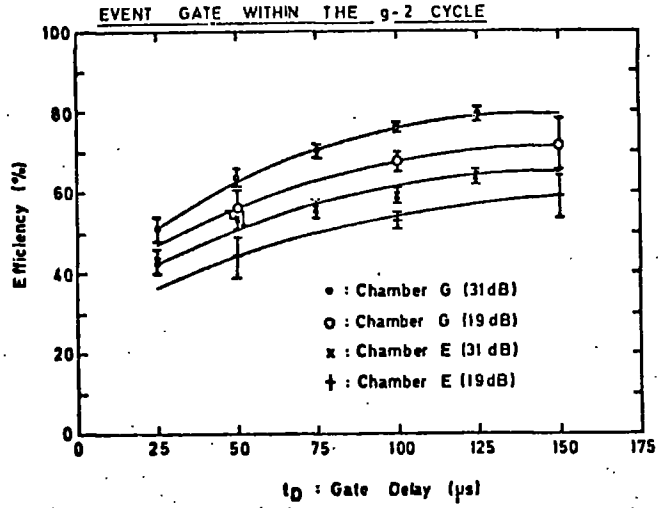

FIG. 7·19 NO OF CHAMBERS HIT BY EMERGENT ELECTRONS OF DIFFERENT ENERGIES.

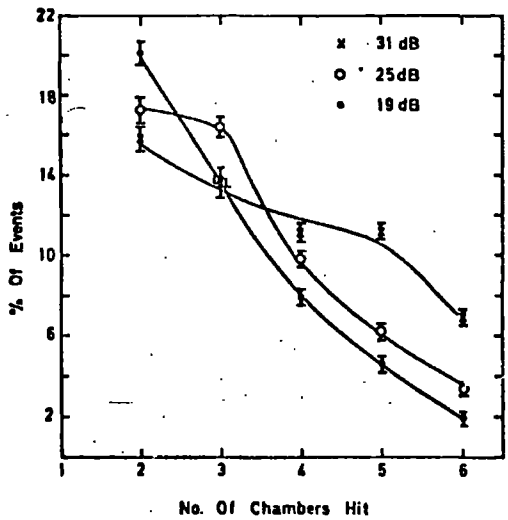

FIG. 7·20. No. of Events showing ≥ a fixed No. of chambers hit, As a Function of Event - Gate Delay (31 dB Attenuation)

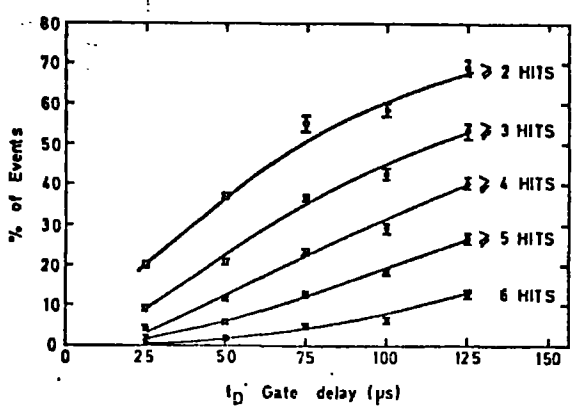

selected).

An efficiency plateau was not attained until the event gate was delayed 125 μs into the g-2 cycle and, for runs where timing information was available, the good tracks observed for low t_D settings were always associated with long times. Efficiency was observed to increase with energy threshold, indicating more spurious counts for lower attenuation levels in the shower counter line. Also indicated in figure 7.18 are efficiency curves for chamber E (immediately upstream of the event selecting telescope) which show the same form of variation but, for geometrical reasons, give lower plateau levels.

A similar inefficiency at low event times within the cycle has been recorded for the M.W.P.C's of the array and is now attributed to a paralysis of the chambers caused by the initial pion burst (of estimated intensity 10^6 particles per chamber and occurring within a few ns). Although the pion pulse of figure 7.2 is only a few hundred ns long, the much slower positive ion swarms resulting from the avalanches will cause a severe restriction on the gain in the sense wire region.

7.4.3 Chamber Hits

Figure 7.19 shows the number of chambers hit by emergent electrons as a function of threshold energy. Due to the radius of curvature (R) of tracks increasing with energy, in general, more chambers were hit at higher threshold settings as predicted for this array (4), and more tracks of high curvature (1/R) were observed at low thresholds.

The amounts of data containing tracks of $\geqslant 2$, $\geqslant 3$, $\geqslant 4$, $\geqslant 5$

and 6 chambers hit are plotted as functions of t_D in figure 7.20. Once again, the inefficiency effect at low t_D values is apparent and the seriousness of this problem is emphasised by the fact that the curves are still rising after 125 μs. (For the initial track analysis to be discussed in section 7.4.5, the criterion of $\geqslant 3$ or $\geqslant 4$ hits was demanded and for a more sophisticated analysis, as much as possible of the data will be utilised; hence a restoration of full efficiency at low t_D values is highly desireable.)

7.4.4 Electron Tracks

From a knowledge of the sense wire spatial locations, and using the predicted drift velocity variation across the chamber, the digitized drift times recorded were processed into Cartesian coordinates in the system where chamber C sense wire plane represented the Y-axis and the origin was the centre of the storage ring (ie. a 6-chamber system). The positions of the sense wires and shower counter in this coordinate system are indicated in figure 7.21 where the "ambiguous pairs" representing hit positions for an electron track passing through all chambers are also plotted.

From these possible hit points, an eye fit can be drawn to represent the electron trajectory. As seen from the figure, the latter is uniquely constructed using one point from each pair in a chamber, thus, the array aided by the magnetic field, has provided a geometrical solution to the left-right ambiguity. The characteristic track shape can be observed, that is, a decreasing curvature with distance from the storage tank, due to the magnetic fringe field fall off.

To reconstruct the muon decay coordinates for a track, the

FIG 7.21 THE SENSE WIRE COORDINATES OF THE SIX-CHAMBER SYSTEM SHOWING THE AMBIGUOUS HIT PAIRS OF A DECAY ELECTRON TRACK
(predicted muon radius: 6942·6 mm)

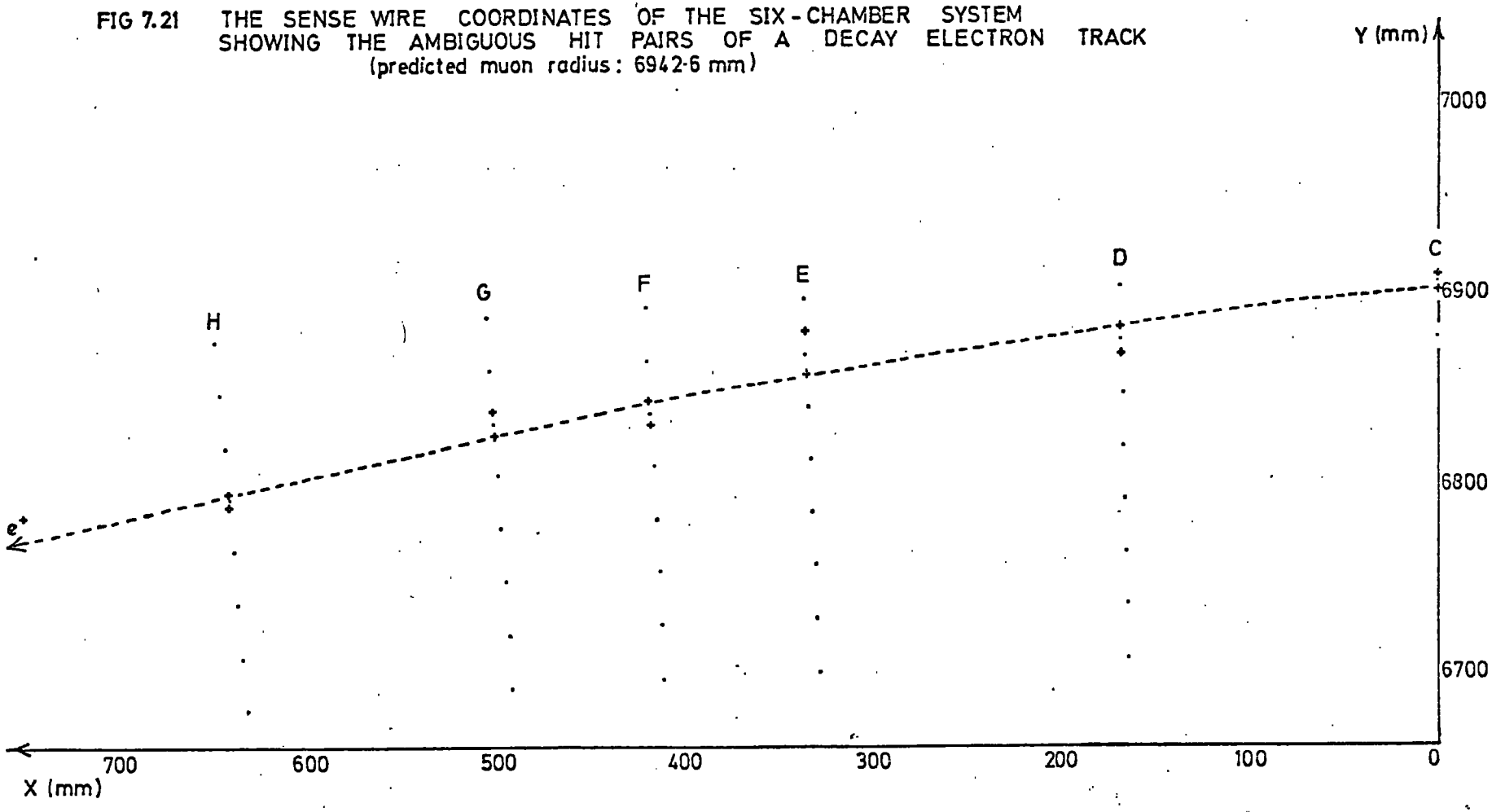

following proceedure was adopted:-

Only those events exhibiting clean hits (one cell only) in $\geqslant$ four chambers were selected for processing. The eight possible circles were constructed through the first three (upstream) ambiguous pairs encountered and those which could not possibly be considered as particle tracks (for example, bending the wrong way) were rejected. The condition of proximity to a hit coordinate in the fourth chamber reduced the number of possible tracks and the final selection was made in the decay point reconstruction stage of the programme. The parent muon decay coordinates were determined by extrapolating the circular fit upstream until tangentiallity with the orbit circles occurred. This analysis assumes that for the first three chambers hit, the electron is in an approximately uniform magnetic field, thus validating a circular fit.

Figure 7.22 shows several examples of electron tracks obtained, with their extrapolated circle fits. The relative positions of the shower counter and storage tank, and the predicted muon decay points are indicated. Many of the track reconstructions predicted the latter to lie outside the storage tank which is obviously impossible. Several examples of this effect are clearly illustrated in figure 7.22 and possible explanations are to be suggested in the following section.

7.4.5 The Circulating Beam Profile

By binning the predicted values of muon radius obtained from the electron tracks, a first estimate of the reconstructed beam intensity profile was made, and is presented in figure 7.23 where the relative position of the storage tank is also shown. As a result of

FIG 7.22 EXAMPLES OF "CLEAN" DECAY ELECTRON EVENTS OBSERVED IN THE SIX-CHAMBER SYSTEM

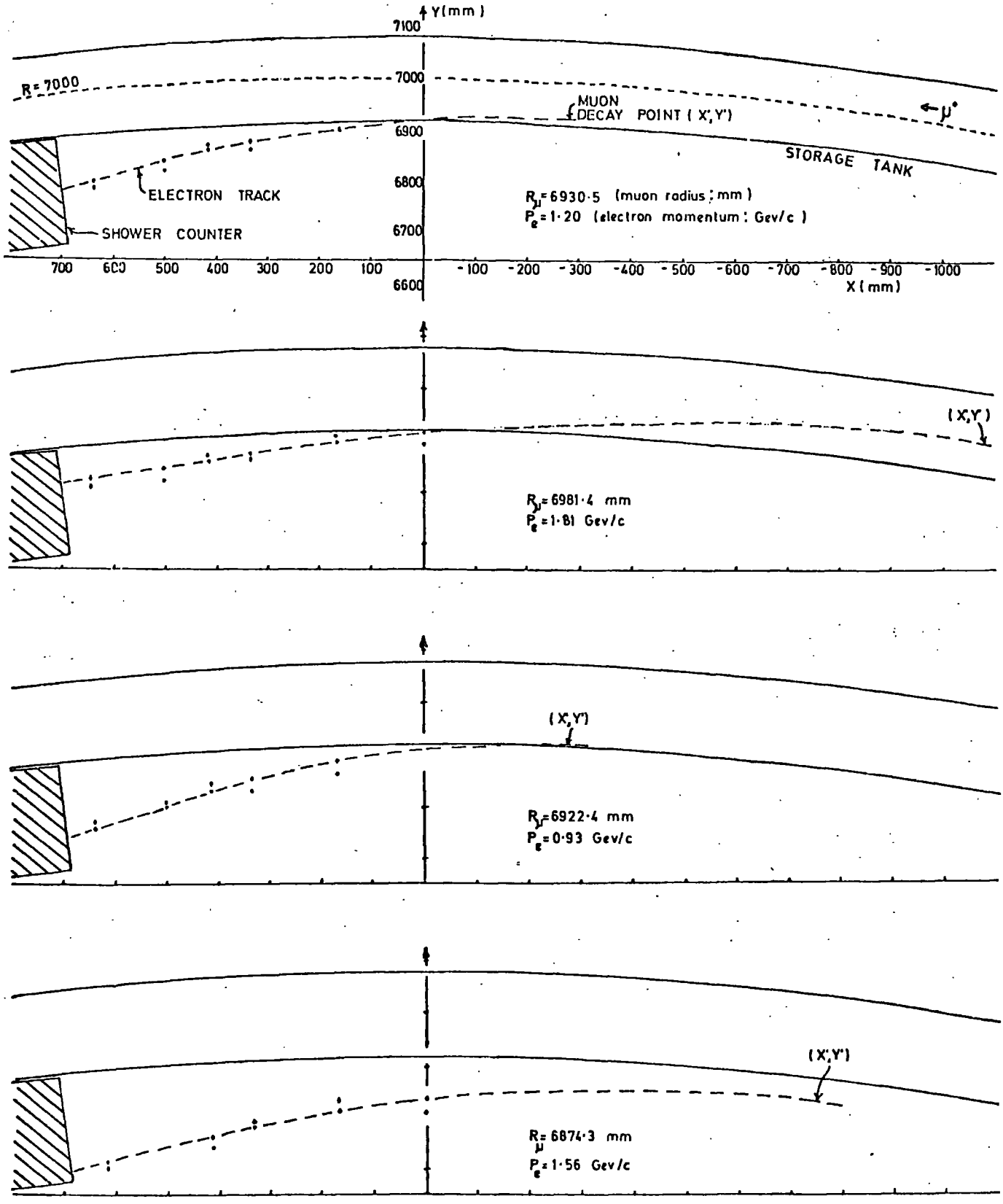

FIG 7.22 (cont.)

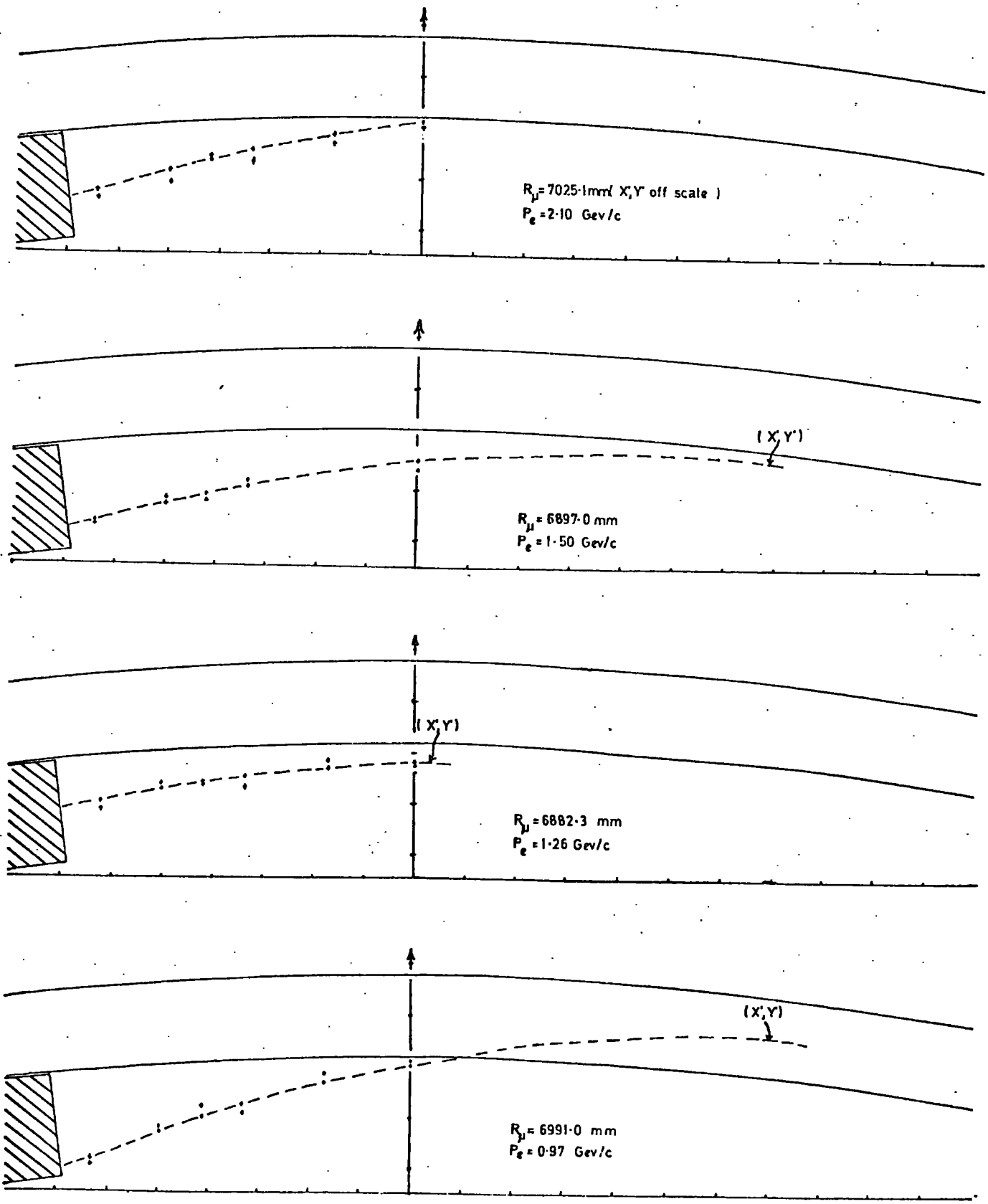
R_μ = 7025·1mm(X',Y' off scale)
P_e = 2·10 Gev/c
(X', Y')
R_μ = 6897·0 mm
P_e = 1·50 Gev/c
(X', Y')
R_μ = 6882·3 mm
P_e = 1·26 Gev/c
(X', Y')
R_μ = 6991·0 mm
P_e = 0·97 Gev/c

FIG 7.23 THE CIRCULATING MUON BEAM PROFILE RECONSTRUCTED FROM ELECTRON TRACKS

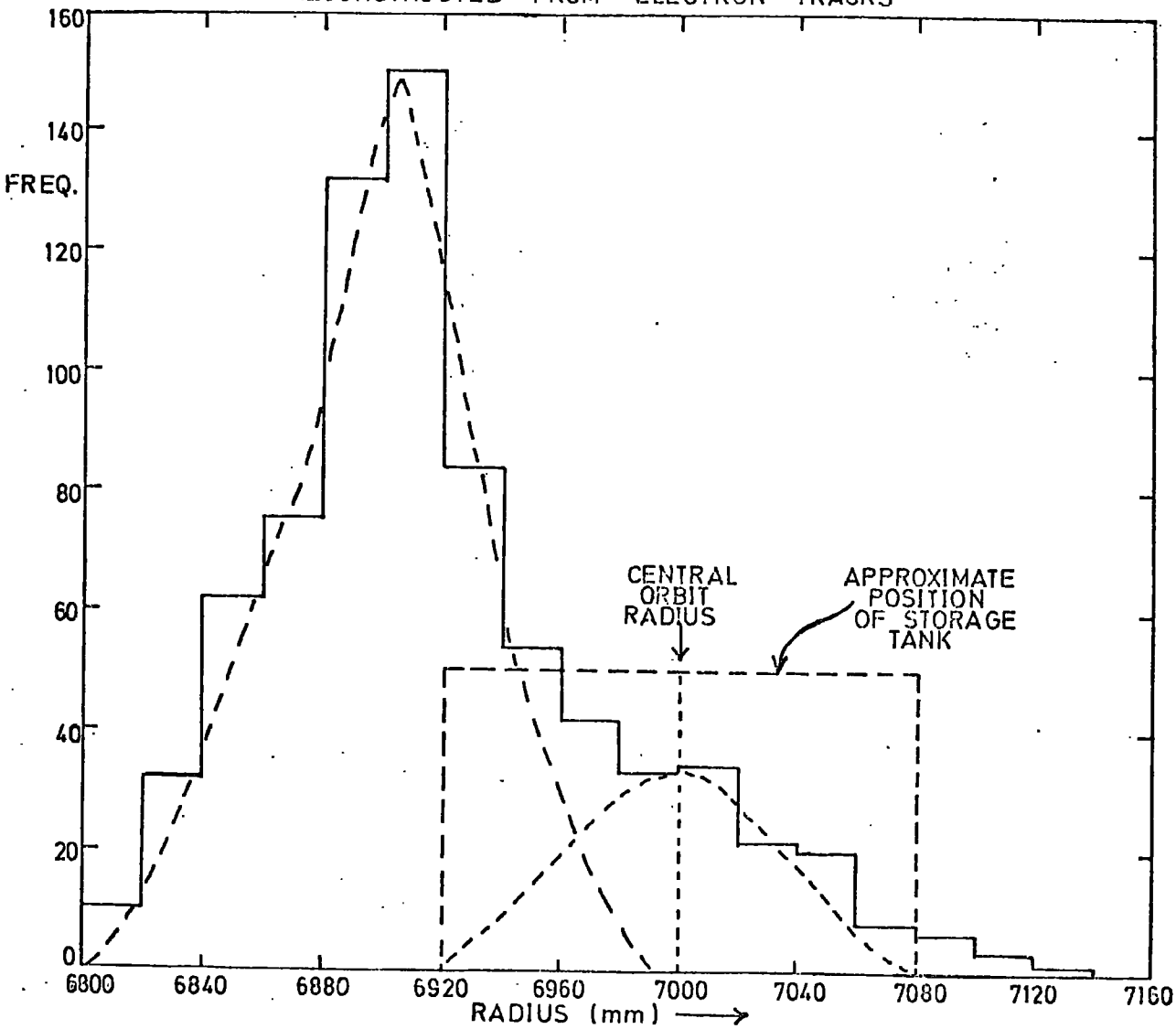

FIG 7.24 SCHEMATIC REPRESENTATION OF A POSSIBLE TRAJECTORY OF AN ELECTRON ENTERING THE DRIFT CHAMBER ARRAY BY AN "INDIRECT PATH"

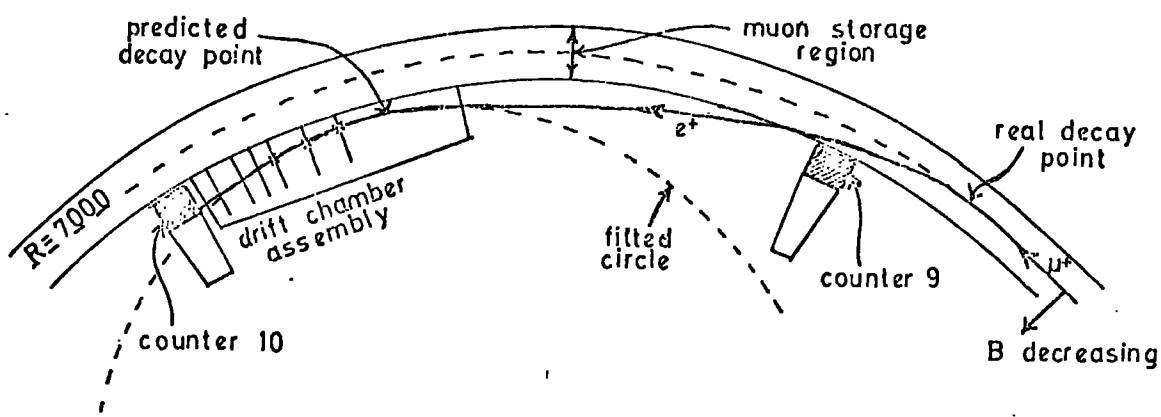

the many recorded tracks appearing to originate from a point inside the storage ring, the radial distribution is seen to peak at a distance ~90 mm from the centre of the vacuum tank. The distribution shapes obtained were approximately as expected (the profile has been estimated to be of a semicircular nature (4)), however the positional shift is somewhat surprising considering the fact that a circular fit for a track extending into a weakening magnetic field would tend to project the predicted muon radius towards larger values.

Attempts to shift the distribution have included:-

artificially skewing the baseplate in the programme to investigate the possibility of leverage of the fit. A tilt of 0.6^{o} (6 mm difference across the array) shifted the profile by only 20 mm.

adjusting individual wire positions in the programme. This alters the fitted circle completely, however, alterations of several mm were necessary to produce the required shift (in approximate accordance with the calculations of appendix I).

altering the inserted drift velocity values which affected the profiles slightly but peak movements were minimal.

Some possible explanations of the observed profile are as follows:-

It is not impossible that a chamber positional error was made and, as all the data were collected from one alignment system, future runs will investigate this possibility.

The circle fitting technique is by no means satisfactory but has served to perform an initial analysis. The selected points for the fit are assumed to be absolutely correct using this method, whereas a fit of the least squares type does not necessarily pass

through the data points and also utilises all data. The final track fitting technique will be complicated and take time to develop, however, better results will be yielded and peak shifts are feasible.

A significant contribution to the data may be from electrons emerging from the storage tank at a point far upstream of the array and following the sort of trajectory indicated in figure 7.24, that is, a "straightening" due to the decrease in magnetic field strength encountered which results in the particle eventually reentering the high field region and experiencing further bending; the circular fit will now predict a false muon radius. Part of the data will certainly be collected in this way when using the present system, as, for this particular g-2 run, counter 10 has been moved close to counter 11 and used as an event trigger for the array, leaving a large sector of the inner storage tank wall without any electron absorbing material (ie. a shower counter).

By suitable relocation of electronic readout channels, a short run was made to observe electron tracks in eight chambers and an example of an event from this system is shown in figure 7.25 where the trajectory observed is of a similar form to that of figure 7.24.

The distributions constructed showed tails at high values of muon radius and thus, the possible contributions to the beam profile have been illustrated in figure 7.23 where the shape of the curves drawn can be compared with those of the profiles obtained from a previous experiment (5). The fact that the contribution attributed to the unusual trajectories of far-upstream ("indirect track") particles appears to be greater than that from particles emerging directly into the array ("direct track") is probably due to the programme selection proce dure. As only "clean tracks" have been selected for analysis,

FIG 7.25 EXAMPLE OF AN EVENT WITH EIGHT RECORDED CHAMBER HITS

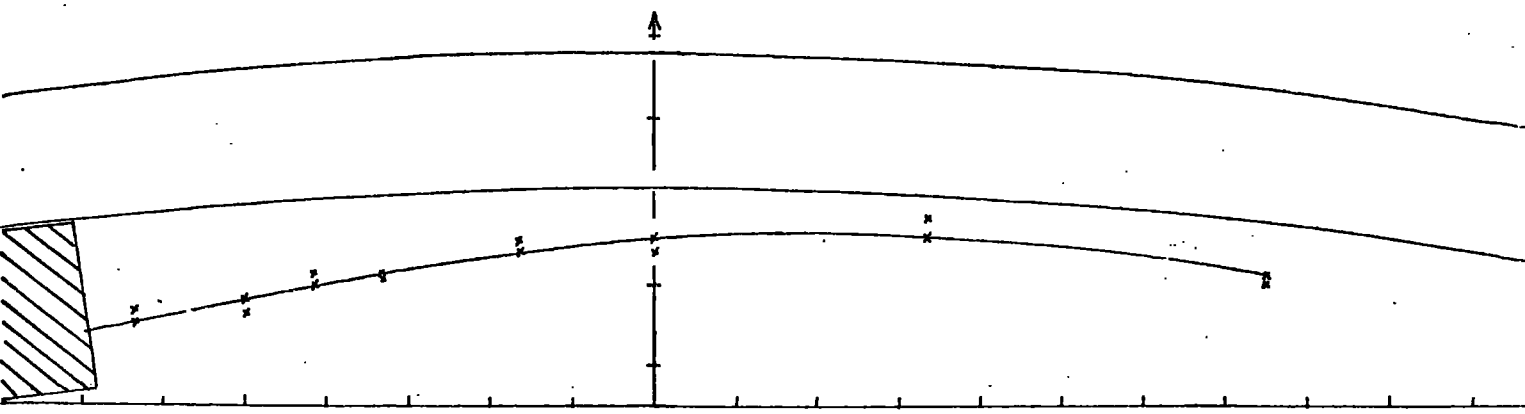

FIG 7.26 EXAMPLE OF A "MULTIPLE CELL HIT" EVENT

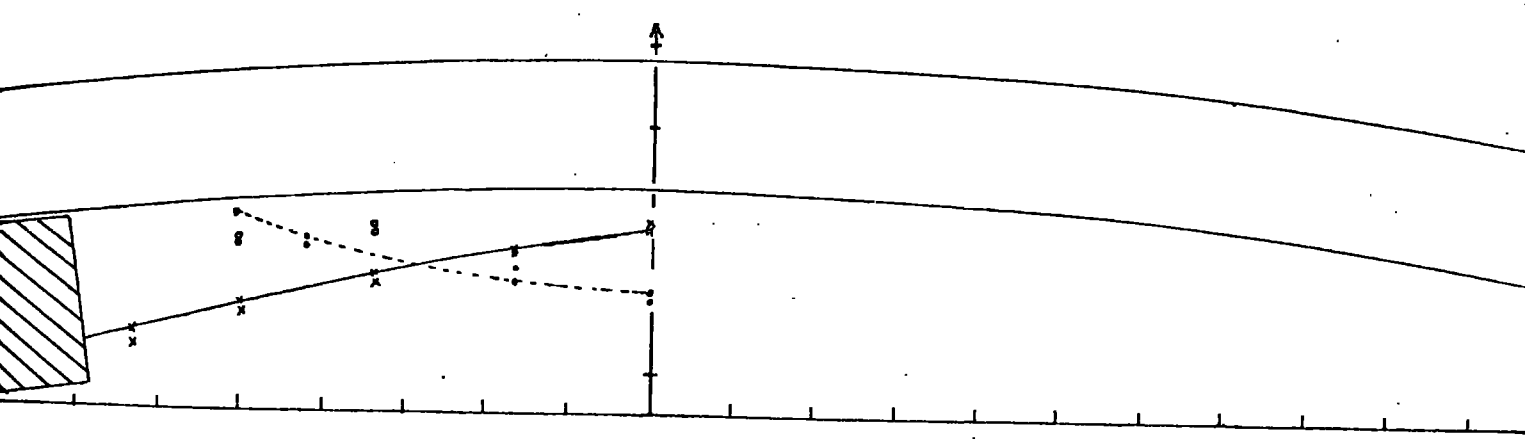

those events where showering has occurred and, for example, an electron-positron pair has entered the array, will be rejected. An example of a "multiple hit" event is presented in figure 7.26 where the possible trajectories of two oppositely charged particles are constructed by eye, however, it is difficult to correctly decipher such an individual event and spurious pulses cannot be ruled out.

Multiple hit events are more likely to be observed for the direct tracks as an "electron" with opposite charge to that of the circulating muons is rapidly bent the "wrong" way into the magnet blocks. If the showering factor is still significant for the thin wall section ($\sim$35% of analyzable events ($\geq$4 hits) contained multiple cell hits in at least one chamber), the rejection of such data for the direct track events will reduce the comparative contribution to the profile of the latter.

The ratio of the relative contributions from the two sources is also dependent on the ratio of the relative lengths of sectors of circle producing tracks in the array. Note that the three points used for fitting trajectories for the indirect tracks are more likely to lie in the non-uniform field region and thus, the resultant part of the profile will be moved to higher radii, thus reducing the possibility of observing distinctly separate peaks from the two contributions.

7.4.6 The Momentum Distribution of Electrons

The momentum (in GeV/c) of a particle bending with radius of curvature R (in metres) in the g-2 magnetic field (14.745 KGauss) can be determined using the expression:-

$$Pc = R/2.26 \qquad (7.1)$$

Thus, by using the circle fitting technique and determining the radius of curvature of a decay electron observed in the drift chamber array, its momentum can be found if the assumption of a uniform magnetic field persisting in the region of the three fitted points is made.

The momentum spectrum determined in this way, for particles appearing to emerge from the storage region ($6920 < R_{\mu} < 7080$) is shown in figure 7.27. A low momentum cut off is observed at ~ 900 MeV/c due to the threshold setting for this run and a high momentum cut off appears at ~ 2500 MeV/c. The latter is due to the geometrical acceptance of the array which, for the whole run, was set back a distance of ~ 2 cm from the storage tank wall, thus reducing the cut off level normally expected of say 2.9 GeV/c (note that, although electrons of up to the maximum muon momentum of ~ 3.1 GeV/c can be produced, a 3.1 GeV/c electron, for example, would continue in stored orbit).

To compare briefly the initial electron momenta measurements with those observed in the g-2 shower counters, the integral spectrum is displayed in figure 7.28 in terms of the "pulse height bit" levels discussed in section 7.2.3. Comparing, then, figures 7.7 and 7.28, slight reductions in the "600 MeV" and "pulse height D" levels are apparent in the drift chamber measurements, due in both cases to the spectrum cut offs, otherwise a similar "step" form is indicated.

7.5 Particle Trajectories in Non-Uniform Magnetic Fields

For a set of data points obtained when a particle, travelling in a magnetic field crosses a wire chamber array, there are several possible methods of determining the trajectory:-

FIG 7.27 THE DIFFERENTIAL MOMENTUM SPECTRUM OF THE DECAY ELECTRONS

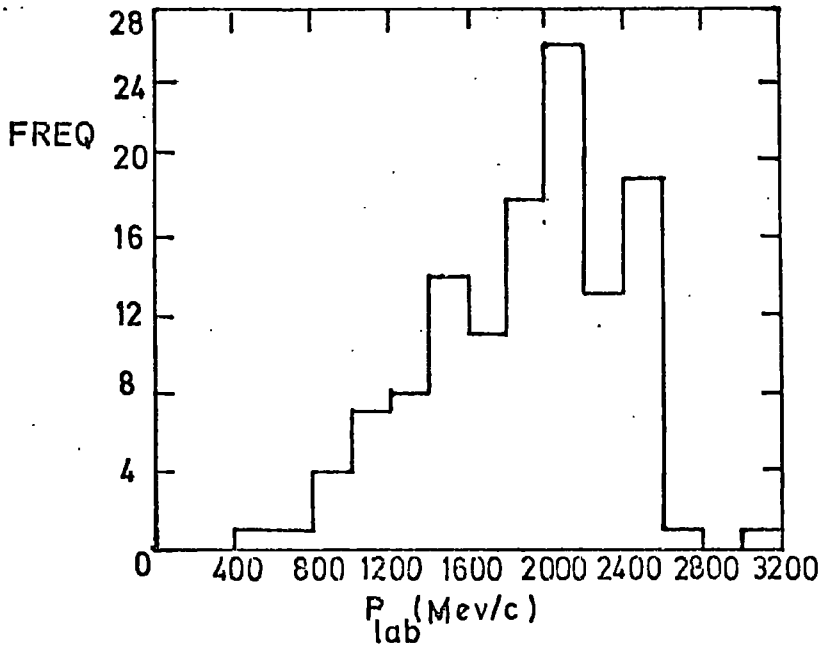

FIG 7.28 THE INTEGRAL MOMENTUM SPECTRUM OF THE DECAY ELECTRONS (in terms of the "pulse height bit" levels)

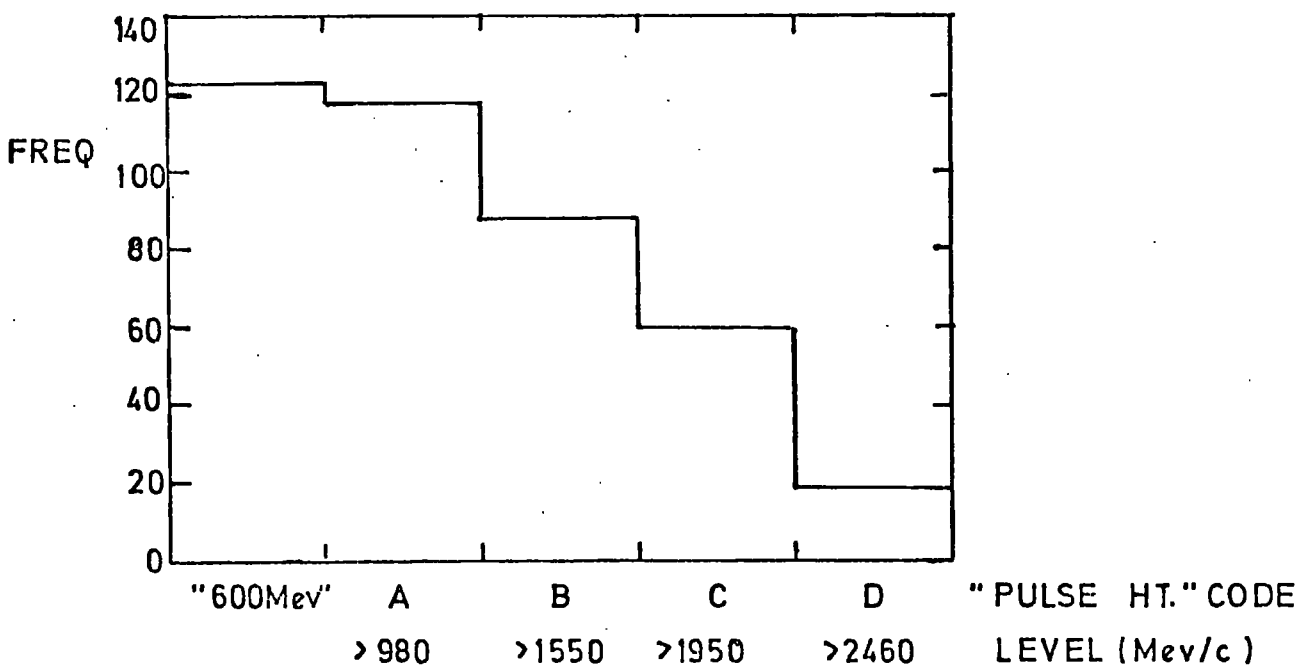

The simplest method, which has been employed in the g-2 data analysis to date, is to fit a circle through the first three points on the track. This is reasonable in the g-2 array as the latter points are often in a region of fairly uniform magnetic field and, although this fit yields an untrue impression of the rest of the trajectory in the downstream direction, the upstream extrapolation will be of the correct (circular) form.

For the field encountered in this experiment, the tracks produced suggest that a parabolic fit to the data would be a reasonable estimate. Hence, the circle technique would be applied to the first three ambiguous hit pairs in order to select a suitable track and would then be replaced by a least squares fit of the form $Y = a + bx + cx^2$. The curve obtained would be used to select the correct coordinate from the fourth hit pair which would then allow a more accurate fit, and so on through all the data points.

The best track reconstruction technique will neccessarily include a magnetic field parameter (often the vector potential). For a non-uniform field as encountered in this experiment (approximately an exponential fall off of the form $B(R) \simeq B_0(1 - e^{-\lambda R^2})$ for radii $R \lesssim$ 6880 mm), the problem is non-trivial and several methods have been developed in high energy laboratories (6) for similar circumstances. The modification of such an existing programme or the development of a similar technique will be implemented in the near future. Such a fitting method will be capable of predicting the correct birth points of any "indirect track" electrons.

7.6 Conclusion and Future Work

A working drift chamber array and data acquisition system

have been installed in the g-2 experiment and the operation of the chambers in this environment has included a study of external noise sources, a brief and encouraging comparison between predicted and observed drift velocities using drift time distributions, and the observing of chamber efficiencies.

The latter quantity was found to be dependent on time within the g-2 cycle because of the many positive ions produced in the chambers by the pions of the initial flash. It is important to reduce this effect as the amount of electron data decreases exponentially with time and work is presently in progress on the application of pulsed clearing fields to the drift chambers. This involves applying a positive square pulse of a few hundred volts magnitude to the H.T. wires near each sense wire at the time of the initial flash. Hence the build up of positive ion clouds as a result of the avalanche process will be supressed, and the negative ions produced by pions in the gas will quickly find a path to earth via the sense wire (there still existing a drift field). This idea has been tested on one short run during the last g-2 cycle, using a thyratron based circuit which was designed to apply a blanking pulse to the shower counters during the initial flash. The application of a 50 volt, 10 μs pulse to one chamber improved the "firing rate" in that chamber by 50%. However, statistics were too low to make any definite conclusion and a thorough testing of the circuit is planned for future runs.

Many electron track events were collected and analysed producing a beam profile which suggested a major contribution from particles following "indirect paths"; this would be reduced by replacing counter 10 in its usual position. (A severe mistake in the chamber alignment or a deficiency in the tracking technique cannot be

ruled out.) The showering factor appeared to be much reduced for the thin wall section, but was still significant.

A more sophisticated tracking technique, as referred to in section 7.5, will be developed and will also include various software corrections (for example, the magnetic field change over the length of a magnet block as illustrated in figure 6.6). Future calibrations on alignment will probably utilise horizontal cosmic rays and high energy leakage particles from the CERN P.S. Measurements on the chamber resolutions and drift times in the curved end will be possible in this way and a complete calibration of drift velocity will be carried out when the CERN drift time digitizers are employed.

The data acquisition system will eventually be integrated with that of the main experiment and will also incorporate information from the M.W.P.C's. In this way, information concerning three dimensional beam profiles, allowing a complete analysis in terms of individual particle momenta and track multiplicity and direction, will be available.

Reversals of the stored muon polarity will necessitate the removal of the chambers to reverse the electric field tilts. Thorough internal cleaning will be carried out on such occasions to minimise any long term time degeneracy of performance (7).

References

1 J.M. Breare, R. Browell, K.A. Short. Durham University Internal Report, NI-74-6

2 J.M. Breare. Private Communication, CERN 1975

3 R. Bouclier, G. Charpak, E. Chesi, L. Dumps, H.G. Fischer, H.J. Hilke, P.G. Innocenti, G. Maurin, A. Minten, L. Nanmann, F. Piuz, J.C. Santiard, O. Ullaland. Nucl. Inst. Meth. 115 (1974) 235

4 J.H. Field. Private Communication, CERN 1975

5 F. Combley, E. Picasso. Phys. Reports 14C (1975) 1

6 See for example: M.W. Peters. Nucl. Inst. Meth. 113 (1973) 371

7 G. Charpak, H.G. Fischer, C.R. Gruhn, A. Minten, F. Sauli, G. Plch, G. Flügge. Nucl. Inst. Meth. 99 (1972) 279

CHAPTER 8

CONCLUDING REMARKS AND FUTURE WORK

8.1 Comments on the Performance of the g-2 Drift Chambers

The mechanical and electrical construction of the production model chambers have been proved to be of sound design and the performance in laboratory and accelerator tests of all cells and chambers has been verified as uniform before experimental installation. A set of operating parameters has been chosen under which good results have been obtained, in particular: spatial resolutions of the order expected of drift chambers ($\sim$0.1 mm), space-time linearity (uniformity of drift velocity), 100% efficiency levels, an energy resolution of $\lesssim$15% for Fe 55 X-rays, minimum diffusion and successful operation in non-uniform magnetic fields of strength up to 15 KGauss have been achieved. The chambers have enabled the successful study of several effects including: fluctuations in pulse height, efficiency and resolution, the effect of varying the gas mixture and, briefly, slanted electric fields and angled tracks.

The curved end shape of the chambers has enabled maximum sensitive detection area within the g-2 magnet pole pieces and electron drift has been achieved in this region with spatial

resolutions of the order 0.3 mm at B = 0. By applying high electric fields, this region has been successfully operated in strong magnetic fields, but the performance parameters have not yet been fully determined under these conditions.

The resolution of normal cells in magnetic fields of strength up to 7.5 KGauss has been observed to be comparable with that at B = 0, and together with the high efficiencies observed under this condition, is primarily due to the short drift spaces involved.

A simple model used to design a magnetic field compensation mechanism and predicting the drift time-distance variation expected in the g-2 magnetic field has been presented. Initial drift time distributions have suggested good agreement between observation and prediction, however, these calibrations are by no means complete as yet, due to the limited time range of the commercial timing devices employed.

The drift chamber array has been commissioned at CERN and electron tracks have been observed successfully (resolving automatically the left-right ambiguity). The initial analysis of the track data has been simple and has predicted a circulating beam profile of the correct shape but shifted by ~9 cm. It is suggested that the main contribution to this profile comes from particles emerging from the storage tank far upstream and entering the array after following an indirect path. A more rigorous curve fitting routine and the continuation of calibration measurements are considered necessary.

A source of severe chamber inhibition has been encountered (section 7.4.2) which has limited efficient data collection to times $\gtrsim 100\,\mu$s after pion inflection. A possible method of reducing the

paralysis time has been mentioned.

8.2 Footnote: The Present State of the g-2 Experiment

The latest value of the anomaly presented by the CERN muon storage ring collaboration (1) is: $a(\mu^+) = (1,165,895 \pm 27) \times 10^{-9}$, meaning that $a_{exp} - (a_{QED} + a_{had}) = (-13 \pm 29) \times 10^{-9}$. This result has been achieved by the collection of some 40 million decay electron events. The above precision represents a measurement to the level of 27 ppm which is an order of magnitude improvement on the previous measurement and validates the theoretical value. The accuracy of measurement will be further improved by the continuation of data taking into 1976, the continued mapping of the magnetic field and the inclusion of data from the g-2 drift chamber array; it is intended to measure (g-2) to 10 ppm. Results for μ^- will also be forthcoming and it is hoped that a similar amount of data will be collected for both particle polarities.

8.3 Concluding Discussion

The main objectives of this work have been:-

1) To devise a full series of experimental tests necessary to the development of drift chambers for use in a high energy physics experiment.

2) To carry out these tests, and more generally, make a study of the properties and problems associated with drift chambers and the electron drift process. (Because of the effort in this field over the past four years, comparison of certain results with those collected independently by other workers can readily be made).

3) To design and build a set of chambers with certain

specialist features for the g-2 experiment, applying the tests of 1), and thus measuring and optimizing various chamber parameters.

4) To install a drift chamber array and data readout-acquisition system in the g-2 muon storage ring and assure its proper working order (while making a study of the effect on drift chambers of this particular environment).

The fulfilment of the above objectives has resulted in the following:-

1) A study of Argon(90)-Methane(10) as a drift chamber gas has been made.

2) The operation of drift chambers in the non-uniform fringe fields of bending magnets has been achieved and has exemplified another method for solving the left-right ambiguity problem.

3) The problems associated with narrow frame chambers and unconventional drift spaces have been investigated (as well as a general study of the principles and operating problems of wire chambers).

4) The collection of initial results from the g-2 array has served as a guide to future work on the system.

By complementing the work of other groups and by successfully operating drift chambers in an experiment, this study has illustrated the feasibility of using such detectors in high energy physics, and presently, the drift chamber is well favoured in the design of new experimental arrays.

8.4 Some Recent Ideas in Drift Chamber Work

To date, the drift chamber technique has by no means been fully exploited and many new developments are currently under study. For instance, some new ideas concerning drift chambers were presented by Charpak in May 1975 (2):-

By scattering protons of the energy range 0.5 - 1.0 GeV from a solid object, a three-dimensional image of the object can be obtained with the use of high accuracy drift chambers. Initial results have implied possible applications of this technique to radiology in medical physics.

With novel-design chambers incorporating converter materials, neutral radiation of various energies has been detected and accurately located using drift chamber techniques (3).

Drift chambers have been instrumental in the study of crystal lattices, their high spatial accuracy giving the required resolution in determining the angular distributions of scattered high energy particles.

A novel detector, the "scintillating drift chamber", makes use of the light emitted on the deexcitation of atoms undergoing collisions with ionization electrons. The photons produced can be wavelength shifted and detected in standard photomultiplier tubes. By using low drift fields throughout most of the chamber (reducing the gas multiplication and thus decreasing the number of positive ions produced), high operating rates can be achieved by this device.

There has recently been work done on the simplification of drift chamber construction. By using large drift spaces the number of sense wires can be reduced, leaving the H.T. wire planes as the only

complicated part of the constructional technique. Atac and Taylor have reported (4) the successful laboratory testing of a prototype drift chamber in which parallel, 50 μm thick Aluminium foils have replaced H.T. wires as a field shaping device. Spatial reolutions of 100 - 150 μm were obtained with 10 mm drift spaces and a gas mixture of Ar/ C_2H_2/CH_4.

The replacement of H.T. wires by planes with deposited metal strips would enable electric field distributions and cell construction to assimilate the type of chamber mostly considered in this thesis. Initial work on this technique carried out by the Nuclear Instrumentation (N.I.) group at Durham has uncovered problems of dielectric charge-up of certain materials used for H.T. plane bases, thus producing non-uniform and unstable gain properties in the chamber.

The techniques developed in this thesis have enabled the planning of future work and some further studies to be made at Durham involving drift chamber techniques together with possible future developments of these detectors will be discussed next.

8.5 Future Work on Drift Chambers

Work is continuing on the g-2 drift chamber array as discussed in section 7.6 and it is intended to continue collecting data for approximately one year with hopefully a resulting contribution to the accuracy of the main experimental measurement.

Two other major drift chamber projects are currently under consideration by the Durham N.I. group:-

Work has started on extending the X-ray imaging techniques

reported by other groups (3) prime interests being to optimize the X-ray converter efficiency and improve energy resolution (5); future medical applications are implied.

It is intended to use a system of multiwire drift chambers as a fast event trigger for a rapid cycling bubble chamber in the investigation of Λ-p interactions at the Rutherford Laboratory (6). A three hundred wire system is envisaged (7), 5 cm drift spaces will be employed and a 20 KGauss magnetic field will be encountered. New constructional techniques will be applied, in particular, curved chambers will probably be used to surround the bubble chamber, thus producing near-normal directions of particle incidence as an alternative to the problems of angled trajectories in an already complicated three dimensional track measuring system.

The Durham University Astrophysics group has recently been involved in work on a drift chamber array for use in high energy gamma ray astronomy studies involving a transatlantic balloon flight (8). The experiment is a Southampton University-E.S.T.E.C. collaboration and the chambers will be built by the I.R.D. company. Spatial resolutions of 0.5 mm in each chamber, angular resolutions of the order 2^{o} and a detection efficiency for 100 MeV γ-rays of 15% are expected for the whole array. The γ-ray converters are incorporated into the chamber design in the form of 1% radiation length perspex windows.

Work has been done on low pressure drift chambers (9) with the advantage of presenting small stopping power to strongly ionizing particles, and complementing the need of extremely thin windows for such radiation. Varying the pressure in drift chambers may receive

future study, in particular, liquid drift chambers offer interesting possibilities.

In general, future developments concerning the basic principle of the drift chamber detector will involve improving the spatial resolution capabilities (with particular emphasis on operating gas mixtures), and developing cheaper and faster readout methods.

References

1 J.M. Bailey, K. Borer, F. Combley, H. Drumm, C. Eck, F.J.M. Farley, J.H. Field, W. Flegel, P.M. Hattersley, F. Krienen, F. Lange, G. Petrucci, E. Picasso, H.I. Pizer, O. Runolfsson, R.W. Williams, S. Wojcicki. Phys. Letters, 55B (1975) 420

2 G. Charpak. CERN Courier, No. 6, Vol. 15, June 1975

3 G. Charpak, Z. Hajduk, A. Jeavons, R. Kahn, R.J. Stubbs. Nucl. Inst. Meth. 122 (1974) 307

4 M. Atac, W.E. Taylor. National Accelerator Laboratory Internal Report, N.A.L. 74/22

5 A.R. Hedge, B. Sitar. Private Communication, University of Durham, 1975

6 J.V. Major. Draft Proposal, University of Durham, May 1975

7 J.M. Breare. Draft Proposal, University of Durham, July 1975

8 D. Ramsden, A.J. Dean, S. McKechnie, B.G. Taylor, R. Bennett, R.D. Wills. Proposal J, "Transatlantic Balloon Facility, a Scientific Case", University of Southampton, November 1974

9 A. Breskin, G. Charpak, F. Sauli. CERN NP Internal Report, January 1974

APPENDIX I

SOME GEOMETRICAL CONSIDERATIONS OF THE g-2 DRIFT CHAMBER ARRAY

a) Angles of Particle Incidence

The radius of curvature (R) of electrons in a magnetic field (B) is determined by the classical expression:-

$$Bev = mv^2/R$$

$$\text{ie. } R = \gamma m_o c/Be = E/Bec$$

which for energy (E) in GeV and R in metres reduces to (for a 15 KGauss field):-

$$R = 2.22\ E \qquad (i)$$

Consider an electron emerging from the centre of the vacuum vessel and intersecting the final drift chamber after travelling a radial distance inwards x (figure A 1). For the maximum angle of incidence on this chamber, $x \simeq 0.3$ m (0.22 m from the shower counter sensitive length). The geometry of figure A 1 thus yields for the maximum angle of incidence ($\alpha(E)$) subtended by the tangent T:-

FIG A1 CONSTRUCTION FOR ANGLED TRAJECTORIES OF DECAY ELECTRONS IN THE DRIFT CHAMBERS

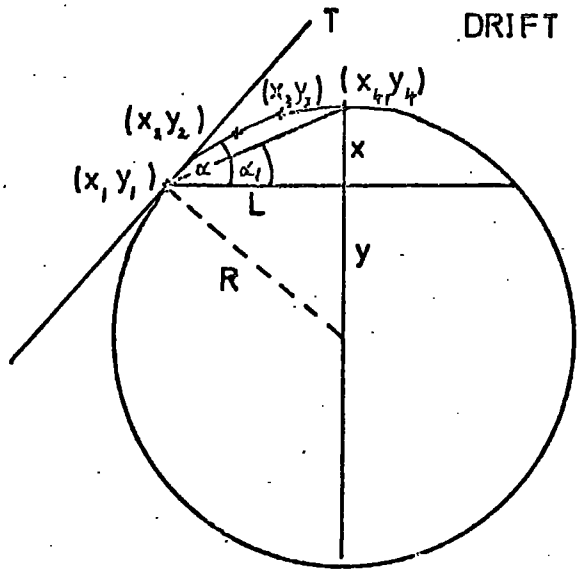

FIG A2 CONSTRUCTION FOR DETERMINING THE ERROR IN THE MUON DECAY RADIUS

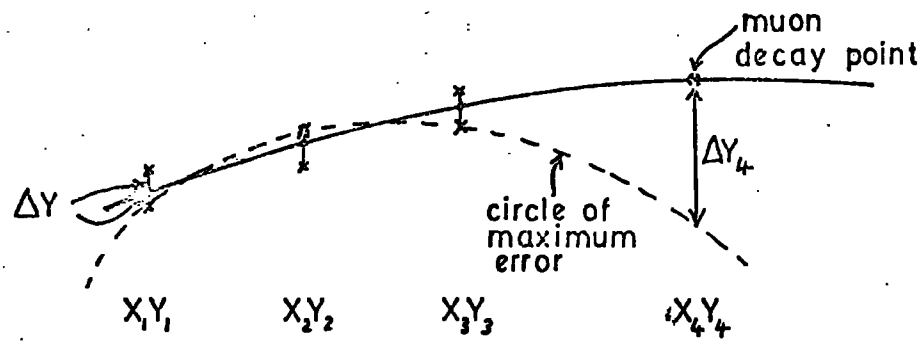

FIG A3 CONSTRUCTION FOR DETERMINING THE MUON DECAY RADIUS

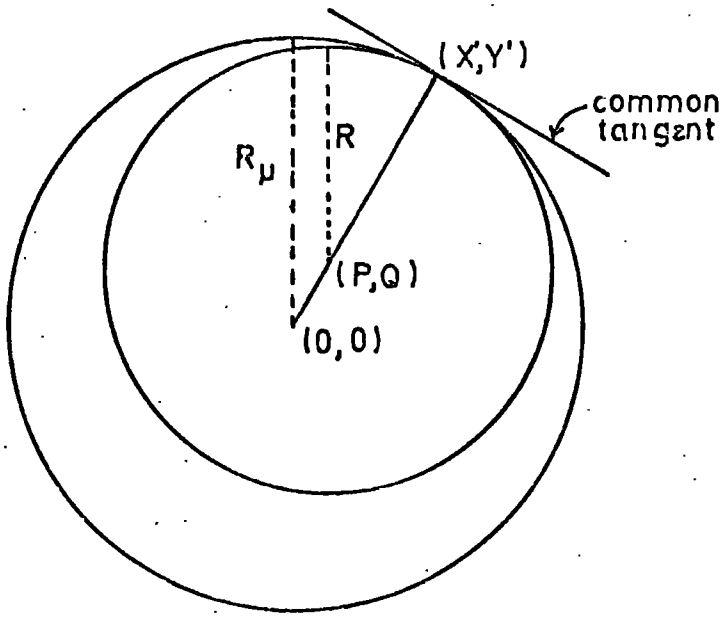

$$\alpha(E) = \arctan\left(\frac{L}{y}\right) = \arctan\left(\frac{\sqrt{0.6\ R - x^2}}{R - x}\right) \qquad \text{(ii)}$$

However, this will be an overestimation as the tracks will straighten as B decreases radially inwards; therefore a second estimate of the maximum angle is:-

$$\alpha_1(E) = \arctan\left(\frac{x}{L}\right) = \arctan\left(\frac{x}{\sqrt{0.6\ R - x^2}}\right) \qquad \text{(iii)}$$

Thus, for various electron energies we have:-

E(GeV)	α^{o}	α_1^{o}
1.0	30.1	15.1
1.5	24.5	12.3
2.0	21.2	10.6
2.5	18.9	9.5
3.0	17.3	8.6

The true values ($\alpha_{max}(E)$) of the upper limit of angle of incidence will be between the values of α and α_1 but, on consideration of all trajectories and all chambers, angles will be mostly much less than α_{max} and thus cause little disturbance to the space-time characteristics.

b) Approximate Errors in Track Reconstruction

Assuming the centre of the circle uniquely defined by three points (X_1, Y_1), (X_2, Y_2), (X_3, Y_3) on the track defines an origin,

the equation of the circle is:-

$$Y^2 + X^2 = R^2 \qquad \text{(iv)}$$

The three simultaneous equations obtained on inserting these points into equation (iv) may be reduced to the single equation:-

$$R^2 = Y_1^2 - \frac{X_1^2(Y_2^2 - Y_3^2)}{(X_2^2 - X_3^2)} \qquad \text{(v)}$$

For an error in each Y-value of ΔY, the maximum error (ΔR) on the radius occurs when ΔY for Y_2 is in the opposite sense to those for Y_1 and Y_3 as indicated in figure A 2 (note that the erroneous circle is not centred on the origin, however, assume this does not affect the following calculation). Thus:-

$$(R + \Delta R)^2 = (Y_1 + \Delta Y)^2 - \frac{X_1((Y_2 + \Delta Y)^2 - (Y_3 - \Delta Y)^2)}{(X_2^2 - X_3^2)} \qquad \text{(vi)}$$

subtracting (v) from (vi) gives:-

$$2R\Delta R + \Delta R^2 = \Delta Y^2 - 2\Delta Y Y_1 - \frac{2\Delta Y X_1^2(Y_2 - Y_3)}{(X_2^2 - X_3^2)} \qquad \text{(vii)}$$

Now, if (X_4, Y_4) is the point of birth of the electron, lying on the circle determined by equation (iv), then:-

$$Y_4^2 = R^2 - X_4^2$$

$$\therefore \quad (Y_4 + \Delta Y_4)^2 = (R + \Delta R)^2 - X_4^2$$

$$\text{thus } 2Y_4\Delta Y_4 + \Delta Y_4^2 = 2R\Delta R + \Delta R^2$$

which from equation (vii) gives:-

$$\Delta Y^2 - 2\Delta Y\left(Y_1 + \frac{X_1^2(Y_2 + Y_3)}{(X_2^2 - X_3^2)}\right) - (2Y_4\Delta Y_4 + \Delta Y_4^2) = 0$$

solving this quadratic in ΔY gives:-

$$\Delta Y = A \pm \sqrt{A^2 + (2Y_4\Delta Y_4 + \Delta Y_4^2)} \qquad \text{(viii)}$$

$$\left(\text{where } A = Y_1 + \frac{X_1^2(Y_2 + Y_3)}{(X_2^2 - X_3^2)}\right).$$

From figures A 1 and A 2, and knowing the separation of the drift chambers, fitting circles through the three downstream chambers we have that: $X_1 \simeq L$, $X_2 \simeq (L - 0.1)$, $X_3 \simeq (L - 0.2)$ and $X_4 = 0$ (all in metres), from whence the values of Y_1, Y_2 and Y_3 can be determined for certain energy tracks. Thus, the following table can be formed, using equation (viii):-

E(GeV)	Required Values of ΔY	
	For ΔY_4 = 1 mm	For ΔY_4 = 2 mm
1	0.08 mm	0.16 mm
2	0.06 mm	0.11 mm

Similarly, assuming $\Delta Y \simeq 0.1$ mm gives the following errors in the radius of electron birth:-

E(GeV)	ΔY_4
1	1.2 mm
2	1.8 mm

These calculations have considered maximum leverage in track reconstruction and in only an approximate way, however, the order of magnitude of results indicates the requirements in this experiment of detectors capable of spatial resolutions of a fraction of a mm.

c) Beam Profile Reconstruction

Drift times from three chambers can be converted into cartesian coordinates (X_1, Y_1), (X_2, Y_2) and (X_3, Y_3) in the system where (0, 0) is the centre of the storage ring, and determine the unique circle (radius R, centre (p, q)):-

$$(X - p)^2 + (Y - q)^2 = R^2 \qquad \text{(ix)}$$

p, q and R are determined from the solution of the three simultaneous

equations utilizing the above track data and equation (ix), and are given by:-

$$p = \frac{F/A\ (D - C) - E + C}{2(BF/A - G)} \qquad (x)$$

$$q = \frac{D - C - 2Bp}{2A} \qquad (xi)$$

$$R = \sqrt{q^2 - 2Y_1 q + p^2 - 2X_1 p + C} \qquad (xii)$$

where:

$$A = Y_2 - Y_1$$

$$B = X_2 - X_1$$

$$C = Y_1^2 + X_1^2$$

$$D = Y_2^2 + X_2^2$$

$$E = Y_3^2 + X_3^2$$

$$F = Y_3 - Y_1$$

$$G = X_3 - X_1$$

(From the left-right ambiguity, three pairs of points are obtained, allowing eight possible circles to be constructed. The correct circle is chosen as mentioned in the main text.)

Tangentiallity (within the storage tank) of this reconstructed track with the muon orbit circle, determines the point of birth (X', Y') of the electron. From figure A 3, this condition is observed when the line $Y = (q/p).X$ intersects the circle of equation (ix), thus in terms of Y' this requires:-

$$((p/q)Y' - p)^2 + (Y' - q)^2 = R^2$$

$$\text{ie. } Y'^2((p^2/q^2) + 1) - Y'((2p^2/q) + 2q) + (p^2 + q^2 - R^2) = 0$$

where the highest root, $q + \sqrt{R^2/(1 + p^2/q^2)}$, determines Y' , and $X' = (p/q)Y'$. The muon radius for a particular track is then given by:-

$$R_\mu = \sqrt{X'^2 + Y'^2} \qquad \text{(xiii)}$$

APPENDIX II

MEASUREMENTS INVOLVING TILTED ELECTRIC FIELDS AT B = 0

a) Efficiencies

Figure A4 shows the efficiency-voltage characteristics obtained for various electric field tilts (1, 2 and 3 H.T. wire spacings) in g-2 chamber cells, using a collimated 1 mCi Sr90 β-source at a distance of 7 mm from the sense wire. The data have been corrected for background counts but are otherwise unnormalised. The results were recorded using a carefully-positioned, low-noise P.M.-scintillator trigger of well defined sensitive area (less than that of the drift chamber cell), with a T.A.C.-P.H.A. timing system generating a gate width of 1.0 μs. Low input impedance amplifiers were employed with output discrimination levels of 100 mV and the outputs from each of the cells adjacent to that under investigation were ORed into the stop line in order to obtain a faithful efficiency characteristic throughout the cell.

Plateau levels of ~100% are observed and the curves obtained for 1 and 2 tilts are almost inseparable and of similar values to the untilted field case, whereas that obtained from a 3 tilt configuration displays a plateau being reached at lower applied voltages. These variations are in accordance with the pulse height variations of

FIG A4 : EFFICIENCY - VOLTAGE CURVES (FOR TILTED ELECTRIC FIELD CONFIGURATIONS) AT A DISTANCE OF 7mm FROM THE S.W.

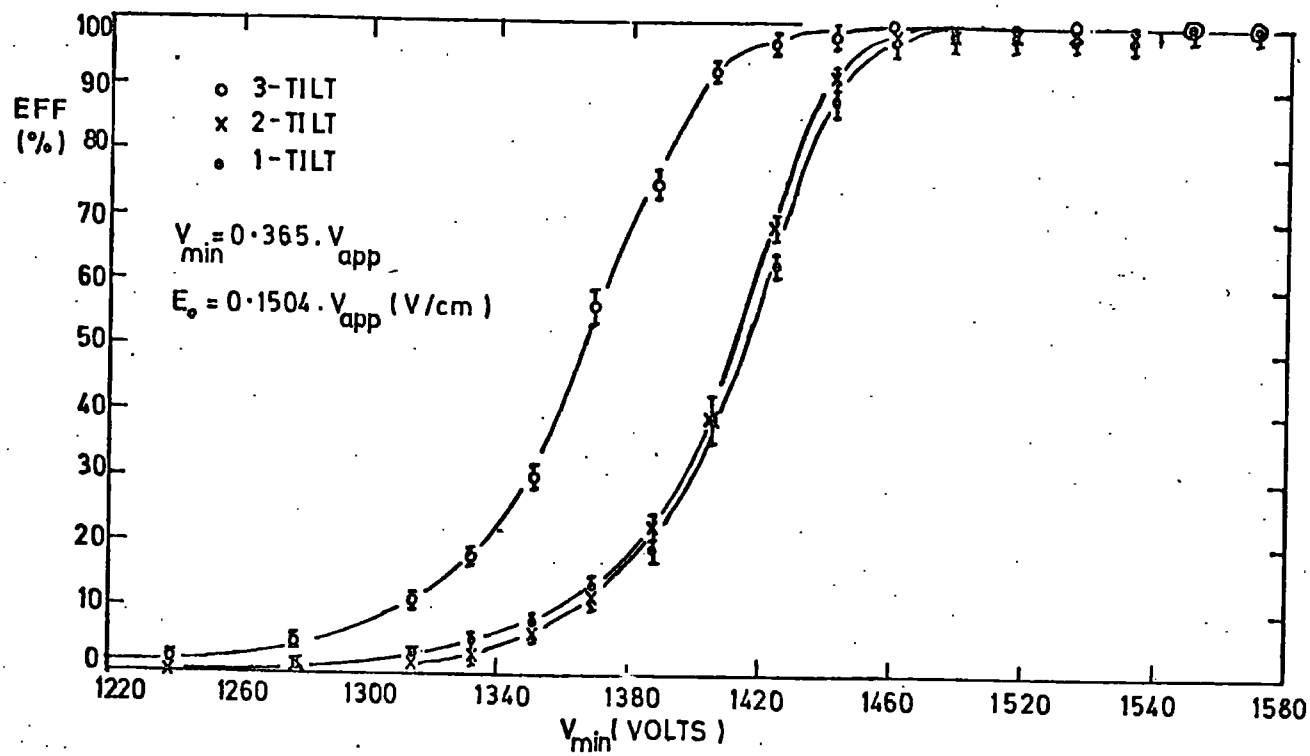

FIG A5 : EFFICIENCY - VOLTAGE CURVES (FOR TILTED ELECTRIC FIELD CONFIGURATIONS) AT A DISTANCE OF 13 mm FROM THE S.W.

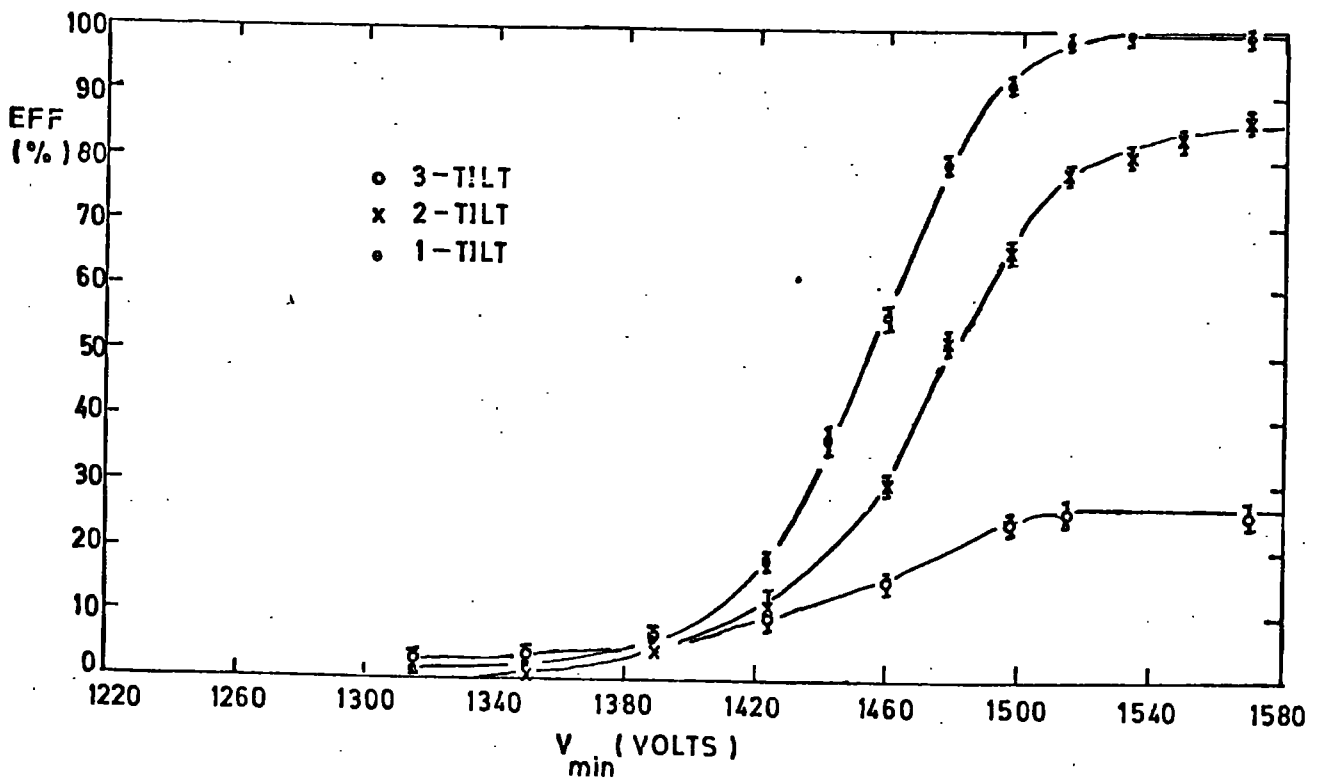

figure 4.6 and dependent on discrimination level. It was also noticed, as might be expected, that breakdown occurred at lower applied voltage levels as the tilt was increased.

Figure A5 shows a similar series of curves obtained at a collimating slit distance of 13 mm from the sense wire (1 mm from the potential wire). Here, the curves do not attain plateau levels until higher voltages are applied and the levels decrease as field tilt is increased. The former effect is due to a certain fraction of the ions formed in the gas being ejected from the chamber (due to the angle of the drift field), resulting in a decrease in pulse height and thus a decrease in efficiency at any particular voltage (for a constant discrimination level). As the field is increased, for the 1-tilt case, the multiplicity in the avalanche process is sufficient to restore $\sim$100% efficiency in spite of the depleted number of swarm electrons; for 2 and 3 tilts, greater losses result in lower plateau levels. To explain the plateau levels in a more quantitative manner would require a precise knowledge of the electron flow lines, the latter being responsible for the 100% efficiency plateaus obtained throughout much of the cell (as for example in figure A4).

Figure A6 shows an efficiency scan across the potential wire region for 1, 2 and 3 tilts of a basic electric field (E_o) of 617 Vcm^{-1} (V_{min} = 1497 V). Efficiency troughs resulting from the ejection of deposited ions are clearly seen and the inefficiency increases with tilt. However, due to the flow line trajectories of the drifting swarm, $\sim$ 100% efficiency is restored at a distance of $\sim$5 mm from the potential wire for the 3-tilt configuration. Also indicated in the figure is the predicted variation of the percentage of deposited ionization collected at the sense wire for a 2-tilt electric

FIG A6: THE EFFICIENCY IN THE P.W. REGION OF A CELL FOR VARIOUS TILTS OF ELECTRIC FIELD (B = 0)

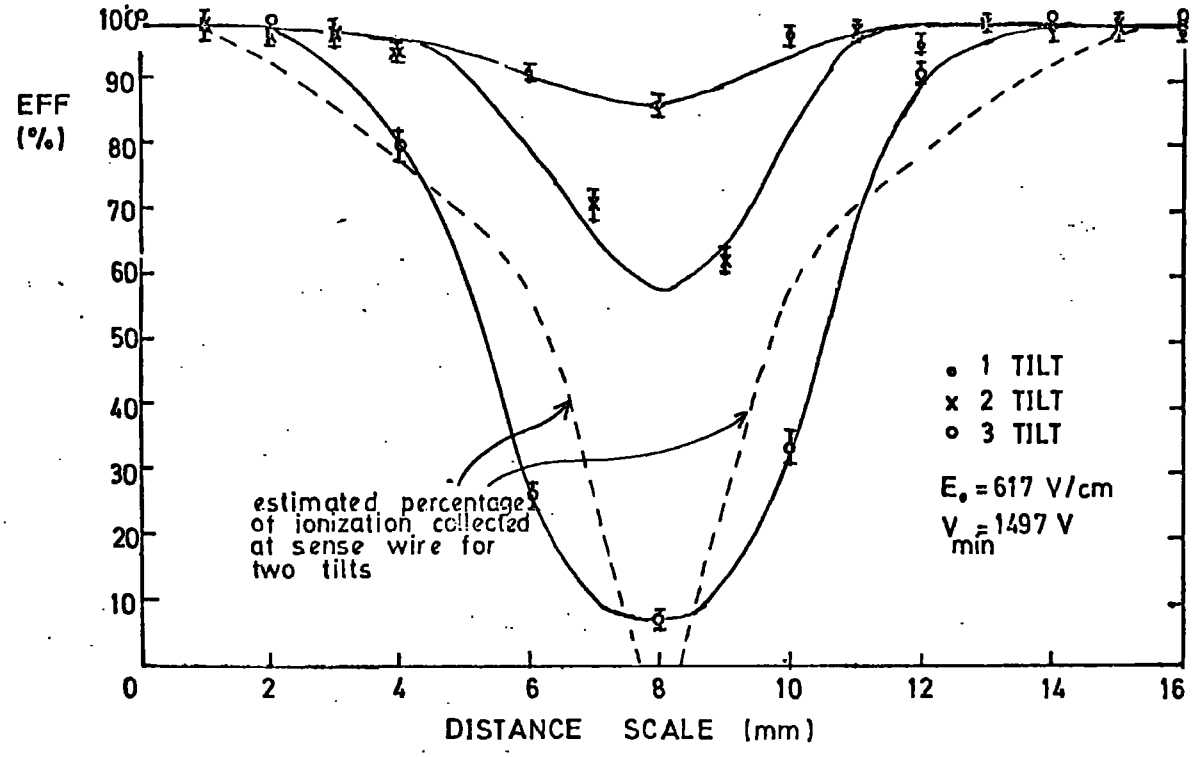

FIG A7: INEFFICIENCIES AND "DEAD SPACES" CAUSED BY TILTED ELECTRIC FIELD CONFIGURATIONS (B = 0)

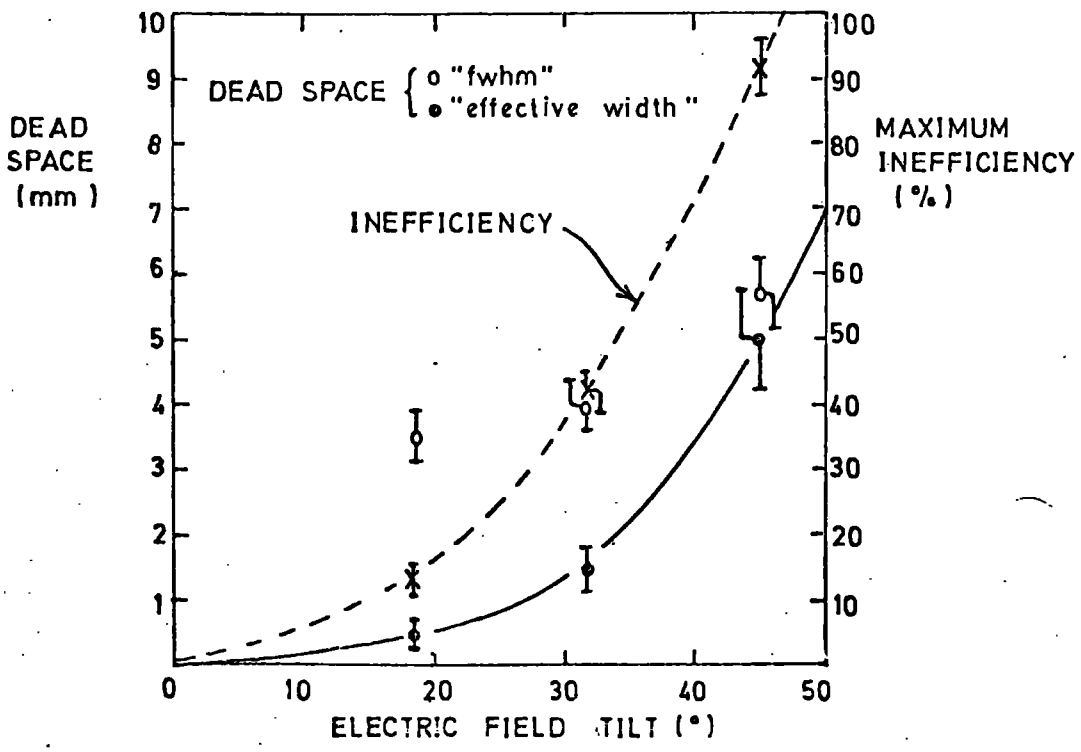

field. This was based on a simple geometrical model which considered the probable paths of electrons starting from the initial track (across the gap between high voltage planes) and travelling in an electric potential configuration similar to (but simplified) that of figure 3.9. The maximum inefficiency incurred by such a tilt of electric field is not as great as that suggested by this model and is probably a result of the potential barriers presented to the drift electrons by the H.T. planes which help to contain the swarms within the cell.

The variations of the F.W.H.M's of the troughs with angle of electric field is indicated in figure A7. On defining a "dead space" as the effective width of a region with 100% inefficiency having the same area as the measured partially-inefficient region, a smooth variation of this quantity with electric field angle is observed as shown in the same figure. Also in figure A7, the maximum inefficiency is shown to be a rapidly increasing function of electric field tilt. From these results, an inefficient region in the last few mm of a g-2 cell is expected for an electric field at 45° to the sense wire plane operating in no magnetic field. It must be mentioned that this effect would be more serious for longer drift spaces, but for a g-2 cell, will be rapidly reduced as B is increased towards ~15 KGauss.

The investigations described above were continued for various values of high voltage ($V_{p.w.}$) applied to the potential wire and it was found that no significant worsening of the efficiency variation in this region was apparent until $V_{p.w.} \leq V_4$ of figure 3.8. The efficiency curve was also seen to be a function of V_{min} (V_{app}) as expected.

b) Drift Times

Figure A8 shows the result of scanning a g-2 prototype chamber across the collimated β-ray beam and measuring the positions on the P.H.A. display of timing distribution peaks at 2 mm intervals. The electric field configuration in the chamber for this test was: 3 tilts for cells 1 and 2, 2 tilts for cells 3, 4 and 5 and 1 tilt for cells 6, 7 and 8 (E_o = 574 Vcm^{-1}). The outputs from all cells were ORed into the stop line.

Linear space-time variations are observed throughout most of the drift spaces, but some deviation from this form is seen to occur at cell boundaries. The flow line trajectories of electron swarms in such a configuration are complicated; the basic drift direction will be at an angle (γ) equalling the electric field tilt angle, but, because of the containing H.T. barriers and the field configuration in the sense wire region, many paths are possible for ions deposited along tracks normal to the sense wire plane. In general, greater values of γ would be expected to produce more diverse flow lines and hence longer observed drift times. This effect was verified on considering the following values of drift velocity ($w_{//}$) derived by averaging the gradients of the uniform parts of the space-time variations ($w_{//}(\gamma = 0) = 35.6$ mm μs^{-1}):-

γ (^{o})	$w_{//}(\gamma, E)$ (mm μs^{-1})
18.4	35.2
33.7	31.1
45.0	29.3

In the presence of a magnetic field, the basic angle of

FIG A8 DRIFT TIMES ACROSS A g-2 CHAMBER (E_o = 574 V/cm, cells 1,2 : γ = 45°
cells 3,4,5: γ = 33·7°
cells 6,7,8: γ = 18·4°)

(vertical scale : 4·5 ns / channel)

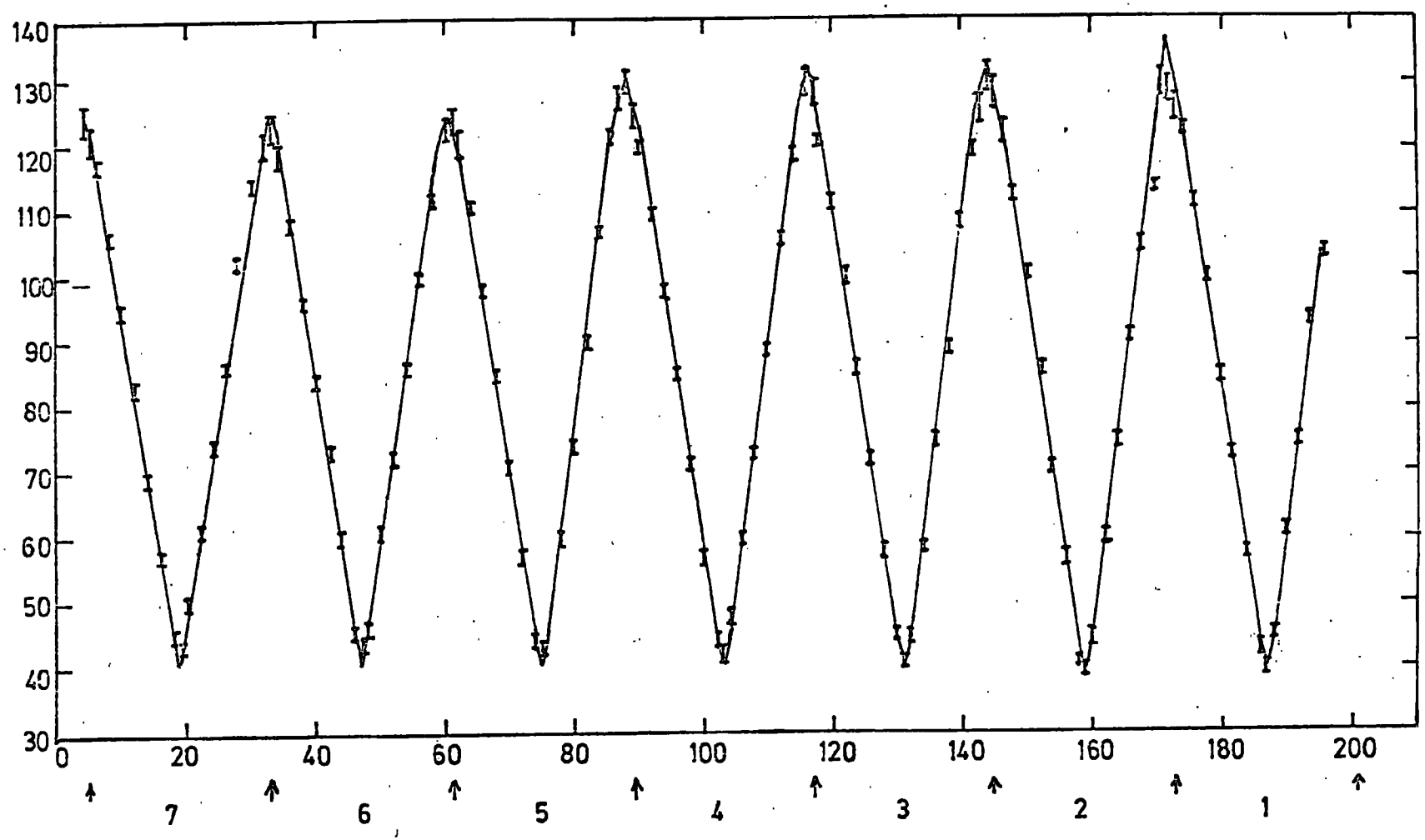

drift ($(\gamma - \theta)$ from chapter 6) is often small compared with the above angles, hence many electrons will flow in such a direction for much of their existence and thus the expected values of $w_{//}(\gamma, E, B)$ can be more readily predicted.

ACKNOWLEDGEMENTS

The author would like to thank Professor A.W. Wolfendale for his support of this work and the use of laboratory facilities. He is indebted to his supervisor, Dr. J.M. Breare for his continual guidance and advice, and also for the effort he himself has put into this project. Mr. R. Browell and Mr. M. Comyn are thanked for their help and collaboration in parts of this work and the technical skills of Mr. J. Webster are appreciated as well as his willingness to take an interest in this project. Members, past and present, of the Nuclear Instrumentation group are thanked for their support and stimulating discussion.

Mr. R. McDermott is thanked for constructing the prototype model frames and several experimental support structures and Mr. A. Robertshaw and his colleagues of the International Research and Development Co. are acknowledged for manufacturing the production chambers.

The author would like to thank the staff of the Daresbury Laboratory for their help and use of facilities. In particular, he is indebted to Dr. J.M. Bailey and Mr. M.D. Rousseau for their support and advice. Dr. P.A. Ridley and Mr. P. Smith are thanked for their endeavours with the computing facilities and the interest expressed by members of other groups has been welcomed.

The author would like to thank Professor E. Picasso for his kind permission to work on the g-2 experiment and the CERN staff are thanked for their help. The interest and encouragement of all members of the Muon Storage Ring collaboration is sincerely appreciated. He would like to thank Mr. W.Glessing for his work on the chamber mounting facility and Mr. P. Scharff-Hansen for his provision of the computer facility.

Dr. F.W. Stubbs is thanked for her excellent transcription of the hand written text as is Dr. R.J. Stubbs for his useful criticisms. Mr. M. Lee, Mrs. E. Johnston and Miss. D. Dixon are thanked for their help with photographs and diagrams.

The S.R.C. is thanked for the provision of an award and additional expenses and, lastly but by no means least, the author would like to thank his parents and Jill for their constant encouragement and patience.